

VOLUME 15

NUMBER 1

2022

ISSN 2218-7979
eISSN 2409-370X

International Journal of
Biology
and **Chemistry**



Al-Farabi Kazakh National University

International Journal of Biology and Chemistry is published twice a year by
al-Farabi Kazakh National University, al-Farabi ave., 71, 050040, Almaty, Kazakhstan
website: <http://ijbch.kaznu.kz/>

Any inquiry for subscriptions should be sent to:
Prof. Mukhambetkali Burkitbayev, al-Farabi Kazakh National University
al-Farabi ave., 71, 050040, Almaty, Kazakhstan
e-mail: [Mukhambetkali Burkitbayev@kaznu.kz](mailto:Mukhambetkali.Burkitbayev@kaznu.kz)

EDITORIAL

The most significant achievements in the field of natural sciences are reached in joint collaboration, where important roles are taken by biology and chemistry. Therefore publication of a Journal, displaying results of current studies in the field of biology and chemistry, facilitates highlighting theoretical and practical issues and distribution of scientific discoveries.

One of the basic goals of the Journal is to promote the extensive exchange of information between the scientists from all over the world. We welcome publishing original papers and materials of biological and chemical conferences, held in different countries (by prior agreement, after the process of their subsequent selection).

Creation of International Journal of Biology and Chemistry is of great importance, since scientists worldwide, including other continents, might publish their articles, which will help to widen the geography of future collaboration.

The Journal aims to publish the results of the experimental and theoretical studies in the field of biology, biotechnology, chemistry and chemical technology. Among the emphasized subjects are: modern issues of technologies for organic synthesis; scientific basis of the production of biologically active preparations; modern issues of technologies for processing of raw materials; production of new materials and technologies; study on chemical and physical properties and structure of oil and coal; theoretical and practical issues in processing of hydrocarbons; modern achievements in the field of nanotechnology; results of studies in various branches of biology, chemistry and related technologies.

We hope to receive papers from the leading scientific centers, which are involved in the application of the scientific principles of biological and chemical sciences on practice and fundamental research, related to production of new materials, technologies well ecological issues.

A.A. Malysheva¹ , A.M. Kokhmetova^{1*} , M.K. Kumarbayeva¹ ,
 D.K. Zhanuzak¹ , A.A. Bolatbekova¹ , Zh.S. Keishilov¹ ,
 E.I. Gulyaeva² , A.M. Kokhmetova¹ , V. Tsygankov³ ,
 Y.B. Dutbayev⁴ , S.B. Dubekova⁵ 

¹Institute of Plant Biology and Biotechnology, Almaty, Kazakhstan

²All-Russian Research Institute of Plant Protection, St. Petersburg, Russia

³LLP «Aktobe Agricultural Experimental Station», Aktobe region, Kazakhstan

⁴Kazakh National Agrarian Research University, Almaty, Kazakhstan

⁵LLP «Kazakh Research Institute of Agriculture and Plant growing», Almaty, Kazakhstan

*e-mail: gen_kalma@mail.ru

(Received 22 April 2022; received in revised form 16 May 2022; accepted 20 May 2022)

Identification of carriers of *Puccinia striiformis* resistance genes in the population of recombinant inbred wheat lines

Abstract. Stripe rust (yellow rust) caused by *Puccinia striiformis* (*Pst*) f. sp. *tritici* is one of the most dangerous diseases of wheat. Marker assisted selection (MAS) accelerates the selection of resistance gene donors in wheat recombinant inbred lines Almaty/Avocet (S) and to evaluate their response to *Pst*. Evaluation of seedling resistance to *Pst* allowed us to select 2 lines simultaneously resistant to races 111E231 and 7E63. Race 7E63 was avirulent to most samples, and 111E231 was highly virulent. All the studied lines demonstrated a resistant and moderately resistant reaction to the causative agent of yellow rust at the adult plant stage (R-MR). Molecular screening revealed the presence of a marker allele associated with the *Yr18/Lr34* gene complex in 5 RIL. The frequency of resistant genotypes inheriting the *Yr18* gene was 22.7%. The results can be used in MAS wheat breeding programs to increase resistance to yellow rust of wheat.

Key words: wheat, yellow rust, *Puccinia striiformis*, resistance genes, molecular markers.

Introduction

Wheat (*Triticum aestivum* L.) is a significant food crop at the global level, and its production is the basis of food security throughout the world [1]. World wheat production currently reaches 777.8 million tons, and world consumption per capita is 67.6 kg/year [2]. On average Kazakhstan produces 18-20 million tons of wheat grain, but output is highly dependent on weather and in recent years has fluctuated between 10 and 17 million tons [3]. Wheat production in Kazakhstan is constrained due to rust diseases (stem, stripe and leaf rust) [4-10], as well as leaf spot diseases (tan spot and rust) [11-16].

Yellow rust caused by *Puccinia striiformis* Westend f. sp. *tritici* (*Pst*) is one of the most dangerous diseases of wheat worldwide. When epiphytotic occur, losses can vary from 20 to 40% or more [17-18]. A decrease in yield is observed as a

result of a decrease in the number of grains in the ear and grain weight in highly sensitive wheat varieties [4, 19]. In the period from 2009 to 2016, stripe rust epidemics occurred annually in Kazakhstan, and yield losses of susceptible wheat varieties reached 20-50% [4]. The rust pathogen population overcomes the protection of resistant cultivars due to the emergence of virulent pathogen races [18]. The cultivation of resistant varieties is the most economical and environmentally friendly approach, which makes it possible to abandon the use of fungicides and reduce crop losses due to yellow rust [20]. However, traditional breeding methods are not always effective. Marker-assisted selection (MAS) using identified target genes makes the process of developing the wheat cultivars more accurate and reliable [21] MAS methods are effectively used to shorten the breeding cycle, increase resistance to biotic and abiotic stresses and maintain potential

wheat yields [22]. Currently, more than 80 genes for resistance to stripe rust have been identified [22]. Based on recent evaluations in Kazakhstan, genes *Yr5*, *Yr10*, *Yr15* and *Yr18* are still effective [9]. The locus *Lr34/Yr18/Pm38* confers partial and durable resistance against the devastating fungal pathogens leaf rust, stripe rust, and powdery mildew. *Yr18/Lr34* genes have been used in breeding programs for a century and so far, no pathogen adaptability has been found [23]. Wheat cultivars containing these genes occupy more than 26 million ha in various developing countries alone and contribute substantially to yield savings in epidemic years [24]. The gene complex *Yr18/Lr34* is of great interest as a donor of valuable traits. Therefore, identification of novel sources of resistance in a breeding material is of foremost importance for the effective disease control. In view of these facts, recombinant inbred lines of bread wheat developed in our laboratory were evaluated in this study for yellow rust resistance. The goal of this study was to determine the presence/absence of yellow rust resistance genes in wheat recombinant inbred lines Almalý/Avocet (S) and to evaluate their response to *Pst*.

Materials and methods

Twenty-two RILs used in this study were established at F₆ generation by the single-seed descent method (SSD) from an F₂ family between a high yielding Kazakh winter wheat variety 'Almalý' and an Australian spring wheat variety 'Avocet (S)'. Almalý is a Kazakh variety of common winter wheat, developed in 2002, pedigree [(R6862/50431) xBezostaya1], is widely used as a parent in breeding programs in Kazakhstan and Central Asian countries. Almalý has a high yield potential and moderately high resistance to 3 species of rust, is a carrier of genes *Lr1*, *Lr28* and *Lr34* [6]. The pedigree of the cultivar contains Bezostaya1, a carrier of the leaf rust resistance genes *Lr34*, *Lr3a* and *Lr13* (<https://maswheat.ucdavis.edu>). Second parent is 'Avocet (S)', spring wheat cultivar, is considered to be universally susceptible to the three types of rust and is widely used in rust resistance tests. The parents were selected on the basis of their contrasting phenotypic expression of resistance to stripe rust. The highly susceptible Morocco, as well as the near-isogenic lines (NIL *Lr34/TC*6/PI58548* for *Yr18*) of Thatcher, are used in field and laboratory tests as controls.

It is known that in order to develop a mapping population, it is necessary to cross parents that are contrasting in terms of the target trait. Therefore, the Almalý variety, moderately resistant to the disease, served as the maternal parent, and the Avocet (S) variety, susceptible to stripe rust, was used as the father. This made it possible to obtain a mapping population consisting of 186 RILs with a wide range of genetic diversity for stripe rust, susceptibility to which varied from 0 to 100%. These RILs will be the objects of further studies: on the basis of QTL mapping, genetic loci of quantitative traits associated with resistance to YR of wheat will be identified and mapped. However, in this study, we will study only 22 RILs that demonstrated field resistance to stripe rust. These lines were selected based on their field and laboratory phytopathological screening for resistance to *Pst*, where cv. Almalý was resistant and Avocet (S) was susceptible.

The phenotyping of the material was carried out in the conditions of the Kazakh Research Institute of Agriculture and Crop Production (KazNIIZiR), Almalýbak (43°13'09"N, 76°36'17"E), Almatý region in 2019-2020 cropping season. Each entry was planted in 1 m² plot in the middle of September. Experiment was conducted using randomized complete block design with two replications and recommended cultural practices were used for trial management. For the replicated data means were calculated. The stripe rust susceptible cultivar Morocco was planted in every 10th row and as a spreader border around the nursery to ensure uniform infection. In mid-April, stripe rust induced susceptible cultivar Morocco, was inoculated with mixed races of *Pst* at seedling stage in the field in Kazakhstan to serve as spreader of stripe rust pathogen to the experimental plots. Weather conditions in Almatý in 2019 and in 2020 were favorable for the development of stripe rust, and the infection on susceptible checks reached 100S. The resistant assessment was carried out according to the method developed by CIMMYT [25]. Five infection types described as the following: 0 – immune; R – resistant; MR – moderately resistant; MS – moderately susceptible; and S – susceptible. Severity of disease was recorded in terms of per cent leaf area infection and pustule type was recorded as response.

Spore collection, storage, and reproduction were then conducted in accordance with the methods of Roelfs *et al.* [25]. Spores of *P. striiformis* were used to determine the pathotypes of stripe rust isolated from wheat leaves in the different regions of Kazakhstan. The determination of race-specific seedling resistance

was performed according to the method of Roelfs et al. (1992) [25] using highly virulent *Pst* races – 111E231 (virulence 60%) and 7E63 (virulence 73%). The 111E231 pathotype was characterized by avirulence to varieties-differentiators with *Yr* genes *SU*, *SD*, *Yr10*, *Yr3v*, *Yr2*, and *Sp* and virulence to varieties with *Yr6*, *Yr7*, *Yr1*, *Yr12*, *Yr8*, *3N*, *Yr6+*, *Yr7+*, and *Yr4+* genes. The 7E63 pathotype showed avirulence to the differentials with *SU*, *SD*, *Yr10*, and *Sp* genes and virulence to varieties with *Yr3v*, *Yr6*, *Yr7*, *Yr1*, *Yr2*, *Yr12*, *Yr8*, *3N*, *Yr6+*, *Yr7+*, and *Yr4+* genes. The results were evaluated on 15-20 days according to the Gassner and Straib accounting scale (IT from 0 to 4) [26].

Genomic DNA was extracted at the stage of 3–5-day-old wheat seedlings using the CTAB method [27]. The presence of the *Lr34/Yr18* gene complex was identified using a specific codominant STS marker csLV34 (*Yr18*) [28], PCR was performed in a Bio-Rad T100TM amplifier (Bio-RAD, Hercules, California, USA). The PCR mixture contained 2.5 µl of genomic DNA (30 ng), 1 µl of each primer (1 pM/µl) (SigmaAldrich, St. Louis, Michigan, USA), 2.5 µl of dNTP mixture (2.5 mM, dCTP, dGTP, dTTP and dATP (aqueous solution) (Silex CJSC, Russia), 2.5 µl MgCl₂ (25 mM), 0.2 µl Taq polymerase (5 units. mcl) (CJSC “Silex”, Russia), 2.5 mcl 10X buffer for PCR and 12.8 mcl ddH₂O. PCR was performed at initial denaturation of 94 °C for 5 minutes, 40 cycles: 94°C – 40 s., 55°C – 30 s., 72°C – 1 min., final elongation at 72 °C – 7 min. The separation of PCR products was carried out in a 2% agarose gel using a TBE buffer (45 mM Tris-borate, 1 mM EDTA, pH 8) with the addition of ethidium bromide. The lengths of the amplicon fragments were determined using a 100-bp DNA marker. Visualization of the results was performed using the gel documentation system (Gel Doc XR+, BIO-RAD, Hercules, California, USA)

Results and discussion

The parent variety Almaly is characterized by high yields and a moderate degree of resistance to stripe rust. There is a variety of Bezostaya 1 in Almaly's pedigree, which is a carrier of the *Yr18* gene [29]. The Australian variety Avocet (S), on the contrary, has a high degree of susceptibility to stripe rust. The results of phytopathological evaluation of the breeding material under artificial infectious background allowed us to select 22 RIL Almaly/Avocet(S) lines that showed a high degree of resistance to the stripe rust pathogen *Pst* at the adult plant stage (0-20MR). From the two parents, ‘Almaly’ showed a moderate degree of resistance (20MR), while ‘Avocet(S)’ and the susceptible control Morocco showed a high degree of susceptibility (100S, both) (Table 1). The other control line NIL *Lr34/TC*6/PI58548* for *Yr18*, the carrier of gene *Yr18* showed a moderate susceptibility with low severity (10MS).

In greenhouse experiment for seedling resistance lines investigated showed a different infectious type (ITs) for the two races of *Pst*. Avirulence of race 7E63 was shown to the majority of the studied RIL entries (91%) (IT-0), while 2 lines (9%) had only moderate resistance to the pathogen (IT-2). Evaluations for race 111E231 showed the following results: 14 RILs had a high degree of susceptibility (IT-4), 6 lines were moderately susceptible (IT-3), one line was moderately resistant and one immune (IT-2 and IT-0, respectively). The susceptible parent ‘Avocet (S)’ and the control ‘Morocco’ both showed a high susceptibility (IT-4) for both races, while the parent ‘Almaly’ and the isogenic line *Lr34/TC*6/PI58548* (carrier of gene *Yr18*) were moderately resistant (IT-2) to race 111E231 and was immune (IT-0) to race 7E63.

Table 1 – Yellow rust severity and the presence of the *Yr18* gene in the genotypes of the population of recombinant inbred lines Almaly/Avocet

#	Genotype	Origin ^a	APR ^b	111E231 ^c	7E63 ^c	CSLV34 ^d	Yr gene detected based on linked marker
♀	Almaly	KZ	20MR	2	0	+	Yr18
♂	Avocet (S)	AUS	100S	4	4	-	-
1	RIL Al/Av(S)-951-664	KZ	0	3	0	-	-
2	RIL Al/Av(S)-1094-817	KZ	0	3	0	+	Yr18
3	RIL Al/Av(S)-1085-808	KZ	20MR	3	0	-	-
4	RIL Al/Av(S)-1086-809	KZ	10MR	3	0	-	-

Continuation of the table

#	Genotype	Origin ^a	APR ^b	111E231 ^c	7E63 ^c	CSLV34 ^d	Yr gene detected based on linked marker
5	RIL Al/Av(S)-852-560	KZ	20R	4	0	+	Yr18
6	RIL Al/Av(S)-882-589	KZ	0	4	0	-	-
7	RIL Al/Av(S)-883-590	KZ	0	4	0	-	-
8	RIL Al/Av(S)-968-682	KZ	20MR	4	0	-	-
9	RIL Al/Av(S)-975-691	KZ	0	4	0	-	-
10	RIL Al/Av(S)-976-692	KZ	0	4	0	-	-
11	RIL Al/Av(S)-982-698	KZ	20MR	4	0	-	-
12	RIL Al/Av(S)-986-702	KZ	0	4	0	-	-
13	RIL Al/Av(S)-993-710	KZ	20MR	4	0	-	-
14	RIL Al/Av(S)-994-711	KZ	20MR	4	0	-	-
15	RIL Al/Av(S)-1058-781	KZ	5R	4	0	-	-
16	RIL Al/Av(S)-1097-821	KZ	0	4	0	-	-
17	RIL Al/Av(S)-1099-823	KZ	0	4	0	-	-
18	RIL Al/Av(S)-1053-776	KZ	10MR	3	2	+	Yr18
19	RIL Al/Av(S)-1054-777	KZ	10MR	3	2	+	Yr18
20	RIL Al/Av(S)-1052-775	KZ	0	4	2	+	Yr18
21	RIL Al/Av(S)-1067-790	KZ	0	0	0	-	-
22	RIL Al/Av(S)-1009-725	KZ	20MR	2	0	-	-
	Controls						
23	NIL Lr34/TC*6/PI58548	USA	10MS	2	0	+	Yr18
24	Morocco	MA	100S	4	4	-	-

a – Origin include countries and organizations: KZ – Kazakhstan, AUS – Australia, USA – United States of America, MA – Morocco, Almaty – Institute of Plant Biology and Biotechnology;

b – Values indicate severity;

c – IT – infection type/ reaction type;

d – “+”, “-” – indicate the presence and absence allele of corresponding gene, respectively.

The STS marker csLV34 is a diagnostic marker for the *Yr18/Lr34* gene complex, which allows determining the allelic state of a gene. Two alleles demonstrate amplicons that are clearly distinguishable in the agarose gel (150 bp for the dominant state and 229 bp for the recessive state). Molecular screening revealed the presence of a marker allele associated with *Yr18/Lr34* in 5 RIL Almaty/Avocet(S) (1094-817, 852-560, 1053-776, 1054-777, 1052-775) (Table 1, Figures 1 and 2). Thus, the frequency of resistant genotypes inheriting the *Yr18* gene was 22.7%. The heterozygous state of alleles of the *Yr18/Lr34* gene was not detected. (Figures 1 and 2.)

The complex of resistance genes *Yr18/Lr34/ Sr57/ Pm38* is important in the breeding of resistant varieties to

yellow, leaf, and also partially to stem rust and powdery mildew [30]. This gene retains its effectiveness for about 100 years, which is due to the molecular characteristics of the defense mechanism. The activity of *Yr18/Lr34* induces necrosis of the tip of the flag leaf.

However, the observed reaction cannot be used as a phenotypic marker for *Yr18/Lr34*, which also manifests itself with other resistance genes (such as *Lr46/Yr29/Pm39*) [31], which indicates the need for molecular screening. *Yr18/Lr34* is a gene for adult plant resistance (APR), nevertheless able to impart resistance at the seedling stage to some rust races [32]. It is possible that the processes induced by *Yr18/Lr34* make the tissue less favorable for biotrophic pathogens [33].

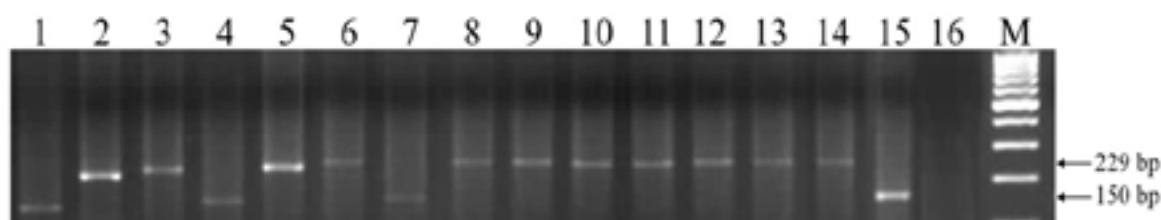


Figure 1 – Wheat DNA amplification products using primers to the STS csLV34 locus linked to the *Yr18/Lr34* resistance gene. Note: 1 – Almalý, 2 – Avocet(S), 3 –14 RIL Almalý/Avocet: 3 – RIL 951-664, 4 – RIL 1094-817, 5 – RIL 1085-808, 6 – RIL 1086-809, 7 – RIL 852-560, 8 – RIL 882-589, 9 – RIL 883-590, 10 – RIL 968-682, 11 – RIL 975-691, 12 – RIL 976-692, 13 – RIL 982-698, 14 – RIL 986-702; 15 – Yr18/NIL-Lr34/TC-6/PI58548, 16 – dd H₂O, M – Gene –Ruler 100 bp DNA Ladder

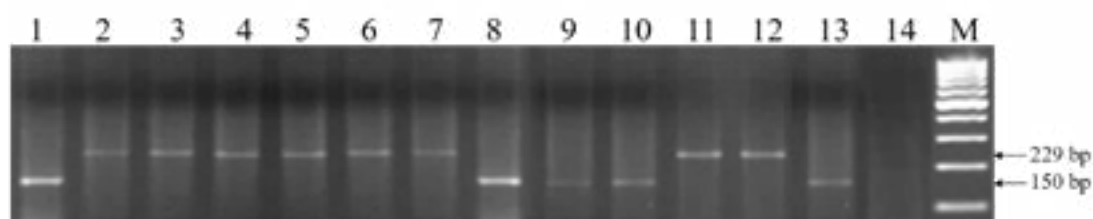


Figure 2 – Wheat DNA amplification products using primers to the STS csLV34 locus linked to the *Yr18/Lr34* resistance gene (continued). Note: 1 – Almalý, 2 – Avocet(S), 3 –14 RIL Almalý/Avocet: 3 – RIL 993-710, 4 – RIL 994-711, 5 – RIL 1058-781, 6 – RIL 1097-821, 7 – RIL 1099-823, 8 – RIL 1053-776, 9 – RIL 1054-777, 10 – RIL 1052-777, 11 – RIL 1067-790, 12 – RIL 1009-725; 13 – Yr18/NIL-Lr34/TC-6/PI58548, 14 – dd H₂O, M – Gene –Ruler 100 bp DNA Ladder

It was previously shown that *Yr18/Lr34* provides a sufficiently high level of resistance in the conditions of an artificial epidemic. The effect of this gene is enhanced in combination with other resistance genes, such as *Yr5* and *Yr10* [5]. Molecular screening revealed 5 (22.7%) carriers of the *Yr18* gene (RIL Almalý/Avocet(S) 1094-817, 852-560, 1053-756, 1054-777 and 1052-775) from 22 studied samples, which indicates a high degree of its inheritance among resistant lines. No resistance genes were found in 71% of the studied samples, however, a high level of immunity to the pathogen *Pst* was noted in the field (0-20MR).

Conclusion

The results of field phytopathological screening of collection of RILs Almalý/Anza in field conditions to yellow rust caused by *Pst* allowed to select 22 resistance wheat lines, presumably carriers of resistance genes. The results of the evaluation of the selected lines of seedling resistance showed a contrasting reaction to two races of yellow rust: race 7E63 was avirulent to most samples, and 111E231 was highly virulent. Evaluation of the resistance

of seedlings to *Pst* allowed us to identify 2 lines that were simultaneously resistant to both races. Molecular screening revealed the presence of a marker allele associated with the *Yr18/Lr34* gene complex in 5 samples. The frequency of resistant genotypes inheriting the *Yr18* gene was 22.7%.

The data obtained indicate the possibility of increasing the resistance of the material due to hybridization with productive wheat varieties and lines. The selected lines can be used in breeding programs to breed varieties resistant to yellow rust. Marker selection methods significantly simplify the process of selecting donors of resistance genes, which has a positive effect on the prospects for the development of the agricultural sector in Kazakhstan.

Acknowledgments

The research was carried out within the framework of the OR11465424 program “Development and implementation of highly effective diagnostic systems for identifying the most dangerous diseases and increasing the genetic potential of crop resistance”, task 03 “Development of DNA markers for creating

a system for identifying resistance genes based on mapping loci of quantitative traits associated with resistance to yellow rust in the population of recombinant inbred wheat lines” for 2021-2022 with the financial support of the Ministry of Science and Higher Education of the Republic of Kazakhstan.

References

1. Bouvet L., Holdgate S., James L., Thomas J., Mackay I. J., Cockram J. (2021) The evolving battle between yellow rust and wheat: implications for global food security. *Theoretical and Applied Genetics*. <https://doi.org/10.1007/s00122-021-03983-z>.
2. Statista. Available online: <https://www.statista.com/> Jan 27, 2022.
3. Kokhmetova A., Sapakhova Z., Urazaliev R., Yessimbekova M., Yeleshev R., Morgounov A. (2014) Effect of spring biomass removal on expression of agronomic traits of winter wheat. *World Applied Sciences Journal*, vol. 30, no. 3, pp. 322-329, 2014. <https://doi.org/10.5829/idosi.wasj.2014.30.03.14026>.
4. Koyshibaev M. K. (2018) Diseases of wheat. FAO, Ankara.
5. Kokhmetova A., Rsaliyev A., Malysheva A., Atishova M., Kumarbayeva M., Keishilov Z. (2021). Identification of stripe rust resistance genes in common wheat cultivars and breeding lines from Kazakhstan. *Plants*, vol. 10, no. 11, pp. 2303. <https://doi.org/10.3390/plants10112303>.
6. Kokhmetova A., Rsaliyev S., Atishova M., Kumarbayeva M., Malysheva A., Keishilov Z., Zhanuzak D., Bolatbekova A. (2021) Evaluation of wheat germplasm for resistance to leaf rust (*Puccinia triticina*) and identification of the sources of *Lr* resistance genes using molecular markers. *Plants*, vol. 10, no. 7, pp. 1484. <https://doi.org/10.3390/plants10071484>
7. Kokhmetova A.A., Morgounov S., Rsaliyev A., Rsaliyev G., Yessenbekova M., Typina L. (2011) Wheat germplasm screening for stem rust resistance using conventional and Rust resistance in wheat molecular techniques. *Czech J. Genet. Plant Breed*, vol. 47, pp. 146–154. <https://doi.org/10.17221/3270-CJGPB>.
8. Morgounov A., Akin B., Demir L.Ä., Keser M., Kokhmetova A., Martynov S., Orhan Ä., Ozdemir F., Äzseven Ä., Sapakhova Z., Yessimbekova M. (2015) Yield gain in leaf rust resistant and susceptible winter wheat varieties due to fungicide application. *Crop and Pasture Science*, vol. 66, no. 7, pp. 649-659. <http://dx.doi.org/10.1071/CP14158>.
9. Kokhmetova A., Sharma R., Rsaliyev S., Galymbek K., Baymagambetova K., Ziyayev Z., Morgounov A. (2018) Evaluation of Central Asian wheat germplasm for stripe rust resistance. *Plant Genet. Resour*, vol. 16, pp. 178–184. <https://doi.org/10.1017/S1479262117000132>.
10. Kokhmetova A., Madenova M., Purnhauser L., Kampitova G., Urazaliev R., Yessimbekova M. (2016) Identification of leaf rust resistance genes in wheat cultivars produced in Kazakhstan. *Cereal Res. Commun*, vol. 44, pp. 240–250. <https://doi.org/10.1556/0806.43.2015.056>.
11. Kokhmetova A.M., Ali S., Sapakhova Z., Atishova M.N. (2018) Identification of genotypes-carriers of resistance to tan spot *Ptr ToxA* and *Ptr ToxB* of *Pyrenophora tritici-repentis* in common wheat collection. *Vavilov J. Genet. Breed*, vol. 22, pp. 978–986, <https://doi.org/10.18699/vj18.440>.
12. Kokhmetova A.M., Atishova M.N., Madenova A.K., Kumarbayeva M.T. (2019) Genotyping of wheat germplasm for resistance to toxins of tan spot *Pyrenophora tritici-repentis*. *J. Biotechnol*, vol. 305, pp. 53. <https://doi.org/10.1016/j.jbiotec.2019.05.188>.
13. Kokhmetova A., Kremneva O., Volkova G., Atishova M., Sapakhova Z. (2017) Evaluation of wheat cultivars growing in Kazakhstan and Russia for resistance to tan spot. *J. Plant Pathol.*, vol. 99, pp. 161–167. <https://doi.org/10.4454/jpp.v99i1.3812>.
14. Kokhmetova A.M., Kovalenko N.M., Kumarbaeva M.T. (2020) *Pyrenophora tritici-repentis* population structure in the Republic of Kazakhstan and identification of wheat germplasm resistant to tan spot. *Vavilov J. Genet. Breed.*, vol. 24, pp. 722–729. <https://doi.org/10.18699/VJ20.666>.
15. Kokhmetova A., Sehgal D., Ali S., Atishova M., Kumarbayeva M., Leonova I., Dreisigacker S. (2021) Genome-Wide association study of tan spot resistance in a hexaploid wheat collection from Kazakhstan. *Front. Genet*, vol. 11, pp. 581214. <https://doi.org/10.3389/fgene.2020.581214>.
16. Kokhmetova A., Kumarbayeva M., Atishova M., Nehe A., Riley I.T., Morgounov A. (2021) Identification of high-yielding wheat genotypes resistant to *Pyrenophora tritici-repentis* (tan spot). *Euphytica*, vol. 217, pp. 97. <https://doi.org/10.1007/s10681-021-02822-y>.
17. Wellings C.R. (2004) Pathogen dynamics associated with historic stripe (yellow) rust epidemics in Australia in 2002 and 2003. Proceedings of the 11th International Cereal Rusts and Powdery Mildews Conference, John Innes Centre, Norwich, UK. Mode of access: <http://www.crpmb.org/icrpmb11/abstracts.htm>

18. Chen X. M. (2005). Epidemiology and control of stripe rust [*Puccinia striiformis* sp. *tritici*] on wheat. *Canadian Journal of Plant Pathology*, vol. 27, no. 3, pp. 314-337. <https://doi.org/10.1080/07060660509507230>.
19. Khan M. H., Bukhari A., Dar Z. A., Rizvi, S. M. (2013) Status and strategies in breeding for rust resistance in wheat. *Agricultural Sciences*, vol. 04, no. 6, pp. 292-301. <https://doi.org/10.4236/as.2013.46042>.
20. Sabouri H., Kazerani B., Fallahi H. A., Dehghan M. A., Alegh S. M., Dadras A. R., Mastinu A. (2022) Association analysis of yellow rust, fusarium head blight, tan spot, powdery mildew, and brown rust horizontal resistance genes in wheat. *Physiological and Molecular Plant Pathology*, vol. 118, pp. 101808. <https://doi.org/10.1016/j.pmpp.2022.101808>.
21. Soriano, J. M., Royo, C. (2015). Dissecting the genetic architecture of leaf rust resistance in wheat by QTL meta-analysis. *Phytopathology*, vol. 105, pp. 1585–1593. <https://doi.org/10.1094/PHYTO-05-15-0130-R>.
22. Pandurangan S., Workman C., Nilsen K., Kumar S. (2022) Introduction to Marker-Assisted Selection in Wheat Breeding. In: Bilichak A., Laurie J.D. (eds) Accelerated Breeding of Cereal Crops. Springer Protocols Handbooks. Humana, New York, NY. https://doi.org/10.1007/978-1-0716-1526-3_3
23. Krattinger S.G., Sucher, J., Selter L.L., Chauhan H., Zhou B., Tang M.Z., Upadhyaya N.M., Mieulet D., Guiderdoni E., Weidenbach D. (2016) The wheat durable, multipathogen resistance gene *Lr34* confers partial blast resistance in rice. *Plant Biotechnol. J.* vol. 14, pp. 1261–1268. <https://doi.org/10.1111/pbi.12491>
24. Kolmer J.A., Singh R.P., Garvin D.F., Viccars L., William H.M., Huerta-Espino J., Ogonnaya F.C., Raman H., Orford S., Bariana E.S., Lagudah E.S. (2008) Analysis of the *Lr34/Yr18* rust resistance region in wheat germplasm. *Crop Sci*, vol. 48, pp. 1841–1852.
25. Roelfs A.P., R.P. Singh, E.E. Saari. (1992) Rust Diseases of Wheat: Concepts and methods of disease management. Mexico, D.F.: CIMMYT. ISBN: 968-6127-47-X
26. Gassner G., Straib W. (1929) Experimentelle Untersuchungen über das Verhalten der Weizensorten gegen *Puccinia glumarum*. *Phytopathology Zeitschrift*, vol. 1, no. 3, pp. 215–275.
27. Riede C.R., Anderson J.A. (1996) Linkage of RFLP markers to an aluminum tolerance gene in wheat. *Crop Science*, vol. 36, pp. 905–909.
28. Lagudah E.S., McFadden H., Singh R.P., Huerta-Espino J., Bariana H.S., Spielmeier W. (2006) Molecular genetic characterization of the *Lr34/Yr18* slow rusting resistance gene region in wheat. *Theoretical and Applied Genetics*, vol. 114, pp. 21–30. <https://doi.org/10.1007/s00122-006-0406-z>.
29. Catalog of varieties of wheat and barley released in Central Asia (2003). GTZ-CIMMYT, Almaty, P. 144.
30. Lagudah E. S., Krattinger S. G., Herrera-Foessel S., Singh R. P., Huerta-Espino J., Spielmeier W., Keller B. (2009). Gene-specific markers for the wheat gene *Lr34/Yr18/Pm38* which confers resistance to multiple fungal pathogens. *Theoretical and Applied Genetics*, vol. 119, no. 5, pp. 889–898. <https://doi.org/10.1007/s00122-009-1097-z>.
31. Lillemo M., Asalf B., Singh R.P., Huerta-Espino J., Chen X.M., He Z.H., Bjørnstad Å. (2008) The adult plant rust resistance loci *Lr34/Yr18* and *Lr46/Yr29* are important determinants of partial resistance to powdery mildew in bread wheat line Saar. *Theoretical and Applied Genetics*, vol. 116, pp. 1155–1166. <https://doi.org/10.1007/s00122-008-0743-1>
32. Dyck P.L., Samborski D.J. (1982) The inheritance of resistance to *Puccinia recondita* in a group of common wheat cultivars. *Canadian Journal of Genetics and Cytology*, vol. 24, pp. 273–283. <https://doi.org/10.1139/g82-029>.
33. Keller B., Lagudah E.S., Selter L.L., Risk J.M., Harsh C., Krattinger S.G. (2015) How has *Lr 34/Yr 18* conferred effective rust resistance in wheat for so long? Proceedings of the Borlaug Global Rust Initiative, Technical Workshop, Beijing, China. P.46-56. ISBN: 13: 978-0-615-70429-6.

© This is an open access article under the (CC)BY-NC license (<https://creativecommons.org/licenses/by-nc/4.0/>). Funded by Al-Farabi KazNU

A. Perfilyeva¹, K. Bespalova^{1,2*}, G. Abylkassymova¹,
B. Bekmanov^{1,2}, L. Djansugurova^{1,2}

¹Institute of Genetics and Physiology, Almaty, Kazakhstan

²Al-Farabi Kazakh National University, Almaty, Kazakhstan

*e-mail: kira.b.bespalova@gmail.com

(Received 12 May 2022; received in revised form 24 May 2022; accepted 31 May 2022)

RS2710102 polymorphism of the *CNTNAP2* gene is related to autism susceptibility in a Kazakhstani population

Abstract. Autism spectrum disorders (ASDs) represent serious mental development disorders characterized by deficits in verbal and non-verbal communication, reciprocal social interactions and stereotypical behaviors. Genetically determined pathologies of neurodevelopment and synaptic functioning are increasingly considered to be a cause of ASDs. Contactin associated protein-like 2 (*CNTNAP2*) gene encodes a protein, which plays an essential role in brain development. Genetic variations in the *CNTNAP2* gene can perturb its functions, contributing to the genetic predisposition to ASDs. The study aimed to investigate an association of the *CNTNAP2* rs2710102 with ASDs in a Kazakhstani population. The study involved patients diagnosed with ASDs and healthy controls of Kazakhstani origin. PCR-RFLP assay was used for the genotyping rs2710102 *CNTNAP2* SNP. The distribution of the rs2710102 genotype was under the Hardy-Weinberg equilibrium in both cases and controls. C allele and CC genotype were associated with a significantly increased risk of ASDs (OR = 3.04, 95% CI = 1.96-4.72, $p < 0.001$ and OR = 6.41, 95% CI = 2.47-16.63, $p < 0.001$, respectively), which was also confirmed for males (OR = 2.25, 95% CI = 1.23-4.10, $p = 0.007$ and OR = 2.95, 95% CI = 1.06-8.18, $p = 0.029$, respectively) and females (OR = 4.75, 95% CI = 1.91-11.77, $p < 0.001$ and OR = 7.20, 95% CI = 0.89-58.53, $p = 0.002$, respectively). In contrast, there was no statistically significant association of the rs2710102 with deficits of verbal communication in ASD patients. The obtained results provide the first significant link between rs2710102 *CNTNAP2* and autism susceptibility in Asian populations.

Key words: Autism spectrum disorders (ASDs), *CNTNAP2* gene, single-nucleotide polymorphism, genetic susceptibility, Kazakhstani population, neurodevelopment.

Introduction

Autism spectrum disorders (ASDs) are a group of heterogeneous neurodevelopmental diseases, which are characterized by deficits in verbal and non-verbal communication, reciprocal social interactions and stereotypical behavior. In Kazakhstan, as everywhere in the world, the number of children with ASDs has been increasing annually. In Kazakhstan, according to the Service of psychological, medical and pedagogical consultation, autism was diagnosed in 3820 children (in the 2020 year), however, according to the international experts, the real number of children with ASD significantly exceeds this figure. For, according to the Institute of Autism at Oregon State University (USA), in our country 59 thousand children have autism spectrum disorders.

Genetic factors are one of the main components of ASDs. Literature shows hundreds of candidate genes

for ASDs, which may be a subject of closer attention and deserve a separate study. Here, we focused on the contactin associated protein-like 2, which has been proposed to be a candidate gene for ASDs [1].

CNTNAP2 gene is located in 7q35–36 and encodes the transmembrane protein Caspr2, which is a member of the neurexin family. This protein is localized at the juxtaparanodes of myelinated axons providing interactions between neurons and glia during nervous system development. It is also involved in clustering K⁺ channels in myelinated axons [2].

Several genetic, neurobiological and mouse model studies have supported the role of *CNTNAP2* in ASDs and other related neurodevelopmental disorders. In the Old Order Amish community, the mutations of *CNTNAP2* have been identified as causes of symptomatic childhood-onset epilepsy, characterized by the presence of neuronal migration

abnormalities, intellectual disability, language regression, seizures, hyperactivity, impulsive/aggressive behavior, as well as ASDs [3].

In mouse models, *CNTNAP2* deficiency has shown extraordinary similarity to the main deficits of behavioral and cognitive functions of ASD patients. Neurophysiological features, such as cortical neuronal migration abnormalities, observed in *CNTNAP2*^{-/-} mice, further supported the involvement of the *CNTNAP2* gene in ASD pathologies [4]. The migration of neurons in the developing cerebral cortex plays a key role in the development of brain and brain networks [5]. A number of neuroimaging studies demonstrated abnormal connectivity and altered brain networks in individuals with ASDs [6–8]. Moreover, mouse model studies have demonstrated a capacity of anti-Caspr2 auto-ABS to generate ASD-like behavior [9, 10].

Besides, the *CNTNAP2* gene is expressed in language-related cortical areas [11]. Hence, given the speech impairment in autism, *CNTNAP2* becomes a strong candidate gene for autism.

Genetic variations in the *CNTNAP2* gene can affect its functions contributing to the genetic predisposition to ASDs. It has been shown that the loss of even one *CNTNAP2* allele leads to elicit axonal growth alterations [12]. Several common and rare variants of *CNTNAP2* have been reported to be associated with autism as well as related to phenotypes such as intellectual deficiency, impaired language, abnormal social behavior, epilepsy and schizophrenia [13–17].

The single-nucleotide polymorphism (SNP) rs2710102 is located at intron 13. There are still insufficient data on the relation of this common variant with ASDs in Asian populations. Therefore, in the present study, we carried out a case–control association study between rs2710102 and ASDs in a Kazakhstani population.

Materials and methods

The study involved patients diagnosed with ASDs and healthy controls of Kazakhstani origin. A total of 51 healthy individuals and 280 ASD patients had been recruited in rehabilitation centers of Kazakhstan starting from March 2018 to December 2020.

Collection of the clinical material in families with children with ASD was carried out in the “Autism Pobedim” Foundation based on the Memorandum of Cooperation, as well as in public funds, working with ASD children in Almaty, Astana, Zhezkazgan, Karaganda, Kokshetau, Kyzyl-Orda, Pavlodar, Petropavlovsk, Temirtau, Ust-Kamenogorsk, Shymkent, Ekibastuz and South Kazakhstan region.

Buccal epithelium samples were collected from patients with ASDs, as well as from healthy individuals using sterile cotton-tipped applicators. The collected material was transported to the Institute of General Genetics and Cytology in a portable refrigerated container and frozen at -80° C for further molecular-genetic studies.

The collection of biomaterial was conducted exclusively voluntarily after signing an informed consent by at least one of the parents. The protocol of the study was approved by the Ethics Committee of S. Asfendiyarov Kazakh National Medical University (Protocol #57 from 05.09.2017).

The clinical diagnosis of autism was established by senior psychiatrists and assessed by the CARS for children over 3 years and the M-Chat-R for children under three years old. CARS and M-Chat-R have been used as standardized, investigator-based instruments for the detection of ASDs [19, 20]. ASD patients with M-CHAT or CARS scores in the low-risk range were excluded from the study. Additional exclusion criteria were a recognizable neurological or genetic disorder (Rett syndrome, Fragile X syndrome and others), noncitizens of Kazakhstan.

For the control group, the exclusion criteria were the presence of autism or other mental disorders in personal and family history, M-CHAT or CARS scores in the medium/high-risk range, noncitizens of Kazakhstan.

Verbal communication in the ASD group was assessed by interviewing parents of ASD children and classified as without (verbal communication is appropriate for age and situation) or with speech disorders (delayed speech, echolalia, meaningless speech, etc.).

DNA from buccal swabs was isolated using a DNA extraction kit (AmpliSens). DNA samples were stored at -20°C and -80°C. PCR-RFLP assay was used for the genotyping rs2710102 *CNTNAP2* SNP as described earlier [18].

Statistical analysis was performed using “Case-Control Study Estimating Calculator” by TAPOTILI company (Laboratory of Molecular Diagnostics and Genomic Dactyloscopy of “GosNIIGenetika” State Scientific Centre of Russian Federation). Hardy-Weinberg equilibrium (HWE) test was used to compare the observed and expected genotype frequencies. Relative risks were estimated by odds ratios (OR) with a logistic regression 95% confidence interval. Statistical analysis considering the models of inheritance—the multiplicative, dominant, and recessive—was conducted for the examined SNP. $P < 0.05$ was considered statistically significant.

Results and discussion

General Characteristics of Patients.

Characteristics of the ASD patients and healthy controls are summarized in Table 1. The ethnic heterogeneity of both groups was Kazakh, Russian and other Europeans and Asians. The mean age for

the ASD group and control subjects was 7.41 ± 8.39 years (range 2-34 years) and 7.08 ± 4.42 years (range 1-39 years), respectively. In the ASD group, 79.3% were males and 20.7% were females. In the control group, 47.1% were males and 52.9% were females. 173 ASD patients had speech disorders and 68 without.

Table 1 – Characteristics of ASD and control groups

Characteristic		ASD N	(%)	Controls N	(%)
Sample size		280		51	
Ethnicity	Kazakh	180	64.3	39	76.5
	Russian	68	24.3	5	9.8
	Other Europeans	3.2	9.0	4	7.8
	Other Asians	8.2	23.0	3	5.9
Age (years)	Median	7.41 ± 8.39		7.08 ± 4.42	
Gender	Male	222	79.3	24	47.1
	Female	58	20.7	27	52.9

Analysis of the Association of the rs2710102 CNTNAP2 Polymorphism with the Risk of ASD in a Kazakhstani Population. The genotype distributions of the rs2710102 polymorphism were under Hardy-Weinberg equilibrium (HWE) for both control ($p=0.585$) and ASD cases ($p=0.818$). The distribution of rs2710102 CNTNAP2 genotypes is presented in Table 2.

As shown in Table 2, the CNTNAP2 C allele and CC genotype were associated with a significantly increased risk of ASD (OR = 3.04, 95% CI = 1.96-4.72, $p<0.001$ and OR = 6.41, 95% CI = 2.47-16.63, $p<0.001$, respectively). Furthermore, a significantly increased risk of ASD was found for CC+CT genotypes versus the TT genotype in the dominant model (OR = 3.56, 95% CI = 1.84-6.89, $p<0.001$) and for CC genotype versus the combined variant

of CT+TT genotypes in the recessive model (OR = 6.41, 95% CI = 2.47-16.63, $p<0.001$).

Due to a gender difference in rates of ASDs we further calculated the association of the rs2710102 CNTNAP2 polymorphism with ASD risk in the subgroups stratified into genders (Table 2). C allele and CC genotype showed a significant association with ASD in both males (OR = 2.25, 95% CI = 1.23-4.10, $p=0.007$ and OR = 2.95, 95% CI = 1.06-8.18, $p=0.029$, respectively) and females (OR = 4.75, 95% CI = 1.91-11.77, $p<0.001$ and OR = 7.20, 95% CI = 0.89-58.53, $p=0.002$, respectively). Furthermore, the C allelotype (CC+CT genotypes) had a high risk for ASD development in both male and female patients in the dominant model (OR = 2.85, 95% CI = 1.09-7.49, $p=0.027$ and OR = 7.03, 95% CI = 2.16-22.88, $p=0.001$, respectively).

Table 2 – Genotype and allele distributions of CNTNAP2 in ASD patients and controls

rs2710102 CNTNAP2	ASD Patients 280	Controls 51	OR	95% CI	p-Value
CC	115	5	6.41	2.47-16.63	<0.001
CT	125	27	0.72	0.39-1.30	
TT	40	19	0.28	0.15-0.54	
Dominant model					
CC+CT	240	32	3.56	1.84-6.89	<0.001
TT	40	19	0.28	0.15-0.54	

Continuation of the table

rs2710102 <i>CNTNAP2</i>	ASD Patients 280	Controls 51	OR	95% CI	p-Value
Recessive model					
CC	115	5	6.41	2.47-16.63	<i><0.001</i>
CT+TT	165	46	0.16	0.06-0.40	
Allele					
C	355	37	3.04	1.96-4.72	<i><0.001</i>
T	205	65	0.33	0.21-0.51	
Male					
CC	97	5	2.95	1.06-8.18	<i>0.029</i>
CT	97	12	0.78	0.33-1.80	
TT	28	7	0.35	0.13-0.92	
Dominant model					
CC+CT	194	17	2.85	1.09-7.49	<i>0.027</i>
TT	28	7	0.35	0.13-0.92	
Recessive model					
CC	97	5	2.95	1.06-8.18	<i>0.031</i>
CT+TT	125	19	0.34	0.12-0.94	
Allele					
C	291	22	2.25	1.23-4.10	<i>0.007</i>
T	153	26	0.44	0.24-0.81	
Female					
CC	18	1	7.20	0.89-58.53	<i>0.002</i>
CT	28	5	2.24	0.70-7.17	
TT	12	11	0.14	0.04-0.46	
Dominant model					
CC+CT	46	5	7.03	2.16-22.88	<i>0.001</i>
TT	12	12	0.14	0.04-0.46	
Recessive model					
CC	18	0	7.20	0.89-58.53	<i>0.036</i>
CT+TT	40	17	0.14	0.02-1.13	
Allele					
C	64	7	4.75	1.91-11.77	<i><0.001</i>
T	52	27	0.21	0.08-0.52	

OR analysis was performed to evaluate the effect of rs2710102 *CNTNAP2* on verbal communication in ASD subjects. As shown in Table 3, there was no statistically significant association of the polymorphism with speech impairments in patients with ASD in the general group, as well as in males or females.

We carried out a case-control association study of the rs2710102 *CNTNAP2* in 280 patients and 51 controls to assess the genetic contribution of this

genetic variant to ASDs in a Kazakhstani population. The results of the study showed significant associations between rs2710102 *CNTNAP2* and autism both in males and females. Further analysis found no significant association between the rs2710102 *CNTNAP2* and speech impediments in ASD patients.

Discordant results have been reported by previous studies. No association was reported between the rs2710102 *CNTNAP2* and autism in

640 trios of Han Chinese descent [19]. No significant differences between the frequencies of the CC risk genotype were demonstrated in the 210 autistic patients and 200 controls representing a Brazilian population [18]. A study of 67 autism cases and 100 controls did not find significant associations between the rs2710102 *CNTNAP2* gene polymorphism and autism in an Iranian population [20]. A case-

control association study of 322 Spanish autistic patients and 524 controls found no association of this polymorphism with autism [21]. Finally, the rs2710102 variant was not significantly associated with autistic-like traits in a Swedish study of 12,319 subjects [22]. Moreover, an updated meta-analysis found no association between the rs2710102 *CNTNAP2* and autism [19].

Table 3 – The relation between rs2710102 *CNTNAP2* and verbal communication in ASD subjects

rs2710102 <i>CNTNAP2</i>	ASD Patients with speech disorders	ASD Patients without speech disorders	OR	95% CI	p-Value
	173	68			
CC	77	25	1.38	0.77-2.46	0.298
CT	70	35	0.64	0.36-1.13	
TT	26	8	1.33	0.57-3.10	
Dominant model					
CC+CT	147	60	0.75	0.32-1.76	0.512
TT	26	8	1.33	0.57-3.10	
Recessive model					
CC	77	25	1.38	0.77-2.46	0.273
CT+TT	96	43	0.72	0.41-1.29	
Allele					
C	224	85	1.10	0.73-1.66	0.645
T	122	51	0.91	0.60-1.37	
<i>Male</i>					
CC	65	21	1.66	0.88-3.13	0.115
CT	50	31	0.52	0.28-0.97	
TT	19	6	1.43	0.54-3.79	
Dominant model					
CC+CT	115	52	0.70	0.26-1.85	0.469
TT	19	6	1.43	0.54-3.79	
Recessive model					
CC	65	21	1.66	0.88-3.13	0.116
CT+TT	69	37	0.60	0.32-1.14	
Allele					
C	180	73	1.20	0.76-1.90	0.422
T	88	43	0.83	0.53-1.31	
<i>Female</i>					
CC	12	4	0.67	0.16-2.80	0.805
CT	20	4	1.58	0.38-6.48	
TT	7	2	0.88	0.15-5.05	
Dominant model					
CC+CT	32	8	1.14	0.20-6.59	0.881
TT	7	2	0.88	0.15-5.05	

Continuation of the table

rs2710102 <i>CNTNAP2</i>	ASD Patients with speech disorders	ASD Patients without speech disorders	OR	95% CI	p-Value
	173	68			
Recessive model					
CC	12	4	0.67	0.16-2.80	0.579
CT+TT	27	6	1.50	0.36-6.31	
Allele					
C	44	12	0.86	0.32-2.35	0.772
T	34	8	1.16	0.43-3.15	

Contrary, some studies suggested associations between the rs2710102 SNP and predisposition to ASDs. A relationship between frontal lobar connectivity and rs2710102 genetic variant was demonstrated by functional neuroimaging, which indirectly confirms its contribution to ASDs [23]. A positive association of the rs2710102 with ASDs has been found in a study of 152 families from the Autism Genetic Resource Exchange [24].

Besides, previous studies have demonstrated the relation of the rs2710102 with language problems, signifying its essential role in ASD pathogenicity. This SNP was associated with non-word repetition [25] and specific language impairment [26]. The risk C allele of rs2710102 was significantly associated with a delayed onset of speech, as measured by the "age at the first word", in ASD children [27]. Non-autistic homozygous for the C allele demonstrated significantly increased activation in contralateral areas of traditional left-sided language regions: the frontal operculum and middle temporal gyrus [28]. Finally, it was suggested that rs2710102, as a part of specific 4-SNP haplotypes, may influence early language development in the general population [29].

In contrast, two studies failed to replicate positive results on the association between the rs2710102 and impaired language development in ASD patients [21, 22]. Similarly, we also found no association between *CNTNAP2* and speech disorders. The reason for this could be insufficient tools to assess speech impairment based on only interviewing parents.

Nevertheless, our results indicate a significant statistical association between the rs2710102 variant and autism in the general group and for both men and women. It is well known that genetic heterogeneity of different populations affects the results of case-control association studies. In this way, the analysis

of genetic predisposition to ASD may require different genetic markers for different populations. The majority of case-control studies of the rs2710102 variant and autism association were performed in European and American populations. To the best of our knowledge, only two studies have been carried out in Asian populations (Chinese and Iranian) so far [19, 20]. This circumstance can explain the discrepancy between our data and the data of the above-mentioned studies.

In addition, the limitations of this study must be taken into account. The control sample is small compared to the ASD sample and not matched for gender with the ASD sample (males in ASD is 79,3% and controls is 47,1%). Subdivision of all the individuals into male and female groups, as well as into groups with and without speech disorders resulted in relatively small sample sizes, so the power of these subgroup results was < 80%, indicating that additional high-level studies are still needed. The current work investigated only one polymorphism of the *CNTNAP2* gene. However, we cannot exclude a possibility that other variants in the *CNTNAP2* gene may be involved in ASDs and language impairment. Further population-based studies that will investigate the effect of genetic variations on ASDs are needed to better understand the genetics of autism and related disorders.

Conclusion

Genetically determined pathologies of neurodevelopment and synaptic functioning are increasingly considered to be a cause of ASDs. Contactin associated protein-like 2 (*CNTNAP2*) gene encodes a protein, which plays an essential role in brain development. Genetic variations in the *CNTNAP2* gene can perturb its functions, contributing to the genetic predisposition to ASDs.

In the current study, we provide the first significant link between rs2710102 CNTNAP2 and autism susceptibility in Asian populations. Our results suggest that the SNP rs2710102 of the CNTNAP2 gene may be associated with autism susceptibility in Kazakhstani population, but it not seems to be involved with speech disorders in the same population.

Acknowledgments

This work was supported by the grant OR11465435 received from the Committee of Science, Ministry of Education and Science of Republic of Kazakhstan in 2021. The authors are grateful to the parents and children participating in the study, as well as the heads of the rehabilitation centers, who, through recruitment, have made a valuable contribution to the success of the study. They would particularly like to thank Demeuova Regina, Darmenova Ainur, Seitova Adina, Kvan Olga, Zhumashev Gamali, as well as Perfilyeva Yuliya for critical reading of the manuscript.

References

1. D.E. Arking, D.J. Cutler, C.W. Brune, T.M. Teslovich, K. West, M. Ikeda, A. Rea, M. Guy, S. Lin, E.H. Cook, A. Chakravarti, A Common Genetic Variant in the Neurexin Superfamily Member CNTNAP2 Increases Familial Risk of Autism, *Am. J. Hum. Genet.* (2008). <https://doi.org/10.1016/j.ajhg.2007.09.015>.
2. S. Poliak, L. Gollan, R. Martinez, A. Custer, S. Einheber, J.L. Salzer, J.S. Trimmer, P. Shrager, E. Peles, Caspr2, a new member of the Neurexin superfamily, is localized at the juxtaparanodes of myelinated axons and associates with K⁺ channels, *Neuron.* (1999). [https://doi.org/10.1016/S0896-6273\(00\)81049-1](https://doi.org/10.1016/S0896-6273(00)81049-1).
3. K.A. Strauss, E.G. Puffenberger, M.J. Huentelman, S. Gottlieb, S.E. Dobrin, J.M. Parod, D.A. Stephan, D.H. Morton, Recessive symptomatic focal epilepsy and mutant contactin-associated protein-like 2, *N. Engl. J. Med.* (2006). <https://doi.org/10.1056/NEJMoa052773>.
4. O. Peñagarikano, B.S. Abrahams, E.I. Herman, K.D. Winden, A. Gdalyahu, H. Dong, L.I. Sonnenblick, R. Gruver, J. Almajano, A. Bragin, P. Golshani, J.T. Trachtenberg, E. Peles, D.H. Geschwind, Absence of CNTNAP2 leads to epilepsy, neuronal migration abnormalities, and core autism-related deficits, *Cell.* (2011). <https://doi.org/10.1016/j.cell.2011.08.040>.
5. J.J. Dudok, P.E.G. Leonards, J. Wijnholds, Genetic and molecular approaches to study neuronal migration in the developing cerebral cortex, *Brain Sci.* (2017). <https://doi.org/10.3390/brainsci7050053>.
6. S. Ha, I.-J. Sohn, N. Kim, H.J. Sim, K.-A. Cheon, Characteristics of Brains in Autism Spectrum Disorder: Structure, Function and Connectivity across the Lifespan, *Exp. Neurobiol.* (2015). <https://doi.org/10.5607/en.2015.24.4.273>.
7. K. Zeng, J. Kang, G. Ouyang, J. Li, J. Han, Y. Wang, E.M. Sokhadze, M.F. Casanova, X. Li, Disrupted brain network in children with autism spectrum disorder, *Sci. Rep.* (2017). <https://doi.org/10.1038/s41598-017-16440-z>.
8. F.H. Duffy, H. Als, A stable pattern of EEG spectral coherence distinguishes children with autism from neuro-typical controls – a large case control study, *BMC Med.* (2012). <https://doi.org/10.1186/1741-7015-10-64>.
9. E. Coutinho, D.A. Menassa, L. Jacobson, S.J. West, J. Domingos, T.C. Moloney, B. Lang, P.J. Harrison, D.L.H. Bennett, D. Bannerman, A. Vincent, Persistent microglial activation and synaptic loss with behavioral abnormalities in mouse offspring exposed to CASPR2-antibodies in utero, *Acta Neuropathol.* (2017). <https://doi.org/10.1007/s00401-017-1751-5>.
10. O. Varea, M.D. Martin-de-Saavedra, K.J. Kopeikina, B. Schürmann, H.J. Fleming, J.M. Fawcett-Patel, A. Bach, S. Jang, E. Peles, E. Kim, P. Penzes, Synaptic abnormalities and cytoplasmic glutamate receptor aggregates in contactin associated protein-like 2/Caspr2 knockout neurons, *Proc. Natl. Acad. Sci. U. S. A.* (2015). <https://doi.org/10.1073/pnas.1423205112>.
11. A. Gordon, D. Salomon, N. Barak, Y. Pen, M. Tsoory, T. Kimchi, E. Peles, Expression of Cntnap2 (Caspr2) in multiple levels of sensory systems, *Mol. Cell. Neurosci.* (2016). <https://doi.org/10.1016/j.mcn.2015.11.012>.
12. G. Canali, M. Garcia, B. Hivert, D. Pinatel, A. Goullancourt, K. Oguievetskaia, M. Saint-Martin, J.A. Girault, C. Faivre-Sarrailh, L. Goutebroze, Genetic variants in autism-related CNTNAP2 impair axonal growth of cortical neurons, *Hum. Mol. Genet.* (2018). <https://doi.org/10.1093/hmg/ddy102>.
13. B. Bakkaloglu, B.J. O’Roak, A. Louvi, A.R. Gupta, J.F. Abelson, T.M. Morgan, K. Chawarska, A. Klin, A.G. Ercan-Sencicek, A.A. Stillman, G. Tanriver, B.S. Abrahams, J.A. Duvall, E.M. Robbins, D.H. Geschwind, T. Biederer, M. Gunel,

- R.P. Lifton, M.W. State, Molecular Cytogenetic Analysis and Resequencing of Contactin Associated Protein-Like 2 in Autism Spectrum Disorders, *Am. J. Hum. Genet.* (2008). <https://doi.org/10.1016/j.ajhg.2007.09.017>.
14. A. Gregor, B. Albrecht, I. Bader, E.K. Bijlsma, A.B. Ekici, H. Engels, K. Hackmann, D. Horn, J. Hoyer, J. Klapecki, J. Kohlhase, I. Maystadt, S. Nagl, E. Prott, S. Tinschert, R. Ullmann, E. Wohlleber, G. Woods, A. Reis, A. Rauch, C. Zweier, Expanding the clinical spectrum associated with defects in *CNTNAP2* and *NRXN1*, *BMC Med. Genet.* (2011). <https://doi.org/10.1186/1471-2350-12-106>.
15. A.G. Chiocchetti, M. Kopp, R. Waltes, D. Haslinger, E. Duketis, T.A. Jarczok, F. Poustka, A. Voran, U. Graab, J. Meyer, S.M. Klauck, S. Fulda, C.M. Freitag, Variants of the *CNTNAP2* 5' promoter as risk factors for autism spectrum disorders: A genetic and functional approach, *Mol. Psychiatry.* (2015). <https://doi.org/10.1038/mp.2014.103>.
16. R. Polimanti, R. Squitti, M. Pantaleo, S. Giglio, G. Zito, Duplication of *FOXP2* binding sites within *CNTNAP2* gene in a girl with neurodevelopmental delay, *Minerva Pediatr.* (2017). <https://doi.org/10.23736/S0026-4946.16.04326-7>.
17. J.I. Friedman, T. Vrijenhoek, S. Markx, I.M. Janssen, W.A. Van Der Vliet, B.H.W. Faas, N. V. Knoers, W. Cahn, R.S. Kahn, L. Edelmann, K.L. Davis, J.M. Silverman, H.G. Brunner, A.G. Van Kessel, C. Wijmenga, R.A. Ophoff, J.A. Veltman, *CNTNAP2* gene dosage variation is associated with schizophrenia and epilepsy, *Mol. Psychiatry.* (2008). <https://doi.org/10.1038/sj.mp.4002049>.
18. P.P. Nascimento, A.L. Bossolani-Martins, D.B.A. Rosan, L.C. Mattos, C. Brandão-Mattos, A.C. Fett-Conte, Single nucleotide polymorphisms in the *CNTNAP2* gene in Brazilian patients with autistic spectrum disorder, *Genet. Mol. Res.* (2016). <https://doi.org/10.4238/gmr.15017422>.
19. T. Zhang, J. Zhang, Z. Wang, M. Jia, T. Lu, H. Wang, W. Yue, D. Zhang, J. Li, L. Wang, Association between *CNTNAP2* polymorphisms and autism: A family-based study in the Chinese Han population and a meta-analysis combined with GWAS data of psychiatric genomics consortium, *Autism Res.* (2019). <https://doi.org/10.1002/aur.2078>.
20. F. Beiranvandi, M. Akouchekian, G.R. Javadi, H. Darvish, The association of *CNTNAP2* rs2710102 and *ENGRAILED-2* rs1861972 genes polymorphism and autism in Iranian population, *Meta Gene.* (2020). <https://doi.org/10.1016/j.mgene.2020.100664>.
21. C. Toma, A. Hervás, B. Torrico, N. Balmaña, M. Salgado, M. Maristany, E. Vilella, R. Martínez-Leal, M.I. Planelles, I. Cuscó, M. Del Campo, L.A. Pérez-Jurado, R. Caballero-Andaluz, Y. De Diego-Otero, L. Pérez-Costillas, J.A. Ramos-Quiroga, M. Ribasés, M. Bayés, B. Cormand, Analysis of two language-related genes in Autism: A case-control association study of *FOXP2* and *CNTNAP2*, *Psychiatr. Genet.* (2013). <https://doi.org/10.1097/YPG.0b013e32835d6fc6>.
22. L. Jonsson, A. Zettergren, E. Pettersson, D. Hovey, H. Anckarsäter, L. Westberg, P. Lichtenstein, S. Lundström, J. Melke, Association study between autistic-like traits and polymorphisms in the autism candidate regions *RELN*, *CNTNAP2*, *SHANK3*, and *CDH9/10*, *Mol. Autism.* (2014). <https://doi.org/10.1186/2040-2392-5-55>.
23. A.A. Scott-Van Zeeland, B.S. Abrahams, A.I. Alvarez-Retuerto, L.I. Sonnenblick, J.D. Rudie, D. Ghahremani, J.A. Mumford, R.A. Poldrack, M. Dapretto, D.H. Geschwind, S.Y. Bookheimer, Altered functional connectivity in frontal lobe circuits is associated with variation in the autism risk gene *CNTNAP*, *Sci. Transl. Med.* (2010). <https://doi.org/10.1126/scitranslmed.3001344>.
24. M. Alarcón, B.S. Abrahams, J.L. Stone, J.A. Duvall, J. V. Perederiy, J.M. Bomar, J. Sebat, M. Wigler, C.L. Martin, D.H. Ledbetter, S.F. Nelson, R.M. Cantor, D.H. Geschwind, Linkage, Association, and Gene-Expression Analyses Identify *CNTNAP2* as an Autism-Susceptibility Gene, *Am. J. Hum. Genet.* (2008). <https://doi.org/10.1016/j.ajhg.2007.09.005>.
25. B. Peter, W.H. Raskind, M. Matsushita, M. Lisowski, T. Vu, V.W. Berninger, E.M. Wijsman, Z. Brkanac, Replication of *CNTNAP2* association with nonword repetition and support for *FOXP2* association with timed reading and motor activities in a dyslexia family sample, *J. Neurodev. Disord.* (2011). <https://doi.org/10.1007/s11689-010-9065-0>.
26. D.F. Newbury, S. Paracchini, T.S. Scerri, L. Winchester, L. Addis, A.J. Richardson, J. Walter, J.F. Stein, J.B. Talcott, A.P. Monaco, Investigation of dyslexia and SLI risk variants in reading- and language-impaired subjects, *Behav. Genet.* (2011). <https://doi.org/10.1007/s10519-010-9424-3>.
27. M. Alarcón, R.M. Cantor, J. Liu, T.C. Gilliam, D.H. Geschwind, D.H. Geschwind, M. Bucan, W.T. Brown, J.D. Buxbaum, T.C. Gilliam, D.A. Greenberg, D.H. Ledbetter, B.L. Miller, S.F. Nelson, J. Pevsner, J.I. Rotter, G.D. Schellenberg, C. Samango-Sprouse, R.E. Tanzi, K.C.

Wilhelmsen, Evidence for a language quantitative trait locus on chromosome 7q in multiplex autism families, *Am. J. Hum. Genet.* (2002). <https://doi.org/10.1086/338241>.

28. H.C. Whalley, G. O'Connell, J.E. Sussmann, A. Peel, A.C. Stanfield, M.E. Hayiou-Thomas, E.C. Johnstone, S.M. Lawrie, A.M. McIntosh, J. Hall, Genetic variation in CNTNAP2 alters brain function

during linguistic processing in healthy individuals, *Am. J. Med. Genet. Part B Neuropsychiatr. Genet.* (2011). <https://doi.org/10.1002/ajmg.b.31241>.

29. A.J.O. Whitehouse, D.V.M. Bishop, Q.W. Ang, C.E. Pennell, S.E. Fisher, CNTNAP2 variants affect early language development in the general population, *Genes, Brain Behav.* (2011). <https://doi.org/10.1111/j.1601-183X.2011.00684.x>.

© *This is an open access article under the (CC)BY-NC license (<https://creativecommons.org/licenses/by-nc/4.0/>). Funded by Al-Farabi KazNU*

M.A. Zhaksylyk^{1*}, M.S. Kyrykbayeva², A.M. Kalimagambetov¹¹Al-Farabi Kazakh National University, Almaty, Kazakhstan²LPP “Center for Molecular Medicine”, Almaty, Kazakhstan

*e-mail: moldirzhaksylyk98@gmail.com

(Received 12 April 2022; received in revised form 29 April 2022; accepted 13 May 2022)

Results of the comprehensive study in newborn babies with congenital phenylketonuria

Abstract. The timely detection of newborns with congenital phenylketonuria, in which the metabolism of the amino acid phenylalanine is disturbed due to the lack of the enzyme phenylalanine hydroxylase, remains an urgent issue. Increase in the level of phenylalanine and its toxic products in the cell leads to severe brain damage, which manifests itself in the form of mental retardation. Prompt diagnosis of phenylketonuria can prevent severe dementia and serious mental disorders. The aim of the work is a comprehensive study of newborns with congenital phenylketonuria for which enzymatic immunoassay, real-time PCR, tandem mass spectrometry were applied. Out of 5,293 newborns screened at the genetic laboratory of LPP “Center for Molecular Medicine” (Almaty, Kazakhstan) in 2019, two newborns were diagnosed with congenital phenylketonuria. The molecular genetic study in both of them indicated the presence of the *R408W* mutation in the heterozygous state in phenylalanine hydroxylase *PAH* gene. Upon application of the appropriate dietary therapy, the concentrations of phenylalanine in the blood reached 62.9 $\mu\text{M/L}$ in the 1st and 173 $\mu\text{M/L}$ in the 2nd newborn, which corresponds to its reference value. For the effective treatment of congenital phenylketonuria with a confirmed diagnosis based on molecular genetic studies (detection of a mutation in the *PAH* gene) in newborns, it is proposed to conduct additional biochemical studies for possible metabolic disorders.

Key words: newborn screening, congenital phenylketonuria, enzyme immunoassay, PCR, tandem mass spectrometry.

Introduction

Hereditary metabolic disorders are common worldwide and play an important role in human hereditary pathology. These diseases are characterized by severe and in many cases fatal symptoms. According to the statistics, 5% of children are born with genetic or congenital disorders [1].

Monogenic forms of metabolic disorders are characterized by impaired metabolism of amino acids and organic acids resulting in the accumulation of toxic metabolites in organs and tissues. Study of the molecular basics of monogenic disorders and their prevalence in different regions of the world is an urgent issue of medical human genetics.

One of the diseases detected by selective screening is congenital phenylketonuria (PKU), which is a severe autosomal recessive disease caused by a genetic deficiency of the enzyme phenylalanine hydroxylase (PAH). Without enzymatic activity, phenylalanine is not converted to tyrosine. Deficiency of the PAH enzyme leads to a marked increase in

the level of phenylalanine (substrate), decrease in the level of tyrosine (product), appearance of phenylalanine metabolites, such as phenylpyruvic acid, phenyllactic acid and phenylacetic acid in the blood and urine, violation of the formation of tyrosine as well as adrenaline, norepinephrine and melanin synthesized from it, and a violation of tryptophan metabolism. A mutant gene in the *PAH* locus located on the long arm of chromosome 12 in the region q22-q24 [2] leads to the absence of *PAH* activity [3]. The protein coding sequence (cDNA) is approximately 90 kb long and consists of 13 exons. Most pathological changes in the *PAH* gene are single nucleotide substitutions, including missense (64%), splicing (13%) and nonsense (6%) mutations and neutral polymorphisms (6%) [4].

It was found that nearly 20 missense mutations affect highly mutagenic CpG dinucleotides. The remaining changes are the result of various deletions or insertions. Currently, more than 490 different variants of the *PAH* gene have been found with a high degree of variability and significant

interpopulation variance. The *R408W* missense mutation is the most common (major) *PAH* gene mutation in European populations. The *R408W* mutation leads to a severe form of PKU and reduces enzyme activity to 1–2.7% [5], while the genetic anomaly is associated with the replacement of C (cytosine) with T (thymine) in exon 12, which leads to the replacement of arginine with tryptophan at position 408 of the protein PAH [6].

In order to determine the prevalence of PKU in the Republic of Kazakhstan, the data on the mass newborn screening conducted in Almaty from 1989 to 1996 was analyzed, according to which the frequency of PKU was 1:6980, on average, with 80–90% of examined infants. State program for screening newborns for phenylketonuria and congenital hypothyroidism was initiated in 2007. According to the Republican Medical Genetic Consultation, the incidence of PKU in Kazakhstan is one case per 1:22 500 newborns (Public Foundation “Help Today”). According to the statistics of the public fund for 2019, almost 167 patients were registered with PKU in Kazakhstan [7].

The disease begins to develop as soon as phenylalanine enters the child’s body with mother’s milk. Symptoms of PKU appear in the first year of life, usually between 2 and 6 months of age. Children with PKU appear healthy at birth, despite the presence of such specific features as blond hair, blue eyes, and dry skin [8]. The child’s lethargy, lack of interest in the environment, sometimes irritability, restlessness, regurgitation, problems with muscle tone (often muscle hypotension), seizures, and symptoms of allergic dermatitis are early signs of the condition. There is a characteristic “mouse” smell. Microcephaly (incomplete development of the brain or abnormal smallness of the brain), delayed static-motor and psychoverbal development are often observed [9].

An effective treatment for PKU is diet therapy based on food low in phenylalanine [10]. High degree of dementia and severe mental disorders develop in patients in the absence of a phenylalanine-free diet from the first days of life due to the accumulation and toxic effect of phenylalanine and its derivatives on tissues and, especially, brain cells. Without special therapy, the condition worsens slowly; mental retardation usually reaches a severe degree with 20 units on IQ test [10]. In the psychological state of patients, there is a lack of development of game and objective activity, illegibility of emotional reactions, lack of expressive and vivid speech. Motor stereotypes, aggressive movements, psychopathic or schizophrenic states are possible.

The diagnosis is based on a combination of genealogical data, clinical and biochemical findings:

- possible consanguineous marriage of the parents of a sick child;
- similar pathology in relatives;
- convulsions, impaired muscle tone; eczematous skin changes;
- hypopigmentation of hair, skin, iris;
- a peculiar “mouse” smell of urine;
- increase in the level of phenylalanine in the blood > 2.1 mg/dL [11; 12].

Symptoms of the disease are practically removed at the time of early detection and treatment. Such a study helps prevent high-grade dementia and severe mental disorders, as well as deaths due to long-term monitoring of congenital malformations.

The aim of the work is a comprehensive study of newborns with congenital phenylketonuria for which enzymatic immunoassay, real-time PCR, tandem mass spectrometry were applied.

Materials and methods

The object of research. Out of 5,293 newborns screened at the genetic laboratory of LPP “Center for Molecular Medicine” (Almaty, Kazakhstan) in 2019, two newborns were diagnosed with congenital phenylketonuria. They underwent clinical studies, including analysis of amino acids in blood, and assessment of the quantitative content of pathological metabolites of phenylalanine and tyrosine in biological fluids. The *PAH* gene mutation was analyzed by PCR and amino acid analysis, including the spectra of phenylalanine and acylcarnitine, by tandem mass spectrometry.

Methods of research. Neonatal screening was conducted using the “Delfia Neonatal Phenylalanine” kit (Perkin Elmer, Finland). Blood sampling for PKU was carried out 3 hours after feeding, in full-term newborns on the 2–3rd day of life (25–72 hours of life), in premature infants – on the 7–14th day of life. A few drops of blood were applied to a special filter paper (Whatman 903, GE Healthcare Life Sciences, Buckinghamshire, UK) used to collect biomaterial for study of hereditary metabolic diseases. For newborn blood spot screening, bloodstain samples in the form of discs were transferred to the wells of microplates with a V-shaped bottom, containing 15 mL of the prepared extraction solution (for which three parts of zinc sulfate were mixed with two parts of 90% ethyl alcohol), and left at room temperature. After incubation for 30–60 minutes on shaker (to ensure that all disks were soaked in), 40 µL of deionized water were consequently added to each well. Blood

spots were freed with a needle. 50 µL of PKU reagent (a bottle of dry PKU reagent was dissolved in 6.5 mL of PKU Reconstitution Buffer) were added and incubated at 60°C for 30-40 minutes. 200 µL of copper blue reagent solution were added and incubated at the room temperature for 35 minutes. The analysis was performed on an immunofluorescent analyzer (Victor2™ D, Perkin Elmer, Finland) with the “85PKU” program for automatic measurement and calculation of results [13].

Isolation of genomic DNA from the peripheral blood of the subjects was carried out using the method of phenol-chloroform extraction. To do this, distilled water was added to 100 µL of blood, mixed and left for 15 minutes. Next, the sample was centrifuged at 5,000 rpm for 10 minutes. The supernatant was discarded and the cell pellet was washed with saline-sodium citrate (SSC) buffer, centrifuged again and the supernatant was discarded. Then, 54 µL of 0.2 M sodium acetate and 6 µL of 10% SDS (sodium dodecyl sulfate) were added to the pellet. The cell pellet was thoroughly resuspended using a vortex and incubated for 30-60 min at 37°C to destroy the cells. Two volumes of Tris-EDTA (TE) buffer (single buffer of 10 mM Tris: 1 mM EDTA) were added and phenolic deproteinization of the sample was carried out with the aqueous phase (top layer) collected in a clean tube without capturing the precipitate. The same was repeated with a mixture of chloroform-isoamyl alcohol to remove residual phenol. The test sample was purified from proteins. To this 1/10 volume of solution III (3 M potassium acetate: 29 g potassium acetate, 11 mL glacial acetic acid and 60 mL distilled water, bring the volume to 100 mL) was added and stirred. DNA was precipitated by adding the two and a half volumes of cold 96% ethyl alcohol. Sample was placed in the freezer for 1-2 hours. The resulting sample was centrifuged for 10 minutes, then the supernatant was discarded. The precipitate was washed with 70% ethyl alcohol. The resulting DNA pellet was dried and dissolved in 20 µL of TE buffer. DNA isolated in this way was used for PCR analysis [14].

PCR-analysis of mutations in the *PAH* gene was carried out using commercial diagnostic kit PKU-8L manufactured by LLC “Center for Molecular Genetics” at the Moscow State Scientific Center of the Russian Academy of Medical Sciences, Russia. For the study, the diagnostic set of primers and restrictases (DNA technology, Russia) were used to determine common mutations in the *PAH* gene: *R408W*, *R261Q*, *R252W*, *IVS10-11*, *IVS12+1*, *R158Q*, *P281L*, *IVS14+5*. Amplification by PCR with

addition of neonatal DNA was carried out according to the kit instructions [15].

Tandem mass-spectrometry for quantitative assessment of enzyme activity was conducted using the NeoBase kit (Perkin Elmer, Finland) that includes the NeoBase Flow solution and Extraction solution and NeoLSD™ kit. To identify congenital metabolic disorders, in particular, to detect elevated levels of the amino acid phenylalanine, acylcarnitines, and free carnitine with electrospray ionization tandem mass-spectrometry (QSight™ 210 MD Screening system, Perkin Elmer, Finland) was used. The material for the study was capillary blood collected on a special filter paper No. 903. This analysis allows the measurement of 75 metabolites for the simultaneous screening of 49 hereditary metabolic disorders [16; 19]. NeoBase™ amino acid assay kits and NeoLSD enzyme kits were used [20; 21].

Results and discussion

Peripheral blood was obtained from 5,293 children who passed newborn screening for phenylketonuria as part of the healthcare genetic consultation in January-December, 2019. The results of neonatal biochemical screening for PKU (Table 1).

Table 1 – The number of tests and the re-tests of newborns for congenital phenylketonuria

No.	Months of 2019	The number of tests for congenital phenylketonuria	The number of the re-tests	Detected PkU newborns
1	January	347	8	0
2	February	405	4	1
3	March	648	9	0
4	April	328	2	0
5	May	385	7	0
6	June	431	2	0
7	July	486	6	1
8	August	307	2	0
9	September	295	3	0
10	October	585	5	0
11	November	601	9	0
12	December	475	11	0
13	Total	5293	68	2

According to the results presented in Table 1, s, both false positive and false negative results are possible during the screening. In that case, the false

positive result determined in 68 children, and they were re-examined, thus the frequency of re-examination estimated 1.2%. Data shows that a false-positive diagnosis of congenital phenylketonuria is possible in about 2% of cases during neonatal screening. When a high level of phenylalanine was confirmed in the retest from the primary dry blood spot of the newborn, within 72 hours after receiving the first result, the dry blood spot of the newborn was retaken and delivered for re-analysis. Repeated dry blood spots were delivered to the laboratory in a separate envelope marked "Repeat PKU". A new blood test for a newborn baby was performed within 36 hours of receiving the blood sample. The increased content of the substance relative to the control with a double re-examination suggests the presence of pathology. As can be seen from Table 1, two newborns after a second examination revealed data corresponding to congenital phenylketonuria. According to the results, the probability of having children with congenital phenylketonuria per 10,000 was 2 cases, which was 10 times higher than the average for Kazakhstan (one in 22,500) [7].

During the neonatal screening in 2019, only two confirmed case of congenital phenylketonuria were detected in newborns. The results of enzyme immunoassay are presented in Table 2. Table 3 shows the reference values of the norm.

As can be seen from Table 2, the results of neonatal screening and retest exceed the reference values (Table 3) of the phenylalanine content in the first newborn by more than 3.5 and 12.4 times. These values for the second newborn were more than 6.3

and 10.8 times, respectively. PKU was diagnosed in newborns based on enzyme immunoassay, including clinical examinations.

Table 2 – The level of phenylalanine in the blood of two newborns

The level of phenylalanine in the blood	The result of 1 – newborn, mg/dL	The result of 2 – newborn, mg/dL
1 result	7.31	13.34
2 result (re-test)	26.20	22.86

Table 3 – Indicator level of congenital phenylketonuria [11; 12]

Meaning	The level of phenylalanine in the blood, mg/dL	The level of phenylalanine in the blood, $\mu\text{mol/L}$
Potentially negative result	< 2.1	< 127
Unclear zone	2.1 – 3.0	127 – 182
Potentially positive result	> 3.0	> 182
Conversion factor: 1 $\mu\text{mol/L}$ to mg/dL equals 60		

When monitoring treatment and dietary therapy, the values of phenylalanine for the first and second newborn were 62.9 $\mu\text{M/L}$ and 173 $\mu\text{M/L}$, respectively, presented in Table 4. The concentration of phenylalanine in two newborns varied within the normal range of 20-265 $\mu\text{M/L}$.

Table 4 – Amino acid values of blood of two babies

No.	Amino acids		Standard values, $\mu\text{M/L}$	The result of 1 – newborn, $\mu\text{M/L}$	The result of 2 – newborn, $\mu\text{M/L}$
1	Alanine	Ala	85 – 910	345	217
2	Arginine	Arg	2 – 125	63	26.7
3	ASA-total	ASA-total	–	0.54	0.19
4	Citrulline	Cit	4 – 80	19.9	23.4
5	Glutamine	Gin	–	50	555
6	Glutamate	Glu	62 – 615	338	127
7	Glycine	Gly	95 – 945	408	220
8	Leucine	Leu	35 – 380	191	93.5
9	Methionine	Met	6 – 155	33.1	9.55
10	Ornithine	Orn	22 – 405	118	64.1
11	Phenylalanine	Phe	20 – 265	62.9	173
12	Proline	Pro	30 – 490	167	131
13	Tyrosine	Tyr	15 – 235	76.9	64.1
14	Valine	Val	45 – 430	178	136

Subsequently, studies were carried out on the content of pathological metabolites of phenylalanine in biological fluids, the determination of *PAH* gene mutations using PCR methods and tandem mass spectrometry (determination of the spectrum of acylcarnitines, amino acids).

To clarify the clinical diagnosis of newborns, a molecular genetic study was performed for the presence of mutations in the *PAH* gene – phenylalanine hydroxylase among the eight most common mutations *R408W*, *R261Q*, *R252W*, *IVS10-11*, *IVS12+1*, *R158Q*, *P281L* and *IVS14+5*. The material for the study was DNA isolated from peripheral blood according to the standard method. Allele-specific ligation followed by amplification and registration of results in a polyacrylamide gel in both newborns revealed *R408W* mutations in the heterozygous state. It was discovered 93 base pairs fragment along with a fragment of 89 base pairs corresponding to the norm (Figure 1).

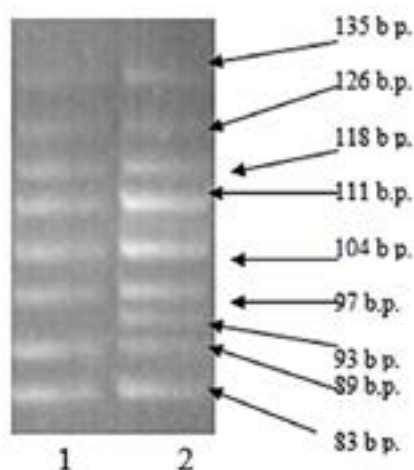


Figure 1 – Electrophoregram of two newborns.
Note: 1 – control DNA; 2-DNA of newborns;
b.p. stands for base pairs

It should be noted that, in order to detect congenital phenylketonuria and confirm the diagnosis, except mass screening and molecular genetic analysis, newborns with congenital phenylketonuria need to undergo an additional examination, since they are predisposed to diseases. An additional examination should include an analysis of the spectrum of amino acids and acylcarnitines by tandem mass spectrometry for hereditary metabolic diseases. When the possibility of a metabolic disorder is identified, certain key metabolic screening tests should be

performed. These tests include plasma amino acid analysis. The amino acid profile may be indicative of a specific metabolic disorder causing neonatal disease, i.e., an increased or decreased amino acid content may indicate the presence of genetic diseases.

Based on the study of the spectrum of amino acids and acylcarnitines by tandem mass spectrometry, according to its multi-parametric nature, was made an analysis of the metabolism of amino acids, carnitines, organic acids to defects in β -oxidation of fatty acids and the amount of enzymes that accompany Gaucher's disease (deficiency of 3-glycocerebrosidase), Niemann-pick (deficiency of sphingomyelinase), Krabbe (galactocerebrosidase deficiency), type 1 mucopolysaccharidosis (iduronidase deficiency), Fabry (alpha-galactosidase deficiency), Pompe caused by alpha-glucosidase enzyme deficiency [22].

Tandem mass spectrometry has the advantage of being able to determine the ratio of substrate concentration to its product concentration in a single sample, in this case the ratio of phenylalanine concentration to tyrosine concentration. The results of the study showed that the ratio of the concentration of phenylalanine to tyrosine was within the normal range and amounted to 0.82 $\mu\text{M/L}$ in the 1st newborn, and 2.69 $\mu\text{M/L}$ in the 2nd newborn (it is important to mention that the reference ratios of phenylalanine to tyrosine are 0.25 – 6.5 $\mu\text{M/L}$). The remaining indicators of the ratios of the components are shown in Table 5. Table 6 presents the data of the analysis of the metabolic test for carnitines in both newborns.

As can be seen from Table 6, the results of the metabolic test for carnitines in both newborns corresponded to the reference value. Along with free carnitines, observed the presence of several types of other carnitines, including acetyl, propionyl, malonyl, butyryl, methylmalonyl, isovalerylcarnitine, etc. Also, studied the breakdown of lysophospholipids, nucleosides, ketones, resulting in the formation of the energy, which is necessary for the life of the cell (Table 7).

Each step of the oxidation process is carried out under the action of specific enzymes. In the absence of one of the enzymes, the process is disrupted. The results of the study did not show data for hereditary aminoacidopathy, carnitines, organic aciduria and defects in mitochondrial β -oxidation of fatty acids.

Data for impaired enzymatic activity for the following lysosomal storage diseases: Gaucher disease, Niemann-Pick disease, Pompe disease, Krabbe disease, Fabry disease and mucopolysaccharidosis type I were also not detected in two newborns (Figure 2).

Table 5 – The amino acid ratio indicators of two newborns

Ratio:	Standard values, $\mu\text{M/L}$	The result of 1 – newborn, $\mu\text{M/L}$	The result of 2 – newborn, $\mu\text{M/L}$
Phenylalanine/Tyrosine	0.25-6.50	0.82	2.69
Leucine/Phenylalanine	0 – 3.65	3.03	0.54
Methionine/Leucine	0.02 – 0.47	0.17	0.10
Methionine/ Phenylalanine	0.04 – 0.70	0.53	0.06
Tyrosine/Leucine	-	0.40	0.69
Tyrosine/Methionine	-	2.33	6.71
Citrulline/Arginine	0 – 5.56	0.32	0.88
Valine/ Phenylalanine	0 – 3.00	2.83	0.79
Citrulline/ Phenylalanine	0.10 – 0.67	0.32	0.14

Table 6 – The values of carnitines of two newborns

Types of carnitines:	Standard values, $\mu\text{M/L}$	1 – newborn, $\mu\text{M/L}$	2 – newborn, $\mu\text{M/L}$
Carnitine free C0	8.0 – 155.0	36.40	43.4
Acetylcarnitine C2	6.0 – 55.0	11.40	18.7
Propionylcarnitine C3	0.16 – 6.50	0.91	2.51
Malonylcarnitine C3D3	0 – 10.40	0.07	0.12
Butyrylcarnitine C4	0 – 1.10	0.23	0.44
Methylmalonyl C4DC	0 – 17.0	0.76	0.40
Isovalerycarnitine C5	0 – 0.70	0.14	0.12
Tiglylcarnitine C5:1	0 – 0.15	0.01	0.01
Glutarylcarnitine C5DC	0 – 6.99	0.12	0.08

Table 7 – The values of lysophospholipids, nucleosides, and ketones by TMS (MS/MS) of first and second newborns

Results:	1 – newborn, $\mu\text{M/L}$	2 – newborn, $\mu\text{M/L}$
Lysophospholipids:		
Lysophosphatidylcholine C20:0	0.65	0.63
Lysophosphatidylcholine C22:0	0.49	0.14
Lysophosphatidylcholine C24:0	0.55	0.26
Lysophosphatidylcholine C26:0	0.19	0.14
Nucleosides:		
Adenosine	0.35	0.3
2-deoxyadenosine	0.02	0.02
Ketones:		
Succinylacetone	0.39	0.18

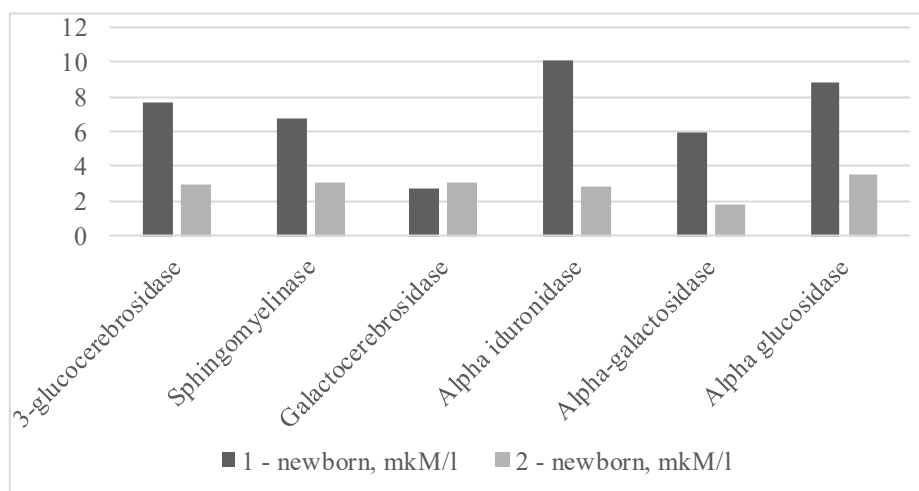


Figure 2 – The amount of specific enzymes in the body in two newborns

Blood donation for immunofluorescence analysis and genetics visits remained mandatory for both newborns once a month, regularly. Every three weeks they had to donate blood for examination. This prevented the complications of innate phenylalanine and allowed control over the amount of phenylalanine they had to consume. The

normal amino acid content is 2.1 mg/dL. Values greater than 2.1 mg/dL represent an increased risk of developing phenylketonuria. Figures 3 and 4 show measurements of phenylalanine in a blood sample for two newborns, respectively. The content of phenylalanine in both newborns showed a steady but significant increase over this period.

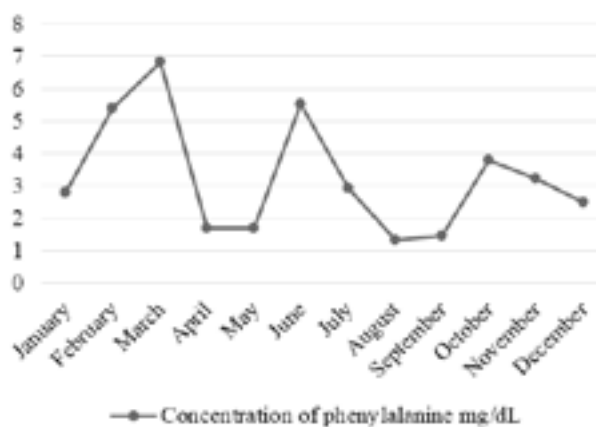


Figure 3 – Distribution of phenylalanine content in the 1st newborn for 2020

It should be noted that in the process of monitoring sharp fluctuations in content of phenylalanine in the process of development were observed in sick children.

According to the Order of the Ministry of Healthcare of the Republic of Kazakhstan No. 105 from March 14, 2018 “On amendments to the

order of the Minister of Healthcare of the Republic of Kazakhstan No. 666 from August 29, 2017 “On approval of the List of medicines and medical devices to provide citizens within the guaranteed volume of free medical care and in the system of compulsory social health insurance, including certain categories of citizens with certain diseases (conditions) free

and(or) subsidized medicines, medical devices and specialized medical products at the outpatient level”” Phenylketonuria section includes therapeutic low-protein products and products with low phenylalanine content: Komida med PKU-formula + LCP (11.8 g protein per 100 g); Komida med PKU – B (31.1 g of

protein per 100 g); Komida med PKU C – 45 (45 g of protein per 100 g); PKU-3 (69 g protein per 100 g); Komida med PKU C-75 (75 g of protein per 100 g); PKU-0 (13 g protein per 100 g); PKU-1 (20 g protein per 100 g); RAM-1 and RAM-2 (75 g of protein per 100 g); Isifen (16.8 g of protein in 1 pack) [23].

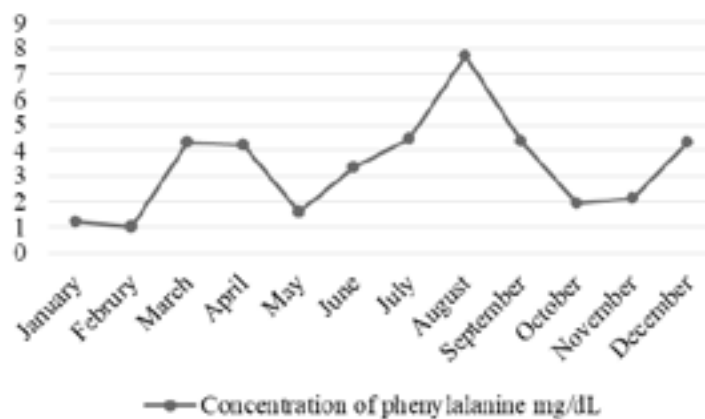


Figure 4 – Distribution of phenylalanine content in the 2nd newborn for 2020

Since good metabolic control in childhood is necessary to prevent cognitive impairment in PKU, it is recommended to treat patients with corrected phenylalanine concentration during the first 12 years [24]. Collaborative study for PKU revealed that discontinuation of diet control correlated with decreased school performance in children and increased behavioral and psychosocial problems in adults [25].

A comprehensive examination of newborns with congenital phenylketonuria will allow timely treatment of critical conditions and metabolic disorders, which will enable them to grow and develop healthy. However, they must be under constant medical supervision, and at the first suspicion of a developmental disorder, complex treatment is required, designed to reduce acute symptoms.

Since one of the main tasks of medicine is diagnosis of genetic pathologies in newborns, a lot of journals and articles have been written in this area, which have a specific purpose and a certain similarity. The significance of our work is a first time comprehensive study of phenylketonuria in newborns after mass neonatal screening. Also studying besides neonatal screening and *PAH* gene mutation, other number of enzymes, which are the causes of lysosomal storage diseases. Our data on the prevalence of PKU can

be used to assess the genetic state of the Republic of Kazakhstan. The frequency of PKU according to our mass screening of newborns in Almaty is 2 cases per 10,000, and this is at the level of the average in Almaty 1 case per 6,980. In both studies, the most frequent mutations were *R408W*, which indicates the similarity of the results of our analysis.

The frequency of mutations in the phenylalanine hydroxylase gene varies in unrelated children diagnosed with PKU [26]. The *R408W* mutation is considered as more typical for Eastern European countries (47.9%) [27].

The average frequency of congenital phenylketonuria varies between 1:10,000 and 15,000 newborns. It varies from country to country, e.g. 1: 4,370 in Turkey and 1: 100,000 in Japan [28]. In addition, among cities of even one country the indices can differ: in Kazakhstan, the number equals to 1:22,500 and in Almaty is equal to 1:6,980 [7].

As mentioned by Levy *et al.* [15], despite the assumption of a normal newborn screen, it is vital to acknowledge the possibility that a child will may have metabolic illness or a related disorder. As a result, testing for all relevant metabolic diseases, including those covered by molecular-genetic analysis, should be included in the evaluation of newborns. In the next work [29] have been highlighted, that the second

sample should be taken if a high phenylalanine level is identified in a newborn screening sample. The latter has the advantage of being able to analyze all amino acids accurately and is preferred when the first phenylalanine is significantly elevated (e.g., above 2.1 mg/dL) [11; 12]. Catabolism can cause an increase in phenylalanine levels in premature and/or severely sick newborns. Under these conditions, it is advised that a full analysis of all amino acids be performed for a limited period of time

Our work emphasizes the importance of expanding "Neonatal medicine" for the early detection of many inborn metabolic errors and making decisions to provide effective treatment and a good results at the end.

Conclusion

One of the main tasks of practical medicine is the diagnosis of hereditary pathologies. The study of the biochemical and molecular-genetic aspects of hereditary diseases is a comprehensive solution to the urgent problems of elucidating the etiology and pathogenesis of this group of diseases. In this regard, in particular, the timely detection of newborns with congenital phenylketonuria remains an urgent problem. As practice shows, a case of late diagnosis can be the cause of severe irreversible developmental disorders of the child. With timely effective treatment, children with this disease do not differ from their peers, develop according to age and study in regular schools. This is possible with neonatal screening, appropriate therapy and proper monitoring of the newborn.

The success of treatment is mainly determined by the extent to which the parents of a sick child have realized the importance of diet therapy, and how strictly they carry it out. The child needs to constantly monitor the content of phenylalanine in the blood, and, depending on laboratory parameters, adjust the composition of those products that, on the one hand, will not increase the level of phenylalanine, and on the other hand, ensure the normal growth and development of the child.

The most important aspect to consider in congenital phenylketonuria – is the psychological aspect. The transition to adulthood – is a period of high risk for patients with PKU. Difficulties are exacerbated by the need to adhere to dietary therapy, there is a risk of loss of metabolic control and a high risk of a complete loss of medical supervision. In this regard, it is necessary to organize psychological support for the families of patients, which should begin from the moment a sick child appears in the

family. Without effective support, many of the benefits gained during early treatment may be lost in adulthood [30].

The results of the study allow us to draw the following conclusions:

1. Neonatal screening of 5,293 newborns revealed two newborns with congenital phenylketonuria: the concentration of phenylalanine in the dry blood spot in the 1st newborn was 7.31 mg/dL, in the retest 26.20 mg/dL, in the 2nd newborn the level of phenylalanine was 13.34 mg/dL in retest 22.86 mg/dL.

2. In these two newborns the *R408W* mutation in *PAH* gene was detected in the heterozygous state.

3. After appropriate dietary therapy, the concentrations of phenylalanine in the blood of the observed newborns decreased to their reference value – 62.9 $\mu\text{M/L}$ in the 1st newborn and 173 $\mu\text{M/L}$ in the 2nd newborn.

4. The ratio of phenylalanine to tyrosine was 0.82 $\mu\text{M/L}$ in the 1st newborn, and 2.69 $\mu\text{M/L}$ in the 2nd newborn.

5. The results of additional studies showed no data for hereditary aminoacidopathy, organic aciduria and defects in mitochondrial β -oxidation of fatty acids. In addition, there were no data for violations of enzymatic activity for the following lysosomal storage diseases: Gaucher disease, Niemann-Pick disease, Pompe disease, Krabbe disease, Fabry disease and mucopolysaccharidosis type I.

For early detection and effective treatment of congenital phenylketonuria, along with mass screening and molecular genetic studies to confirm the diagnosis, it is recommended to conduct additional studies on metabolic disorders in newborns with an established diagnosis due to their predisposition to disease.

References

1. Pechantnikova N.L., Bruhanova N.O., Potechin H.O., Vitkovskaya I.P., Petrikina E.E., Koltunov I.E. (2017) Selektivnyy skринing na nasledstvennyye bolezni obmena veshchestv: Metodicheskiye rekomendatsii no.16 /Departament zdravookhraneniya [Selective screening for hereditary metabolic diseases /Methodical recommendations no.6 /Department of Health]. Moskva. 24 p.
2. Pietro S., Daniela C. (2014) New Strategies for the Treatment of Phenylketonuria (PKU). pp. 1007-1017. <http://doi.org/10.3390/metabo4041007>
3. Hamid R.S., Ali A.H., Mohammad R.B., Zohre B. and Farzaneh Z. (2020) Global prevalence of classic phenylketonuria based on Neonatal Screening Program Data: systematic review and meta-analysis.

Clin Exp Pediatr., pp. 34-43. <http://doi.org/10.3345/kjp.2019.00465>

4. Bushueva T.V. (2010) Sovremennyy vzglyad na problemu fenilketonurii u detey: diagnostika, klinika, lecheniye. Voprosy sovremennoy pediatrii. [A modern view on the problem of phenylketonuria in children: diagnosis, clinic, treatment. Questions of modern pediatrics]. vol. 9, pp. 157-160

5. Hiu M.G., Gerald S., Cary O.H., Beat T. (2019) State-of-the-Art 2019 on Gene Therapy for Phenylketonuria. *Hum. Gene Ther.*, pp. 1274-1283 <http://doi.org/10.1089/hum.2019.111>

6. Blau N., Burton B.K., Thöny B. (2010) Phenylketonuria and BH4 Deficiencies. *J. Inherit. Metab. Dis.*, 3rd edition, 112 p. ISBN 978-3-8374-1526-1

7. Orazgalieva M.G. (2005) Analiz gena fenilalaningidrosilazy u bol'nykh fenilketonuriyey i v populyatsiyakh Respubliki Kazakhstan [Analysis of the phenylalanine hydroxylase gene in patients with phenylketonuria and in the populations of the Republic of Kazakhstan]. Abstract. Ufa. <http://www.dissercat.com/content/analiz-gena-fenilalaningidrosilazy-u-bilnykh-fenilketonuriei-i-v-populyatsiyakh-respubliki-#ixzz4w7GTBkrq>

8. Coakley K.E., Douglas T.D., Goodman M., Ramakrishnan U., Dobrowolski S.F., Singh R.H. (2016) Modeling correlates of low bone mineral density in patients with phenylalanine hydroxylase deficiency. *J Inherit Metab Dis.*, pp. 363–372. <http://doi.org/10.1007/s10545-015-9910-0>

9. Regier D.S., Greene C.L. (2000) Phenylalanine Hydroxylase Deficiency. In: Adam M.P., Ardinger H.H., Pagon R.A., et al., editors. GeneReviews® [Internet]. Seattle (WA): University of Washington, Seattle; 1993-2022. Available from: <https://www.ncbi.nlm.nih.gov/books/NBK1504/>

10. Novikova P.B. (2007) Rukovodstvo po pediatrii. Vrozhdennyye i nasledstvennyye zabolovaniya [Guide to Pediatrics. Congenital and hereditary diseases]. Moskva. Izdatel'skiy dom «Dinastiya», pp. 61-70

11. Gladys H., John C. (2014) Phenylketonuria: translating research into novel therapies. *Transl Pediatr*, pp. 49-62 <http://doi.org/10.3978/j.issn.2224-4336.2014.01.01>

12. Serwet D., Katie E.C., Peter H.B., Carla E.M., Annet M.B., Rani H.S. (2015) Bone health in phenylketonuria: a systematic review and meta-analysis. *Orphanet J Rare Dis*, <http://doi.org/10.1186/s13023-015-0232-y>

13. Christopher J.F., Melissa L.M., Shanthi K., Mary L.L., Tyler R. (2013) Estimating the probability of IQ impairment from blood phenylalanine for

phenylketonuria patients: a hierarchical meta-analysis. *J Inherit Metab Dis.*, pp. 757-766, <http://doi.org/10.1007/s10545-012-9564-0>

14. Kaumov A.R., Gimadutdinov O.A. (2016) Praktikum po molekulyarnoy genetike. Uchebno-metodicheskoye posobiye [Workshop on molecular genetics. Teaching aid]. Kazan: KFU, p. 36

15. Levy H.L., Cornier A.S (1994) Current approaches to genetic metabolic screening in newborns. *Curr Opin Pediatr*, pp. 707-711 <https://doi.org/10.1097/00008480-199412000-00017>

16. Ugeskr L. (2002) Screening of newborns for inborn errors of metabolism by tandem mass spectrometry. *Ugeskr Laeger*, pp. 5607-5612

17. Wilcken B., Haas M., Joy P. (2009) Expanded newborn screening: outcome in screened and unscreened patients at age 6. *Pediatrics*, pp. 241-248 <http://doi.org/10.1542/peds.2008-0586.p241-248>

18. Daly A., Evans S., Chahal S., Santra S., Pinto A., Jackson R., Gingell C., Rocha J., Van F.J., MacDonald A. (2019) Glycomacropeptide: long-term use and impact on blood phenylalanine, growth and nutritional status in children with PKU. *Orphanet J Rare Dis*, 44 p. <http://doi.org/10.1186/s13023-019-1011-y>

19. Anne D., Sharon E., Alex P., Catherine A., Anita M. (2021) Protein Substitutes in PKU: their Historical Evolution. *Nutrients*, 484 p. <http://doi.org/10.3390/nu13020484>

20. NeoBase™2 Non-derivatized MSMS kit. Instructions for use. Perkin Elmer, Walac Oy. Finland. <https://www.perkinelmer.com/product/neobase-non-derivatized-msms-kit-3040-001u>

21. NeoLSD™2 Non-derivatized MSMS kit. Instructions for use. Perkin Elmer. Walac Oy. Finland <https://www.perkinelmer.com/product/neolsd-msms-kit-3093-0020>

22. Robin A.W., Cyril D.M., John R.B. (2008) Phenylketonuria: an inborn error of phenylalanine metabolism. *Clin. Biochem. Rev.*, pp. 31-41

23. Soglasnoprikaza Ministra zdravookhraneniya Respubliki Kazakhstan ot 14 marta 2018 goda no.105 O vnesenii izmeneniy v prikaz Ministra zdravookhraneniya Respubliki Kazakhstan ot 29 avgusta 2017 goda no.666 "Obutverzhdennii Perechnya lekarstvennykh sredstv i izdeliy meditsinskogo naznacheniya dlya obespecheniya grazhdan". Ekspertnoye zaklyucheniye na primeneniye novoy meditsinskoy tekhnologii [According to the Order of the Minister of Health of the Republic of Kazakhstan dated March 14, 2018 No. 105 On amendments to the order of the Minister of Health of the Republic of Kazakhstan dated August 29, 2017 No. 666 "On approval of the List of medicines and medical devices

for providing citizens". new medical technology]. <https://adilet.zan.kz/rus/docs/V1700015856>

24. Christopher J.F., Melissa L.M., Shanthi K., Mary L.L., Tyler R. (2013) Estimating the probability of IQ impairment from blood phenylalanine for phenylketonuria patients: a hierarchical meta-analysis. *J Inherit Metab Dis.*, pp. 757-766. <http://doi.org/10.1007/s10545-012-9564-0>

25. Naz A.H., John C. (2015) Phenylketonuria: a review of current and future treatments. *Transl Pediatr*, pp. 304–317. <http://doi.org/10.3978/j.issn.2224-4336.2015.10.07>

26. Nikiphorova A.I., Abramov D.D., Kadohnikova V.V., Zobkova G.U., Ogurscova K.A., Bruhanova N.O., Shestopalova E.A., Kochetkova T.O., Shubina E.S., Donnikov A.E., Trophimov D.U (2017) Opredeleniye chastoty vstrechayemosti mutatsiy v gene PAH s primeneniym kombinatsii tekhnologiy PCR «V real'nom vremeni» i vysokoproizvoditel'nogo sekvenirovaniya u bol'nykh fenilketonuriyey Moskovskogo regiona [Determination of the frequency of occurrence of

mutations in the PAH gene using a combination of real-time PCR technologies and high-throughput sequencing in patients with phenylketonuria in the Moscow region]. *Vestnik RGMU*, pp. 42-49

27. Johannes Z. (2003) Phenylketonuria mutations in Europe. *Hum Mutat*, pp. 345–356. <http://doi.org/1002/humu.10192>

28. Chastota fenilketonurii v stranakh mira [The frequency of phenylketonuria in the countries of the world]. Moskva. [Electronical resources]. <http://ref-med.geiha.ru/data/30203.htm>

29. Bodamer O.A. (2010) Screening for Phenylketonuria. Institute of Inherited Metabolic Diseases, Paracelsus Medical University. Salzburg, Austria, pp. 53-57. <http://doi.org/10.1159/000312812>

30. Matulevich S.A., Golihina T.A. (2014) Klinicheskiye rekomendatsii po diagnostike i lecheniyu fenilketonurii i narusheniy obmena tetragidrobioterapiya [Clinical guidelines for the diagnosis and treatment of phenylketonuria and metabolic disorders tetrahydrobiotherapy]. Moskva: Izdatel'skiy dom "Akademizdat", 52 p.

© This is an open access article under the (CC)BY-NC license (<https://creativecommons.org/licenses/by-nc/4.0/>). Funded by Al-Farabi KazNU

L. Bekbayeva^{1,2*} , Z. Zakaria² , El-Sayed Negim³ ,
K.M. Al Azzam⁴ , G. Yeligbayeva³ 

¹S. Asfendiyarov Kazakh National Medical University, Almaty, Kazakhstan

²Universiti Sains Malaysia, Penang, Malaysia

³Satbayev University, Almaty, Kazakhstan

⁴Al-Ahliyya Amman University, Amman, Jordan

*e-mail: lyazzat_bk2019@mail.ru

(Received 14 February 2022; received in revised form 17 March 2022; accepted 14 April 2022)

The effect of mixed fertilizers on the vegetative growth and reproductive characteristics of tomatoes (*L. esculentum* Mill)

Abstract. The purpose of this study was to investigate how combination fertilizers based on seaweed liquid extract (SLF) and nitrogen fertilizer (PU) affected tomato vegetative development and reproductive characteristics (*L. esculentum* Mill). The mixed fertilizers had varying amounts of SLF and a constant amount of PU [(5% SLF + PU50), (10% SLF + PU50), 30% SLF + PU50), and (50% SLF + PU50)]. The greenhouse was used to study tomato growth and yield response to mixed fertilizer. The Randomized Complete Block Design (RCBD) was used for the experiment, with five replicates for each treatment. The data were analysed using variance analysis (ANOVA) and compared to a control that did not use fertilizer. The results revealed that the mixed fertilizers resulted in substantial increases in all the evaluated attributes. However, mixed fertilizer (10% SLF + PU50) produced the highest vegetation, flower, and fruit characteristics compared to the control plants and other treatments. These results clearly show that 10% SLF + PU50 is favourable for tomatoes.

Key words: tomato, fertilizer, vegetative, growth.

Introduction

Tomatoes (*Lycopersicon esculentum* Miller) are one of the most significant vegetable crops farmed in the world, both in the field and in greenhouses [1]. In terms of human health, tomato is a vital source of minerals, vitamins, and antioxidants and is a substantial component of many people's daily diets in many countries [2,3]. Using seaweed in such a circumstance is thus a financially advantageous proposition. Seaweed is used as a foliar spray or a soil drench to promote faster growth and production in leafy vegetables, fruits, orchards, and horticultural plants. The presence of plant hormones, particularly cytokinin, has been attributed to a large portion of the benefit derived from the use of seaweed extract.

Various seaweed concentrates contain considerable amounts of cytokinin in addition to other phytohormones [4]. Meanwhile, nitrogen fertilizer is critical for plant growth and final grain yield, and it has been applied at the optimal rate to meet the plant's needs. Urea is one of the most popular nitrogenous fertilizers among farmers due

to its high nitrogen content (46% by weight), which has overtaken other nitrogenous fertilizers. When urea fertilizer inputs to the soil system exceed crop needs, 50% of the applied fertilizer may escape to the environment owing to leaching, surface runoff, decomposition, and ammonium volatilization in the soil, since only a part is absorbed by plants.

The slow-release method was used on urea fertilizer to gradually release the nutrient contents and to correspond with the usage efficiency of plant uptake. It had been reported that PVA was used for seed coating or pre-treatment seed to improve seed germination, seedling growth, or salt resistance [5,6], or used in soil to reduce runoff and soil losses [7], improve root number and root length in jujube [8], and improve rooting percentage in woad and pear clones [9,10]. Copper encapsulated in chitosan and PVA-chitosan increases the development characteristics of tomato plants, according to Hipólito et al. [11] and Pinedo et al. [12]. As a result, the combination of hydrogel and fertilizer has emerged as one of the promising materials for overcoming the shortcomings of conventional fertilizer by significantly improving

plant nutrition, decreasing fertilizer loss rate, reducing environmental impact from water-soluble fertilizer, supplying nutrients sustainably, and lowering irrigation frequency [13]. Mixed fertilizers have the potential to increase crop production stability, maintain improvements in soil fertility, and improve plant development efficiency [14]. Copper encapsulated in chitosan and PVA-chitosan hydrogel, according to Hipólito et al. [11] and Pinedo et al. [12], increases the growth characteristics of tomato plants and plants and pepper.

Evidence suggests that combining organic and inorganic fertilizers improves nutrient availability, optimizes the soil environment, and improves crop productivity [15,16]. The combined use of chemical and organic sources, known as integrated nutrient management, is generally acknowledged as a method of enhancing crop productivity sustainably [17,18]. When compared to NPK fertilizer alone, a combined application of 3 t/ha vermicompost and 50% doses of NPK (60: 30: 30: kg/ha) fertilizer resulted in greater tomato crop growth and yield [19].

Ayeni et al. [20] found that poultry at 20, 30, and 40 t/ha with NPK 15: 15: 15 fertilizers greatly increased plant leaf area, quantity of leaves, branches, and tomato fruit yield. Adnan et al. [21] discovered a significant increase in plant growth and tomato fruit yield because of using organic manures in combination with the recommended dose of inorganic fertilizers. Makinde and Ayoola [22] found that applying a mix of synthetic fertilizers to maize (*Zea mays L.*) yielded higher yields than manure alone. According to Akanbi et al. [23], a combined application of 4 t/ha maize straw compost and N mineral fertilizer at 30 kg/ha increased plant growth and gave higher tomato yield. Dawa et al. [24] discovered that fertilizing tomato plants with mixed fertilizers chicken manure at 6 ton/ha with 50% NPK from the recommended dose, i.e., 75 N, 35 P₂O₅, and 85.5 K₂O kg/ha and sprayed with seaweed extract at a rate of 2.5 mL/L produced the highest values of vegetable growth parameters, chlorophyll, N, P, and K percentages in tomato leaves. Pepper plants fed with mixed fertilizers (seaweed extract and chicken manure as organic fertilizers) in the presence of biofertilizers enhanced vegetative plant growth and NPK percentages in leaves [25]. Awosika et al. [26] fertilized tomatoes using pig manure and NPK (15:15:15) and discovered that 187 kg/ha NPK plus 6 t/ha pig manure had the greatest results in terms of leaf number, plant height, fruit weight, yield, and quality. Prativa and Bhattarai [27] investigated the impact of integrated nutrient management on tomato plant

growth, yield, and soil nutrient status (*Lycopersicon esculentum L.*). The study indicated that combining organic manures with inorganic fertilizers improved overall plant growth, yield, and soil macronutrient status more than either nutrient applied alone. Prakash et al. [28] investigated the influence of humic acid (HA) and SLF on the growth and nutritional quality of *Abelmoschus esculentus*. A combined impact of SLF and HA (8.5%: 0.5 %) was beneficial in enhancing the growth of the plant in the pots that is also reflected in the increased carbohydrate and protein content in *Abelmoschus esculentus*. Mukta et al. [29] found that using vermicompost as an organic fertilizer at a rate of 10 t/ha in conjunction with 50% chemical fertilizer resulted in the best tomato production and quality.

Current study was conducted to increase the growth, yield, and chemical content of tomato (*Lycopersicon Esculentum L. Mill*) treated with mixed fertilizers at different rates (5% SLF + PU50), (10% SLF + PU50), and (30% SLF + PU50), (50% SLF + PU50).

Materials and methods

Seaweed extract preparation (SLF). A fresh sample of seaweed (*Gracilaria manilaensis*) was collected from Pantai Merdeka, Sungai Petani, Kedah. To eliminate adhering material and sand particles, the seaweed was carefully washed with seawater immediately after collecting, followed by freshwater. Clean seaweed was sun-dried for 7 days in the open air before being oven-dried for 48 hours at 60°C and ground to a fine powder with a mixer grinder. The seaweed powder was then used to make seaweed liquid extract (SLE) using the methods described by Srijaya et al. [30], Ganapathy and Sivakumar [31], and Rathore et al. [32].

In a sealed conical flask, four liters of water were added to 1 kg of dried seaweed and heated for 45 minutes at 60°C. The content was filtered through four layers of muslin cloth after cooling. The filtrate collected (2.150 mL) was 100% seaweed liquid fertilizer (SLF), and different concentrations of SLF, namely 5, 10, 30, and 50%, were prepared using distilled water [33]. Using an atomic absorption spectrophotometer, physical observations such as colour, pH, and different components of macronutrients (calcium, magnesium, potassium, phosphorous, nitrogen) and micronutrients (iron, magnesium, zinc, copper, and nitrate) were calculated [34]. Table 1 shows the physicochemical properties of SLF of *Gracilaria manilaensis* before preparation of different concentrations.

Table 1 – The physicochemical analysis of *Gracilaria manilaensis* (SLF)

Parameters	Values
Colour	Brown
pH	6.74
Nitrogen	400 (mg/L)
Calcium	156.06 (mg/L)
Magnesium	110.09 (mg/L)
Sodium	291.04 (mg/L)
Potassium	180.3 (mg/L)
Iron	6.9 (mg/L)
Phosphate	43.06 (mg/L)
Chloride	2180.8 (mg/L)
Sulphate	58.7 (mg/L)
Zinc	1.1 (mg/L)
Copper	1.7 (mg/L)
Nitrate	127.09 (mg/L)

Synthesis of nitrogen fertilizer (PU). The nitrogen fertilizer (PU) based on polyvinyl alcohol (PVA) and urea (U) was synthesized in an aqueous solution using Lewis acid (acetic acid) as a catalyst. The following procedure was used to synthesize PVA/U blends with a constant ratio, i.e., 50:50. (PU50). In an Erlenmeyer flask, the PVA and U were dissolved in 300 mL of distilled water. The solution was stirred using a magnetic stirrer, and the flask was sealed with a septum stopper. The solution was then flushed with nitrogen gas before being administered through a hypodermic needle, and another needle was placed within the stopper for gas outflow. The solution was continually agitated using a magnetic stirrer, and the nitrogen gas was bubbled at 30 minutes intervals.

The appropriate amount of glacial acetic acid was injected into the solution until pH 4 was attained, and nitrogen gas flushing was maintained for another 30 minutes. The nitrogen gas bubbling was stopped, the needles were withdrawn from the stopper, and the flask was sealed with Teflon tape. The temperature of the reaction was kept constant at 90°C by immersing the flask in a constant-temperature oil bath. When the pH remained constant at 4, the process was stopped. The polymer solution was precipitated in an excess of methanol, and the product was dried in a vacuum at 35°C. The nitrogen fertilizer was prepared and analyzed using the methods described earlier by El-Sayed *et al.* [35] (¹H NMR, FTIR, SEM, DSC, and

TGA). The elemental analysis was performed using a Vario Micro Elemental Analyzer (Elementar, Germany) to determine the carbon, nitrogen, and oxygen content of the fertilizers, as indicated in Table 2.

Table 2 – The elemental composition of nitrogen fertilizer (PU)

	Elements	C (%)	N (%)	O (%)
PU50	(PVA: U) (50:50) wt.%	28.79	34.09	37.58

Preparation of mixed fertilizer (SLF+PU50). Mixed fertilizers (SLF+PU50) were a 50/50 w/v mixture of SLF with concentrations ranging from 5, 10, 30, 50, and 50% nitrogen fertilizer PU50. Mixed fertilizers were used with a constant concentration of 1% w/v using distilled water.

Experimental design and treatment. The crop plant selected for the present study was *Lycopersicon esculentum* (tomato). The hybrid tomato seeds (Pearl-F₁) were purchased from the local market and kept for one hour in a glass beaker with fresh water. Only the seeds that sank at the bottom of the beaker were used in the experiment. The seeds were carefully sewn in plastic trays, and the compost soil was kept wet by spraying with water daily. After two weeks, the germinated seedlings were transferred and planted in plastic pots. The seedlings were planted 5 cm deep into the soil and the depression was then loosely covered back by the soil. The soil was air-dried, sieved, and packed (13.5 kg/pot), and was properly filled in 15 pots.

The day on which the seedlings were planted in the pot was treated as day zero (Figure 1). The plants were watered every day or on alternate days depending on the requirement.

All 3 sets were prepared in five replicates. Mixed fertilizer treatment was given to the plants namely (SLF+PU50) and a set of control plants. In each of the treatments, 500 mL (1% w/v) of SLF+PU50 was applied directly to the soil. The first treatment was given to 15-day-old seedlings. Thereafter, the treatments were given at intervals of 15 days each until 90 days. The control set was watered only with tap water without any fertilizers.

Physical and chemical properties of the soil. In this study, the soil's physical and chemical properties were analyzed before the addition of the mixed fertilizers in different concentrations to the experimental soil to know the type and properties

of the soil. The results are presented in Table 3. The ingredients of the experimental soil were a mixture of clay (56.63%), fine sand (14.22%), and silt (24.15%).

The chemical properties of the soil were 1.4 mhos/cm³, 81.0 ppm N, 3.04 ppm P, 40.8 ppm K, 0.6 ppm of organic matter and pH was 7.8.



Figure 1 – Tomato plants after two weeks of germination

Table 3 – The physical and chemical properties of the soil

Physical properties	
Sand	56.63 (%)
Silt	24.15 (%)
Clay	14.22 (%)
Soil texture	Sandy loam
Chemical properties	
pH	7.8
Ec	1.4 (mhos/cm ³)
Available N	81.0 (ppm)
Available P	3.04 (ppm)
Available K	40.8 (ppm)
Organic matter	1.6 (%)

Data recorded. Vegetative growth. Plant height, number of major lateral branches, number of leaves, leaf area, and fresh and dry weights of shoots were measured at 4 and 8 weeks.

Chemical composition. Leaves disks were collected 4 and 8 weeks after transplanting to assess chlorophyll a, b according to the method described by Sartory and Grobbelaar [36]. Total carbohydrate content in dry matter of leaves was determined spectrophotometrically method described by Dubois et al. [37]. Nitrogen, phosphorus, and potassium elements were determined in the leaves of tomato

plants via digestion procedure according to Piper [38]. Nitrogen content was determined by the modified micro-Kjeldahl method as described by Pregl [39]. Phosphorus and potassium contents in the sample were estimated using ammonium molybdate and flame photometer methods respectively, according to Chapman [40].

Flowering and fruit yield. The number of nodes bearing the first flower, the number of flower clusters per plant, the number of flowers per cluster, the number of flowers per plant, the weight, and the number of fruits per plant were all recorded.

Physical characteristics of fruits. The fruit shape index was calculated using the ratio of vertical to horizontal diameters. Fruit volume was determined by using the immersion method.

Chemical characteristics of fruits. The soluble solids content (SSC) was assessed using a hand refractometer and the AOAC technique [41]. The technique published by AOAC [42] was used to calculate titratable acidity. The ascorbic acid concentration (vitamin C) was tested following AOAC guidelines [43]. Lycopene in tomato samples was extracted using hexane: ethanol: acetone (2:1:1) (v/v) mixture according to Sharma and Le Maguer's technique [44].

Statistical analysis. The data calculated on various variables were subjected to analysis of variance (ANOVA) to identify differences between treatments and their interactions. The Least Significant

Difference (LSD at 5%) test was used to separate the means. The ANOVA and LSD were computed using the statistical computer program Statistix 8.1 [45].

Results and discussion

Plant height (cm). The findings shown in Figure 2 showed that the combination fertilizers (SLF + PU50) had a highly significant ($p < 0.05$) effect on plant height at 4 and 8 weeks. Plant height increased when SLF concentrations

decreased from 50 to 10%. Plant height treated with 10% SLF + PU50 was substantially greater than control plants and other treatments at 4 and 8 weeks. Treatments with 10% SLF + PU50 mixed fertilizer performed best, followed by 30% SLF + PU50, 50% SLF + PU50, and 5% SLF + PU50. The increase in tomato plant height caused by combined fertilizer (SLF + PU50) might be attributed to hormone components such as cytokinins and auxins in SLF and nitrogen in PU50, which promote plant height.

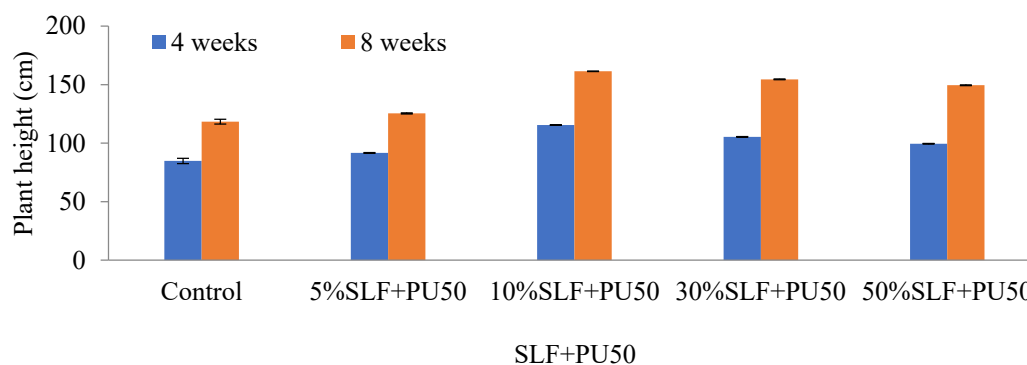


Figure 2 – Effect of mixed fertilizer on tomato plant height

Polyvinyl alcohol-urea blend (PU) has a cross-linked structure of hydrophilic urea. The presence of polyvinyl alcohol improves the ability to adsorb the metals from soil and seaweed. This, in turn, improves the soil's water-holding capacity, regains its fertility, and in sustainable manner for improved plant growth [13,46-48]. Similar results were reported by Wakifatul et al. [49] on soybeans and Cheng et al. [50] on lettuce, who found that fertilizer treatment, i.e., a blend of SLF and organic fertilizer, increased plant height.

Number of lateral branches. The effect of mixed fertilizer (SLF + PU50) on lateral branch numbers per tomato plant is shown in Figure 3. The treatment (10% SLF + PU50) resulted in a substantial increase in lateral branch numbers per tomato plant at the 5% level of probability when compared to the mixed fertilizers (30% SLF + PU50), (50% SLF + PU50), and control plants. At 4 and 8 weeks, the plants treated with mixed fertilizer (10% SLF + PU50) had the most lateral branches compared to the other treatments. The 10% SLF + PU50 treatment increased lateral branch numbers by 61.7 and 79.6% at 4 and 8 weeks, respectively, compared to the control, which was expected due to the positive effect of mixed 10% SLF

with PU50 (N: 34.1%) on soil edifice environmental conditions, which affected tomato plant vegetative growth [51]. These findings were consistent with those reported by Sridhar and Rengasamy [52-54] on *Tagetes erecta* and chili, who discovered that the best two interaction treatments for increasing lateral branch number per plant were 10% SLF combined with 50% recommended rate of chemical fertilizer. The plants treated with 5% SLF + PU50 at 4 and 8 weeks produced the fewest lateral branches.

Number of leaves per plant. Figure 4 shows that the application of mixed fertilizer (SLF + PU50) at 8 weeks induced a substantial increase in the number of leaves per plant at the 5% probability level when compared to the treatment of mixed fertilizer at 4 weeks. The treatment with 10% SLF + PU50 produced the most leaves per plant (78.5 and 125.6) at 4 and 8 weeks, respectively, while the treatment with 5% SLF + PU50 produced the fewest leaves per plant (35.4 and 74.5) at 4 and 8 weeks, respectively. This is due to the continuous release of nutrients from SLF as well as nitrogen from PU50. The increase in leaves number following mixed fertilizer (10% SLF + PU50) treatments proved the effect of mixed fertilizer in enhancing soil physical qualities and promoting

vegetative growth in leafy vegetables [55-57]. Dawa et al. [24, 25] discovered that foliar application of seaweed extract with chicken manure as a source of organic fertilizer and in the presence of biofertilizers increased vegetative plant development and N, P, and

K percentages in leaves on pepper and tomato plants. According to Khan et al. [58], combining N with organic fertilizer resulted in higher plant height and number of leaves of pepper plants than using organic or biofertilizers alone.

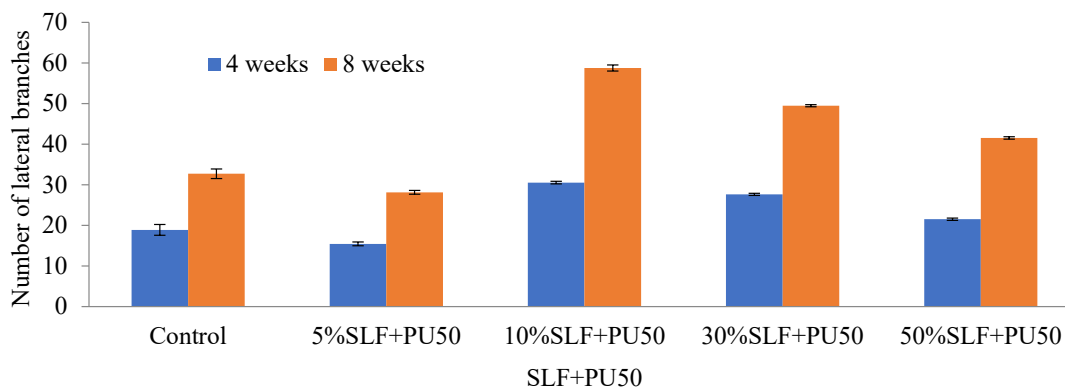


Figure 3 – Effect of mixed fertilizer on the number of lateral branches per tomato plant

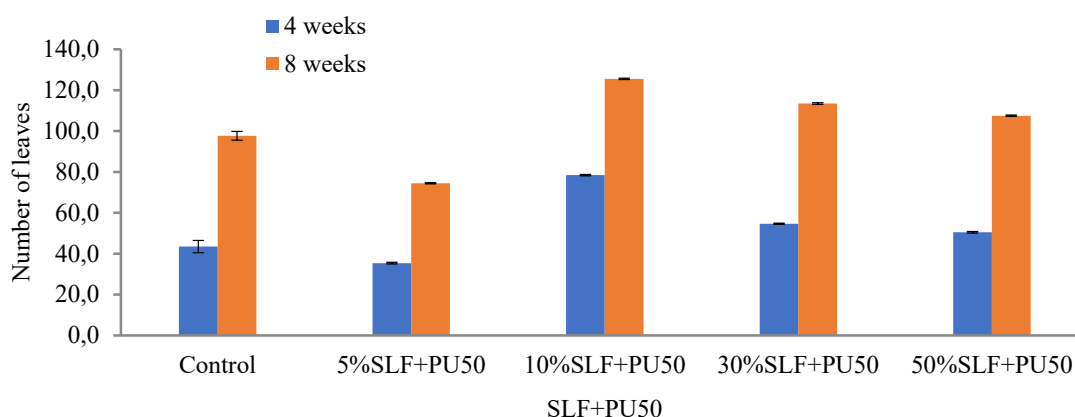


Figure 4 – Effect of mixed fertilizer on the number of leaves per tomato plant

Leaf area (cm²). Figure 5 depicts the effect of a mixed fertilizer (SLF + PU50) on leaf area after 4 and 8 weeks of growth. When compared to control plants, the usage of mixed fertilizer resulted in substantial increases ($p < 0.05$) in leaf area. The tomato plants' leaf area rose when the SLF content in the mixed fertilizer was reduced from 50 to 10%. Plants fertilized with 10% SLF + PU50 had the largest leaf areas, with 265.9 and 291.275 cm², respectively, whereas plants fed with 50% SLF + PU50 had the smallest leaf areas. At 4 and 8 weeks, SLF + PU50 had leaf areas of 231.0 and 256.15 cm², respectively.

Mixed fertilizer (10% SLF + PU50) can be given to tomato plants to improve the nutritional content

of the soil and, as a result, increase the vegetative growth of tomato plants. The leaf area measurement on the control plants was the smallest. These findings agreed with those of Ogundare et al. [59], Dawa et al. [24], and Sridhar and Rengasamy [54], who found that combining SLF with chemical fertilizer enhanced leaf area in tomato plants and chili plants, respectively. Several studies found that combining low-level N fertilizer or NPK with biofertilizer improved citrus plant leaf area more than using high-level N fertilizer or NPK in a single application or coupled with biofertilizer [60,61].

The fresh and dry weight of shoots (g/ plant). Figure 6 shows that the combined fertilizer (10% SLF + PU50) induced a substantial increase in the

fresh and dry weight of shoots at the 5% probability level when compared to the control plants and other treatments. This might be because seaweed contains growth-promoting substances, as well as nitrogen in PU50 fertilizer. Nitrogen is essential for plant growth because it promotes protein synthesis, amino acid synthesis, enzyme, and chlorophyll formation, which affects cell division, the number of leaves and branches per plant, and dry matter accumulation [24, 49, 62].

The increased percentages of fresh weight of shoots over non-fertilized treatments ranged from 14.7 to 34.4 % at 4 weeks and from 88.3 to 160.1% at 8 weeks, with decreasing concentrations of SLF in the mixed fertilizers ranging from 50 to 10%.

The mixed fertilizer 5% SLF+PU50 had no significant effect on the fresh and dry weights of the shoots. The treatment of 10% SLF + PU50 at 8

weeks led to the greatest percentage values of fresh and dry weights of tomato shoots (160.1 and 159.4%, respectively).

Chlorophyll (a, b) content (mg/ dm²). The contents of chlorophyll a and b in tomato leaves were influenced by mixed fertilizer (SLF + PU50) (Figure 7). The treatment (SLF + PU50) resulted in a substantial increase ($p < 0.05$) in leaf chlorophyll a and b contents compared to control plants at 4 and 8 weeks. Plants fertilized with 10% SLF + PU50, on the other hand, had the highest chlorophyll (a, b) concentrations in leaves, followed by plants fertilized with 30% SLF/PU50, 50% SLF + PU50, and 5% SLF + PU50 at 4 and 8 weeks. The increase in chlorophyll content is caused by cytokines found in seaweed extract and nitrogen found in PU fertilizers, both of which drive physiological activities and increase chlorophyll in plants [63, 64].

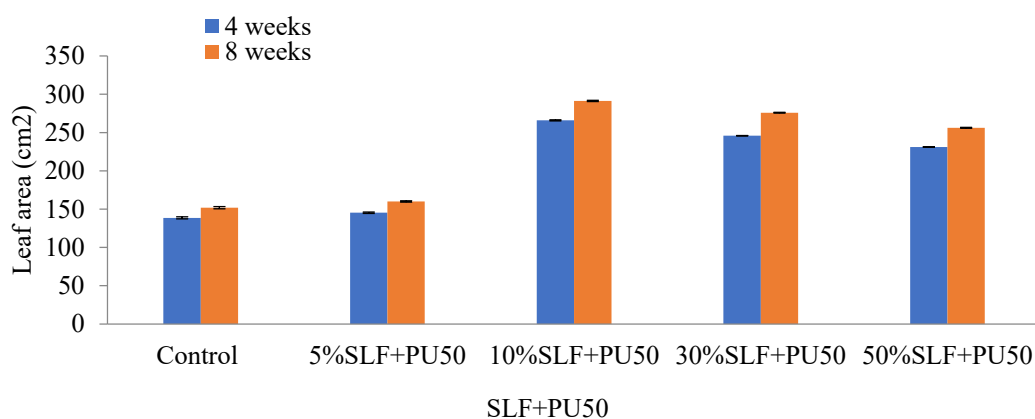


Figure 5 – Effect of mixed fertilizer on the tomato leaf area

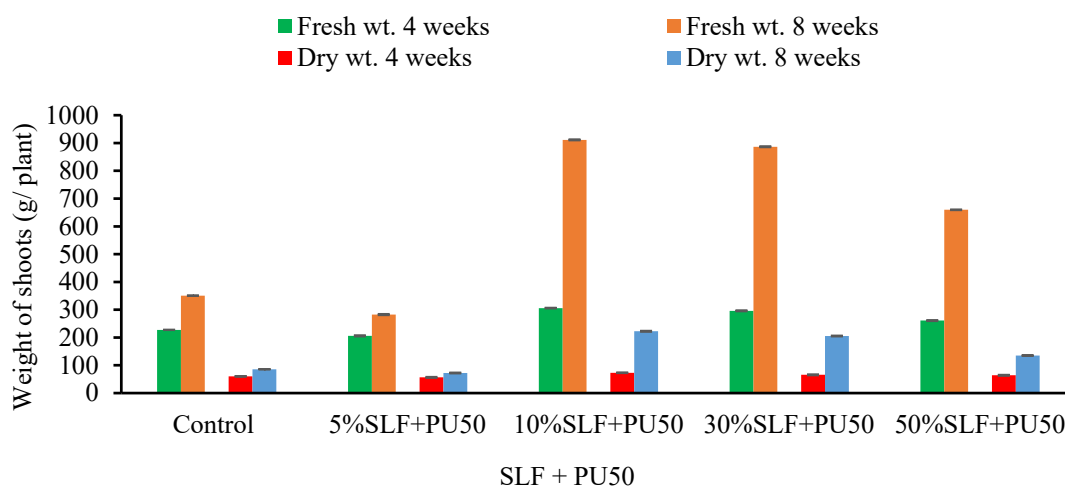


Figure 6 – Effect of mixed fertilizer on shoot fresh and dry weights per tomato plant

These findings were consistent with those reported by Sridhar and Rengasamy [54], Zeid [65], Samane et al. [66], and El-Tantawy [67], who investigated the effect of mixed fertilizers (10% SLF of *S. wightii* + 50% chemical fertilizer including urea, superphosphate, and potash), and spraying

of chitosan and aminofort on the photosynthetic pigments in *A. hypogea*, *C. annuum* (Chilli) and tomato leaves, respectively. The results revealed that the highest concentration of photosynthetic pigments was achieved by the interaction between seaweed extract liquid and nitrogen fertilizers.

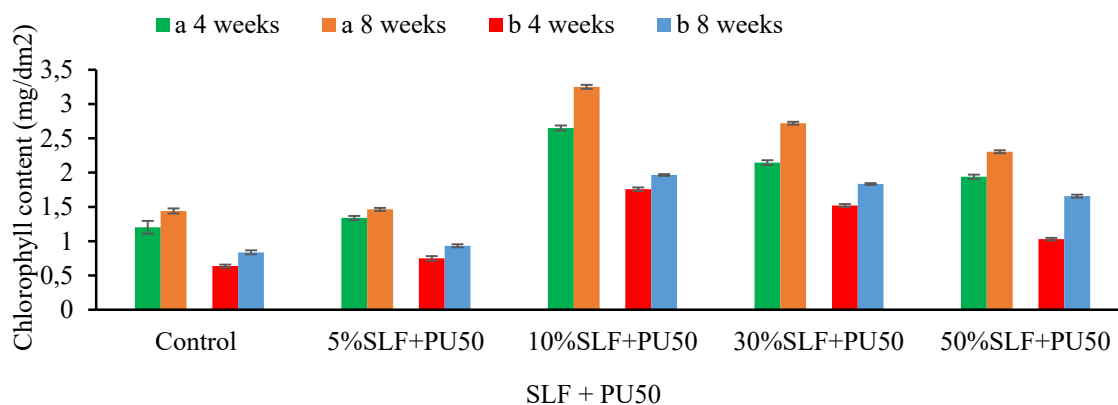


Figure 7 – Effect of mixed fertilizer on chlorophylls a and b in leaves of tomato plants

Carbohydrate content (%). Figure 8 shows the effect of different mixed concentrations of SLF with PU50 (N: 34.1%) on total carbohydrate content in tomato plant leaves. The results revealed that the combined fertilizers (SLF + PU50) induced a significant increment ($p < 0.05$) in leaf carbohydrate content when compared to the control plants. This is due to enhanced nitrogen photosynthetic activity and carbohydrate production and accumulation. Furthermore, the interaction between seaweed and chemical fertilizer played an important role in improving plant growth through the biosynthesis of endogenous hormones of seaweed which are responsible for promoting plant growth [54]. The highest value of total leaf carbohydrate content (17.75%) was detected in tomato plants fertilized with 10% SLF + PU50, whereas the lowest leaf carbohydrate content (12.3%) was obtained from plants fertilized with mixed fertilizer (5% SLF + PU50) at 8 weeks. Therefore, it could be concluded that the combined effect of 10% SLF with PU50 has met the required micronutrients in tomato plants than 30 and 50% SLF combined with PU50. With the use of PU and SLF, nutrients are released at a slower rate throughout the seasons, and plants are able to take up most of the nutrients without waste by leaching. This result following with the study of Nayan et al., [68], who found that polyvinyl alcohol (PVA) blended with starch and chitosan to release the nutrients directly to

the root of the plants, decrease the nitrogen loss and reduce water and soil pollution.

Nitrogen, phosphorus, and potassium content (%). Figure 9 shows the effect of combined fertilizers (SLF + PU50) at varying concentrations of SLF on nutrient content in tomato plant leaves. When compared to control plants, mixed fertilizers caused significant increments ($p < 0.05$) in leaf nitrogen, phosphorus, and potassium percentages. However, higher nitrogen (5.8%), phosphorus (0.78%) and potassium (3.18%) contents were recorded by tomato plants fertilized with 10% SLF + PU50, while lower nitrogen (3.5%), phosphorus (0.45%), and potassium (2.17%) contents were recorded by tomato plants fertilized with 5% SLF + PU50 at 8 weeks as compared to control plants (3.29%, 0.41% and 1.94% respectively) at 8 weeks.

The purpose of combining PU and SLF is to speed up the uptake of nutrients from the soil and SLF, resulting in higher nutrient percentages in plant leaves. These results are supported by Mikkelsen [69, 70]. The presence of marine bioactive substances in seaweed extract and nitrogen in PU enhances stomata uptake efficiency in treated plants compared to non-treated plants [71, 72]. According to Paul and Mannan [73], Asadu and Unagwu [74], Dawa et al. [24], and Sridhar and Rengasamy [54], the nutrient percentages in tomato leaves were influenced by the mixture of different fertilizer compounds such as organic, inorganic, chemical, and seaweed.

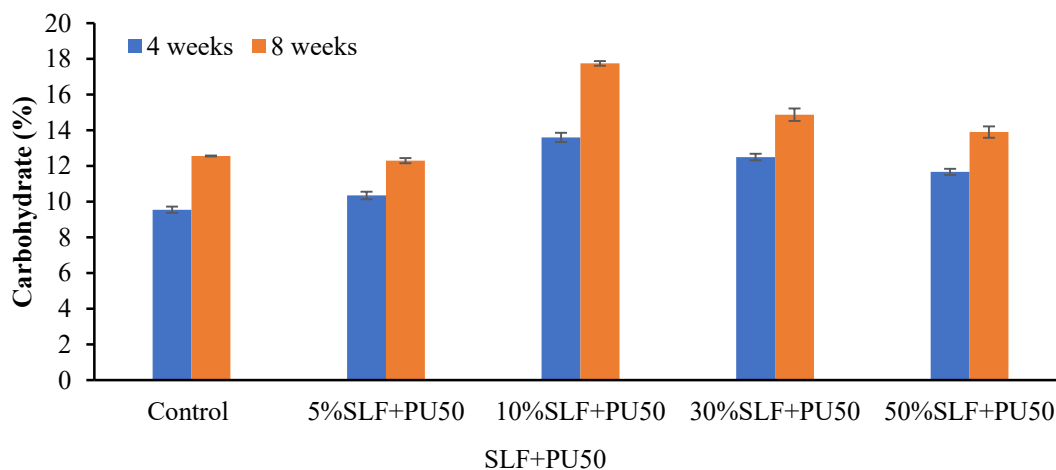


Figure 8 – Effect of mixed fertilizer on carbohydrate in leaves of tomato plant

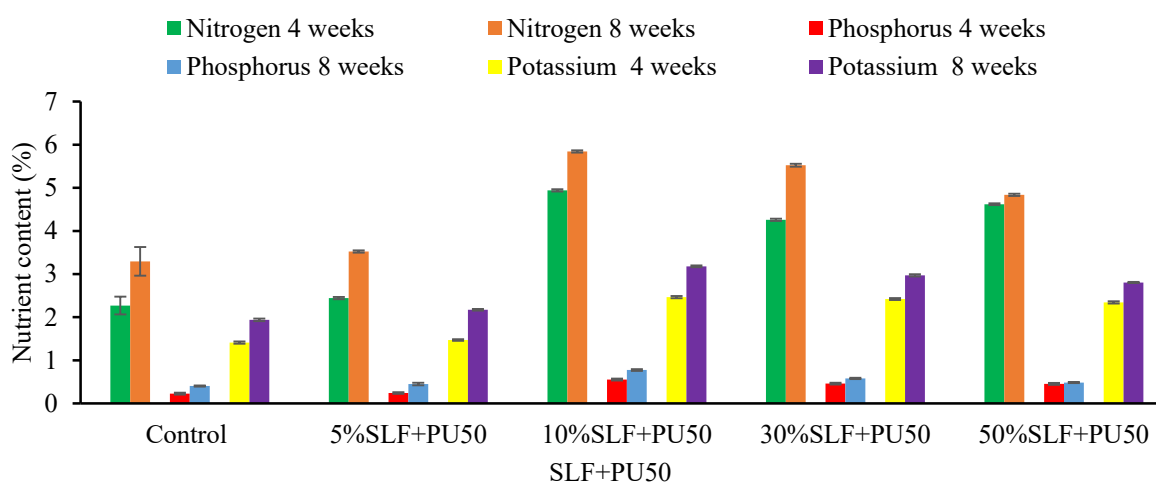


Figure 9 – Effect of mixed fertilizer on nitrogen, phosphorus, and potassium percentages in leaves of tomato plants

Characteristics of flowers. The results in Figures 10 and 11 showed that the mixed fertilizers (SLF + PU50) caused significant increment ($p < 0.05$) in the node number bearing the first flower, the number of flower clusters per plant, and the number of flowers per cluster, compared to the control plants.

An increased in the concentration of SLF in mixed fertilizer (SLF + PU50) from 5 to 10% resulted in increased node number bearing from 6.07 to 9.83, the number of flower clusters per plant from 15.30 to 33.44, the number of flowers per cluster from 4.40 to 9.13 (Figure 10) and the number of flowers per plant from 65.28 to 105.63 (Figure 11).

The concentration of SLF in mixed fertilizer (SLF + PU50) was increased from 10 to 50%, which resulted in a reduction in the above flowering characters. Tomato plants fertilized with 10% SLF

+ PU50 produced more flower characteristics than those treated with 30% SLF + PU50, 50% SLF + PU50, 5% SLF + PU50, and control. This might be attributed to the presence of plant growth regulating substances and hormones in seaweed, as well as nitrogen in PU, which may encourage flowering by initiating robust plant growth.

The findings were consistent with those of Najaf et al. [75] and Ilupeju et al. [76], who detected a highly significant increase in the number of flowers on tomato plants treated with nitrogen fertilizer and two types of biofertilizers. Wakifatul et al. [49] reported that the interaction of seaweed with cattle urine enhanced the flower characters of soybean plants. Sridhar and Rengasamy [52,53] observed a similar behavior while studying the interaction of SLF with chemical fertilizer on the flowers of *Tagetes erecta*.

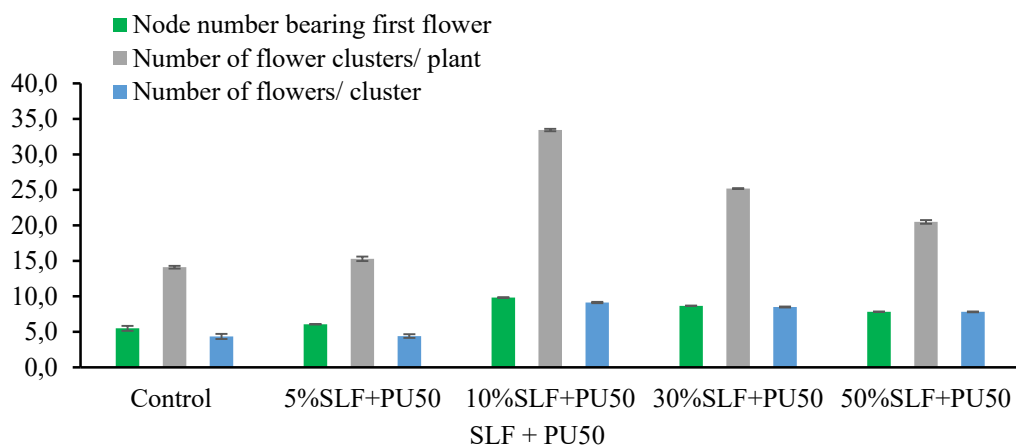


Figure 10 – Effect of mixed fertilizer on node number bearing first flower, number of flower clusters per plant and number of flowers per cluster

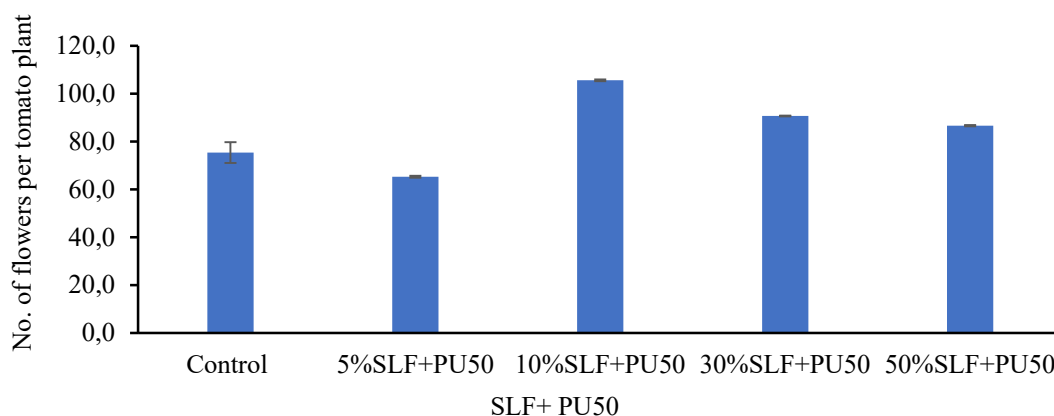


Figure 11 – Effect of mixed fertilizer on the number of flowers per tomato plant

Number of fruits per plant. The results in Figure 12 showed the mixed fertilizer (SLF + PU50) at a concentration of 10% SLF caused a significant increment at 5% probability level in the number of fruits per plant, compared to other treatment and the control plants. The highest number of fruits per plant (37.48) was present in the (10% SLF + PU50) treatment, while the lowest number of fruits per plant (26.25) was observed in (50% SLF + PU50), compared to the control plants (24.25). The increased number of fruits per plant might be due to the presence of some growth-promoting substances in SLF and nitrogen in PU. This might have helped in producing a higher amount of carbohydrates, which might have translocated from source (leaf) to reproductive parts (sink), resulting in a greater number of fruits [77-79]. This result is similar to Juárez-Maldonado et al. [80] and Pinedo et al. [12], who found an increase

in the number of tomato fruits treated with copper encapsulated in chitosan-polyvinyl alcohol. The same behaviour was reported by Ogundare et al. [59] and Libert et al. [81] when they studied the influence of the interaction between organic and inorganic fertilizers on tomato fruit yield.

Weight and volume of fruits. Figures 13-15 showed that the combination fertilizer (SLF + PU50) at a concentration of 10% SLF caused a significant increment at a 5% probability level in the fruit weight, fruit volume and shape index of fruit compared to all other treatments and the control plants. The application 10% SLF + PU50 increased fruit weight (154.9%) (Figure 13), fruit volume (42.7%) (Figure 14) and shape index of fruit (31.8%) (Figure 15), while application 5% SLF + PU50 increased fruit weight (21.6%) and fruit volume (4.2%), compared to the control plants.

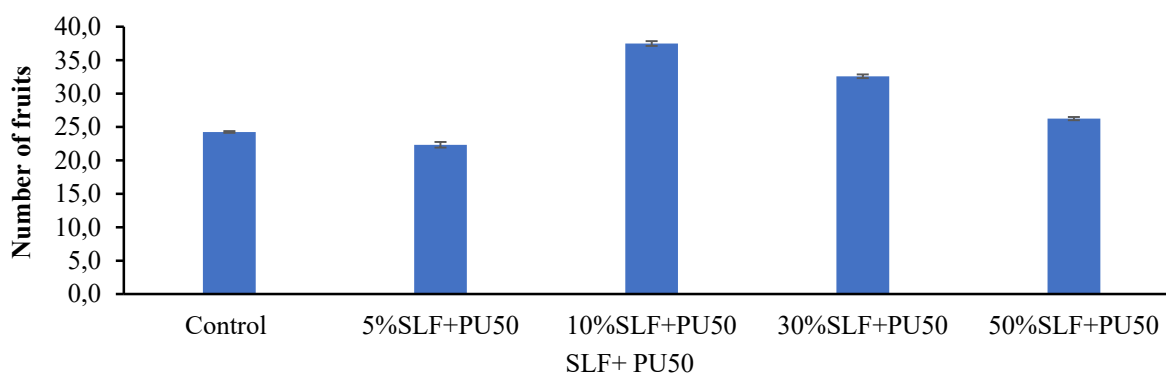


Figure 12 – Effect of mixed fertilizer on the number of fruits per tomato plant

The enhanced weight, volume, and shape index of fruit over the control were attributed to the interaction fertilizer (SLF + PU50) providing the micronutrients to the plants in an optimal range. Similar findings were reported by Dimitrios *et al.* [82], Chanda *et al.* [83], Najaf *et al.* [75], Salama *et*

al. [84], Iiupeju *et al.* [76], and Ogundare *et al.* [59], who found that the application of mixed fertilizers (cow manure + NPK) resulted in the highest tomato fruit growth, which could be interpreted as the release of nutrients from organic and inorganic fertilizers at different times.

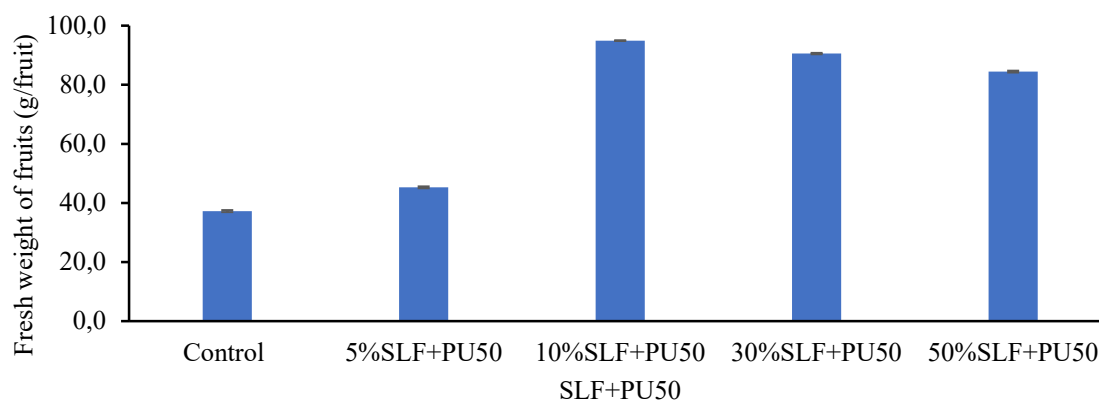


Figure 13 – Effect of mixed fertilizer on the fresh weight of tomato fruits

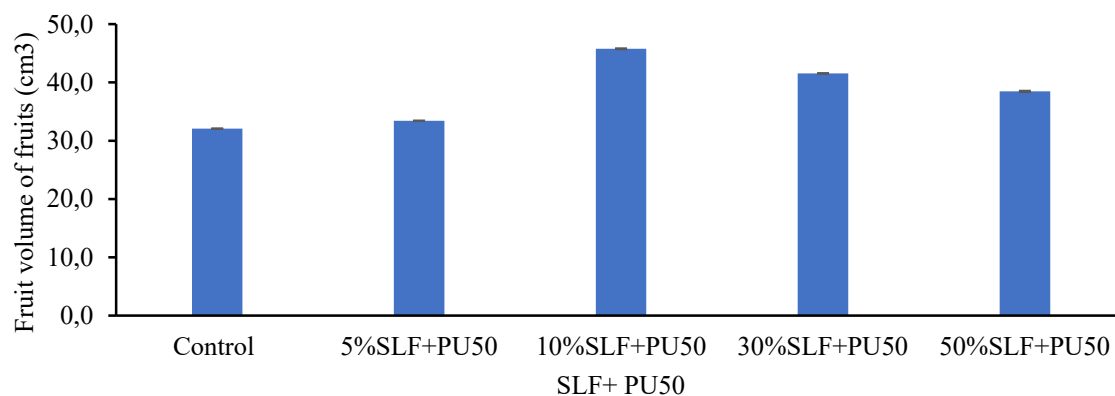


Figure 14 – Effect of mixed fertilizer on the volume of tomato fruits

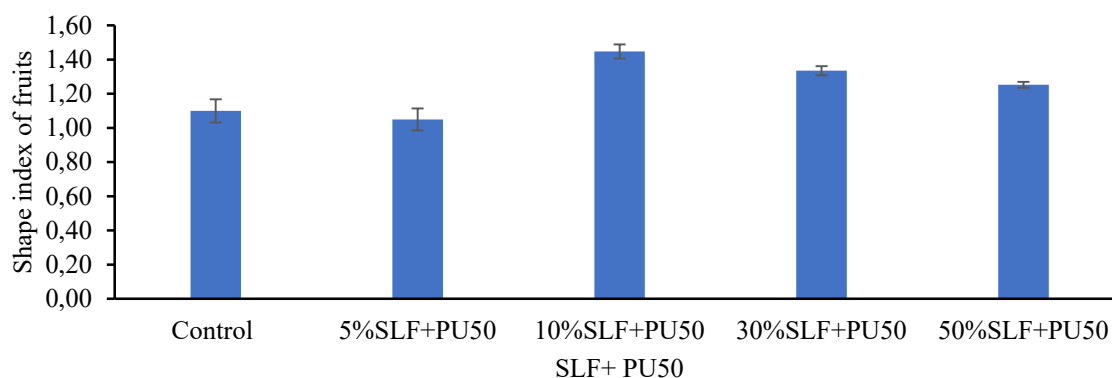


Figure 15 – Effect of mixed fertilizer on the shape index of tomato fruits

Chemical content of fruits. The results in Figures 16 and 17 demonstrated that the mixed fertilizer (SLF + PU50) at a concentration of 10% SLF caused a considerable increase in soluble solids content (SSC), acidity, vitamin C, and lycopene pigment in tomato fruits when compared

to other treatments and control plants. Soluble solid concentration (3.72%) was lower in tomato fruits treated with mixed fertilizer (5% SLF + PU50). While tomato fruits treated with (10% SLF + PU50) had a greater SSC (6.32%) than control plants (3.60%) (Figure 16).

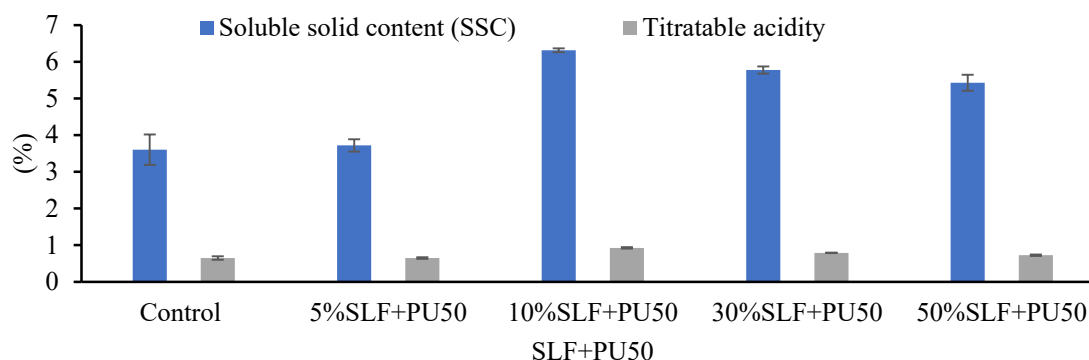


Figure 16 – Effect of mixed fertilizer on SSC and titrateable acidity in tomato fruits

Ilupeju et al. [76] obtained greater total soluble solids with 100% recommended doses of mixed fertilizers and biofertilizers. When compared to the control plants, the 10% SLF + PU50 treatment had the highest titrateable acid content (0.93%) in the tomato fruits, while the 5% SLF + PU50 treatment had the lowest titrateable acid percentage (0.65). Hasanein et al. [85] found a similar effect of biofertilizers and amino acids on tomato fruits. The results can be explained by nutrient availability to the plants and their balanced supply from mixed fertilizers SLF and PU50 in the required amounts during fruit formation.

Figure 17 shows that the ascorbic acid content (23.78) and lycopene (41.75) in tomato fruits treated with mixed fertilizers (10% SLF + PU50) were higher

than in other treatments and control plants. Fruits produced by plants treated with 5% SLF + PU50 and control had lower percentages.

This was consistent with the findings of Peyvast et al. [86], who discovered that mixed fertilizers (nitrogen and potassium) boosted ascorbic acid levels in tomato fruits. These findings confirm that the mixed fertilizer (10% SLF + PU50) has a positive effect on soluble solids content (SSC), acidity, vitamin C, and lycopene levels in tomato fruits. A similar finding was reported by Ilupeju et al. [76] and Makinde et al. [87] when they investigated the effects of organic and inorganic fertilizer interactions on the growth, fruit production, nutritional, and lycopene content of three tomato varieties [88, 89].

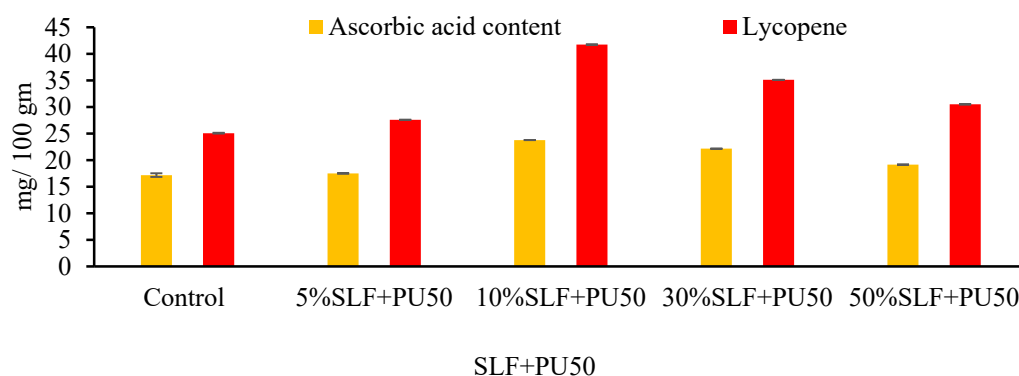


Figure 17 – Effect of mixed fertilizer on ascorbic acid and lycopene in tomato fruits

Conclusion

These experiments aimed to investigate the effect of mixed fertilizer (SLF + PU50) on the growth, yield, and chemical composition of tomato plants (*L. esculentum* Mill). To achieve the goal of this study, the experiment was designed in a randomized complete block design (RCBD) with each treatment replicated five times. The basic properties of the experimental soil have been tested. Soil pH, EC, available N, P and K were 7.8, 1.4 mhos/cm³, 81.0 ppm, 3.04 ppm and 40.8 ppm, respectively. Treatments included: control (without fertilizers), four mixed fertilizer concentrations (SLF + PU50) (5% SLF + PU50, 10SLF + PU50, 30SLF + PU50 and 50% SLF + PU50). The data were analyzed using variance analysis (ANOVA) and compared using fertilizer-free control. Mixed fertilizer-treated tomato plants (10% SLF + PU50) showed maximum growth and control between the various experimental concentrations. Tomato plants fertilized with 10% SLF + PU50 produced the highest vegetative growth, flower, and fruit characteristics. Tomato fruit yields (54.5%) were best applied with mixed fertilizers (SLF + PU50) at 10% SLF + PU50. It may be recommended to use 10% SLF mixed with PU50 to obtain high vegetative growth and yield tomato fruits.

References

1. Nieves-García V., van der Valk O., Elings A. (2011) Mexican Protected Horticulture, Wageningen University and Research, Netherlands.
2. Kotkov Z., Lachman J., Hejtmnkov A., Hejtmnkov K. (2011) Determination of antioxidant activity and antioxidant content in tomato varieties and evaluation of mutual interactions between

antioxidants. *LWT – Food of Science and & Technology*, vol. 44, pp. 1703-1710.

3. Vallverdú-Queralt A., Medina-Remón A., Martínez-Huélamo M., Jáuregui O., et al. (2011) Phenolic profile and hydrophilic antioxidant capacity as chemotaxonomic markers of tomato varieties. *Journal of Agriculture Food Chemistry*, vol. 59, pp. 3994-4001.

4. Sharma H.S.S., Fleming C., Selby C., Rao J.R., et al. (2014) Plant biostimulants: a review on the processing of macroalgae and use of extracts for crop management to reduce abiotic and biotic stresses. *Journal of Applied Phycology*, vol. 26, pp. 465-490.

5. Lin J., Lu H., Chen C. (2003) Effects of seed coating with chitosan-PVA film on quality of rice seedlings. *Subtropical Plant Science*, vol. 32, pp. 19-21.

6. Ruan S., Xue Q. (2002) Effects of chitosan coating on seed germination and salt-tolerance of seedlings in hybrid rice (*Oryza sativa* L.). *Acta Agronomica Sinica*, vol. 28, pp. 803-808.

7. Marsh M.H., Groenevelt P.H. (1992) Effect of surface application of polyvinyl alcohol on phosphorus losses in runoff and on corn growth. *Journal of Environmental Quality*, vol. 21, pp. 36-40.

8. Wang N., Liu M., Qin Z. (2006) Effects of PVA on tissue culture of Dongzao jujube (*Ziziphus jujuba*) and *Z. acidojujuba*. *Journal of Fruit Science*, vol. 23, no. 2, pp. 301-303.

9. Zhang S., Ke S., Zhu W.E.L. (2007) The influence of polyvinyl alcohol on vitrification in tissue culture of woad. *Journal of Tangshan Teach Coll*, vol. 29, no. 5, pp. 36-38.

10. Qingrong S., Hongyan S., Richard L.B., Li X. (2009) Effect of polyvinyl alcohol on in vitro rooting capacity of shoots in pear clones (*Pyrus communis* L.) of different ploidy. *Plant Cell, Tissue and Organ Culture*, vol. 99, pp. 299-304.

11. Hipólito H.-H., Susana G.-M., Adalberto B.-M., Hortensia O.-O., et al. (2018) Effects of Chitosan-PVA and Cu Nanoparticles on the Growth and Antioxidant Capacity of Tomato under Saline Stress. *Molecules*, vol. 23, pp. 1-15.
12. Pinedo G.Z., Hernández F.A., Ortega O.H., Benavides M.A., et al. (2017) Cu Nanoparticles in Hydrogels of Chitosan-PVA Affects the Characteristics of Post-Harvest and Bioactive Compounds of Jalapeño Pepper. *Molecules*, vol. 22, pp. 926, pp. 1-14.
13. Guo M., Liu M., Zhan F., Wu L. (2005) Preparation and properties of a slow-release membrane-encapsulated urea fertilizer with superabsorbent and moisture preservation. *Industrial and Engineering Chemistry Research*, vol. 44, no. 12, pp. 4206-4211.
14. Moe K., Kumudra W.M., Kyaw K.W., Takeo Y. (2017) Combined effect of organic manures and inorganic fertilizers on the growth and yield of hybrid rice (Palethwe-1). *American Journal of Plant Sciences*, vol. 8, pp. 1022-1042.
15. Mubeen K., Iqbal A., Hussain M., Zahoor F., et al. (2013) Impact of Nitrogen and Phosphorus on the Growth, Yield and Quality of Maize (*Zea Mays* L.) Fodder in Pakistan. *Philippine Journal of Crop Science*, vol. 38, no. 2, pp. 43-46.
16. Huang S., Weijian Z.W., Yu X., Huang Q. (2010) Effects of long-term fertilization on corn productivity and its sustainability in an Ultisol of southern China. *Agriculture, Ecosystems and Environment*, vol. 138, pp. 44-50.
17. Mahajan A., Bhagat R.M., Gupta R.D. (2008) Integrated nutrient management in sustainable rice-wheat cropping system for food security in India. *SAARC Journal of Agriculture*, vol. 6, pp.149-163.
18. Schoebitz M., Vidal G. (2016) Microbial consortium and pig slurry to improve chemical properties of degraded soil and nutrient plant uptake. *Journal of Soil Science and Plant Nutrition*, vol. 16, no. 1, pp. 226-236.
19. Singh B.K., Pathak K.A., Boopathi T., Deka B.C. (2010) Vermicompost and NPK fertilizer effects on morpho-physiological traits of plants, yield and quality of tomato fruits (*Solanum lycopersicum* L.). *Vegetable Crops Research Bulletin*, vol. 73, pp. 77-86.
20. Ayeni L.S., Omole T.O., Adeleye E.O., Ojeniyi S.O. (2010) Integrated application of poultry manure and NPK fertilizer on performance of tomato in derived savannah transition zone of Southwest Nigeria. *Nature and Science*, vol. 8, no. 2, pp. 50-54.
21. Adnan A.K., Hamida B., Zahid A., Muhammad S., et al. (2017) Effect of compost and inorganic fertilizers on yield and quality of tomato. *Academia Journal of Agricultural Research*, vol. 5, no. 10, pp. 287-293.
22. Makinde E.A., Ayoola A.A. (2008) Residual influence of early season crop fertilization. *American Journal of Agricultural and Biological Sciences*, vol. 3, no.4, pp. 712-715.
23. Akanbi W.B., Akande M.O., Adediran J.A. (2005) Suitability of composted maize straw and mineral nitrogen fertilizer for tomato production. *Journal of Vegetation Science*, vol. 11, no. 1, pp. 57-65.
24. Dawa K.K.A., Al-Gazar T.M., Abdel-Fatah A.M. (2013) Effect of chicken manure combined with bio-fertilizers, mineral fertilizer and some foliar applications on: 1-vegetative growth and some chemical constituents of tomato leaves. *Journal of Plant Production Mansoura University*, vol. 4, no. 10, pp. 1555-1570.
25. Dawa K.K., Abd El H.M., Nabi E., Swelam, W.E. (2012) Response of sweet pepper plants (vegetative growth and leaf chemical constituents) to organic, biofertilizers and some foliar application treatments, *Journal of Plant Production Mansoura University*, vol. 3, no. 9, pp. 2465 -2478.
26. Awosika O.E., Awodun M.A., Ojeniyi S.O. (2014) Comparative effect of pig manure and NPK fertilizer on agronomic performance of tomato (*Lycopersicon esculentum* Mill). *American Journal of Experimental Agriculture*, vol. 4, no. 11, pp. 1330-1338.
27. Prativa K.C., Bhattarai B.P. (2011) Effect of integrated nutrient management on the growth, yield and soil nutrient status in tomato. *Nepal Journal of Science and Technology*, vol. 12, pp. 23-28. <https://doi.org/10.3126/njst.v12i0.6474>
28. Prakash P., Amitesh M., Ritanjan N., Swetha S. (2018) Effect of seaweed liquid fertilizer and humic acid formulation on the growth and nutritional quality of *Abelmoschus esculentus*. *Asian Journal of Crop Science*, vol. 10, no.1, pp. 48-52.
29. Mukta S., Rahman M.M., Mortuza M.G. (2015) Yield and nutrient content of tomato as influenced by the application of vermicompost and chemical fertilizers. *Journal of Environmental Science & Natural Resources*, vol. 8, no. 2, pp.115-122.
30. Srijaya T.C., Pradeep P.J., Anil Chatterji. (2010) Effect of seaweed extract as an organic fertilizer on the growth enhancement of black mustard plant. *Journal of Coastal Environment*, vol.1, no. 2, pp. 137-150.
31. Ganapathy S.G., Sivakumar G. (2013) Effect of foliar spray from seaweed liquid fertilizer of *Ulva*

reticulata (Forsk) on *Vigna mungo* L. and their elemental composition using SEM-energy dispersive spectroscopic analysis. *Asian Pacific Journal of Reproduction*, vol. 2, no. 2, pp. 119-125.

32. Rathore S.S., Chaudhary D.R., Boricha G.N., Ghosh A. (2009) Effect of seaweed extract on the growth, yield and nutrient uptake of soybean (*Glycine max*) under rainfed condition. *Seaweed Research and Utilisation*, vol. 75, pp. 351-355.

33. Kalaivanan C., Chandrasekaran M., Venkatesalu V. (2012) Effect of seaweed liquid extract of *Caulerpa scalpelliformis* on growth and biochemical constituents of black gram (*Vigna mungo* (L.). *Hepper Phykos*, vol. 42, no. 2, pp. 46-53.

34. Humphries E.C. (1956) Mineral components and ash analysis. In: Rach K, MV Tracer (Eds.). *Modern Methods of Plant Analysis*. Berlin, pp. 468-502.

35. El-Sayed N., Lyazzat B., Hanan A., Yeligbayeva G., et al. (2018) The effect of blend ratios on physico-mechanical properties and miscibility of cross-linked poly (vinyl alcohol)/urea blends. *Journal of Physics Conference Series*, vol. 1123, no. 012066, pp. 1-9.

36. Sartory D.P., Grobbelaar J.U. (1984) Extraction of chlorophyll a, from freshwater phytoplankton for spectrophotometric analysis. *Hydrobiologia*, vol. 114, pp. 177-187.

37. Dubois M., Gilles K.A., Hamilton J., Roberts R., Smith F. (1956) Colorimetric method for determination of sugar and related substances. *Analytical Chemistry*, vol. 28, no. 3, pp. 350-356.

38. Piper C.S. (1947) Soil and Plant Analysis. The University of Adelaide, pp. 258-275.

39. Pregl F. (1945) Quantitative Organic Microanalysis. 4th Ed. J.&A. Churchill, Ltd., London.

40. Chapman H.D., Pratt P.F. (1961) Methods of analysis for soil, plant and water. University California Davis Agric Science, U.S.A.

41. AOAC. (1965). Official Method of Analysis of Association of Agricultural Chemists (10th Ed.).

42. AOAC. (2005). Official Method of Analysis of Association of Agricultural Chemists (15th Ed.).

43. AOAC. (1970). Official Method of Analysis of Association of Agricultural Chemists (10th Ed.).

44. Sharma S.K., Le Maguer M. (1996) Lycopene in tomatoes and tomato pulp fractions.

45. Mead R., Currnow R.N., Harted A.M. (1993) Statistical Methods in Agricultural and Experimental Biology. (2nd Ed.), pp. 54-60.

46. Wiśniewska M., Bogatyrov V., Ostolska I., Szewczuk-Karpisz K., et al. (2016) Impact poly(vinyl alcohol) adsorption on the surface characteristics of mixed oxide $Mn_xO_y-SiO_2$. *Adsorption*, vol. 22, pp. 417-423.

47. Nayan N.H.M., Hamzah M.S.A., Austad A., Muslih E.F., et al. (2019) Effect of Polyvinyl Alcohol/Chitosan Hydrogel Loaded with NPK Compound Fertilizer on *Capsicum sp.* Growth and Fruiting Yield Analysis, *MSAE2019-PFE28*, pp.164-167.

48. Kangkrana S., Kamalika S. (2018) Polyvinyl alcohol based hydrogels for urea release and Fe(III) uptake from soil medium. *Journal of Environmental Chemical Engineering*, vol. 6, pp. 736-744.

49. Wakifatul H., Kaimuddin, Syamsuddin G. (2015) Increasing the production of soybean (*Glycine Max* L.) by using mulch of rice straw and applying Poc (Liquid Organic Fertilizer) from seaweed (*Gracilaria* Sp.) and cattle's urine. *Journal of Biology, Agriculture and Healthcare*, vol. 5, no. 14, pp. 1-8.

50. Cheng-Wei L., Yu S., Bo-Ching C., Hung-Yu L. (2014) Effects of nitrogen fertilizers on the growth and nitrate content of lettuce (*Lactuca sativa* L.). *International Journal of Environmental Research and Public Health*, vol. 11, pp. 4427-4440.

51. Eiasu B.K. (2004) Potato yield and soil physical properties as affected by gel-polymer soil amendments and irrigation management. MSc. Agric. Thesis. University of Pretoria, Pretoria. South Africa.

52. Sridhar S., Rengasamy R. (2010) Effect of seaweed liquid fertilizer on the growth, biochemical constituents and yield of *Tagetes erecta*, under field trial. *Journal of Phytology*, vol. 2, no. 6, pp. 61-68.

53. Sridhar S., Rengasamy R. (2010) Studies on the effect of seaweed liquid fertilizer on the flowering plant *Tagetes erecta* in field trial. *Advances in Bioresearch*, vol. 1, no.2, pp. 29-34.

54. Sridhar S., Rengasamy R. (2012) The effect of *Sargassum wightii* extract on the growth, biochemical composition and yield of *Capsicum annum* under field trial. *International Journal of Current Science*, vol. 4, pp. 35-43.

55. Agyeman K., Osei-Bonsu I., Berchie J.N., Osei M.K., et al. (2014) Effect of poultry manure and different combinations of inorganic fertilizers on growth and yield of four tomato varieties in Ghana. *Agricultural Science*, vol. 2, pp. 27-34.

56. Sainju U.M., Singh B.P., Whitehead W.F. (2001) Comparison of the effects of cover crops and nitrogen fertilizer on tomato yield, root growth, and soil properties. *Scientia Horticulturae*, vol. 91, pp. 201-214.

57. Sethi S.K., Adhikary S.P. (2009) Effect of region-specific *Rhizobium* in combination with seaweed liquid fertilizer on vegetative growth and yield of *Arachis hypogea* and *Vigna mungo*. *Seaweed Research and Utilisation*, vol. 31, pp. 1-8.

58. Khan Z., Tiyagi S.A., Mohamood I., Rizvi R. (2012) Effect of N- fertilization, organic matter and biofertilizers on growth and yield of chili in relation to management of plant-parasitic nematods. *Turkish Journal of Botany*, vol. 36, pp. 73-81. doi:10.3906/bot-1009-60
59. Ogundare S.K., Babalola T.S., Hinmikaiye A.S., Oloniruha J.A. (2015) Growth and fruit yield of tomato as influenced by combined use of organic and inorganic fertilizer in Kabba, Nigeria. *European Journal of Agriculture and Forestry Research*, vol. 3, no. 3, pp. 48-56.
60. Ennab H.A. (2016) Effect of Organic Manures, Biofertilizers and NPK on Vegetative Growth, Yield, Fruit Quality and Soil Fertility of Eureka Lemon Trees (*Citrus limon* (L.) Burm.). *Journal of Soil Sciences and Agricultural Engineering Mansoura University*, vol. 7, no.10, pp. 767-774. doi: 10.21608/JSSAE.2016.40472
61. Khehra S., Bal, J.S. (2014) Influence of organic and inorganic nutrient sources on growth of lemon (*Citrus limon* (L.) Burm.) cv. Baramasi. *Journal of Experimental Biology and Agricultural Sciences*, vol. 2, no. 1S, pp. 126-129.
62. Chen J.S., Zhu R.F., Zhang Y.X. (2013) The effect of nitrogen addition on seed yield and yield components of *Leymus chinensis* in Songnen Plain, China. *Journal of Soil Science and Plant Nutrition*, vol. 13, no. 2, pp. 329-339.
63. Prasanna R., Jaiswal P., Singh Y.V., Singh P.K. (2008) Influence of biofertilizers and organic amendments on nitrogenase activity and phototrophic biomass of soil under wheat. *Acta Agronomica Hungarica*, vol. 56, no. 2, pp. 149-159.
64. Thirumaran G., Arumugam M., Arumugam R., Anantharaman P. (2009) Effect of seaweed liquid fertilizer on growth and pigment concentration of *Cyamopsis tetragonoloba* (L) Taub. *American-Eurasian Journal of Agronomy*, vol. 2, no. 2, pp. 50-56.
65. Zeid I. M. (2009) Effect of arginine and urea on polyamines content and growth of bean under salinity stress. *Acta Physiologiae Plantarum*, vol. 28, pp. 65-70.
66. Samane B.L., Mohammadreza S., Adel D.M., Mohammad M.V. (2014) Changes in nitrogen and chlorophyll density and leaf area of sweet basil (*Ocimum basilicum* L.) affected by biofertilizer and nitrogen application. *International Journal of Biosciences*, vol. 5, no. 9, pp. 256-265.
67. El-Tantawy E.M. (2009) Behavior of tomato plants as affected by spraying with chitosan and amino fort as natural stimulator substances under application of soil organic amendments. *Pakistan Journal of Biological Sciences*, vol. 12, pp. 1164-1173.
68. Nayan N.H.M., Mohd S.A.H., Abdussalam A.M.T., Amirah A.A.R., et al. (2018). Development of Polyvinyl Alcohol/Chitosan Hydrogel Loaded with Fertilizer Compound: Preparation, Properties and Effect on Seed Germination. *Journal of Science and Technology*, vol. 10, pp. 21-27.
69. Mikkelsen R.L. (1994) Using hydrophilic polymers to control nutrient release. *Fertilizer Research*, vol. 38, pp. 53-59.
70. Mikkelsen R. L. (1996) Using hydrophilic polymers to improve uptake of manganese fertilizers by soybeans [1995]. *Fertilizer Research*, vol. 41, pp. 87-92.
71. Mancuso S., Azzarello E., Mugnai S., Briand X. (2006) Marine bioactive substances (IPA extract) improve foliar ion uptake and water tolerance in potted *Vitis vinifera* plants. *Advances in Horticultural Science*, vol. 20, pp.156-161.
72. Khalid K.A. (2013) Effect of nitrogen fertilization on morphological and biochemical traits of some apiaceae crops under and region conditions in Egypt. *Nusantara Bioscience*, vol. 5, pp. 15-21.
73. Paul G.C., Mannan M.A. (2007) An integrated nutrient management approach to improve sugar productivity. *Sugar Tech*, vol. 9, no.1, pp. 28-35.
74. Asadu L.A., Unagwu B.O. (2012) Effect of combined poultry manure, and Inorganic fertilizer on maize performance in an Ultisol of Southeastern Nigeria. *Nigerian Journal of Soil Sciences*, vol. 22, no. 2, pp. 79-87.
75. Najaf D.S., Alemzadeh A.N., Sedighie D.F. (2008) Effect of different levels of nitrogen fertilizer with two types of bio-fertilizers on growth and yield of two cultivars of tomato (*Lycopersicon esculentum* Mill). *Asian Journal of Plant Science*, vol. 7no. 8, pp. 757-761.
76. Ilupeju E.A.O., Akanbi W.B., Olaniyi J.O., Lawal B.A., et al. (2015) Impact of organic and inorganic fertilizers on growth, fruit yield, nutritional and lycopene contents of three varieties of tomato (*Lycopersicon esculentum* Mill) in Ogbomoso, Nigeria. *African Journal of Biotechnology*, vol. 14, no. 31, pp. 2424-2433.
77. Sutharsan S., Nishanthi S., Srikrishnah S. (2014) Effects of foliar application of seaweed (*Sargassum crassifolium*) liquid extract on the performance of *Lycopersicon esculentum* Mill. In sandy regosol of Batticaloa District Sri Lanka. *American-Eurasian Journal of Agriculture & Environmental Science*, vol. 14, no. 12, pp.1386-1396.
78. El-Sharony T.F., El-Gioushy S.F., Amin, O.A. (2015) Effect of Foliar Application with Algae

and Plant Extracts on Growth, Yield and Fruit Quality of Fruitful Mango Trees Cv. Fagri Kalan. *Journal of Horticulture*, vol. 2, no. 4, pp. 1–6.

79. Pise N.M., Sabale A.B. (2010) Effect of seaweed concentrates on the growth and biochemical constituents of *Trigonella foenumgraecum* L. *Journal of Phytology*, vol. 2, pp. 50-56.

80. Juárez-Maldonado A., Ortega-Ortíz H., Pérez-Labrada F., Cadenas-Pliego G., et al. (2016) Cu Nanoparticles absorbed on chitosan hydrogels positively alter morphological, production, and quality characteristics of tomato. *Journal of Applied Botany and Food Quality*, vol. 89, pp. 183-189.

81. Libert B.T., Anne B., Emmanuel Y., Paul V.M., et al. (2009). Impact of organic and inorganic fertilizers on tomato vigor, yield and fruit composition under tropical andosol soil conditions. *Fruits*, vol. 64, pp.167-177.

82. Dimitrios B., Magdalini K., Ioannis R., Panayioti P., et al. (2018). Effects of organic and inorganic fertilization on yield and quality of processing tomato (*Lycopersicon esculentum* Mill). *Folia Horticulture*, vol. 30, no. 2, pp. 321-332.

83. Chanda G.K., Bhunia G., Chakraborty S.K. (2011) The effect of vermicompost and other fertilizers on cultivation of tomato plants. *Journal of Horticulture and Forestry*, vol. 3, no. 2, pp. 42-45.

84. Salama A.A., Nashwa A.I.A., El-Sayed H.E.K. (2017) Effect of deficit irrigation levels and NPK fertilization rates on tomato growth, yield and fruits quality. *Middle East Journal of Agriculture Research*, vol. 6, no.3, pp. 587-604.

85. Hasanein N.M., Abdrabbo M.A.A., El-Khulaifi Y.K. (2014) The effect of biofertilizers and amino acids on tomato production and water productivity under net-house conditions. *Arab Universities Journal of Agricultural Sciences*, vol. 22, no. 1, pp. 43-53.

86. Peyvast G., Olfati J.A., Ramezani-Kharazi P., Kamari-Shahmaleki S. (2009) Uptake of calcium nitrate and potassium phosphate from foliar fertilization by tomato. *Journal of Horticulture and Forestry*, vol. 1, no.1, pp. 007-013.

87. Makinde A.I., Jekanola O.O., Adedeji J.A., Awogbade A.L., et al. (2016) Impact of organic and inorganic fertilizers on the yield, lycopene and some minerals in tomato (*Lycopersicum esculentum*. Mill) fruit. *European Journal of Agriculture and Forestry Research*, vol. 4, no. 1, pp. 18 -26.

88. Bekbayeva L., Zakaria Z., Karpenyuk T., Goncharova A., Negim ES., Kaldanay K. (2021) Effects of NPK Fertilizers on the Growth, Yield and Chemical Content of Tomato (*Lycopersicon esculentum* L. Mill). Proceedings of the 6th International Conference on Fundamental and Applied Sciences. Springer Proceedings in Complexity. Springer, Singapore, 37-50.

89. Zakari Z. Bekbayeva L., Goncharova A.V., Negim E.-S. (2020) Effects of blended polyvinyl alcohol/urea on the growth, yield and chemical content of tomato (*Lycopersicon esculentum* L. Mill). *International Journal of Biology and Chemistry*, vol. 13, no. 2, pp 59-68.

© This is an open access article under the (CC)BY-NC license (<https://creativecommons.org/licenses/by-nc/4.0/>). Funded by Al-Farabi KazNU

E. Altınöz* , E.M. Altuner 

Kastamonu University, Kastamonu, Turkey

*e-mail: altinozedaa@gmail.com

(Received 2 March 2021; received in revised form 30 March 2022; accepted 13 May 2022)

Observing the presence of efflux pump activities in some clinically isolated bacterial strains

Abstract. Chemotherapeutic agents are substances that cure infectious diseases for many years. However, problems arose due to drug resistance that developed over time and it was observed that the drugs failed to kill the bacteria. Studies have been carried out to find the factor caused by drug resistance that adversely affect the disease treatment, and these studies continue today. There are different types of resistance mechanisms. Efflux pumps are just one of these mechanisms. Efflux pumps cannot enter and release the drug into the cell. Thus, the microorganism becomes resistant to the drug used. If this resistance is inhibited, the drug may work. A variety of chemical or natural inhibitors are available for inhibition. However, since they cause toxicity problems, their clinical use is not currently available. Studies in this area are ongoing. There are studies to determine the activity of the efflux pump. The activity of this mechanism can be detected with ethidium bromide (EtBr). In this study, it was aimed to determine the efflux pump activity of some resistant clinically isolated strains using EtBr dye. The strains that are *Acinetobacter baumannii*, *Candida albicans*, *Candida glabrata*, *Candida tropicalis*, *Klebsiella pneumoniae*, *Providencia rustigianii*, *Serratia odorifera*, *Shigella flexneri*, *Staphylococcus aureus* and *Streptococcus pneumoniae* microorganisms. Cartwheel method was applied on agars containing TSB with EtBr with different concentrations (0.0 mg/L, 0.5 mg/L, 1.0 mg/L, 1.5 mg/L, 2.0 mg/L and 2.5 mg/L). After the incubation, activation case was observed under UV light. It is concluded that each strain used has efflux pump activity. EtBr was released at 0.5 mg/L and did not fluoresce. Difference in fluorescence was observed under EtBr UV between 1.0 mg/L and 2.5 mg/L.

Key words: Drug resistance, efflux pump activities, clinically isolated bacterial strains, EtBr, inhibitors, UV.

Introduction

Microbial multidrug resistance (MDR) has reached a very important stage. As a result, the researches to discover new antibiotic hit compounds are accelerated. MDR efflux pumps mechanism is one of the important phenomena for antibiotic resistance.

Gram negative bacteria also have more antibacterial resistance than gram positive bacteria because gram negative bacteria have an outer membrane in addition to the cell wall structure [1-3].

Efflux pumps are transport proteins that play a role in expelling substances from inside towards the outside of the cells [4]. It can be present in all types of living cells [5].

The first exploration of the efflux pump mechanism was the excretion of tetracycline in *Escherichia coli* bacteria identified by Levy et al. [6-9].

There are 5 superfamilies defined for the efflux pumps, which are the ATP Binding Cassette (ABC), Multidrug and Toxic Efflux (MATE),

Major Facilitator Superfamily (MFS), Resistance Nodulation Division (RND) and Small Multidrug Resistance (SMR) [4, 10, 11]. In addition to these, The Proteobacterial Antimicrobial Compound Efflux (PACE) family was also defined in the study published by Du et al. [12] and the Drug Metabolite Transporter (DMT) family by Song and Wu [13]. DMT is a large group of membrane transporters present in eukaryotes, bacteria and archaea, and includes exporters for a wide range of substrates such as toxic compounds and metabolites [13-15].

As a result of inhibiting efflux pumps, the antimicrobial compounds can accumulate inside the cell, which may cause a cell death. Although there are some compounds that inhibit efflux pumps, but they are not commonly used clinically due to their toxicity [16].

Efflux pump inhibitors can act on either gram positive or gram-negative bacteria or both [17]. The examples of some efflux pump inhibitors and their mode of action are as follows.

Verapamil inhibits ABC/MFS family, Thioridazine inhibits NorA pump of the MFS family, Carbonyl Cyanide *m*-Chlorophenyl Hydrazone (CCCP) inhibits MATE/MFS/RND family, Phenylalanyl Arginine Beta Naphtylamid (PAβN/MC-207, 110) inhibits RND/MFS (CmIA and FloR pump) family, Paroxetine inhibits RND/MFS family and Reserpine inhibits RND/MFS family [10, 13, 18-33].

The aim of this study is observing the presence of efflux pump activity in some multidrug resistant (MDR) clinically isolated bacterial strains to define their efflux pump activity profile.

Materials and methods

Enrichment of microorganisms and isolation of pure colonies. In this study, totally 10 clinical isolate MDR strains were used. 7 of the strains are bacteria (*Acinetobacter baumannii*, *Klebsiella pneumoniae*, *Providencia rustigianii*, *Serratia odorifera*, *Shigella flexneri*, *Staphylococcus aureus* and *Streptococcus pneumoniae*) and 3 are yeast (*Candida albicans*, *Candida glabrata* and *Candida tropicalis*). Microorganisms were activated Luria-Bertani (LB) Broth (Merck, Germany) and then transferred to Nutrient Agar (NA) (Merck, Germany) for pure colony formation. Pure colonies obtained in NA were transferred into sterile saline solution (0.9%) and standardized by adjusting according to 0.5 McFarland standards.

Ethidium bromide (EtBr)-Tryptic Soy Agar (TSB) cartwheel method. TSB (Merck, Germany) plates, which included different EtBr (Merck, Germany) concentrations (0.0, 0.5, 1.0, 1.5, 2.0 and 2.5 mg/L) were prepared. Microorganisms were inoculated on the plates according the cartwheel method. Cartwheel methodology was used (Figure 1) [34]. Then the

petri dishes were incubated at 37°C for 24 hours for bacterial strains and 27°C for 48 hours for yeasts.

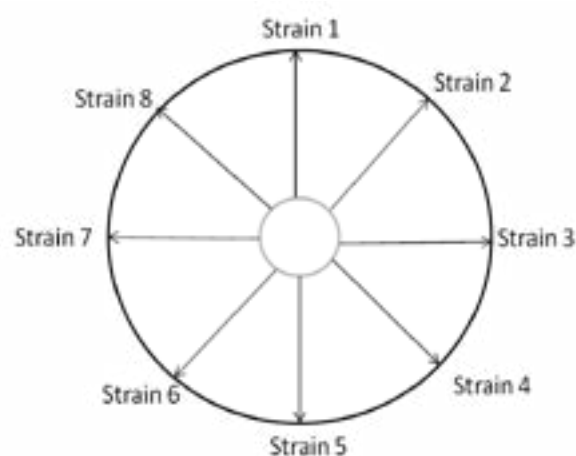


Figure 1 – Cartwheel method

Observing under UV light. After incubation, TSB agar plates containing EtBr were observed under UV light.

Statistical analysis. R Studio, version 4.0.2 was used to conduct a one-way analysis of variance (ANOVA) to analyze the results ($P = 0.05$) [35].

Results and discussion

In order to obtain results, plates were observed under UV light. A fluorescence was observed at different concentrations of EtBr for each microorganism under UV light on TSB agar plates. 0.0 mg/L concentration is the negative control group. Absence of fluorescence was expected as EtBr was absent at 0.0 mg/L. Therefore, no fluorescence was observed for these plates (0.0 mg/L), presented on Figure 2.

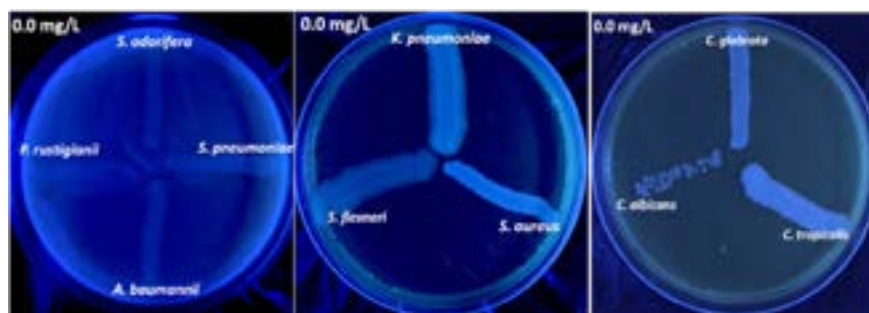


Figure 2 – UV fluorescence for 0.0 mg/L EtBr concentration

Since the amount of EtBr dye at 0.5 mg/L was too low, microorganisms were expected to efflux EtBr out and the results confirmed this, presented on Figure 3.

For 1.0 mg/L of EtBr concentration; as the concentration started to increase, the majority of EtBr began to remain in the cell and a purple fluorescence started to appear. A low

fluorescence for 4 microorganisms (*S. odorifera*, *S. pneumoniae*, *A. baumannii*, *P. rustigianii*) was observed in the first plate. Differences in purple fluorescence of microorganisms were observed on the second plate and the purple fluorescence of *C. albicans* in the third plate is higher than that for *C. glabrata* and *C. tropicalis*. Results presented on Figure 4.

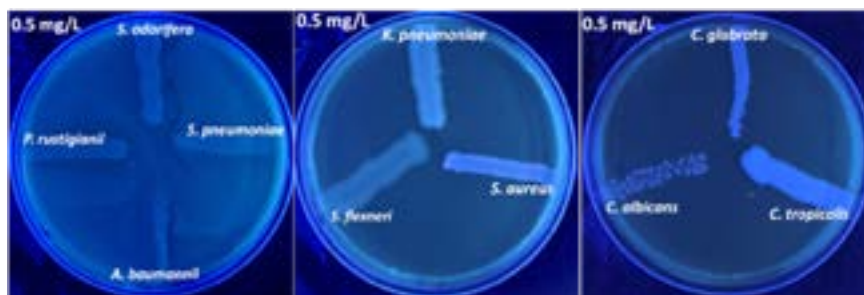


Figure 3 – UV fluorescence for 0.5 mg/L EtBr concentration



Figure 4 – UV fluorescence for 1.0 mg/L EtBr concentration

For 1.5 mg/L of EtBr concentration; EtBr was started to accumulate in the cells of all microorganisms, although there are differences between them. Fluorescence of 4 microorganisms (*S. odorifera*, *S. pneumoniae*, *A. baumannii*, *P. rustigianii*) in the first plate was also observed to be equal. Differences in fluorescence of microorganisms were observed on the second plate. *S. aureus* and *K. pneumoniae* presented equal fluorescence and the purple fluorescence in *S. flexneri* was observed to be more intense. The fluorescence of *C. albicans* in the third plate was found to be higher than the others. Results presented on Figure 5.

For 2.0 mg/L of EtBr concentration; EtBr was accumulated in the cells of all microorganisms,

although there are differences between them. Fluorescence of 4 microorganisms (*S. odorifera*, *S. pneumoniae*, *A. baumannii*, *P. rustigianii*) in the first plate was also observed to be equal. Differences in fluorescence for *S. aureus*, *K. pneumoniae* and *S. flexneri* were observed on the second plate. The fluorescence of *C. albicans* and *C. tropicalis* in the third plate was higher than *C. glabrata*. Results presented on Figure 6.

2.5 mg/L concentration is the highest concentration. EtBr was accumulated in the cells of all microorganisms. Because of the high EtBr concentration, the intensity of fluorescence was higher than other concentrations. Results presented on Figure 7.

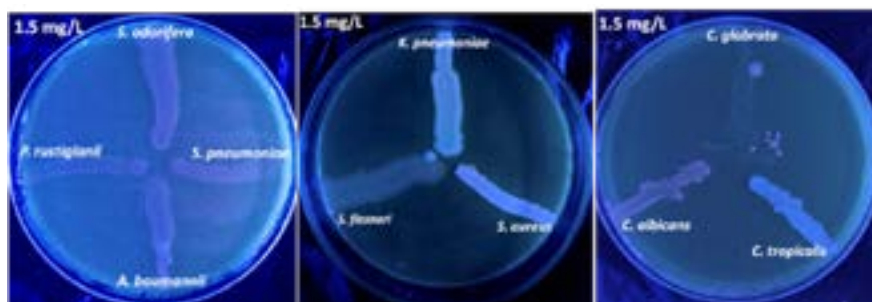


Figure 5 – UV fluorescence for 1.5 mg/L EtBr concentration



Figure 6 – UV fluorescence for 2.0 mg/L EtBr concentration

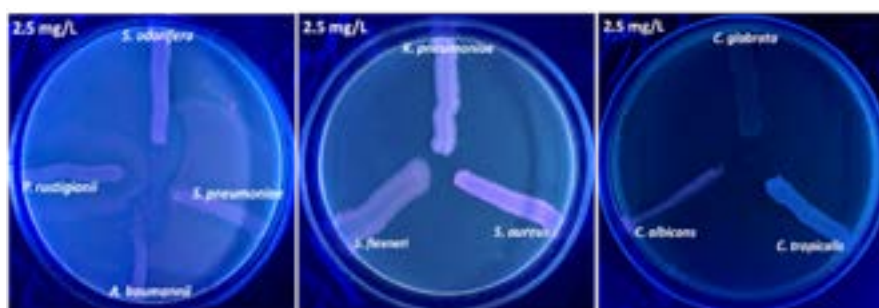


Figure 7 – UV fluorescence for 2.5 mg/L EtBr concentration

According to the results it was observed that the maximum EtBr concentration effluxed out the cell changes between 1.0 and 2.0 mg/L of EtBr for all strains used in the study. In all strains, the intensity of the fluorescence was increased, as the EtBr concentration was increased from 1.0 mg/L to 2.5 mg/L, where the highest fluorescence was at 2.5 mg/L concentration.

In a previous study, which was conducted by MDR *E. coli* strains, the activity of the efflux pumps against commercial efflux pump inhibitors were observed. Cartwheel test with EtBr was applied to microorganisms and similar results were observed under UV light. In addition, verapamil,

thioridazine hydrochloride and phenyl arginine beta naphthylamide (PAβN) inhibitors were tested in combination with some antibiotics for inhibiting bacterial growth and positive results were obtained [11].

In a study by Anbazhagan et al. MDR *Salmonella Typhimurium* strains were used and the efflux pump activity was evaluated. They applied the EtBr cartwheel method in the experiment. They prepared MH agar plates with EtBr containing 0.0 mg/L, 0.5 mg/L, 1.0 mg/L, 1.5 mg/L and 2.0 mg/L. After the incubation, the plates were examined under UV and their fluorescence were observed. It was reported that the efflux activities of 1.0 mg/L and 1.5 mg/L

EtBr on strains are well differentiated. They observed the efflux pump activity of strains by using PA β N inhibitor and some antibiotics. It was stated that 8 out of 9 strains they used in the study showed efflux pump activity and at least one antibiotic had an effect [36]. In the study by Martins et al. MDR *E. coli*, *Salmonella typhimurium*, *Salmonella enteritidis*, *Enterococcus faecalis*, *Enterobacter aerogenes* and *Staphylococcus aureus* bacteria strains were used. They applied the cartwheel method in TSB agars with EtBr at concentrations between 0.0 mg/L and 2.5 mg/L to observe the presence of efflux pumps [34]. Jiang et al. used the LightCycler 96 instrument (Roche, Basel, Switzerland) to measure (533 and 572 nm) the fluorescence of EtBr in the cell in their study. Thus, they studied the role of efflux pump in ciprofloxacin resistance of *Listeria monocytogenes* they used [37].

Conclusion

As stated in other studies, after the efflux pump activity was determined, inhibitor studies were performed with antibiotic combinations. Studies should continue to discover a non-toxic inhibitor and to investigate which efflux pump the inhibitor acts on. Thus, it is thought that it may overcome the major problem of antibiotic resistance. In this study, efflux pump activity was observed in drug resistant strains. Each strain used had efflux pump activity. Especially, different fluorescence was observed under EtBr UV between 1.0 mg/L and 2.5 mg/L. It is clear that, researches about efflux pumps have an extreme importance since they are important in bacterial resistance and this study clearly presents that each strain could have different efflux capacities, so it is important to observe the efflux pump activities of each microorganism before conducting efflux pump inhibition researches. Various results can be obtained by observing efflux pump activity by working with more various microorganisms.

References

1. Gan L., Chen S., Jensen G. (2008) Molecular organization of Gram-negative peptidoglycan. *Proc Natl Acad Sci U S A.*, vol. 105, no. 48, pp. 18953–18957. <https://doi.org/10.1021/jo035397e.s001>.
2. Vollmer W., Blanot D., De Pedro M.A. (2008) Peptidoglycan structure and architecture. *FEMS Microbiol. Rev.*, vol. 32, no. 2, pp. 149-167. <https://doi.org/10.1111/j.1574-6976.2007.00094.x>.
3. Altınöz E., Altuner E.M. (2019) Antibiotic Resistance and Efflux Pumps. *Int. J. Inn. Res. Rev.*, vol. 3, no. 2, pp. 1-9.
4. Webber M.A., Piddock L.J.V. (2003) The importance of efflux pumps in bacterial antibiotic resistance. *J. Antimicrob. Chemother.*, vol. 51, no. 1, pp. 9-11. <https://doi.org/10.1093/jac/dkg050>.
5. Alcalde-Rico M., Hernando-Amado S., Blanco P., Martínez, J. L. (2016) Multidrug efflux pumps at the crossroad between antibiotic resistance and bacterial virulence. *Front. Microbiol.*, vol. 7, no. 1483, pp. 1-14. <https://doi.org/10.3389/fmicb.2016.01483>.
6. McMurry L., Levy S.B. (1978) Two transport systems for tetracycline in sensitive *Escherichia coli*: critical role for an initial rapid uptake system insensitive to energy inhibitors. *Antimicrob Agents Chemother.*, vol. 14, no. 2, pp. 201-209. <https://doi.org/10.1128/aac.14.2.201>.
7. McMurry L., Petrucci R.E., Levy S.B. (1980) Active efflux of tetracycline encoded by four genetically different tetracycline resistance determinants in *Escherichia coli*. *Proc Natl Acad Sci U S A.*, vol. 77, no. 7, pp. 3974-3977. <https://doi.org/10.1073/pnas.77.7.3974>.
8. Nelson M.L., Levy S.B. (2011) The history of the tetracyclines. *Ann N Y Acad Sci.*, vol. 1241, no. 1, pp. 17-32. <https://doi.org/10.1111/j.1749-6632.2011.06354.x>.
9. Kumar S., Varela, M.F. (2013) Molecular mechanisms of bacterial resistance to antimicrobial agents. In A. Méndez-Vilas (Ed.), *Microbial Pathogens and Strategies for Combating Them: Science, Technology and Education* 522-534 p. Badajoz:Formatex Research Center.
10. Lomovskaya O., Warren M.S., Lee, A., et al. (2001) Identification and characterization of inhibitors of multidrug resistance efflux pumps in *Pseudomonas aeruginosa*: novel agents for combination therapy. *Antimicrob Agents Chemother.*, vol. 45, no. 1, pp. 105-116. <https://doi.org/10.1128/AAC.45.1.105-116.2001>.
11. Altınöz E., Altuner E.M. (2020) Responses of some *Escherichia coli* clinical isolate strains with multiple drug resistance and overexpressed efflux pumps against efflux pump inhibitors. *International Journal of Biology and Chemistry*, vol. 13, no. 1, pp. 77-87. <https://doi.org/10.26577/ijbch.2020.v13.i1.08>.
12. Du D., Wang-Kan X., Neuberger A., van Veen H.W., Pos K.M., Piddock L.J., Luisi B.F. (2018) Multidrug efflux pumps: structure, function and regulation. *Nat Rev Microbiol.*, vol. 16, no. 9, pp. 523-539. <https://doi.org/10.1038/s41579-018-0048-6>.

13. Song L., Wu X. (2016) Development of efflux pump inhibitors in antituberculosis therapy. *Int J Antimicrob Agents.*, vol. 47, no. 6, pp. 421-429. <https://doi.org/10.1016/j.ijantimicag.2016.04.007>.
14. Jack D.L., Yang N.M., Saier M.H. (2001) The drug/metabolite transporter superfamily. *Eur J Biochem.*, vol. 268, no. 13, pp. 3620-3639. <https://doi.org/10.1046/j.1432-1327.2001.02265.x>
15. Tsuchiya H., Doki S., Takemoto M., et al. (2016) Structural basis for amino acid export by DMT superfamily transporter YddG. *Nature.*, vol. 534, no. 7607, pp. 417-420. <https://doi.org/10.1038/nature17991>.
16. Abdi S.N., Ghotaslou R., Ganbarov K., Mobed A., Tanomand A., Yousefi M., Asgharzadeh M., Kafil H.S. (2020) Acinetobacter baumannii Efflux Pumps and Antibiotic Resistance. *Infect Drug Resist.*, vol. 13, pp. 423-434. <https://doi.org/10.2147/IDR.S228089>.
17. Kumar R., Pooja Patial S.J. (2016) A review on efflux pump inhibitors of gram-positive and gram-negative bacteria from plant sources. *Int J Curr Microbiol Appl Sci.*, vol. 5, no. 6, pp. 834-855. <https://doi.org/10.20546/ijcmas.2016.506.092>.
18. Van Bambeke F., Lee V.J. (2006) Inhibitors of bacterial efflux pumps as adjuvants in antibiotic treatments and diagnostic tools for detection of resistance by efflux. *Recent Pat Antiinfect Drug Discov.*, vol. 1, no. 2, pp. 157-175. <https://doi.org/10.2174/157489106777452692>.
19. Gupta A.K., Chauhan D.S., Srivastava K., et al. (2006) Estimation of efflux mediated multi-drug resistance and its correlation with expression levels of two major efflux pumps in mycobacteria. *J Infect Dis.*, vol. 38, no. 3, pp. 246-254.
20. Kristiansen M.M., Leandro C., Ordway D., et al. (2006) Thioridazine reduces resistance of methicillin-resistant Staphylococcus aureus by inhibiting a reserpine-sensitive efflux pump. *In vivo.*, vol. 20, no. 3, pp. 361-366.
21. Seeger M.A., Diederichs K., Eicher T., Brandstatter L., Schiefner A., Verrey F., Pos K.M. (2008) The AcrB efflux pump: conformational cycling and peristalsis lead to multidrug resistance. *Curr Drug Targets*, vol. 9, no. 9, pp. 729-749. <https://doi.org/10.2174/138945008785747789>.
22. Li X.Z., Nikaido H. (2009) Efflux-mediated drug resistance in bacteria. *Drugs.*, vol. 69, no. 12, pp. 1555-1623. <https://doi.org/10.2165/11317030-000000000-00000>.
23. Vecchione J.J., Alexander B., Sello, J.K. (2009) Two distinct major facilitator superfamily drug efflux pumps mediate chloramphenicol resistance in Streptomyces coelicolor. *Antimicrob Agents Chemother.*, vol. 53, no. 11, pp. 4673-4677. <https://doi.org/10.1128/AAC.00853-09>.
24. Gupta A.K., Reddy V.P., Lavania M., et al. (2010) jefA (Rv2459), a drug efflux gene in Mycobacterium tuberculosis confers resistance to isoniazid & ethambutol. *Indian J Med Res*, 132(2), 176-188.
25. Okandeji B.O., Greenwald D.M., Wroten J., Sello, J.K. (2011) Synthesis and evaluation of inhibitors of bacterial drug efflux pumps of the major facilitator superfamily. *Bioorg Med Chem.*, vol. 19, no. 24, pp. 7679-7689. <https://doi.org/10.1016/j.bmc.2011.10.011>.
26. Tegos P.G., Haynes M., Strouse J.J., et al. (2011) Microbial efflux pump inhibition: tactics and strategies. *Curr Pharm Des.*, vol. 17, no. 13, pp. 1291-1302. <https://doi.org/10.2174/138161211795703726>.
27. Rodrigues L., Machado D., Couto I., Amaral L., Viveiros, M. (2012) Contribution of efflux activity to isoniazid resistance in the Mycobacterium tuberculosis complex. *Infect Genet Evol.*, vol. 12, no. 4, pp. 695-700. <https://doi.org/10.1016/j.meegid.2011.08.009>.
28. Rodrigues L., Vilellas C., Bailo R., Viveiros M., Ainsa, J.A. (2013) Role of the Mmr efflux pump in drug resistance in Mycobacterium tuberculosis. *Antimicrob Agents Chemother.*, vol. 57, no. 2, pp. 751-757. <https://doi.org/10.1128/AAC.01482-12>.
29. Adams K.N., Szumowski J.D., Ramakrishnan, L. (2014) Verapamil, and its metabolite norverapamil, inhibit macrophage-induced, bacterial efflux pump-mediated tolerance to multiple anti-tubercular drugs. *J. Infect. Dis.*, vol. 210, no. 3, pp. 456-466. <https://doi.org/10.1093/infdis/jiu095>.
30. Spengler G., Csonka Á., Molnár J., Amaral L. (2016) The anticancer activity of the old neuroleptic phenothiazine-type drug thioridazine. *Anticancer Res.*, vol. 36, no. 11, pp. 5701-5706. <https://doi.org/10.21873/anticancer.11153>.
31. Singh G., Srivastava A.K. (2017) Efflux Pump Inhibitors: Enhance Therapy And Cauterize Tuberculosis. *Int J Pharm Sci Res.*, vol. 8, no. 7, pp. 2762-2767. [https://doi.org/10.13040/IJPSR.0975-8232.8\(7\).2762-67](https://doi.org/10.13040/IJPSR.0975-8232.8(7).2762-67).
32. Lawrence R.C., Subramaniapillai S.G., Ulaganathan, V., et al. (2019) Tackling drug resistance with efflux pump inhibitors: from bacteria to cancerous cells. *Crit Rev Microbiol.*, vol. 45, no. 3, pp. 334-353. <https://doi.org/10.1080/1040841X.2019.1607248>.
33. Sharma A., Gupta V.K., Pathania R. 2019. Efflux pump inhibitors for bacterial pathogens: From bench to bedside. *Indian J Med Res.*, vol. 149,

no. 2, pp. 129-145. https://doi.org/10.4103/ijmr.IJMR_2079_17.

34. Martins M., Couto I., Viveiros M., Amaral L. (2010) Identification of efflux-mediated multi-drug resistance in bacterial clinical isolates by two simple methods. In: Antibiotic resistance protocols. Humana Press, 143-157 p. https://doi.org/10.1007/978-1-60327-279-7_11.

35. Core R Team (accessed at December 15, 2020) "R: A language and environment for statistical computing. R Foundation for Statistical Computing." R-project.org. <https://www.R-project.org/>.

36. Anbazhagan P.V., Thavitiki P.R., Varra M., Annamalai L., Putturu R., Lakkineni V.R., Pesingi P.K. (2019) Evaluation of efflux pump activity of multidrug-resistant *Salmonella typhimurium* isolated from poultry wet markets in India. *Infect Drug Resist.*, vol. 12, pp. 1081-1088. <https://doi.org/10.2147/IDR.S185081>.

37. Jiang X., Yu T., Xu P., Xu X., Ji S., Gao W., Shi L. (2018) Role of efflux pumps in the in vitro development of ciprofloxacin resistance in *Listeria monocytogenes*. *Front. Microbiol.*, vol. 9, no. 2350, pp. 1-12. <https://doi.org/10.3389/fmicb.2018.02350>.

© This is an open access article under the (CC)BY-NC license (<https://creativecommons.org/licenses/by-nc/4.0/>). Funded by Al-Farabi KazNU

S.D. Zhantlessova* , Zh. Khamitkyzy , A.B. Talipova ,
I.S. Savitskaya , A.S. Kistaubayeva 

Al-Farabi Kazakh National University, Almaty, Kazakhstan

*e-mail: sirina.zhantlessova@mail.ru

(Received 16 March 2022; received in revised form 19 April 2022; accepted 29 April 2022)

Selection and optimization of cultivation conditions for bacterial cellulose producer

Abstract. The aim of this study was to increase productivity of *Komagataeibacter xylinus* C3 strain on nutrient media using industrial wastes as carbon source. By-product of sugar production, molasses, was selected for the cultivation of bacterial cellulose (BC) producer. It has been shown that the significant accumulation of BC (11.9 g/L) occurs on molasses medium with 7 days of cultivation in static conditions, which is 1.6 times higher than on modified Hestrin and Schramm (MHS) medium. BC synthesized on molasses medium is of high mechanical properties (tensile strength – 38.34 MPa and relative elongation at break – 3.34%). The replacement of carbon source for molasses in MHS medium for BC production did not alter the polymer structure and its microfibrillar nature was not affected by the composition of the medium. The introduction of molasses as nutrient source promoted a significant cost decrease of culture media by almost 2.8 times relating to MHS medium cost.

Key words: bacterial cellulose, industrial waste, morphological properties, mechanical parameters, cost-effective production.

Introduction

The main object of study and practical use for the production of bacterial cellulose (BC) are acetic acid bacteria belonging to the family of *Acetobacteriaceae* [1-3]. Currently, 14 genera are present in this family: *Acetobacter*, *Acidiphilium*, *Acidocella*, *Acidomonas*, *Craurococcus*, *Asaia*, *Gluconobacter*, *Paracraurococcus*, *Rhodopila*, *Roseomonas*, *Stella*, *Kozakia*. The species differ in their ability to develop on media with high concentrations of acetate and glucose. The names of the genera *Acetobacter* and *Gluconobacter* in this family have been known for a long time, but the taxons of the remaining genera were isolated and published only after 1989. Until 1998, the species *Acetobacter xylinum* was considered in the scientific literature as a separate species, but belonged to the subspecies *Acetobacter acetii*. In 1998, this species was again reclassified as *Gluconacetobacter xylinus*. The species *Acetobacter hansenii* has been reclassified as *Gluconacetobacter hansenii*. Later, the genus *Gluconacetobacter* was again reclassified into the genus *Komagataeibacter* [4].

It is believed that the cells of bacteria synthesizing cellulose are immobilized in the polymer net in

order to maintain the entire population in the space between air and liquid. I.e., cellulose biosynthesis is physiologically expedient for producers, and is an important evolutionary mechanism for the survival of producers of this polymer [5].

Bacterial cells created during the synthesis process of glucose chains exit through tiny pores that are present on its cell membrane [6]. Cellulose-synthesizing enzymes involved in the glucose polymerization reaction produce several glucan chains that form 1.5-nanometer subelement fibrils. These fibrils (glucose chains) then combine to form microfibrils, which later assemble and form cellulose ribbons [7]. Typically, 10 to 100 microfibrils form a ribbon approximately 7 nm thick and 70-145 nm wide. These ribbons (nanofibers) subsequently create a web-like net structure with a large number of empty spaces between the fibers [8, 9].

The main factors affecting the productivity of bacteria are the composition of the nutrient medium and the conditions of their cultivation. The optimal choice of nutrient medium and conditions for cultivation is also important for cellulose-forming bacteria, whose productivity depends primarily on the carbon source. They synthesize it from glucose, which is used in the classical Hestrin and Schramm

(HS) medium [10]. However, a number of papers provide information on the influence of other carbon sources on BC biosynthesis [11-13]. Most often their authors used sucrose, fructose, galactose, mannitol and glycerin. It has been shown that sucrose and fructose provide the highest BC yield, followed in descending order by mannitol, glycerin and galactose [13]. The authors explained the results obtained by the ability of bacteria to form glucose from different carbon sources, since any substrate must initially be converted into glucose and only after that it polymerizes into cellulose [13]. When using mannitol, fructose or glucose constant rates of cellulose formation are observed as a result of efficient transport through the cell membrane (initially mannitol is converted into fructose). Galactose has been identified as the least suitable carbon source because its transport through the cell membrane is inefficient.

One of the problems limiting the BC production is a high cost. The price of the fermentation medium is 30-50% of the total cost of the target product, which plays a crucial role in microbial fermentation.

The use of waste and by-products of some industries in fermentation media can increase the profitability of BC production. In this regard, many studies have focused on the development of media using industrial waste: cognac extract [14], fruit juices [15], maple syrup [16], sugar cane juice, wastewater from the production of rice wine [17], grape oilcake [18], wastewater from confectionery factories, corn liquor, dairy and soy whey [19]. In a number of works, agro-industrial wastes were tested for these purposes: wheat straw [20], activated sludge [21], spruce hydrolysate [22], hydrolysates of technical cellulose, as well as waste from biodiesel production, such as crude glycerin and by-products of acetone-butanol-ethanol fermentation [23]. Thus, the range of agricultural and industrial waste that could be used in fermentation media for the growth of producers and the formation of BC by them is quite wide.

In this regard, the purpose of this work is to select and optimize the cultivation conditions that ensure the maximum yield of BC.

Materials and methods

Obtaining BC under surface cultivation conditions. The inoculate was obtained by transferring a colony from an agar culture with *Komagataeibacter xylinus* C-3 strain into 100 ml of modified HS (MHS) medium, and then incubated at 30°C for 48 hours. In MHS medium, in contrast to the classical HS medium, the glucose content is reduced to 1% and ethanol is added at a concentration of 0.5% [24].

Composition of MHS medium (g/L): glucose – 10, sodium hydrogen phosphate – 2.7, peptone – 5, yeast extract – 5, citric acid – 1.15, ethanol – 5.

The resulting culture was vigorously shaken to release the immobilized cells from the synthesized cellulose film, followed by filtration of the suspension through sterile nets. The cells were then precipitated by centrifugation at 10,000 rpm. The titer of cells in the inoculum was determined by optical density and adjusted to a cell density of 5×10^8 CFU/ml using a UV-1601 PC spectrophotometer (Shimadzu, Japan).

Liquid-phase stationary cultivation of the BC producer was carried out in MHS medium with glucose, as well as in a condition where production wastes were used instead of glucose. Nutrient media based on whey, molasses and glycerin of the following compositions:

- medium with whey (g/L): whey – 20, sodium hydrogen phosphate – 2.7, peptone – 5, yeast extract – 5, citric acid – 1.15, ethanol – 5;

- medium with molasses (g/L): molasses – 20, sodium hydrogen phosphate – 2.7, peptone – 5, yeast extract – 5, citric acid – 1.15, ethanol – 5;

- medium with glycerin (g/L): glycerin – 20, peptone – 5, yeast extract – 5, citric acid – 1.15, ethanol – 5.

The media were poured into 100 ml flasks, then 1 ml of inoculate was added. Cultivation was carried out at 30°C for 7 days.

BC films were separated from the culture fluid and periodically washed with 0.5-1% NaOH solution at 80°C heating until the cells were removed. Then, the cellulose samples were washed from the NaOH solution with distilled water, 0.5% acetic acid solution and once more with distilled water until a neutral reaction. The obtained cellulose samples were stored in distilled water at 5°C.

The BC mass was determined after preliminary drying in a dry-burning thermostat at 80°C to a constant weight of the sample.

Characterization of bacterial cellulose samples by scanning electron microscopy. Samples of cellulose were pre-coated with a thin layer of a platinum-palladium alloy (Pt/Pd 80/20) and examined using a JSM-7800F scanning electron microscope (Jeol, Japan). The average diameter of the BC nanofiber was calculated according to the obtained (at least 100) values, calculations were carried out using Origin Pro 9.1 program (Originlab Corporation, USA).

Determination of the strength of films. The mechanical data of BC was measured using the Instron bursting machine (USA) in uniaxial mode according to the parameters: tensile strength (MPa)

and elongation at disruption (%). Tensile tests were conducted with a set sample deformation at constant speed of 100 mm/min.

Statistical analysis. Statistical comparison was performed using an unpaired test, followed by one-way analysis of variance (ANOVA) using Dunnett's multiple comparison test. All statistical data of the analysis were carried out using the SPSS 16.0 software package (SPSS Inc., USA).

Results and discussion

Despite the fact that there are many publications using cheap sources of raw materials for the production of BC [14-23], it is necessary to clarify the technological parameters for each producer and a specific strain. It is impossible to transfer the optimal conditions identified for one strain to another, since it is always necessary to take into account the biosynthetic features of a particular producer. In this regard, at the next stage, studies were conducted to determine the possibility of using cheap carbon and

energy sources as part of the nutrient medium for the *K. xylinus* C-3 strain.

Dairy and sugar production are well developed in the Republic of Kazakhstan, the waste of which are whey and molasses. One of the ways to use them is to develop simple and cheap nutrient media based on them for production BC.

In addition, the number of distilleries, including those producing bioethanol, is increasing every year. One of the main components of organic waste in the production of biofuels is glycerin. A significant amount of glycerin is formed during the industrial distillation of alcohol in distillation columns and the production of bioethanol from vegetable raw materials. Waste disposal occupies one of the key positions in the organization of environmentally safe and cost-effective production.

In this regard, it was decided to use whey, molasses and glycerin, which were introduced into MHS medium instead of glucose as carbon source. Figure 1 shows the results of determining the mass of BC films formed on MHS and waste media.

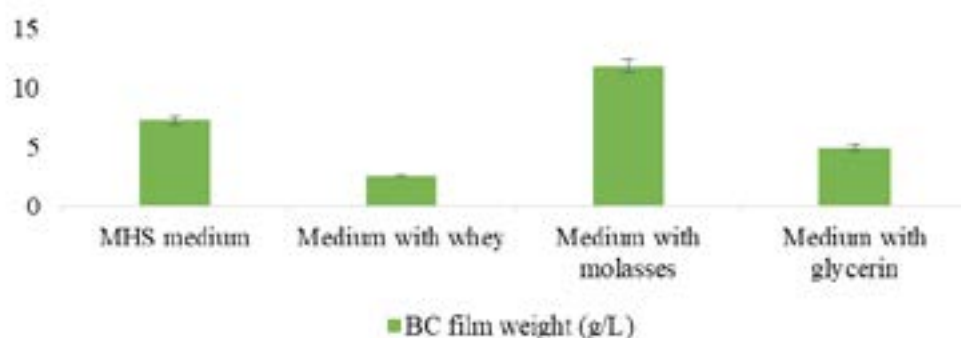


Figure 1 – Productivity of *K. xylinus* C-3 strain on MHS medium and waste-based media

Judging by obtained data, the lowest BC yield was observed on the medium with whey (2.5 g/L). The producer synthesizes cellulose from glucose. Therefore, any sugars contained in the fermented substrate must be converted to glucose. Lactose presented in whey is a disaccharide that breaks down into glucose and galactose. Galactose is considered the least suitable carbon source for cellulose-forming bacteria [13]. Besides, the proportion of mutants that unable to synthesize cellulose increases during cultivation on media with galactose or lactose. The increase in the number of cellulose-negative cells leads to competition for a substrate with a population of cellulose-positive cells. It was found that not a dense, but a gel-like film was formed on these media.

The fact is that the presence in the population of a significant proportion of cellulose-negative mutants not involved in the synthesis of cellulose leads to a noticeable decrease in the overall rate of polymer accumulation, which in turn prevents the formation of a dense film [24]. A similar pattern was observed in our experiments.

It should also be taken into account that whey is a perishable product, which is a significant disadvantage of the widespread use of a nutrient medium based on it.

Low productivity of the strain was also noted on the glycerin medium. The weight of the film synthesized by the strain is 4.87 g/L, which is 32.6% less than on MHS medium. Similar data were

obtained by other authors, who found that with static cultivation, the yield of BC on glycerin medium is lower than on glucose medium [25, 26].

The most favorable medium for BC synthesis is a medium based on molasses [27-29]. It is one of the most economical carbon sources in the microbiological industry. Molasses is a by-product of the final stage of crystallization in the sugar production process. Due to the high content of sucrose in molasses, it is actively used as a raw material for the preparation of nutrient media. Molasses contains about 80% of dry substances that approximately 57% is represented by sugars. However, at such concentration, microorganisms will not be able to grow, so molasses was diluted with distilled water 10 times. The relatively low sugar concentration in molasses is a prerequisite for efficient cellulose production.

It should be noted that molasses contains minerals and heavy metals that have a toxic effect on the growth of microorganisms and the synthesis of the product [30]. Suspended impurities and heavy metals of molasses were removed by treatment with hydrochloric acid at 70-80°C. In addition, this treatment will also allow sucrose to be hydrolyzed to its glucose and fructose monomer.

The polymer mass yield on the molasses medium is 11.9 g/L, which is 1.6 times more than on MHS medium (7.23 g/L). The reason may be that molasses contains a mixture of carbohydrates (sucrose, glucose and fructose). Primarily, the producer consumes glucose, and then gradually other sugars.

There is noted a pH decline cause of glucose oxidation to a gluconic acid that could impact on formation of BC [15]. However, synthesis of gluconic acid is suppressed in a medium based on molasses, and pH stays steady (Figure 2).

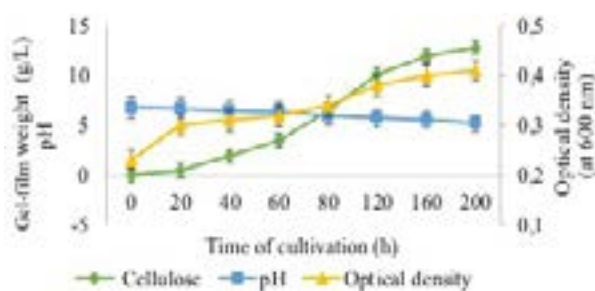


Figure 2 – Dynamics of BC biosynthesis on the medium with molasses

Furthermore, molasses includes phenolic compounds with guaiacyl and syringyl linkages comparable to lignin [29], which are likewise slowly consumed, resulting in a modest pH shift, which was accompanied by an increase in cell proliferation and the synthesis of BC. It was discovered that BC synthesis was linked to the growth of acetic acid bacteria, and that the conditions applied to the highest number of bacteria also correspond to the highest BC production.

Molasses includes nitrogen molecules such as amino acids, nucleic acids, and vitamins apart from carbohydrates. In MHS medium, peptone and yeast extract serve as sources of nitrogen nutrition. Peptone is an expensive component (48,775 tenge/kg). On the one hand, yeast extract also contains nitrogen compounds necessary for microorganisms (peptides, free amino acids and nucleotides). On the other hand, it also contains all the vitamins of group B. And, finally, some researchers point out that the absence of peptone in the nutrient medium does not affect the productivity of *K. xylinus* strain [31]. In this regard, the producer strain was grown under the same conditions, but on a medium without peptone (Table 1).

Table 1 – The mass of the BC film (g/L) formed on media with different concentrations of peptone

Medium	Content of peptone (%)		
	0	3	5
MHS with glucose	7.12±0.3	7.19±0.4	7.23±0.4
Medium with molasses	11.65±0.4	11.79±0.2	11.9±0.4

Note: * in all cases, there were no significant differences between the indicators ($p \geq 0,05$)

Under the conditions of this experiment, no significant difference in the level of productivity of the strain was found, the discrepancy in the mass of the BC films was within the confidence interval, at least in the conditions of the experiment. Probably,

organic nitrogen compounds contained in molasses and yeast extract fill the needs of the strain in this element. This eliminates the need to use an additional source of nitrogen nutrition, such as pepton. The removal of peptone from the medium based on

molasses will reduce the cost of the BC production technology.

Thus, the proposed composition of the medium with molasses (g/L): molasses – 20; sodium hydrophosphate – 2.7; yeast extract – 5; citric acid – 1.15; ethanol – 5. A patent for utility model No. 5756 was obtained for it under the name “Nutrient medium

for the cultivation of the bacterial cellulose producer *Komagateibacter xylinus*” dated 08.01.2021 [32].

The production nutrient medium not only significantly affects the cost of the obtained products, but also determines their quality [16, 21, 33]. The BC was examined on a scanning electron microscope to detect possible differences in the gel film (Figure 3).

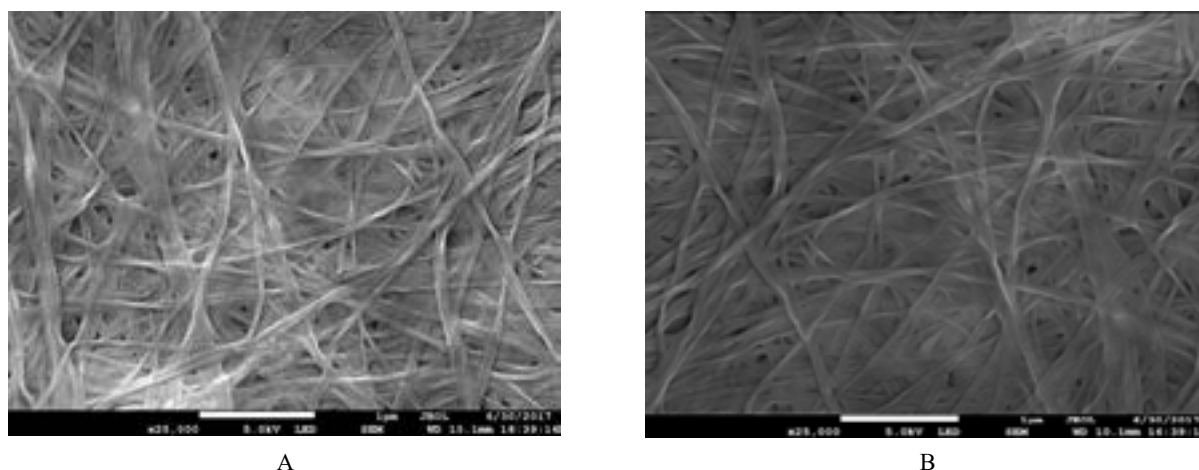


Figure 3 – SEM images of BC films synthesized by the *K. xylinus* C-3 strain on various media.
Note: A – MHS; B – medium with molasses (magnification x25 000)

Microfibrillar ribbons forming a nano-gel film of BC grown on MHS and media based on molasses do not differ from each other. All BC films had a flat and smooth surface. The thickness of BC microfibrils averaged 15–150 nm. The average diameter of BC fibrils was approximately 30 ± 5 nm. The interconnected porous matrix structure of films formed on media had a considerable surface area. BC microfibrils are combined together into one million of a centimeter thick ribbon-like fibers. It is feasible to provide not only the needed vapor and gas permeability, but also to retain different biologically active components in the structure of films.

The presence of a BC framework with uniform fiber distribution density assures that films have a high mechanical strength, which is an important measure of biomaterial quality [34]. The strength of the films was determined on the universal breaking machine Instron (USA) in uniaxial mode by two indicators: tensile strength (MPa) and elongation value (%) (Table 2).

Judging by the results presented in Table 2, the tensile strength of the BC formed on MHS medium was 28.54 ± 0.4 MPa, and the elongation value was 4.89 ± 0.2 . The elongation value (%) of BC gel film

formed on the media based on molasses was 3.34 ± 0.2 . BC films synthesized on molasses medium had the highest strength value (38.34 ± 0.2) compared to those obtained on MHS medium. This value is sufficiently high compared to the mechanical parameters of many flat oriented layers of organic polymers. It is known that high tensile strength correlates with an increase in the number of hydrogen bonds in the material [30]. This suggests that an increase in the strength of BC synthesized on the medium with molasses may be due to the occurrence of hydrogen bonds between OH-groups of cellulose and OH-groups in composition of molasses. The cost of 1 liter of MHS medium is 743 tenge, molasses-based media is 435 tenge (Table 3).

Table 2 – Mechanical properties of BC formed on various nutrient media

Mechanical strength indicators	MHS medium	Medium with molasses
Tensile Strength (MPa)	28.54 ± 0.4	38.34 ± 0.2
Elongation at break (%)	4.89 ± 0.2	3.34 ± 0.2

Table 3 – Calculation of the cost of nutrient media for cultivation of *K. xylinus* C3

Medium	Components of medium	Price (tg per 1 kg)	Number of ingredients (g/L)	Price (tg for 1 liter of medium)
MHS medium	glucose	7,000	10	70
	sodium hydrogen phosphate	103,800	2.7	280
	peptone	48,775	5	244
	yeast extract	26,400	5	132
	citric acid	5,700	1.15	7
	ethanol	2,000	5	10
Total	743			
Medium with molasses	molasses	300	20	6
	sodium hydrophosphate	103,800	2.7	280
	yeast extract	26,400	5	132
	citric acid	5,700	1.15	7
	ethanol	2,000	5	10
Total	435			

The cost of 1 g of BC on MHS medium – 103 tenge and on molasses-based medium – 37 tenge, which reduces the cost of BC production technology by almost 2.8 times (Table 4).

Thus, the new molasses medium is cost-effective for the cultivation of the BC producer as well as provides a high level of gel-film biosynthesis.

Table 4 – Calculation of the cost of BC on different media

Medium	BC output on media (g/L)	The cost of the medium (tg per 1L)	Cost of BC (tg for 1 g/L)
MHS medium	7.23	743	103 tg
Medium with molasses	11.9	435	37 tg

Conclusion

Production of BC is costly with defined chemical medium, i.e., HS medium. Therefore, most researchers are searching alternative from the available wastes in order to reduce the cost. To overcome these difficulties, there has been a research on the enhanced production of BC, by selection and optimization of the producer static cultivation using whey, glycerin and molasses, as substrate.

An optimal nutrient medium based on the waste of sugar production – molasses was selected for the BC producer, which provides a 2.8-fold reduction in the cost of the synthesized biopolymer. Surface cultivation of *K. xylinus* C3 strain on a medium with molasses for 7 days increases the productivity of the film formation to 11.9 g/L.

BC, obtained on the medium with molasses forms a network of micro-(15-35 nm) and macrofibrils (50-150 nm), providing high mechanical properties (tensile strength – 38.34 ± 0.2 MPa; elongation at break – $3.34 \pm 0.2\%$).

Thus, the composition of optimal nutrient medium for BC production was developed using molasses as a substrate. By-product of sugar production promoted significant gains of BC in mass and yield compared to MHS medium, without any difference in microfibrillar structure of polymer.

An optimized nutrient medium based on sugar production waste – molasses can be used to scale the production of BC. The use of media based on food and agro-industrial waste can significantly reduce the cost of technology for obtaining not only BC, but also other products of microbiological synthesis and

opens up broad prospects for the development of new technologies for the disposal of these wastes.

Acknowledgement

Scientific work was conducted within the framework of the project AP09259491 “Biotechnology application in production of combined dairy products using polysaccharide matrix with probiotic biofilms” (2021-2023) supported by the Ministry of Science and Higher Education of the Republic of Kazakhstan.

References

- Aswini K., Gopal N., Uthandi S. (2020) Optimized culture conditions for bacterial cellulose production by *Acetobacter senegalensis* MA1. *BMC Biotechnology*, vol. 20, no. 1, 46 p. <https://doi.org/10.1186/s12896-020-00639-6>
- Yan Z., Chen S., Wang H., Wang B., Jiang J. (2008) Biosynthesis of bacterial cellulose/multi-walled carbon nanotubes in agitated culture. *Carbohydrate Polymers*, vol. 74, no. 3, pp. 659-665. <https://doi.org/10.1016/j.carbpol.2008.04.028>
- Cheng K., Catchmark J. M., & Demirci A. (2011) Effects of CMC addition on bacterial cellulose production in a biofilm reactor and its paper sheets analysis. *Biomacromolecules*, vol. 12, no. 3, pp. 730-736. <https://doi.org/10.1021/bm101363t>
- Yamada Y., Hoshino K., Ishikawa T. (1997) The phylogeny of acetic acid bacteria based on the partial sequences of 16S ribosomal RNA: The elevation of the subgenus *gluconoacetobacter* to the generic level. *Bioscience, Biotechnology, and Biochemistry*, vol. 61, no. 8, pp. 1244-1251. <https://doi.org/10.1271/bbb.61.1244>
- Williams W. S., Cannon R. E. (1989) Alternative environmental roles for cellulose produced by *Acetobacter xylinum*. *Applied and Environmental Microbiology*, vol. 55, no. 10, pp. 2448-2452. <https://doi.org/10.1128/aem.55.10.2448-2452.1989>
- Zaar K. (1979) Visualization of pores (export sites) correlated with cellulose production in the envelope of the gram-negative bacterium *Acetobacter xylinum*. *Journal of Cell Biology*, vol. 80, no. 3, pp. 773-777. <https://doi.org/10.1083/jcb.80.3.773>
- Feng Y., Zhang X., Shen Y., Yoshino K., Feng W. (2012) A mechanically strong, flexible and conductive film based on bacterial cellulose/graphene nanocomposite. *Carbohydrate Polymers*, vol. 87, no. 1, pp. 644-649. <https://doi.org/10.1016/j.carbpol.2011.08.039>
- Ashori A., Sheykhnazari S., Tabarsa T., Shakeri A., Gholipour M. (2012) Bacterial cellulose/silica nanocomposites: Preparation and characterization. *Carbohydrate Polymers*, vol. 90, no. 1, pp. 413-418. <https://doi.org/10.1016/j.carbpol.2012.05.060>
- Bae S., Shoda M. (2004) Bacterial cellulose production by fed-batch fermentation in molasses medium. *Biotechnology Progress*, vol. 20, no. 5, pp. 1366-1371. <https://doi.org/10.1021/bp0498490>
- Hang F.M. (2013) *Biotechnology of bacterial cellulose using the producer strain Gluconoacetobacter hansenii Gh – 1/2008*: (dissertation).
- Wang S., Han Y.H., Chen J.L., Zhang D.C., Shi X., Ye Y., Chen D., Li M. (2018) Insights into bacterial cellulose biosynthesis from different carbon sources and the associated biochemical transformation pathways in *Komagataeibacter* sp., W1. *Polymers*, vol. 10, no. 9, 963 p. <https://doi.org/10.3390/polym10090963>
- Hu Y., Catchmark J. M. (2010) Formation and characterization of spherelike bacterial cellulose particles produced by *Acetobacter xylinum* JCM 9730 strain. *Biomacromolecules*, vol. 11, no. 7, pp. 1727-1734. <https://doi.org/10.1021/bm100060v>
- Gladysheva E., Skiba E. (2014) Influence of the carbon composition of nutrient media on the productivity of cellulose-synthesizing bacteria [Vliyaniye uglerodnogo sostava pitatel'nykh sred na produktivnost' tsellyulozosinteziruyushchikh bakteriy]. *Polzunovskii vestnik*, no.3, pp. 168-173.
- Hong F., Qiu K. (2008) An alternative carbon source from Konjac powder for enhancing production of bacterial cellulose in static cultures by a model strain *Acetobacter aceti* subsp. *xylinus* ATCC 23770. *Carbohydrate Polymers*, vol. 72, no. 3, pp. 545-549. <https://doi.org/10.1016/j.carbpol.2007.09.015>
- Kurosumi A., Sasaki C., Yamashita Y., Nakamura Y. (2009) Utilization of various fruit juices as carbon source for production of bacterial cellulose by *Acetobacter xylinum* NBRC 13693. *Carbohydrate Polymers*, vol. 76, no. 2, pp. 333-335. <https://doi.org/10.1016/j.carbpol.2008.11.009>
- Zeng X., Small D. P., Wan W. (2011) Statistical optimization of culture conditions for bacterial cellulose production by *Acetobacter xylinum* BPR 2001 from Maple Syrup. *Carbohydrate Polymers*, 85(3), pp. 506-513. <https://doi.org/10.1016/j.carbpol.2011.02.034>
- Wu J.M., Liu R. (2012) Thin stillage supplementation greatly enhances bacterial

- cellulose production by *Gluconacetobacter Xylinus*. *Carbohydrate Polymers*, vol. 90, no. 1, pp. 116-121. <https://doi.org/10.1016/j.carbpol.2012.05.003>
18. Vazquez A., Foresti, M. L., Cerrutti P., Galvagno M. (2012) Bacterial cellulose from simple and low cost production media by *Gluconacetobacter Xylinus*. *Journal of Polymers and the Environment*, vol. 21, no. 2, pp. 545-554. <https://doi.org/10.1007/s10924-012-0541-3>
19. Li Z., Wang L., Hua J., Jia S., Zhang J., Liu H. (2015) Production of nano bacterial cellulose from waste water of candied jujube-processing industry using *Acetobacter xylinum*. *Carbohydrate Polymers*, vol. 120, pp. 115-119. <https://doi.org/10.1016/j.carbpol.2014.11.061>
20. Chen L., Hong F., Yang X., Han S. (2013) Biotransformation of wheat straw to bacterial cellulose and its mechanism. *Bioresource Technology*, vol. 135, pp. 464-468. <https://doi.org/10.1016/j.biortech.2012.10.029>
21. Cavka A., Guo X., Tang S., Winestrand S., Jönsson L. J., Hong F. (2013) Production of bacterial cellulose and enzyme from waste fiber sludge. *Biotechnology for Biofuels*, vol. 6, no. 1. <https://doi.org/10.1186/1754-6834-6-25>
22. Guo X., Cavka A., Jönsson L. J., Hong F. (2013) Comparison of methods for detoxification of spruce hydrolysate for bacterial cellulose production. *Microbial Cell Factories*, vol. 12, no. 1. <https://doi.org/10.1186/1475-2859-12-93>
23. Savitskaya I., Kistaubayeva A., Zhantlessova S., Kurmangali A. (2017) Selection of optimal conditions for the growth of the producer and biosynthesis of the gel film of bacterial cellulose under surface cultivation conditions [Podbor optimal'nykh usloviy dlya rosta produtsenta i biosinteza gel'plenki bakterial'noy tsellyulozy v poverkhnostnykh usloviyakh kul'tivirovaniya]. *IV Mezhdunarodnyye farabiyeviskiye chteniya. Materialy mezhdunar. nauch.-prakt. konferentsii «Aktual'nyye problemy biotekhnologii, ekologii i fiziko-khimicheskoy biologii»*, 82 p.
24. Gromovykh T. I., Sadykova V. S., Lutcenko S. V., Dmitrenok A. S., Feldman N. B., Danilchuk T. N., Kashirin V. V. (2017) Bacterial cellulose synthesized by *Gluconacetobacter hansenii* for medical applications. *Applied Biochemistry and Microbiology*, vol. 53, no. 1, pp. 60-67. <https://doi.org/10.1134/s0003683817010094>
25. Tsouko E., Kourmentza C., Ladakis D., Kopsahelis N., Mandala I., Papanikolaou S., Paloukis F., Alves V., Koutinas A. (2015) Bacterial cellulose production from industrial waste and by-product streams. *International Journal of Molecular Sciences*, vol. 16, no. 12, pp. 14832-14849. <https://doi.org/10.3390/ijms160714832>
26. Budaeva V. V., Gladysheva E. K., Skiba E. A., Sakovich G. V. (2015) A method for producing bacterial cellulose – an application for an invention [Text] [Pitateľ' naya sreda dlya kul'tivirovaniya Komagateibacter xylinus produczena bakterial'noj czellyulozy']. Registration No. 2015129304 dated 07/16/2015 [Registracziornyj № 2015129304 ot 16.07.2015].
27. Revin V. V., Dolganov A. V., Liyaskina E. V., Nazarova N. B., Balandina A. V., Devyataeva A. A., Revin V. D. (2021) Characterizing bacterial cellulose produced *Bykomagataeibacter sucrofermentans* H-110 on molasses medium and obtaining a biocomposite based on it for the adsorption of fluoride. *Polymers*, vol. 13, no. 9, 1422 p. <https://doi.org/10.3390/polym13091422>
28. Salari M., Sowti Khiabani M., Rezaei Mokarram R., Ghanbarzadeh B., Samadi Kafil H. (2019) Preparation and characterization of cellulose nanocrystals from bacterial cellulose produced in sugar beet molasses and Cheese Whey Media. *International Journal of Biological Macromolecules*, vol. 122, pp. 280-288. <https://doi.org/10.1016/j.ijbiomac.2018.10.136>
29. Souza E. F., Furtado M. R., Carvalho C. W. P., Freitas-Silva O., Gottschalk L. M. F. (2020) Production and characterization of *Gluconacetobacter xylinus* bacterial cellulose using cashew apple juice and soybean molasses. *International Journal of Biological Macromolecules*, vol. 146, pp. 285-289. <https://doi.org/10.1016/j.ijbiomac.2019.12.180>
30. Kūçūkaşık F., Kazak H., Güney D., Finore I., Poli A., Yenigün O., Nicolaus B., Öner E. T. (2010) Molasses as fermentation substrate for levan production by *Halomonas* sp., *Applied Microbiology and Biotechnology*, vol. 89, no. 6, pp. 1729-1740. <https://doi.org/10.1007/s00253-010-3055-8>
31. Chen X., Lou W., Zong M., Smith T. J. (2011) Optimization of culture conditions to produce high yields of active *ACETOBACTER* SP. CCTCC M209061 cells for anti-Prelog reduction of prochiral ketones. *BMC Biotechnology*, vol. 11, no. 1. <https://doi.org/10.1186/1472-6750-11-110>
32. Kistaubayeva A.S., Savitskaya I.S., Shokataeva D.Kh., Abdulzhanova M.A. (2021) Nutrient medium for cultivation of *Komagateibacter xylinus* of bacterial cellulose producer [Pitateľ' naya sreda dlya kul'tivirovaniya Komagateibacter xylinus

producenta bakterial'noj tsellyulozy']. Patent No. 5756 for utility model from 08.01.2021 of the Republic of Kazakhstan [Patent №5756 na poleznuyu model' ot 08.01.2021 Respubliki Kazakhstan].

33. Rühls P. A., Storz F., López Gómez Y. A., Haug M., Fischer P. (2018) 3D bacterial cellulose biofilms formed by foam templating. *Npj Biofilms and Microbiomes*, vol. 4, no. 1, 21 p. <https://doi.org/10.1038/s41522-018-0064-3>

34. Savitskaya I., Kistaubayeva A., Shokatayeva D. (2017) Physicochemical properties of bacterial cellulose obtained by a new strain of *Komagataeibacter xylinus* C-3 on an optimized nutrient medium [Fiziko-khimicheskiye svoystva bakterial'noy tsellyulozy, poluchennoy novym shtammom *Komagataeibacter xylinus* C-3 na optimizirovannoy pitatel'noy srede]. *KazNU. Experimental Biology*, vol. 3, no. 72, pp. 114-128.

© This is an open access article under the (CC)BY-NC license (<https://creativecommons.org/licenses/by-nc/4.0/>). Funded by Al-Farabi KazNU

M.K. Kumarbayeva^{1*}, A.M. Kokhmetova¹,
 N.M. Kovalenko², O.Yu. Kremneva³, M.N. Atishova¹, Zh.S. Keishilov¹,
 A.A. Malysheva¹, D.K. Zhanuzak¹, A.A. Bolatbekova¹, A.M. Kokhmetova¹

¹Institute of Plant Biology and Biotechnology, Almaty, Kazakhstan

²All-Russian Research Institute of Plant Protection, St. Petersburg, Russia

³Federal Research Center of Biological Plant Protection, Krasnodar, Russia

*e-mail: madina_kumar90@mail.ru

(Received 15 March 2022; received in revised form 19 April 2022; accepted 28 April 2022)

Identification of wheat samples for resistance to toxins of *Pyrenophora tritici-repentis* (Ptr)

Abstract. *Pyrenophora tritici-repentis* (Ptr) is a causal agent of tan spot in wheat in Kazakhstan, as it has been around the world. The pathogen produces host-specific toxins which interact with the wheat host sensitivity loci. The aim of this study was 1) to identify whether selected Kazakhstani isolates of *P. tritici-repentis* possessed the Ptr toxin genes *ToxA* and/or *ToxB* and 2) to identify the wheat varieties resistant to HST ToxA and ToxB. As a result of the analysis of the frequency of occurrence of PTR races, it was found that races 7 (25%) and 8 (41.6%) dominate in isolates from southern Kazakhstan, and race 4 (62.5%) prevails in northern Kazakhstan. Twenty single spore isolates collected from wheat-growing areas of the South and North of Kazakhstan representing the *P. tritici-repentis* population were characterized for the presence of the *Ptr ToxA* and *Ptr ToxB* genes, using two gene specific primers. Eight (40%) Kazakhstani *P. tritici-repentis* isolates were positive for the *ToxA* gene, and two isolates (10%) were positive for the *ToxB* gene. *ToxB* gene was not previously found in our country, but the results of this study show the appearance of this toxin in south Kazakhstan. Eleven (64.7%) wheat varieties resistant to HST ToxA were identified using molecular markers linked to the *tsn1* gene, insensitive to Ptr ToxA. The identified genotypes are recommended for use in breeding for wheat resistance to tan spot.

Key words: *Pyrenophora tritici-repentis*, isolates, host-selective toxins, race, tan spot.

Introduction

Tan spot caused by *Pyrenophora* (*P.*) *tritici-repentis* (syn. *Drechslera tritici-repentis* (Died.) Shoemaker), is an economically important foliar disease of wheat (*Triticum* spp.) worldwide, including Australia, Europe, USA, Canada and South America [1, 2], Russia [3-4]. In Kazakhstan, every year the spectrum of pathogens is growing, which significantly reduce the wheat yield. These pathogens include *Puccinia graminis* f. sp. *Tritici* [5-7], *Puccinia striiformis* West end. f. sp. *tritici* [8], *Puccinia triticina* Erikss. [9], *Tilletia caries* [10]. In recent years there has been increasing distribution and harmfulness of *P. tritici-repentis* in Kazakhstan [11-16].

Tan spot infection can result in two distinct symptoms, necrosis (tan colour) and extensive chlorosis (yellow colour). On leaves, the lesions characteristically have small tan/ brown centres,

surrounded by a yellow circular border. As the plant matures, *P. tritici-repentis* (Ptr) infects the stem where it will begin to develop pseudothecia [17].

The development of the different characteristic symptoms is highly specific and a result of an interaction between host-selective toxins (HST) secreted by the pathogen and the target receptors of a toxin-sensitive host wheat plant [18, 19]. Three HST (Ptr ToxA, Ptr ToxB and Ptr ToxC) have been characterized to date. Both Ptr ToxA, which induces necrosis on susceptible wheat genotypes, and Ptr ToxB, which induces chlorosis on susceptible wheat cultivars, are proteinaceous in nature and are encoded, respectively by the genes *ToxA* [22-24] and a number of multi-copy genes such as *ToxB* [25-27]. At present, it is possible to screen for the presence of both genes *ToxA* and *ToxB* using specific molecular primers [28]. In contrast, although Ptr ToxC, which can induce chlorosis on specific wheat genotypes, has been suggested to be a non-ionic polar molecule,

its exact nature and the gene(s) encoding it have not been identified [27]. Additionally, there are also two other, uncharacterized HST, known as Ptr ToxD toxins, whose exact targets and functions have yet to be elucidated [28]. Studies of *P. tritici-repentis* populations in the USA, Canada, South America, Australia, the Baltic States and Romania have shown that Ptr ToxA has been the predominant HST found in these populations, with Ptr ToxB almost completely absent [19, 22, 26, 29].

Based on the ability of isolates to produce the different HSTs (and thereby necrosis or chlorosis) on a set of differential wheat cultivars, currently eight races of *P. tritici-repentis* have been identified worldwide [30]. However, there is little information on the presence of Ptr ToxA and/ or Ptr ToxB in populations of Kazakhstan *P. tritici-repentis* isolates.

An integrated plant disease control requires a combination of several tools to effectively combat the disease. In the case of tan spot, the use of resistant wheat varieties is the best option to sustainably manage the disease. In addition, it is the most cost-effective and environmentally friendly method of disease control. To this end, the breeding of resistant wheat varieties should be one of the main objectives of the tan spot control strategy, which should include assessment of germplasm diseases [31]. The aim of this study was 1) to identify whether selected Kazakhstani isolates of *P. tritici-repentis* possessed the Ptr toxin genes *ToxA* and/or *ToxB* and 2) to identify the wheat varieties resistant to HST ToxA and ToxB.

Materials and methods

In 2020, a collection of 113 single-pore isolates of *P. tritici-repentis* was created, of which 20 isolates were selected for further study.

Detection of Ptr-ToxA and Ptr-ToxB using PCR. The 20 Kazakhstani *P. tritici-repentis* single-spore isolates were screened using PCR for the presence of the Ptr ToxA and Ptr ToxB genes using ToxA and ToxB specific primers, respectively. The genomic DNA of 2 Ptr isolates, used as a control known to be either positive or negative for Ptr ToxA and Ptr ToxB, and from a range of different Ptr races, were obtained to validate the PCR and for comparison against the local Kazakhstani Ptr isolates. Genomic DNA for the 2 international *Ptr* isolates (control) from different geographic origin (Pskov and Greece 9) were provided by Dr Mironenko (All-Russian Research Institute of Plant Protection, St. Petersburg, Russia).

Genomic DNA extraction from P. tritici-repentis. The isolates of Ptr were grown for 3 weeks in liquid Fries medium amended with 1.5% yeast extract [30]. The mycelial mats were used for genomic DNA extraction. Briefly, 40 mg of lyophilized mycelium from each isolate was extracted with a Wizard® Genomic DNA Extraction Kit (Promega Corp, Madison, WI) in accordance with the protocol for plant material of the manufacturer. After these two extractions with phenol-chloroform (1:1 v/v) followed by one extraction with chloroform were performed. DNA concentration was measured using a NanoDrop-ND-1000 spectrophotometer (NanoDrop Technologies, United States of America) and DNA concentrations were diluted to 10–20 ng/μL for PCR. [19].

The Ptr isolates were screened for the presence of either the *ToxA* and *ToxB* genes using Ptr ToxA and Ptr ToxB gene-specific primers as described by Antoni *et al.* [26]. The forward (F) and reverse (R) primers for ToxA were: TA51F (5'-GCGTTCTATCCTCGTACTTC-3') and TA52R (5'-GCATTCTCCAATTTTCACG-3'); and the *ToxB* primers were TB71F (5'-GCTACTTGCTGTGGCTATC-3') and TB60R (5'-ACTAACAACGTCCTCCACTTTG-3'). Primer for *CHS-1* [31], the gene for chitin synthase, were included as an internal control for fungal DNA and produced a 275-bp amplification product (Table 1).

Each PCR reaction volume was made up to 25 μL containing 1xPCR buffer (Roche), 200 μM dNTPs, 10 μM primer, 1 U FastStart Taq polymerase (Roche) and 1 μL template DNA. A negative control with 1 μL sterile water instead of the template DNA was included. A 7–10 μL aliquot of each PCR product combined with 3 μL loading dye was separated by electrophoresis at 10V/cm for 50 min in a 1% agarose gel (Bioline USA Inc.) alongside the 1 Kb plus DNA Ladder (Invitrogen™, Thermo Fisher Scientific Inc., USA). Gels were stained in ethidium bromide solution and visualised on a UV transilluminator (UVItec Cambridge Imaging System, Total Lab Systems Ltd). The presence of a band with the expected size for each gene indicated the presence of the *Tox* gene. [34].

Identification of carriers of wheat varieties resistant to Ptr ToxA and Ptr ToxB. Genomic DNA extracted at two-leaf seedling stage for each individual plant using the CTAB method [19]. DNA concentration measured using a spectrophotometer SmartSpec™ Plus (Bio RAD). The DNA concentration for each sample was adjusted to 30 ng/μL. Samples were genotyped using the SSR marker *Xfcp623* designed to detect alleles of the

Tsn1 gene. The sequence of primers and PCR reaction conditions are given by [35]. The carriers of the *Tsn1* gene were also detected using PCR protocol for SSR marker *Xfcp623* published at the WheatCAP website <http://maswheat.ucdavis.edu/protocols>. The amplification products were separated on 2%-agarose gels, to determine the

length of the amplification fragment 100 bp DNA Ladder (Ferments, Lithuania) was used. Gels were visualized on Gel Documentation System (Gel Doc XR+, BIO-RAD, Hercules, USA) for documentation of allele types in cultivars. Wheat entries Salamouni and Glenlea served as positive and negative controls, respectively [36].

Table 1 – Primers used for amplification of the Ptr ToxA and Ptr ToxB genes in *P. tritici-repentis* isolates

Gene	Primer for singleplex PCR	Sequence	Estimated band size (bp)	Reference
<i>ToxA</i>	TA51F TA52R	5'-GCATTCTCCAATTTTCACG-3 5'-GCTACTTGCTGTGGCTATC-3	573	[32]
<i>ToxB</i>	TB71F TB60R	5'-GCTACTTGCTGTGGCTATC-3 5'-ACTAACAACGTCTCCACTTTG-3'	232	[32], [33]
<i>CHS-1</i>	CHS-79F CHS-354R	5'-TGGGGCAAGGATGCTTGGAAGAAG-3' 5'-TGGAAGAACCATCTGTGAGAGTTG-3'	275	[32]

Results and discussion

P. tritici-repentis is a necrotrophic pathogen and a well characterized producer of host-specific toxin effectors. The results of previous studies have shown that, in 2016, it was shown that races 1 and 8 were dominant in Kazakhstan [37, 38]. Monosporic isolates of *P. tritici-repentis* isolated from the southeastern region in 2020 were assigned to certain races based on the manifestation of symptoms of necrosis/chlorosis on standard differentials (Glenlea, 6B662, 6B365).

In this study, a virulence was determined within the study of 113 single-spore isolates, which were isolated from infectious wheat material collected in the different regions of Kazakhstan during 2020

growing season. A total of 20 single spore Ptr isolates were recovered and characterized in this study (Table 2). Analysis of virulence of isolates from southern Kazakhstan allowed to determine the presence of five races: 4 (8.3%), 5 (16.6%), 6 (8.3%), 7 (50%) and 8 (16.6%). Isolates from northern Kazakhstan are determined by virulence to three races, including race 2 (12.5%), race 4 (62.5%), and race 7(25%).

Earlier five races of *P. tritici-repentis* have been identified, including races 1, 2, 3, 7 and 8; it has been shown that races 1 and 8 of *P. tritici-repentis* are dominant [38, 39]. As a result of current research, it was found that races 7 (25%) and 8 (41.6%) are the dominating in isolates from southern Kazakhstan, and race 4 is prevailing in northern Kazakhstan.

Table 2 – Molecular screening of Kazakhstan isolates of *P. tritici-repentis* for the presence of *ToxA* and *ToxB*, *CHS-1* genes

*Isolate code	Race	PCR reaction			Region/Country collected
		<i>ToxA</i>	<i>ToxB</i>	<i>CHS1</i>	
KAZ-S-1-2021	7	-	-	275 bp	Almaty oblast, Kazakhstan
KAZ-S-2-2021	7	573 bp	-	275 bp	Almaty oblast, Kazakhstan
KAZ-S-3-2021	5	-	232 bp	275 bp	Almaty oblast, Kazakhstan
KAZ-S-4-2021	6	573 bp	-	275 bp	Almaty oblast, Kazakhstan
KAZ-S-5-2021	4	-	-	275 bp	Almaty oblast, Kazakhstan
KAZ-S-6-2021	7	-	-	275 bp	Almaty oblast, Kazakhstan
KAZ-S-7-2021	7	-	-	275 bp	Almaty oblast, Kazakhstan
KAZ-S-8-2021	8	573 bp	-	275 bp	Almaty oblast, Kazakhstan
KAZ-S-9-2021	7	-	-	275 bp	Almaty oblast, Kazakhstan

Continuation of the table

*Isolate code	Race	PCR reaction			Region/Country collected
		<i>ToxA</i>	<i>ToxB</i>	<i>CHS1</i>	
KAZ-S-10-2021	5	-	232 bp	275 bp	Almaty oblast, Kazakhstan
KAZ-S-11-2021	8	573 bp	-	275 bp	Almaty oblast, Kazakhstan
KAZ-S-12-2021	8	573 bp	-	275 bp	Almaty oblast, Kazakhstan
KAZ-N -1-2021	4	-	-	275 bp	Kostanay oblast, Kazakhstan
KAZ-N -2-2021	4	-	-	275 bp	Kostanay oblast, Kazakhstan
KAZ-N -3-2021	7	-	-	275 bp	Kostanay oblast, Kazakhstan
KAZ-N -4-2021	7	-	-	275 bp	Kostanay oblast, Kazakhstan
KAZ-N -5-2021	4	-	-	275 bp	Kostanay oblast, Kazakhstan
KAZ-N -6-2021	4	-	-	275 bp	Kostanay oblast, Kazakhstan
KAZ-N -7-2021	2	573 bp	-	275 bp	Kostanay oblast, Kazakhstan
KAZ-N -8-2021	4	573 bp	-	275 bp	Kostanay oblast, Kazakhstan
Spb-Pskov (Control for <i>ToxA</i> gene)	1	573 bp	-	275 bp	St. Petersburg, Russia
Spb-Greece 9 (Control for <i>ToxB</i> gene)	5	-	232 bp	275 bp	St. Petersburg, Russia

Notes: *Isolates designation: KZ for Kazakhstan, the number after the KAZ, indicates the number of the field, N or S is the southern or northern region from which isolates was collected, and the number after the dashed line is denoted for the particular isolates included in this study

Using molecular markers detection of *Ptr ToxA* and *Ptr ToxB* was carried out. To control the ability to amplification of isolates DNA the primers for *CHS1* gene (the gene for chitin synthase) were used. It was found that *CHS1* gene amplified a 275-bp amplification product from all isolates tested (Table 2). The *Ptr ToxA* specific primers amplified a band of 573 bp from the genomic DNA of 8 (40%) of the *P. tritici-repentis* isolates (KAZ-S-2-2021, KAZ-S-4-2021, KAZ-S-8-2021, KAZ-S-1-2021,

KAZ-S-11-2021, KAZ-S-1-2021, KAZ-N-7-2021, KAZ-N-8-2021 and KAZ-S-12-2021). No amplification products of 573 bp were found in 13 isolates (KAZ-S-1-2021, KAZ-S-3-2021, KAZ-S-5-2021, KAZ-S-6-2021, KAZ-S-7-2021, KAZ-S-9-2021, KAZ-S-10-2021, KAZ-N-1-2021, KAZ-N-2-2021, KAZ-N-3-2021, KAZ-N-4-2021, KAZ-N-5-2021, KAZ-N-6-2021) indicating the absence of toxin *ToxA*, which accounted for 65% of the number of isolates studied.



Figure 1 – PCR amplification assays with primer for *ToxA* gene. Note: Lane: M, DNA ladder; 1, KAZ-S-1-2021; 2, KAZ-S-3-2021; 3, KAZ-S-2-2021; 4, KAZ-S-4-2021; 5, KAZ-S-5-2021; 6, KAZ-S-6-2021; 7, KAZ-S-7-2021; 8, KAZ-S-8-2021; 9, KAZ-S-9-2021; 10, KAZ-S-10-2021; 11, KAZ-S-11-2021, 12, KAZ-S-12-2021; 13, KAZ-N -1-2021; 14, KAZ-N -2-2021; 15, KAZ-N -3-2021; 16, KAZ-N -4-2021; 17, KAZ-N -5-2021; 18, KAZ-N -7-2021; 19, KAZ-N -8-2021, 20, KAZ-N -6-2021; 21, Pskov (positive control for *ToxA* gene); 22, ddH₂O (negative control for *ToxA* gene), M, DNA ladder

The ToxB specific primers amplified a band of 232 bp from the genomic DNA of the *P. tritici-repentis* isolates KAZ-S-3-2021 (Race 5) and KAZ-S-10-2021 (Race 5). A band of 232 bp were also observed in Greece 9, the reference positive control for ToxB gene (Figure 2). No PCR product was amplified using the ToxB specific primers in the 18 tested isolates of *P. tritici-repentis* (KAZ-S-1-2021, KAZ-S-2-2021, KAZ-S-4-2021, KAZ-S-5-2021,

KAZ-S-6-2021, KAZ-S-7-2021, KAZ-S-8-2021, KAZ-S-9-2021, KAZ-S-11-2021, KAZ-S-12-2021, KAZ-N-1-2021, KAZ-N-2-2021, KAZ-N -3-2021, KAZ-N -4-2021, KAZ-N -5-2021, KAZ-N -6-2021, KAZ-N -7-2021, KAZ-N -8-2021).

The results of genotyping of 17 wheat entries with marker *Xfcp623* are given in Table 3. Of the tested 17 samples, 11 (64.7%) varieties and promising lines with insensitivity to Ptr ToxA were identified.



Figure 2 – PCR amplification assays with primer for *ToxB* gene. Note: Lane: M, DNA ladder; 1, KAZ-S-1-2021; 2, KAZ-S-2-2021; 3, KAZ-S-3-2021; 4, KAZ-S-4-2021; 5, KAZ-S-5-2021; 6, KAZ-S-6-2021; 7, KAZ-S-7-2021; 8, KAZ-S-8-2021; M, DNA ladder; 9, KAZ-S-9-2021; 10, KAZ-S-10-2021; 11, KAZ-S-11-2021; 12, KAZ-S-12-2021; 13, KAZ-N -1-2021; 14, KAZ-N -2-2021; 15, KAZ-N -3-2021; 16, KAZ-N -4-2021; 17, KAZ-N -5-2021; 18 KAZ-N -6-2021; 19, KAZ-N -7-2021; 20, KAZ-N -8-2021, 21, Greece 9 (positive control for *ToxB* gene); 22, ddH₂O (negative control for *ToxB* gene)

Table 3 – Results of genotyping wheat samples using the *Xfcp623* marker

Accessions	Host, cultivar	<i>Xfcp623</i>	
		bp	gene
Oral	<i>Triticum aestivum</i>	null	<i>tsn1</i>
KZ-KP32-2021	<i>Triticum aestivum</i>	380	<i>Tsn1</i>
KZ-KP33-2021	<i>Triticum aestivum</i>	null	<i>tsn1</i>
KZ-KP34-2021	<i>Triticum aestivum</i>	null	<i>tsn1</i>
KZ-KP35-2021	<i>Triticum aestivum</i>	380	<i>Tsn1</i>
KZ-KP36-2021	<i>Triticum aestivum</i>	null	<i>tsn1</i>
Akbiday	<i>Triticum aestivum</i>	380	<i>Tsn1</i>
Koksu	<i>Triticum aestivum</i>	null	<i>tsn1</i>
Alem	<i>Triticum aestivum</i>	380	<i>Tsn1</i>
Rosinka 3	<i>Triticum aestivum</i>	380	<i>Tsn1</i>
KZ-KP40-2021	<i>Triticum aestivum</i>	380	<i>Tsn1</i>
Aliya	<i>Triticum aestivum</i>	null	<i>tsn1</i>
KZ-KP44-2021	<i>Triticum aestivum</i>	null	<i>tsn1</i>
Reke	<i>Triticum aestivum</i>	null	<i>tsn1</i>
KSI16-2021	<i>Triticum aestivum</i>	null	<i>tsn1</i>
KSI17-2021	<i>Triticum aestivum</i>	null	<i>tsn1</i>
KZ-KP46-2021	<i>Triticum aestivum</i>	null	<i>tsn1</i>
Salamouni	<i>Triticum aestivum</i>	null	<i>tsn1</i>
Glenlea	<i>Triticum aestivum</i>	380	<i>Tsn1</i>

Note: *Xfcp623* – SSR marker of the *Tsn1* locus sensitive to Ptr ToxA amplifies a 380 bp DNA fragment

As an example, the PCR results for 19 wheat samples are shown in the Figure 3. Seven entries (KZ-KP32-2021, KZ-KP35-2021, Akbiday, Alem, Rosinka 3, KZ-KP40-2021 and Glenlea) had 380 bp fragment, indicative of the dominant *Tsn1* allele conferring toxin *Ptr ToxA* sensitivity. Eleven

entries (Oral, KZ-KP33-2021, KZ-KP34-2021, KZ-KP36-2021, Aliya, Koksus, KZ-KP44-2021, Reke, KSI16-2021, KSI17-2021 and Salamouni) had no amplification product (null allele), indicative of the recessive *tsn1* allele conferring toxin *Ptr ToxA* insensitivity.

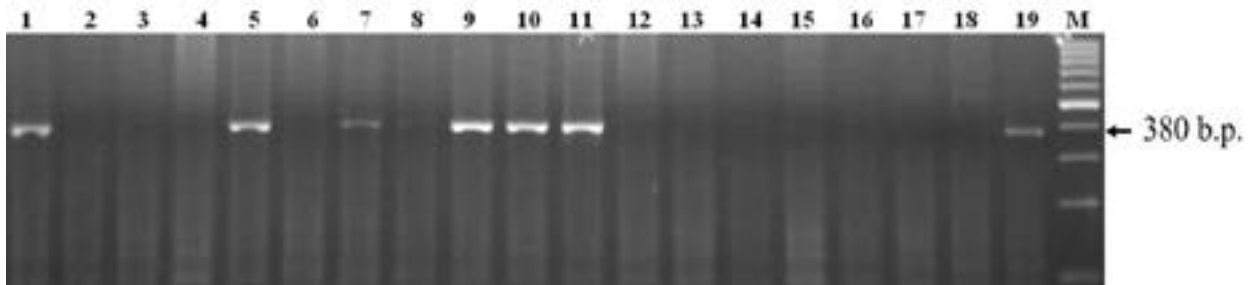


Figure 3 – DNA amplification product for wheat cultivars and elite lines obtained with diagnostic marker *Xfcp623* linked to the *Tsn1* gene sensitive to *Ptr ToxA*. Lane: 1, KZ-KP32-2021; 2, Oral; 3, KZ-KP33-2021; 4, KZ-KP34-2021; 5, KZ-KP35-2021; 6, KZ-KP36-2021; 7, Akbiday; 8, Koksus; 9, Alem; 10, Rosinka 3; 11, KZ-KP40-2021; 12, Aliya; 13, KZ-KP44-2021; 14, Reke; 15, KSI16-2021; 16, KSI17-2021; 17, KZ-KP46-2021; 18, Salamouni (resistant reference cultivar for race 1, insensitive to *Ptr ToxA*, with recessive gene *tsn1*); 19, Glenlea (susceptible reference cultivar for race 1, sensitive to *Ptr ToxA*, with dominant gene *Tsn1*); M, DNA ladder. Fragments amplified by *Xfcp623* were separated in 2% agarose gels. The bands are 380 bp for the *Tsn1* allele (lanes 1, 5, 7, 9, 10, 11 and 19), sensitive to *Ptr ToxA* and null allele for the *tsn1* allele, insensitive to *Ptr ToxA* (lanes 2, 3, 4, 6, 8, 12, 13, 15, 16, 17 and 18)

Determination of the prevalence of genes encoding toxins in the local population, and the susceptibility of commonly grown wheat cultivars to *Ptr* aid selection of wheat cultivars to reduce disease risk. Thus, according to the results of our research, five races of *Ptr* (4, 5, 6, 7 and 8) have been identified from southern Kazakhstan, and three races (2, 4 and 7) from northern Kazakhstan. *ToxB* was not previously found in Kazakhstan, but the results of this study show the appearance and spread of this toxin in south Kazakhstan. According to the obtained data, the frequency of occurrence of isolates with the *ToxB* gene was 10.0%. A similar observations of occurrence frequency of *ToxB* was noted in studies by Kamel *et al* in 2019 in Tunisia [40]. In the present study, the wheat entries were genotyped with *Xfcp623* marker to predict reaction to the *Ptr ToxA*. Eleven wheat varieties resistant to HST *ToxA* were identified using molecular markers linked to the *tsn1* gene insensitive to *Ptr ToxA*.

Conclusion

Our results indicate an annual fluctuation in the population structure of *P. tritici-repentis* in the regions of Kazakhstan. Identification of six *Ptr* races on wheat

demonstrates the high diversity of the pathogen population in Kazakhstan, which requires further in-depth annual studies. It was found that races 7 and 8 dominate in isolates from southern Kazakhstan, and race 4 prevails in northern Kazakhstan. Twenty single spore isolates of *P. tritici-repentis* were characterized for the presence of the *Ptr ToxA* and *Ptr ToxB* genes. Seven isolates were positive for the *ToxA* gene, and two isolates were positive for the *ToxB* gene. Eleven wheat varieties resistant to HST *ToxA* were identified using molecular markers linked to the *tsn1* gene, insensitive to *Ptr ToxA*. Our results have important practical implications for breeders when studying the distribution of *P. tritici-repentis*.

Acknowledgments

This study was conducted within the framework of the program OR11465424 “Development and implementation of highly effective diagnostic systems for identifying the most dangerous diseases and increasing the genetic potential of crop resistance”, task 01 “Monitoring the development of diseases to determine the level of danger of pathogens of brown, yellow rust and diseases of wheat leaf spots” for 2021-2022 supported by the Ministry of Science and

Higher Education of the Republic of Kazakhstan. The funders had no role in study design, data collection and analysis, decision to publish or preparation of the manuscript.

References

1. Lamari L., Strelkov S.E. (2010) *Pyrenophora tritici-repentis* interaction: progress towards an understanding of tan spot disease. *Can J Plant Path.*, vol. 32, no. 1, pp. 4-10.
2. Phuke R.M., He X., Juliana P., Bishnoi S.K., et al. (2020) Association mapping of seedling resistance to tan spot (*Pyrenophora tritici-repentis* Race 1) in CIMMYT and South Asian Wheat Germplasm. *Front Plant Sci.*, vol. 11, p. 1309.
3. Kremneva O.Yu., Volkova G.V., Kovalenko N.M. (2019) The Dynamics of the Race Structure of *Pyrenophora tritici-repentis* in the North Caucasus Region. *Mikologiya I Fitopatologiya.*, vol. 53, no. 4, pp. 246-253 <https://doi.org/10.1134/S0026364819040056>
4. Kremneva O.Yu., Mironenko N.V., Volkova G.V., Baranova O.A., Kim Y.S., Kovalenko N. M. (2021) Resistance of winter wheat varieties to tan spot in the North Caucasus region of Russia. *Saudi Journal of Biological Sciences.*, vol. 28, no. 3, pp. 1787-1794. <https://doi.org/10.1016/j.sjbs.2020.12.021>
5. Kokhmetova A., Madenova A., Kampitova G., Urazaliev R., et al. (2016) Identification of leaf rust resistance genes in wheat cultivars produced in Kazakhstan. *Cereal Res. Commun.*, vol. 44, no. 2, pp. 240-250. <https://doi.org/10.1556/0806.43.2015.056>.
6. Kokhmetova, A., Sharma, R., Rsaliyev S., Galymbek, K., et al. (2018) Evaluation of Central Asian wheat germplasm for stripe rust resistance. *Plant Genet. Resour.*, vol. 16, no. 2, pp. 178-184. <https://doi.org/10.1017/S1479262117000132>.
7. Kokhmetova A.M., Atishova M.N., Galymbek K., et al. (2020) Identification of wheat germplasm resistant to leaf, stripe and stem rust using molecular markers. *Bulletin of NAS RK.*, vol. 2, no. 384, pp. 45-52. <https://doi.org/10.32014/2020.2518-1467.40>
8. Kokhmetova A., Rsaliyev Sh., Atishova M., Kumarbayeva M., et al. (2021) Evaluation of wheat germplasm for resistance to leaf rust (*Puccinia triticina*) and identification the sources of *Lr* resistance genes using molecular markers. *Plants.*, vol. 10, no. 7, p. 1484. <https://doi.org/10.3390/plants10071484>
9. Kokhmetova A., Rsaliyev A., Malysheva A., Atishova M., et al. (2021) Identification of Stripe Rust Resistance Genes in Common Wheat Cultivars and Breeding Lines from Kazakhstan. *Plants.*, vol. 10, no. 11, p. 2303. <https://doi.org/10.3390/plants10112303>.
10. Madenova, A.; Sapakhova, Z.; Bakirov, S.; Galymbek K., et al. (2021) Screening of wheat genotypes for the presence of common bunt resistance genes. *Saudi. J. Biol. Sci.*, vol. 28, pp. 2816-2823. <https://doi.org/10.1016/j.sjbs.2021.02.013>
11. Kokhmetova A., Atishova M. (2020) Identification wheat genotypes resistant to tan spot *Pyrenophora tritici-repentis*. *Bulletin of NAS RK.*, vol. 2, no. 384, pp. 29-35. <https://doi.org/10.32014/2020.2518-1467.38>
12. Kokhmetova A., Atishova M., Kumarbayeva M., Leonova I.N. (2019) Phytopathological screening and molecular marker analysis of wheat germplasm from Kazakhstan and CIMMYT for resistance to tan spot. *Vavilov J. Genet. Breed.* 23, 879–886. <https://doi.org/10.18699/vj19.562>
13. Kokhmetova, A., Kumarbayeva, M., Atishova, M., Nehe, A., et al. (2021) Identification of high-yielding wheat genotypes resistant to *Pyrenophora tritici-repentis* (tan spot). *Euphytica.*, vol. 217, p. 97. <https://doi.org/10.1007/s10681-021-02822-y>
14. Kokhmetova A., Sehgal D., Ali S., Atishova M., et al. (2021) Genome-Wide Association Study of Tan Spot Resistance in a Hexaploid Wheat Collection From Kazakhstan. *Front. Genet.*, vol. 11, p. 581214. <https://doi.org/10.3389/fgene.2020.581214>
15. Kokhmetova, A.M., Ali, S., Sapakhova, Z., Atishova, M.N. (2018) Identification of genotypes-carriers of resistance to tan spot Ptr ToxA and Ptr ToxB of *Pyrenophora tritici-repentis* in common wheat collection. *Vavilov J. Genet. Breed.*, vol. 22, pp. 978–986. <https://doi.org/10.18699/vj18.440>
16. Kokhmetova, A.M., Atishova, M.N., Madenova, A.K., Kumarbayeva, M.T. (2019) Genotyping of wheat germplasm for resistance to toxins of tan spot *Pyrenophora tritici-repentis*. *J. Biotechnol. Proc. of European Biotechnology Congress. Valencia, Spain, April 11-13, 2019.* <https://doi.org/10.1016/j.jbiotec.2019.05.188>
17. Weith S. (2015) *Pyrenophora tritici-repentis* the causal agent of tan spot: characterisation of New Zealand populations. Master's thesis, Lincoln University, New Zealand. https://researcharchive.lincoln.ac.nz/bitstream/handle/10182/6849/Weith_MSc_open.pdf
18. Singh P.K., Singh R.P., Duveiller E., Mergoum M., et al. (2010) Genetics of wheat-*Pyrenophora tritici-repentis* interactions. *Euphytica.*

vol. 171, pp. 1-13. <https://doi.org/10.1007/s10681-009-0074-6>

19. Aboukhaddour R., Turkington T.K., Strelkov S.E. (2013) Race structure of *Pyrenophora tritici-repentis* (tan spot of wheat) in Alberta, Canada. *Canadian Journal of Plant Pathology.*, vol. 35, pp. 256-268. <https://doi.org/10.1080/07060661.2013.782470>

20. Ballance G.M., Lamari L., Bernier C.C. (1989) Purification and characterization of a host-selective necrosis toxin from *Pyrenophora tritici-repentis*. *Physiological and Molecular Plant Pathology.*, vol. 35, pp. 203-213. [https://doi.org/10.1016/0885-5765\(89\)90051-9](https://doi.org/10.1016/0885-5765(89)90051-9)

21. Tomás A., Feng G.H., Reeck G.R., Bockus W.W., et al. (1990) Purification of a cultivar-specific toxin from *Pyrenophora tritici-repentis*, causal agent of tan spot of wheat. *Molecular Plant-Microbe Interactions.*, vol. 3, p. 221-224. <https://doi.org/10.1094/MPMI-3-22>

22. Tuori A., Wolpert T.J., Ciuffetti L.M. (1995) Purification and immunological characterization of toxic components from cultures of *Pyrenophora tritici-repentis*. *Molecular Plant-Microbe Interactions.*, vol. 8, pp. 41-48. <https://doi.org/10.1094/MPMI-8-0041>

23. Strelkov S.E., Lamari L. (2003) Host-parasite interactions in tan spot (*Pyrenophora tritici-repentis*) of wheat. *Canadian Journal of Plant Pathology.*, vol. 25, pp. 339-349. <https://doi.org/10.1080/07060660309507089>

24. Lamari L., Strelkov S.E., Yahyaoui A., Amedov M., et al. (2005) Virulence of *Pyrenophora tritici-repentis* in the countries of the Silk Road. *Canadian Journal of Plant Pathology.*, vol. 27, pp. 383-388. <https://doi.org/10.1080/07060660509507236>

25. Martinez J.P., Oesch N.W., Ciuffetti L.M. (2004) Characterization of the multiple-copy host-selective toxin gene, *ToxB*, in pathogenic and nonpathogenic isolates of *Pyrenophora tritici-repentis*. *Molecular Plant Microbe Interactions.*, vol. 17, pp. 467-474. <https://doi.org/10.1094/MPMI.2004.17.5.467>

26. Antoni E.A., Rybak K., Tucker M.P., Hane J.K., et al. (2010) Ubiquity of *ToxA* and absence of *ToxB* in Australian populations of *Pyrenophora tritici-repentis*. *Australasian Plant Pathology.*, vol. 39, pp. 63-68. <https://doi.org/10.1071/AP09056> Effertz RJ, Meinhardt SW, Anderson

27. JA, Jordahl JG, Francl LJ 2002. Identification of a chlorosis-inducing toxin from *Pyrenophora tritici-repentis* and the chromosomal location of an insensitivity locus in

wheat. *Phytopathology* 92: 527-533. <https://doi.org/10.1094/PHTO.2002.92.5.527>

28. Faris J.D., Liu Z., Xu S.S. (2013) Genetics of tan spot resistance in wheat. *Theoretical and Applied Genetics.*, vol. 126, pp. 2197-2217. <https://doi.org/10.1007/s00122-013-2157-y>

29. Abdullah S., Sehgal S.K., Ali S., Liatukas Z. (2017) Characterization of *Pyrenophora tritici-repentis* (tan spot of wheat) races in Baltic States and Romania. *Plant Pathology Journal.*, vol. 33, pp. 133-139. <https://doi.org/10.5423/PPJ.OA.10.2016.0214>

30. Ali S., Gurung S., Adhikari T.B. (2010) Identification and characterization of novel isolates of *Pyrenophora tritici-repentis* from Arkansas. *Plant Disease.*, vol. 94, pp. 229-235. <https://doi.org/10.1094/PDIS-94-2-0229>

31. Engle J.S., Madden L.V., Lipps P.E. (2006) Distribution and pathogenic characterization of *Pyrenophora tritici-repentis* and *Stagonospora nodorum* in Ohio. *Phytopathology.*, vol. 96, pp. 1355-1362. <https://doi.org/10.1094/PHTO-96-1355>

32. Andrie R.M., Pandelova I., Ciuffetti L.M. (2007) A combination of phenotypic and genotypic characterization strengthens *Pyrenophora tritici-repentis* race identification. *Phytopathology.*, vol. 97, pp. 694-701.

33. Martinez J.P., Ottum S.A., Ali S., Francl L.J., et al. (2001) Characterization of the *ToxB* gene from *Pyrenophora tritici-repentis*. *Mol. Plant-Microbe Interact.*, vol. 14, pp. 675-677.

34. Abdullah S., Sehgal S.K., Ali S. (2017) Race Diversity of *Pyrenophora tritici-repentis* in South Dakota and Response of Predominant Wheat Cultivars to Tan Spot. *J. Plant. Pathol. Microbiol.*, vol. 8, p. 409. <https://doi.org/10.4172/2157-7471.1000409>

35. Faris JD, Zhang Z, Lu H, Lu S, et al. (2010) A unique wheat disease resistance-like gene governs effector-triggered susceptibility to necrotrophic pathogens, *Proc Natl Acad Sci U S A.*, 107(30):13544-13549. DOI: 10.1073/pnas.1004090107.

36. Riede C.R., Anderson J.A. (1996) Linkage of RFLP markers to an aluminum tolerance gene in wheat, *Crop Sci*, 36(4):905-909. DOI:10.2135/crops ci1996.0011183X0036000400015x.

37. Kokhmetova A.M., Kremneva O.Yu., Keyshilov Zh.S., Sultanova N.Zh. (2016b). Race range and virulence of *Pyrenophora tritici-repentis* isolates in the Republic of Kazakhstan and the North Caucasus region of Russia. *Eurasian J. Appl. Biotechnol.*, vol. 3, pp. 57-66. (in Russian)

38. Kokhmetova A., Kremneva O., Volkova G., Atishova M., et al. (2017) Evaluation of

wheat cultivars growing in Kazakhstan and Russia for resistance to tan spot. *J. Plant Pathol.*, vol. 99, pp. 161–167. <https://doi.org/10.4454/jpp.v99i1.3812>.

39. Kokhmetova A.M., Kovalenko N.M., Kumarbaeva M.T. (2020) *Pyrenophora tritici-repentis* population structure in the Republic of Kazakhstan and identification of wheat germplasm

resistant to tan spot. *Vavilov. J. Genet. Breed.*, vol. 24, no. 7, pp. 722–729. <https://doi.org/10.18699/VJ20.666>

40. Kamel S., Cherif M., Hafez M., Despins T., et al. (2019) *Pyrenophora tritici-repentis* in Tunisia: Race Structure and Effector Genes. *Front. Plant Sci.*, vol. 10, p. 1562. <https://doi.org/10.3389/fpls.2019.01562>

© This is an open access article under the (CC)BY-NC license (<https://creativecommons.org/licenses/by-nc/4.0/>). Funded by Al-Farabi KazNU

S. Syraiyl^{1*}, A. Ydyrys¹, A. Ahmet²,
R. Aitbekov¹, M.T. Imanaliyeva¹

¹Al-Farabi Kazakh National University, Almaty, Kazakhstan

²Akdeniz University, Antalya, Turkey

*e-mail: aksoy@akdeniz.edu.tr

(Received 19 April 2022; received in revised form 23 May 2022; accepted 31 May 2022)

Phytochemical composition and antioxidant activity of three medicinal plants from southeastern Kazakhstan

Abstract. Main results on study of phytochemical composition and antioxidant activity of three plants growing in southeastern part of Kazakhstan, namely *A. schrenkiana*, *L. turkestanicus* and *C. tianschanica*. Plant material was collected on flowering stage in July 2020. This study was carried out to evaluate the phytochemical constituents and antioxidant potential in order to validate the medicinal potential of these herbs. The antioxidant activity of alcoholic extracts was evaluated using 2,2 diphenyl-1-picrylhydrazyl (DPPH) assays. The total polyphenol and flavonoid content were determined according respectively to Spanos-Wrolstad and Zhishen method. The essential oil composition of samples was analyzed by gas chromatography (GC) (Agilent 7890A) coupled by flame ionization detector and mass spectrometry (Agilent 5975C) using capillary column (HP Innowax Capillary; 60.0 m×0.25 mm×0.25 μm). Phenols in *A. schrenkiana* (2.83 mg OE/g), in *L. turkestanicus* (2.86 mg OE/g), in *C. tianschanica* (16.08 mg OE/g). Flavonoids in *C. tianschanica* (21.79 mg RE/g), in *L. turkestanicus* (4.29 mg RE/g), in *A. schrenkiana* (3.8 mg RE/g). *C. tianschanica* (IC₅₀ = 0.78 μg.mL) had greater antioxidant activity than *A. schrenkiana* (IC₅₀ = 3.7 μg.mL) and *L. turkestanicus* (IC₅₀ = 3.38 μg.mL). The components of the essential oil of *A. schrenkiana* revealed 13 types of chemical elements, of which the indicators of camphor (44.79%) and 1.8-cineole (29.05%) were high.

Key words: *Artemisia schrenkiana* Ledeb, *Leonurus turkestanicus* V.I.Krecz, *Cerasus tianschanica* Pojark, antioxidant activity, phytochemical composition.

Introduction

More than 8,000 polyphenolic compounds have been identified in various plant species [1]. Polyphenolic compounds are natural antioxidants used for protection against oxidative damage to such important biological molecules like DNA, lipids, and proteins involved in numerous diseases, this means that they can stop the reaction of free radicals with other molecules in the body, preventing DNA damage, as well as long-term health effects [2]. In the scavenging of various free radicals, flavonoids are highly effective by their redox potential as they can destroy free radicals. They help in DNA repair, as well as inhibit angiogenesis and tumor invasion. There has been an increasing interest in research on plant flavonoids since their pharmacological properties are directly linked with their antioxidant potential [3]. Like in 2,2-diphenyl-1-picrylhydrazyl (DPPH) assay, a purple-colored solution of DPPH

radical, which by accepting electron is converted to discolour DPPH. In fact, the degree of color change is related to the concentration and effectiveness of the antioxidants. The degree of discoloration with respect to the decrease in the absorbance of the reaction mixture indicates the free radical scavenging action [4].

Many species of *Artemisia* is a valuable forage plant in Central Asia. It has a corresponding economic value as ornamental crops, medicinal and aromatic plants, many species of these plants are a source of essential oils used in medicine, cosmetics and pharmaceutical industry [5-6]. For example, new phytopreparations with antibiotic, antimicrobial, phytohormonal and antioxidant action were developed on the basis of santonin derivatives isolated from *A. cina* in the Institute of Phytochemistry of Medical University Karaganda (Kazakhstan) [7]. *A. schrenkiana* is used in folk medicine for allergies, skin diseases, respiratory diseases, as it contains many

biologically active substances, such as essential oils, saponins, tannins, phenolic compounds, vitamins, amino acids, organic acids, enzymes, absiogin and santonin [8].

Second plant *L. turkestanicus* is a perennial Woody rhizomatous plant belonging to the Lamiaceae family [9]. Plant species from the Lamiaceae family have been used in traditional herbal medicine for thousands of years. Traditional applications of plants from the Lamiaceae family are as a common tea, as an insect repellent, in flu control, and as an anti-inflammatory, sedative and analgesic agent. Tea and infusion from the aerial parts of *L. turkestanicus* is used in Uzbekistan to treat nervous disorders, hypertonia, hysteria, epilepsy, tachycardia, and gastrointestinal and female diseases and as soporific, anti-inflammatory, pathogenic, and laxative agents [10]. A previous phytochemical study of the aerial part of *L. turkestanicus* revealed the presence of the flavonoid genkwanin and iridoids 6-deoxy-8-acetylharpagide, 8-acetylharpagide, and harpagide [11].

The third plant, *C. tianschanica* is a tree-shrub plant belonging to the Rosaceae family. It grows in tropical and subtropical regions. It grows only in Central Asia (in the Pamirs and Tien Shan). In our country, it is distributed mainly in the Almaty region, where it can often be found in the foothills of the Takyr mountains [12]. It is used in folk medicine to treat skin rashes and can also be used for decorative purposes. It has been a favorite food of the local ethnic minorities in China since ancient times and was known as the "sacred xueyu fruit" [13]. It contains alkaloids (0.15%), tannins (10.4%), various sugars, malic acids and a very small amount of essential oil, fiber, vitamin C, carotenoids, and anthocyanins, each of which play an important role in cancer prevention. One of the most important groups of biologically active compounds in the composition are phenolic compounds. Their action on the human and animal body is diverse and underlies a number of vital functions and processes, in particular, metabolism, hematopoiesis, strengthening of vessel walls, etc. [14, 15].

Studied plants were long used in folk medicine to treat various diseases. However, despite their promising biological activities, these plants have been little studied in Kazakhstan. We aimed to focus on studying the total content of phenols and flavonoids and antioxidant activity of specimens from southeastern Kazakhstan. The composition of the essential oils of *A. schrenkiana* was determined as well.

Materials and methods

Objects of study. Three plants have been evaluated in this study, namely *A. schrenkiana*, *L. turkestanicus* and *C. tianschanica*. It is well known that the quantitative concentration of biologically active compounds changes depending on the stage of plant growth and development. For harvesting the plants, the best time for harvesting was determined. The three plants were gathered in August 2020. *C. tianschanica* plant was collected from the territory of Mount Sogeti of Almaty region (43° 27' 0" N, 78° 54' 0" E), *A. schrenkiana* plant was collected from the territory of Urdzhar District of eastern Kazakhstan region (47° 6' 13" N, 81° 33' 16" E), and *L. turkestanicus* was collected from the mountain Alma-Arasan gorge located in the south-western part of Almaty (43° 5' 11" N, 76° 54' 25" E).

The aerial parts were air dried in shade for ten days, then grinded to fine powder by using electric blender (Ruian Kangyuan Pharmaceutical Machinery limited company, China).

Preparation of the plant extracts. 20 mL methanol with 80% purity was added to the 2 g plant sample and extraction is made in the orbital shaker for 1 hour. The tube was centrifuged in 5,000 rpm during 5 minutes. Later, the liquid phase was collected in a test tube by filtering the solution. 5 mL methanol with 80% purity added to the residual part in the tube and the same process were recurred three times. After this, the extracts were taken to the 50 mL volumetric flask and it was diluted to the volume of the volumetric flask [16].

Determination of total phenolics. The total phenolic contents of the plant samples were determined as spectrophotometrically in accordance with the method of Spanos and Wrolstad [17]. For this goal, 100 µL were taken from the extracts and 900 µL deionized water, 4 mL Na₂CO₄ solution (75 g/L), 5 mL 0.2 N Folin Ciocalteu reactive was added. The mixture was stored at a dark place for 2 hours. The absorbance of the mixture was read in 765 nm wavelength in spectrophotometer device (Shimadzu UV-Vis 160A, Japan). At the end of the experiment, results were calculated as a gallic acid equivalent [18].

Determination of total flavonoids. The total flavonoid contents of the extracts were determined as spectrophotometrically according to the method of Zhishen. To achieve this goal, 1 mL was taken from the extracts and 4 mL deionized water and 0.3 mL NaNO₂ solution (5%) were added. After waiting 5 minutes, 0.60 mL AlCl₃ solution (10%) was added.

Then, 2 mL NaOH (4%) was added after 5 minutes. Total volume was completed with deionized water to 10 mL. The absorbance of the mixture was read in 510 nm.

Antioxidant activity. DPPH radical scavenging assay was performed by dilution with methanol after extraction. The 1mM DPPH radical solution was prepared depending on the number of samples; 600 μ L of DPPH was added to each of the tubes. Different amounts (20, 40, 60, 80, 100 μ l) of plant extract were added to the test tubes, the total volume of the tube was filled with up to 6 ml of methanol. All tubes were vortexed; the incubation procedure was made during 15 minutes in a dark place in the room temperature (25°C). 5,400 μ l MeOH was added to the 600 μ L DPPH for using as a replicate sample. Incubation of the copied sample was carried out within 15 minutes. The absorption values of the samples were read on a spectrophotometer with a wavelength of 517 nm at the end of the incubation procedure. The percentage inhibition values corresponding to the sample size were calculated according to the equation below.

$$\% \text{ Inhibition} = \frac{(\text{Abs}_{\text{DPPH}} - \text{Abs}_{\text{extract}}) / \text{Abs}_{\text{DPPH}} \times 100}$$

Certain inhibition values were shown on a graph showing the values of the sample volume, and a linear regression analysis was also performed, and curved equation was determined depending on the sample. The value of IC_{50} was calculated based on this equation. Obtaining the DPPH ($1/\text{IC}_{50}$) value showed a reverse value converted to mg for the new plant, which inhibits 50% of the 1 g DPPH radical [19].

Essential oil. The each dried samples were weighted as 20 g, the weighed sample was put into the Clevenger apparatus, deionized water was added as 200 mL, the hydrodistillation was realized as 2 hours. Essential oil content was calculated by using essential oil amount and weighed plant material [20].

Essential oil composition. The essential oil composition of plant samples was analysed by gas chromatography (Agilent 7890A, Agilent, USA) coupled by flame ionization detector and mass spectrometry (Agilent 5975C, Agilent, USA) using capillary column (HP Innowax Capillary, Agilent, USA; 60.0 m \times 0.25 mm \times 0.25 μ m). Essential oils were diluted 1:50 ratio with hexane. Gas chromatography (Agilent 7890A)-mass detector (Agilent 5975C) (GC-MS/FID) analysis was carried out at split mode of 40:1. Injection volume and temperature were adjusted as 1 μ L and 250 °C, respectively. Helium was the carrier gas at a constant flow rate of 0.8 mL/min. The oven temperature was programmed as follows:

60 °C for 10 minutes, increased at 4 °C/minute to 220 °C, and held at 220 °C for 10 minutes. Mass spectrometry (MS) spectra was recorded between 35 to 450 amu and the ionization mode used was electronic impact at 70eV. The relative percentage of the components was calculated from GC-FID peak areas [21].

Results and discussion

The results of quantitative determination of the content of biologically active substances in the studied samples of medicinal plants are presented in the drawings. The data obtained show that the content of biologically active substances in plants varies widely. Thus, for example, the mass fraction of phenolic and flavonoids in plant raw materials varies considerably from ~ 0.5% in *A. schrenkiana* to ~ 8% in *C. tianschanica*.

In this study, the amount of total phenols varied in the three plants and ranged from 2.02 to 20.81 mg/g dry matter. The highest level of phenols was found in *C. tianschanica*. It was noted that the total amount of phenolic compounds in Rosaceae varieties, it is higher than in other families. Relatively low levels of phenols were found in *A. schrenkiana* (2.83 mg EHA/g), *C. tianschanica* (16.08 mg EHA/g) and *L. turkestanicus* (2.86 mg EHA/g dry weight) (Figure 1).



Figure 1 – Total phenol contents for the studied plants, mg GAE/g dry weight

Flavonoids are considered one of the most common groups of natural compounds found in plants. The Zhishen method, most commonly used for determining the total flavonoid content, showed relatively good reproducibility. *C. tianschanica* was distinguished by the highest content of flavonoids (21.79 mGRE/g), *A. schrenkiana* (3.80 mGRE/g) and *L. turkestanicus* (4.29 mGRE/g) (Figure 2).

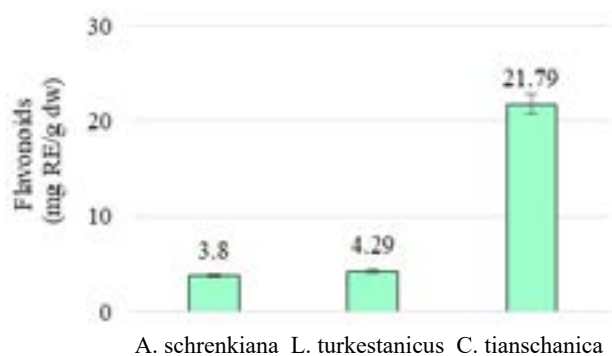


Figure 2 – Total flavonoid contents for the studied plants mg RE/g dry weight

Antioxidant activity. Among extracts tested for antioxidant activity by DPPH, crude methanol extracts of *C. tianschanica*. IC_{50} 0.78 $\mu\text{g/mL}$, *A. schrenkiana* and *L. turkestanicus* showed antioxidant activity with (IC_{50}) values of 3.7 $\mu\text{g/mL}$ and (3, 38 $\mu\text{g/ml}$) respectively. The results show that the antioxidant activity of the crude extract of *C. tianschanica* is relatively high compared to the other two plants (Figure 3).

A. schrenkiana is a valuable fodder and medicinal plant and contains a large amount of essential oils.

The amount of essential oil collected from the *A. schrenkiana* plant was 0.15 ml and the composition of the essential oil in the plant *A. schrenkiana* is 0.37%. The main components of the essential oil: camphene – 3.65%, 1,8-cineole – 29.05%, g-terpinene – 0.30%, p-cymene – 1.08%, α -thujone – 0.35%, camphor – 44.79%, bornyl acetate – 0.93%, terpinen-4-ol – 1.16%, borneol – 4.26%, carvone – 0.70%, β -oplophenone – 1.57%, spatulenol – 3.76% and others – 8.40%. These components are displayed on the histogram (Figure 4).

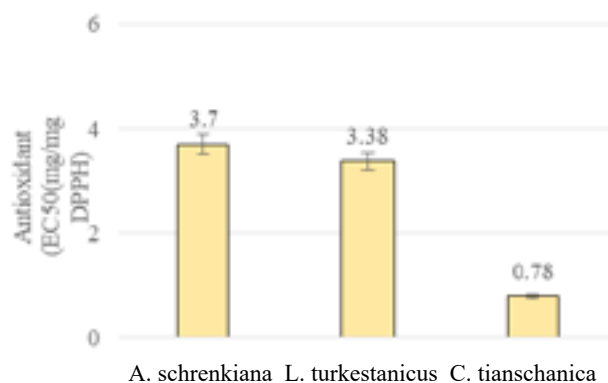


Figure 3 – The value of antioxidant activity ($\mu\text{g/ml}$ DPPH)

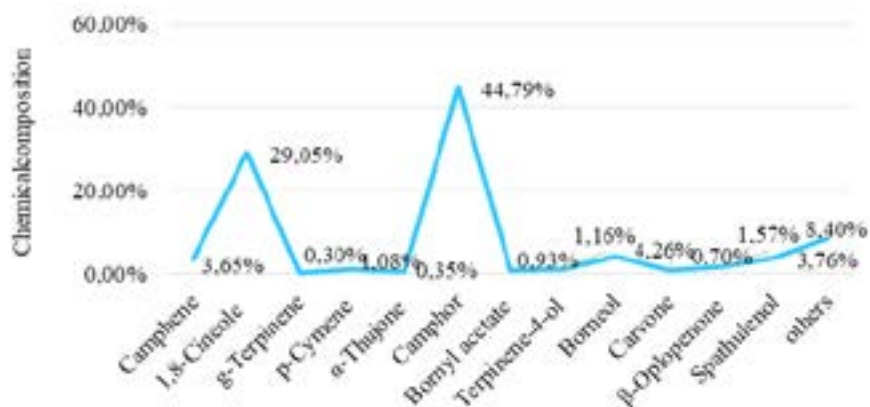


Figure 4 – Chemical composition of *A. schrenkiana* essential oil

We have previously studied nine different elements in *A. schrenkiana*, including macro and microelements lead, cadmium, zinc, copper, iron, manganese, sodium, and potassium [22]. A second study was on the effect of *A. schrenkiana* herbal extract on insulin, glucose, and homeostatic model for assessing insulin resistance (HOMA-IR) serum

levels in diabetic rats and *A. schrenkiana* extract improved the alloxan-induced diabetic metabolic abnormality [23].

Phenols are valuable secondary plant metabolites found in plants and their products, which might potentially be associated with antioxidant, anti-inflammatory, anticancer,

hypoglycemic, hypocholesterolemic, antibacterial, antifungal, antiviral, and analgesic activities [24-26]. Interestingly in some cases the cytotoxic effect of many plant extracts might be related to their antioxidant activity. According to the US National Cancer Institute, the IC₅₀ value should be <20 g/mL for plant extract to be considered as a potential cytotoxic agent, and <4 mcg/ml for isolated compounds [27]. Higher content of total phenols and flavonoids was observed in *C. tianschanica* (13.869 mg GAE/g and 21.79 mg RE/g). All three different plants analyzed have high antioxidant properties, however the highest antioxidant activity was observed in *A. schrenkiana*.

A plant growing in different places has different phytochemical components. For example, in Kazakhstan, *A. schrenkiana* had high levels of camphor (44.79%) and 1,8-cineole (29.05%). The reason for this phenomenon might be the favorable climate and fertile soils of southeastern Kazakhstan. They give plants unique healing properties. In particular, it is a common tea used as an anti-inflammatory, sedative and analgesic for influenza, and due to 1,8-cineol, it can be used in therapeutic soaps, sprays or cosmetic flavors and other hygiene products, such as toothpaste, which have a bactericidal effect [28, 29].

Conclusion

It was found that despite the higher content of total phenols and flavonoids in *C. tianschanica* (13.869 mg GAE/g and 21.79 mg RE/g), higher antioxidant activity was observed in *A. schrenkiana*, which looks promising by the composition of its essential oil, in which prevailing compounds are camphor (44.79%) and 1,8-cineole (29.05%).

Acknowledgments

Scientific work was conducted within the framework of the project AP13067924 Comprehensive studies of some promising medicinal plant species from the Asteraceae family for the industrial development, funded by the Ministry of Science and Higher Education.

References

- Kondratyuk T.P., Pezzuto J.M. (2004) Natural Product Polyphenols of Relevance to Human Health. *Pharm Biol.* <https://doi.org/10.3109/13880200490893519>
- Soobrattee M. A., Neergheen V. S., et al. (2005) Phenolics as potential antioxidant therapeutic agents: mechanism and actions. *Mutation Research.* doi:10.1016/j.mrfmmm.2005.03.023
- Zhishen J., Mengcheng T., Jianming W. (1999) The determination of flavonoid contents in mulberry and their scavenging effects on superoxide radicals. doi:10.1016/s0308-8146(98)00102-2
- Krishnaiah D., Devi T., Bono A., Sarbatly R. (2009). Studies on phytochemical constituents of six Malaysian medicinal plants. *Medicinal Plants Research.* <https://doi.org/10.5897/JMPR.9001153>
- Rahil R. B., Muneeb U. R., Ambreen S., Manzoor U. R., et al. (2019) Chemical Composition and Biological Uses of *Artemisia absinthium* (Wormwood). [Plant and Human Health] Switzerland: the company Springer Nature Switzerland AG, 151 p. ISBN: 978-3-030-04408.
- Teixeira D.S., Jaime A. (2004) Mining the essential oils of the Anthemideae. [African Journal of Biotechnology] Japan: Faculty of Agriculture, Kagawa University, 706 p. eISSN: 1684-5315.
- Kemelbek M., Syraiyl S., Ydyrys A., Xiaofeng M., Jenis J. (2020) Biological, Phytochemical features and medicinal use of plant species belonging to the genus *Artemisia* of South-eastern Kazakhstan. [Astana medical journal] Kazakhstan: Astana medical university, 162 p. ISSN: 1562-2940.
- Godwill A. E. (2018) Free radicals and the role of plant phytochemicals as antioxidants against oxidative stress-related diseases. doi: 10.5772/intechopen.76719.
- Dewick, P. M. (2002) a biosynthetic approach [Medicinal natural products] India: Chennai, 2 p. ISBN: 047-1-496-413.
- Brahmi F., Khodir M., Mohamed C., Pierre D. (2017) Chemical composition and biological activities of *Mentha* species. In: *Aromatic and Medicinal Plants-Back to Nature.* Egypt: Cairo University, 51 p. ISBN 978-953-51-2978-3.
- Isaev I. M., Agzamova M. A., Isaev M. I. (2011) Genkwanin and iridoid glycosides from *Leonurus turkestanicus*. *Chemistry of Natural Compounds*, <https://doi.org/10.1007/s10600-011-9857-9>
- Potter D., Eriksson T., Evans R. C., Morgan D. R., M. et al. (2007) Phylogeny and classification of Rosaceae. doi:10.1007/s00606-007-0539-9
- Kanat N. S. (2018) Medicinally Important Plants of Kazakhstan. doi:10.1007/978-3-319-99728-5_10
- Mamedov N., Mamadalieva N. (2016) Medicinal plants of former USSR used for treatment of depression [Herbal Medicine in Depression] Uzbekistan: Academy of Sciences of Uzbekistan, 183 p. ISBN: 978-3-319-14021-6.

15. Solovyova V. (2011) Olma Media Group/ Enlightenment, [Encyclopedia of medicinal plants]. Kazakhstan pp. 78-79. ISBN978-8472081598.
16. Nair S., Nagar R., Gupta R. (1998) Antioxidant phenolics and flavonoids in common Indian foods. [Journal of the Association of Physicians of India]. India, 708 p. ISSN/ISBN: 0004-5772.
17. Ena A., Pintucci C., Carozzi P. (2012) The recovery of polyphenols from olive mill waste using two adsorbing vegetable matrices. doi: 10.1016/j.jbiotec.2011.06.027.
18. Abulude F. O., Ogunkoya M. O., Akinjagunla Y. S. (2010) Phytochemical screening of leaves and stem of cashew tree (*Anacardium occidentale*). [Cookies on CAB Direct], Spain: Faculty of Science, University of Vigo et Ourense, 815-819 p. ISSN:1579-4377.
19. Re R., Pellegrini N., Proteggente A., Pannala A., Yang M., Rice-Evans C., et al. (2009) Antioxidant activity applying an improved ABTS radical cation decolorization assay. doi: 10.1016/s0891-5849(98)00315-3.
20. Spanos G. A., Wrolstad R. E. (1990) Phenolics of apple, pear, and white grape juices and their changes with processing and storage. doi:10.1021/jf00021a002.
21. Uysal Bayar F., Çinar O. (2020) Yield and quality parameters of some cultivated *Origanum* spp. species. <https://doi.org/10.16882/derim.2020.605745>.
22. Syraiyl S., Kemelbek M. (2020) Determination of biological activity of phytochemical composition of *Artemisia schrenkiana* Ledeb plant. [International scientific conference Farabi Alemi]. Kazakhstan, pp. 42. ISBN 978-601-04-5238-9.
23. Ydyrys A., Syraiyl S., Abdolla N., Erkenova N. (2020) Study of the effect of *Artemisia schrenkiana* Ledeb plant extract on insulin, glucose and HOMA-IR serum levels in diabetic squirrels. [Astana medical Journal], Kazakhstan Astana medical university, pp. 67-76. ISSN: 1562-2940.
24. Takeda Y., Tomonari M., Arimoto S., Masuda T., Otsuka H., Matsunami K., Ashurmetov O. A. (2008) A new phenolic glucoside from an Uzbek medicinal plant, *Origanum tyttanthum*. doi: 10.1007/s11418-007-0187-y.
25. Kaur C., Kapoor H. C. (2002) Antioxidant activity and total phenolic content of some Asian vegetables. <https://doi.org/10.1046/j.1365-2621.2002.00552.x>
26. Halliwell B., Gutteridge J. M. (1992) Free radicals, antioxidants and human disease. <https://doi.org/10.1146/annurev.nu.16.070196.000341>.
27. Atanassova M., Georgieva S., Ivancheva K. (2011) Total phenolic and total flavonoid contents, antioxidant capacity and biological contaminants in medicinal herbs. [Journal of the University of Chemical Technology & Metallurgy], Bulgaria: University of Chemical Technology and Metallurgy, 12 p. ISSN 1314-7978.
28. Abad M. J., Bedoya L. M., Apaza L., Bermejo P. (2012) The *Artemisia* L. genus: a review of bioactive essential oils. doi: 10.3390/molecules17032542.
29. Mamadalieva N. Z., Akramov D. K., et al. (2017) Aromatic medicinal plants of the Lamiaceae family from Uzbekistan: Ethnopharmacology, essential oils composition, and biological activities. doi: 10.3390/medicines4010008

© This is an open access article under the (CC)BY-NC license (<https://creativecommons.org/licenses/by-nc/4.0/>). Funded by Al-Farabi KazNU

N.V. Khan^{1*}, M. Baláž², M.M. Burkitbayev¹,
 B.B Tatykayev¹, Zh.S. Shalabayev³, A.I. Niyazbayeva¹,
 F.Kh. Urakaev^{1,4}

¹Al-Farabi Kazakh National University, Almaty, Kazakhstan

²Institute of Geotechnics, Košice, Slovakia

³Scientific Center of Anti-infectious Drugs, Almaty, Kazakhstan

⁴Sobolev Institute of Geology and Mineralogy, Novosibirsk, Russia

*e-mail: Natalya.Khan@kaznu.edu.kz

(Received 2 May 2022; received in revised form 17 May 2022; accepted 07 June 2022)

Solvothermal DMSO-mediated synthesis of the S/AgI microstructures and their testing as photocatalysts and biological agents

Abstract. S/AgI microstructures were produced by solvothermal DMSO-mediated synthesis using two methods of sulfur precipitation: at room temperature (method 1) and by water (method 2). The samples were obtained with different percentages of AgI: 10, 30 and 50 %. Microstructures were investigated with help of XRD, Raman spectroscopy and SEM/EDS (elemental mapping). XRD and Raman spectroscopy confirmed the presence of sulfur and AgI. EDS elemental mapping revealed that samples were composed of large grains of sulfur covered by smaller grains of AgI. The obtained SEM micrographs revealed that the 1st method gave larger grains of sulfur in comparison with the 2nd method. Testing of the microstructures as photocatalysts showed the low activity; as the prepared samples were able to degrade no more than 7 % of the molecules of Orange II. Significant biological activity was detected only for S/AgI (2) 50 % sample, as it was able to suppress test strains of *S. aureus* ATCC BAA-39, *P.aeruginosa* ATCC 9027 and *Erwinia amylovora* at MBC/MFC 5000 µg/mL, and *E. coli* ATCC 8739 at 2500 µg/mL.

Key words: sulfur; silver iodide; solvothermal synthesis; microstructures; photocatalytic activity; biological activity.

Introduction

Micro- and nano-structures are widely used in various fields [1-3]. Among them are structures based on sulfur and silver iodide (AgI) [4, 5]. The necessity of obtaining such structures is explained by the possibility of their application in photocatalysis, biochemistry and electrochemistry. The production of silver halides is caused by high cost of the feedstock, so the question arises of using cheaper accompanying components that could enhance certain properties and reduce the amount of used silver halide. Sulfur can potentially serve as such a cheap and accessible component.

Sulfur is an inorganic substance, which used in wide range of the science and technology [6]. It is often used in production of batteries, because of its semiconductor properties [7, 8]; in drugs production because of its anti-inflammatory properties and the ability to treat different diseases

[6, 9]. In the production of fertilizers, sulfur used in oxidized form, which improves the ability of plants to absorb the necessary components [10]; in the production of antibacterial and antifungal agents, sulfur is more active in nano-state [11, 12]. Sulfur is also used in photocatalytic CO₂-reduction [13] and hydrogen evolution [14] in combination with C₃N₄. For degradation of organic dyes, sulfur doping by ZnO and PbO is also used [15, 12].

AgI is inorganic substance with specific properties. The most common application of the AgI is photocatalysis [16-22] because of its photosensitivity. In degradation of model solutions and various contaminants, AgI is used with other materials for obtaining of the enhanced properties. For example, it can be TiO₂, Ag, Bi₅O₇I, BiOI, C₃N₄, SnS₂ and others [17-19]. Another application field of AgI is microbiology, more accurately, the production of antimicrobial agents [13, 17-19, 21]. Here AgI

also used in combinations with other substances, like, PVA, ZnO and chlorophyll [18].

Preparation methods of above mentioned materials encompass mainly from hydrothermal to solid-phase route [6-15, 20-24]. In our case, we have chosen the solvothermal DMSO-mediated method of synthesis. DMSO is aprotic and bipolar solvent, which is used in medicine, biotechnologies, chemistry and other fields [25]. DMSO is less dangerous and toxic in comparison with other aprotic and polar organic solvents; it can serve as a source of sulfur and dilute a big number of substances [26-28]. Our research group have already studied the behavior and solubility of the sulfur in DMSO media [29] and synthesized sulfur-containing materials with silver compounds [30, 31]. In the present case, we have used similar methodology to [30], however, the mass ratios of the components was changed and in the process of precipitation of sulfur by water, the volume of it was different. Hence, this research work is devoted to the synthesis of microstructures based on sulfur and AgI, and further study of the effect of the method of obtaining and the percentage of components on the manifestation of photocatalytic and biological activities.

Materials and methods

Materials. Silver nitrate, ammonia iodide, sulfur, Orange II were provided by Sigma Aldrich (Germany). Dimethyl sulfoxide and sodium chloride were supplied by OJSC Mikhailovsky Plant of Chemical Reagents (Russia). Mueller Hinton Agar (M173) and Mueller Hinton Broth (M391) were purchased from HiMedia (India). All reagents were of analytical grade and deionized water was used in experiments.

Characterization. X-ray diffraction (XRD) was used for determination of the phase composition of the samples. Analysis was conducted with Rigaku MiniFlex 600 X-ray diffractometer using copper radiation ($\lambda = 0.15405$ nm). The XRD patterns were processed with help of the ICCD-PDF2 release 2016 database.

Raman spectroscopy was conducted for identification of the samples composition and proving the XRD results. Analysis was made on Solver Spectrum (NT MDT Instruments, Russia) spectrometer using an 1800/500 diffraction grating.

The morphology and size of the particles were studied by scanning electron microscopy (SEM) and particle distribution by Energy Dispersive X-ray mapping analysis (EDS mapping). Analysis was conducted on Quanta 200i 3D microscope (FEI,

Netherlands). The analyses were conducted in the NNLOT laboratory of al-Farabi Kazakh National University.

Absorption spectra of the samples were obtained with help of SF-56 (OKB Spektr, Russia) spectrophotometer, using wavelength range from 350 to 700 nm.

Synthesis of the S/AgI microstructures (sulfur deposition at room temperature), (1) The process of the synthesis was conducted with using an apparatus, which consist of three-neck round bottomed flask, thermometer, backflow condenser and magnetic stirrer. The similar procedure was used in [30]. For obtaining silver iodide, the solutions of AgNO_3 and NH_4I in DMSO were used (50 mL of each solution). The required amount of sulfur was dissolved in 100 ml of DMSO at 120 °C with constant stirring. Then 1/10 part of the NH_4I was added drop by drop to the reaction mixture and the content of the flask was stirred for 15 minutes. After that, a solution of AgNO_3 and NH_4I were introduced into the flask alternately, drop by drop. Thus, AgI is formed because of the ion exchange reaction (1). Then, the resulting mixture was cooled at room temperature for 12 hours for complete precipitation of sulfur from the DMSO solution. Further, the mixture was stirred and precipitated in a centrifuge (Rotina 380, Hettich, Germany) (4000 rpm, 10 min), washed 2 times with deionized water and dried for 12-14 hours, at 70 °C.



The marking of the samples depending on the content of AgI and synthesis method was adopted as follows: S/AgI (1) 10, 30, 50 % and S/AgI (2) 10, 30, 50 %. Here 10, 30, 50 % shows the content of AgI, the rest is sulfur, (1) – a synthesis method in which sulfur precipitates at room temperature and (2) – a synthesis method in which sulfur precipitates by diluting the reaction mixture with water.

Synthesis of the S/AgI microstructures (sulfur deposition by water), (2) The initial steps of synthesis were identical to the previous method described above. However, the process of the precipitation of sulfur was different. After adding solutions of AgNO_3 and NH_4I to the flask, deionized water was poured into the mixture. The volume ratio of water to the reaction mixture was 1:1. At final step, the products were precipitated, washed and dried.

Synthesis of pure AgI. The procedure of obtaining of pure AgI was the same as the previous, but the step of introducing of sulfur to the reaction mixture was excepted.

Synthesis of pure S. The procedure of obtaining of pure S was the same as the previous, but the step of introducing of solutions of AgNO_3 and NH_4I to the reaction mixture was skipped.

Photocatalytic activity. 20 mg of the microstructure was introduced to 40 mL of the Orange II (10 mg/L). For uniform distribution of the sample in the volume of the solution, ultrasound treatment was used (3 min). To stabilize the samples, the adsorption-desorption test was conducted in the dark conditions for 1 hour (the sample was covered with aluminum foil). When the adsorption process is complete and the sample is stable, the visible light exposure begins. The source of visible light was a 300 W Osram Vita-lux lamp equipped with a UV filter. The irradiation intensity was 15 mW/cm^2 . Sampling was carried out every 30 minutes. Then, the sample was centrifuged (Rotina Micro 200, Hettich, Germany) for 3 min at 10000 rpm. The photocatalytic activity of the samples was studied with help of UV-Vis spectrophotometer. Each study was conducted twice to confirm the results.

Biological activity. For study of the biological activity the following bacterial strains of American Type Culture Collection (ATCC) were used: *Staphylococcus aureus* ATCC 6538-P (collection sensitive strain); *Candida albicans* ATCC 10231 (collection sensitive strain); *Escherichia coli* ATCC 8739 (collection sensitive strain); *Pseudomonas aeruginosa* ATCC 9027 (collection sensitive strain); *Erwinia amylovora* (phytopathogenic strain), *Staphylococcus aureus* (subsp. aureus) ATCC BAA-39 and *Escherichia coli* ATCC BAA-196TM. The sensitivity of microorganisms was studied on standard nutrient media [32].

Preparation of bacterial suspension. For preparation of the bacterial solution 5 mL of saline solution was poured to the test tube, then the test strain was added, and vigorously stirred. The result suspension was tested for the following characteristics: for bacteria, the turbidity was 0.5 McFarland units (which corresponds to a concentration of 1.5×10^8 CFU/mL); for yeast – like fungi, the turbidity was 2.5 (which corresponds to a concentration of 7.5×10^8 CFU/mL). 1 mL of the suspension was transferred in 9 mL of sterile saline solution for tenfold dilutions. As a result, a concentration of 1.5×10^6 CFU/mL for bacteria and 7.5×10^6 CFU/mL for yeast-like fungi, was obtained. The purity of bacterial strains was examined before each experiment.

Method of two-fold serial dilutions. The biological activity was studied on water suspensions of microstructures (10 mg/mL).

In typical experiment, 0.5 mL of Muller-Hinton broth was poured to the plate with 48 wells. Then, 0.5 mL of the water solution of microstructure was poured in the first well of the row and stirred. Hence, 1:1 dilution was obtained. For 1:2 dilution, 0.5 mL of mixture from the first well was stirred and transferred to the second well. In that way other two-fold serial dilutions up to 1:128 were prepared. After that, 0.05 mL of test strains of microorganisms were added to all wells. For each series of dilutions, medium control and strain growth control were used. Experimental procedures were carried out in two repetitions for all samples [32, 33].

The incubation of the samples was conducted for 48 hours at a temperature of $(22 \pm 1)^\circ\text{C}$ for fungi and for 18-24 hours at $(37 \pm 1)^\circ\text{C}$ for bacteria. The seeding at Petri dish was carried out to determine the number of living cells. The incubation conditions were similar to conditions described above.

The biological activity was determined by examining the visible growth of microorganisms on the surface of a solid nutrient medium. The minimal bactericidal (fungicidal) concentration (MBC or MFC) was considered as a measure of the biological activity.

All experiments were performed in three repetitions.

Results and discussion

XRD analysis. In the Figure 1 the XRD patterns of the S/AgI (1, 2) 10, 30, 50 %, pure AgI and S (1, 2) are shown. According to the obtained results there are three noticeable peaks of AgI at 23.76 , 39.24 and 46.36° , which correspond to its gamma modification. Also, with an increase in the content of AgI, the intensity of these peaks increases. As for sulfur, it can be seen that samples represented by one clear peak at about 23.18° and small peaks in the range between 25 and 30° . There is also an increase in the intensity of peaks, with an increase in the sulfur content in the samples. In order to confirm the presence of identified phases, the Raman spectroscopy measurements have been conducted.

Raman spectroscopy. In the Figure 2 the Raman spectra of S/AgI (1, 2) 10, 20, 50 %, pure AgI and S (1, 2) are shown. Pure AgI (orange spectrum) is represented by two peaks at 74 and 109 cm^{-1} , while pure sulfur (red and blue spectra) has four clear peaks at 89 , 158 , 223 and 477 cm^{-1} . The obtained results correspond to the [34]. The signals corresponding to both phases could be identified in S/AgI. Hence, synthesized samples contain both S and AgI.

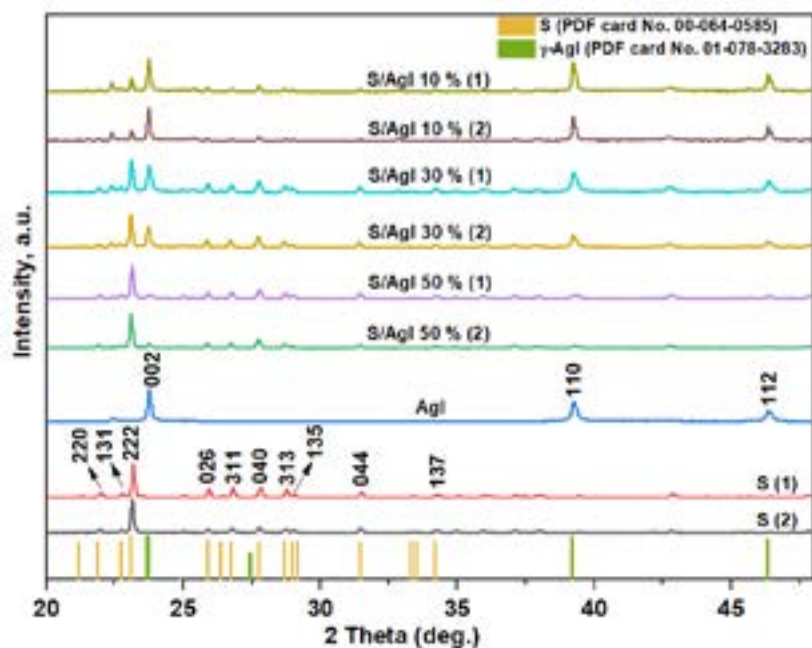


Figure 1 – XRD patterns the S/AgI (1, 2) 10, 30, 50%, AgI and S (1, 2)

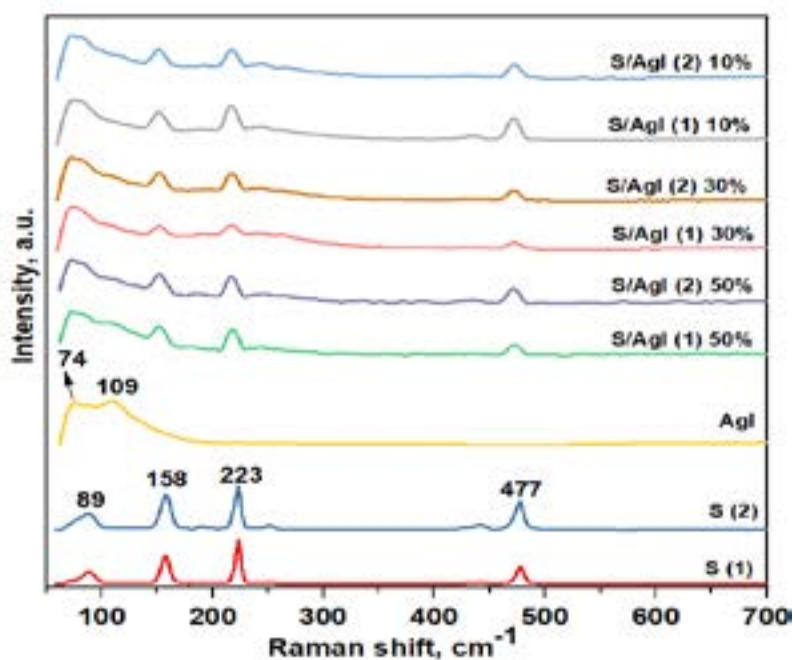


Figure 2 – Raman spectra of the S/AgI (1, 2) 10, 30, 50 %, AgI and S (1, 2)

SEM/EDS analyses. For understanding of distribution of all components of the samples the EDX mapping have been conducted. For this analysis only 50 % samples were analyzed, because the samples with a higher sulfur content melted.

In Figure 3 (a-h), the results for S/AgI (1, 2) 50 % are shown. In the case of S/AgI (1) 50 % sample, large sulfur grains were detected (Figure 3a). However, the small grains of sulfur also can be seen (Figure 3 b). As for Ag and I – it is evenly distributed

on the surface of the sulfur particles. Thus, the large grains of the sulfur are covered by a layer of the AgI [31]. For S/AgI (2) 50 % the presence of large grains

was not evidenced. In general, more homogeneous distribution of all elements was detected for this samples.

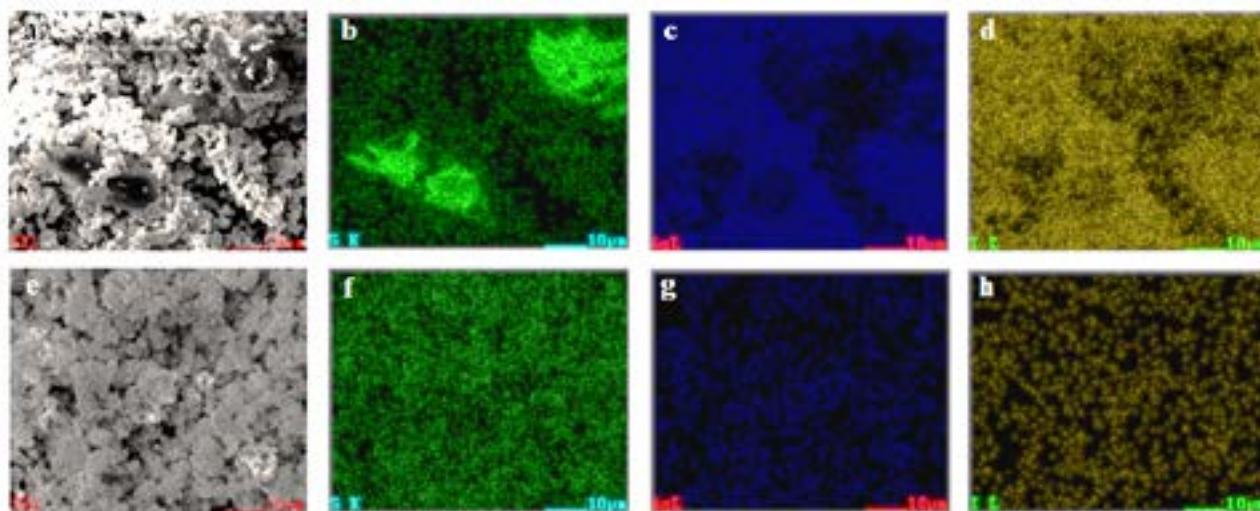


Figure 3 – EDS mapping of S/AgI 50% (1) (a-d), (2) (e-h). a, e – EDS layered images; b, f – EDS image of S distribution; c, g – EDS image of Ag distribution; d, h – EDS image of I distribution

To further confirm the presence of small AgI particles on the surface of sulfur grains, a more detailed SEM analysis was performed (Figures 4 – 6). In general, the presence of big particles covered by smaller ones can be seen in all samples. It is highly probable that sulfur is represented by dark large particles with irregular form and AgI by small light particles with even and clear boundaries.

The results of SEM analysis of S/AgI (1) 10 % are shown in the Figure 4 (a – c) and of S/AgI (2) 10% – in the Figure 4 (d – f). Here the first method gives the largest grains of the sulfur. The average size of sulfur in the S/AgI (1) 10 % is fluctuated from 20 to 50 µm, while for the S/AgI (2) 10 % it has size range from 10 to 20 µm. AgI particles obtained by method 1 have clear and smooth triangle and hexagonal form with the average size of 0.5 – 3 µm. AgI particles in the S/AgI (2) 10 % are irregular with size from 0.3 to 0.9 µm.

In Figure 5, 6 (a – f) the SEM of the S/AgI (1, 2) 30, 50 % are given. Here also the 1st method gave sulfur with bigger size in comparison to the 2nd method. The morphology and the size of the sulfur is similar to the samples with 10 % AgI content. The AgI particles obtained by method 1 have also triangular and hexagonal form with smooth surface

and in the method 2 the AgI particles exhibit irregular shape with loose surface. The size of AgI in the S/AgI (1) 30 % is in the range from 0.2 to 0.6 µm and for S/AgI (2) 30 % from 0.4 to 1 µm. In 50 % samples the 1st method produced sulfur particles with the size range from 20 to 50 µm and the 2nd method – from 5 to 10 µm. AgI grains are represented by size from 1 to 3 µm and from 0.5 to 2 µm for both method 1 and 2, respectively.

For easier perception of the data on the particle sizes of microstructures, we have given all the data in Table 1.

Photocatalytic activity. Figure 7a shows a comparison of the photocatalytic activity of the S/AgI (1, 2) 10, 30, 50 % micro-structures and pure AgI and S (1, 2). The results show that pure AgI is able to degrade 99 % molecules of Orange II after 180 minutes of exposure to visible light, while after the same duration, the S/AgI (1, 2) samples of all compositions and pure sulfur do not show photodegradation higher than 7 %. Hence, the synthesized microstructures do not possess photocatalytic activity. Such result can be explained by the micro-size of the sulfur, which probably passivates otherwise photocatalytically active AgI. Maybe the higher content of the AgI could solve this problem.

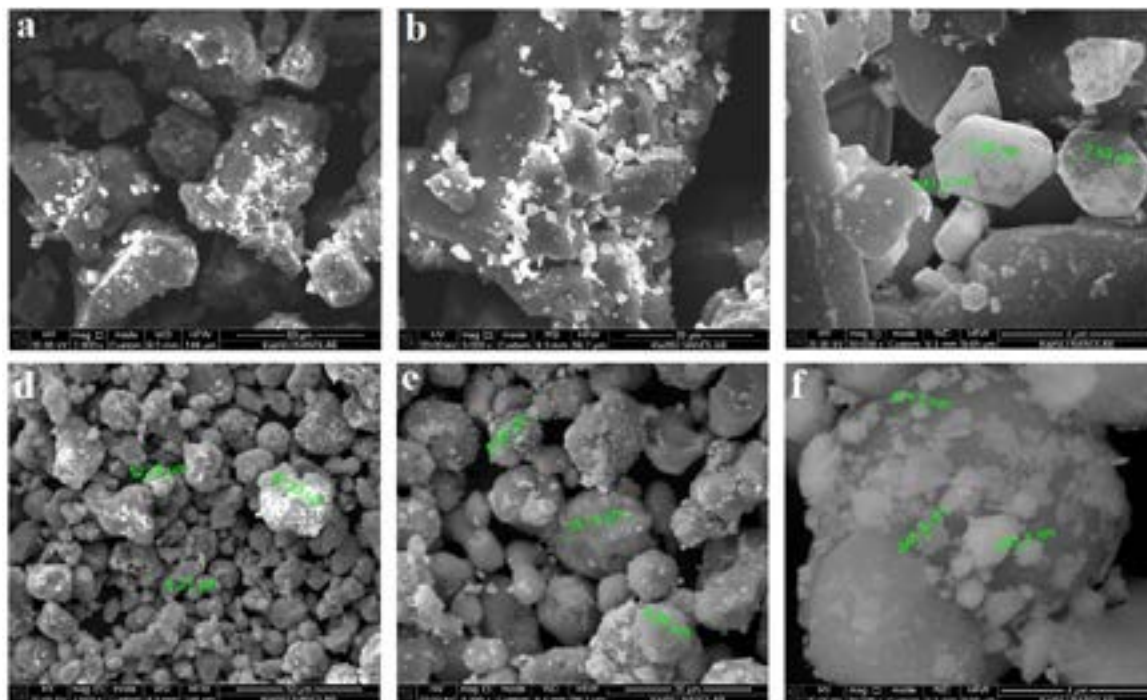


Figure 4 – SEM analysis of the: S/AgI (1) 10 % (a – 2000x; b – 5000x, c – 30000x magnification); S/AgI (2) 10 % (d – 2000x; e – 5000x, f – 30000x magnification)

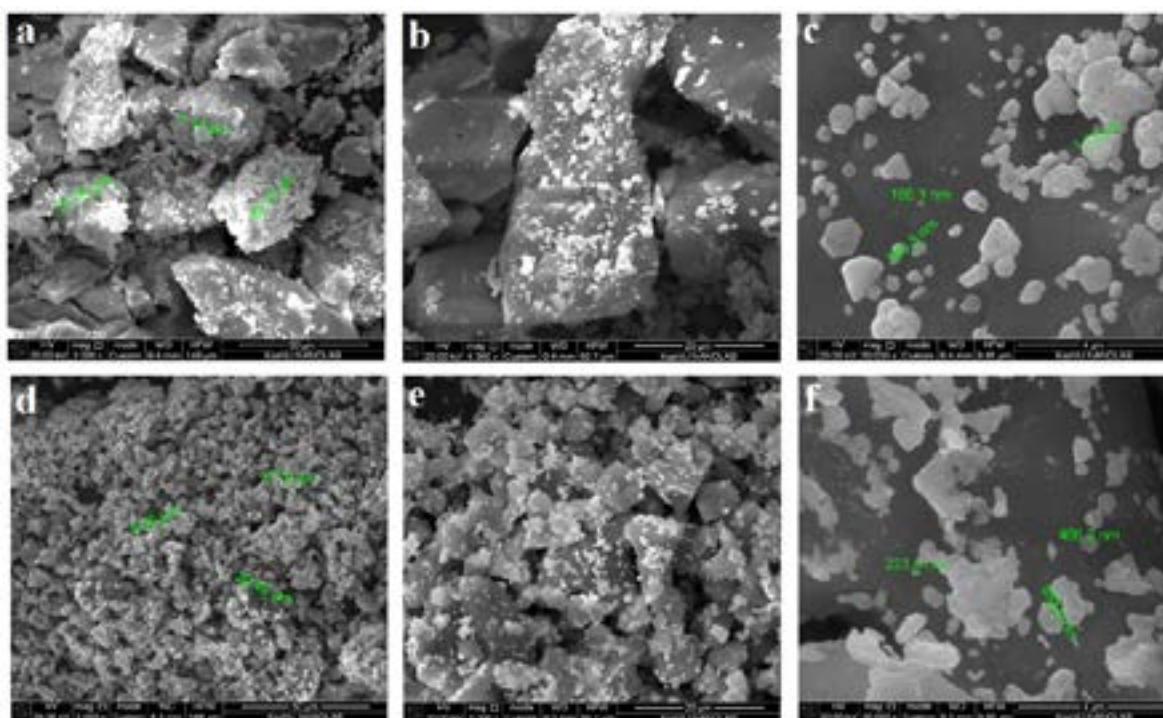


Figure 5 – SEM analysis of the: S/AgI (1) 30 % (a – 2000x; b – 5000x, c – 30000x magnification); S/AgI (2) 30 % (d – 2000x; e – 5000x, f – 30000x magnification)

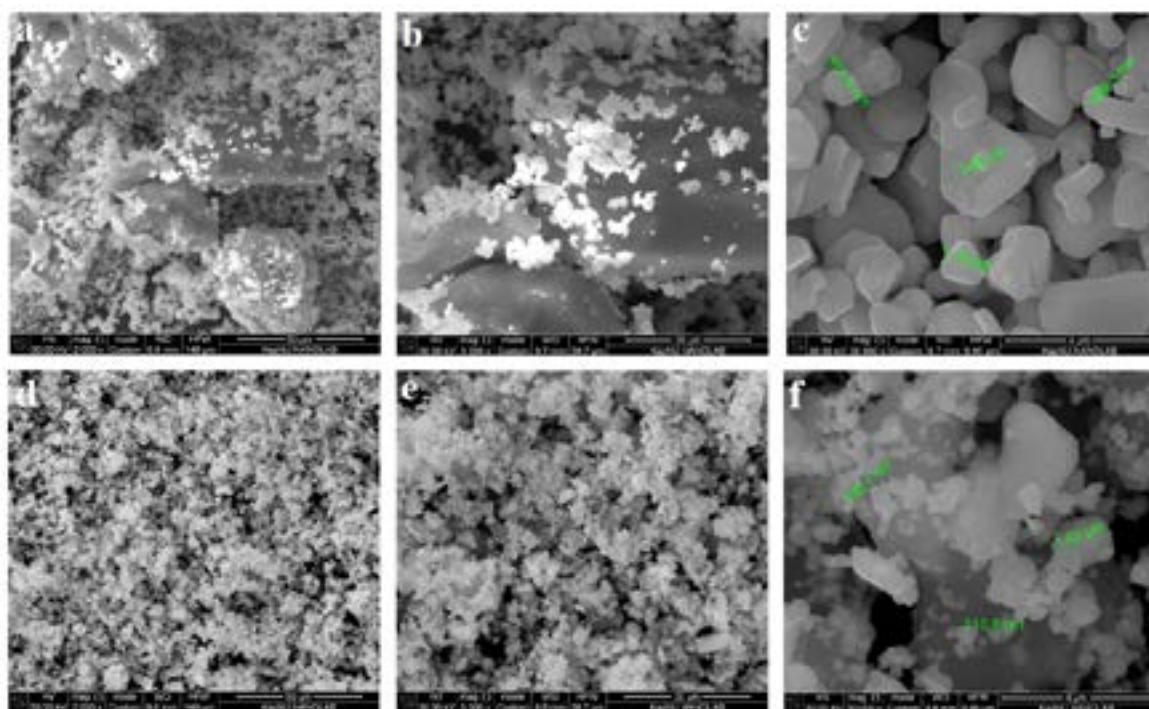


Figure 6 – SEM analysis of the: S/AgI (1) 50 % (a – 2000x; b – 5000x, c – 30000x magnification); S/AgI (2) 50 % (d – 2000x; e – 5000x, f – 30000x magnification)

Table 1 – The size ranges of the microstructures

Microstructure	The size range of the sulfur, μm	The size range of the AgI, μm
S/AgI (1) 10 %	20-50	0.5-3.0
S/AgI (2) 10 %	10-20	0.3-0.9
S/AgI (1) 30 %	20-50	0.2-0.3
S/AgI (2) 30 %	5-10	0.4-1.0
S/AgI (1) 50 %	20-50	1.0-3.0
S/AgI (2) 50 %	5-10	0.5-2.0

The kinetics of the photocatalytic process was accepted as a pseudo-first-order reaction: $\ln(C_0/C) = kt$. C_0 and C are initial and final concentrations, respectively, of model solution in moment of time t ; k (min^{-1}) is the rate constant of the photocatalytic reaction [35]. Other kinetics models were also studied, but the most suitable one was the pseudo-first-order reaction. The k

was found from the linear graphs. High Pearson's correlation coefficient r was a proof of the kinetic order of model solution degradation. Figure 8 b shows the pseudo-first order kinetics for photocatalytic degradation of Orange II by S/AgI (1, 2) 10, 30, 50 % microstructures. In the Table 2, the values of k and r for all synthesized samples can be found.

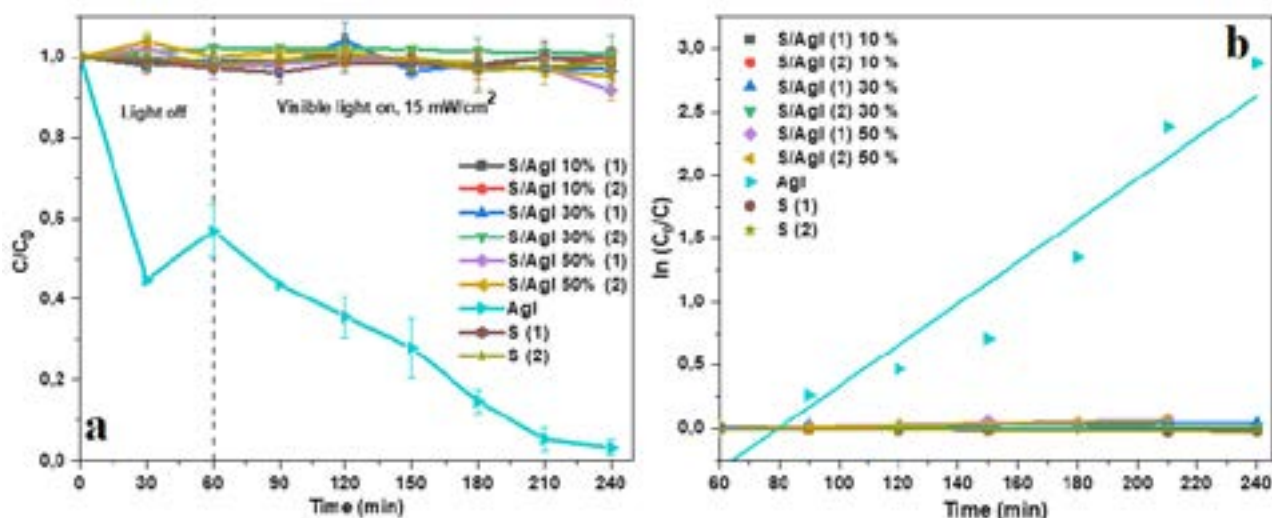


Figure 7 – Photocatalytic degradation of Orange II: a – comparison of the photocatalytic activity of the S/AgI (1, 2) 10, 30, 50 %, pure sulfur and AgI; b – Pseudo-first-order kinetics for photocatalytic degradation of the Orange II by all samples

Table 2 – Pseudo-first order rate constants of photocatalytic degradation of the Orange II for all samples

Sample	The rate constant, $k \cdot 10^2 \text{ min}^{-1}$	Pearson's coefficient, r
S/AgI (1) 10 %	0.006	0.974
S/AgI (2) 10 %	0.008	0.912
S/AgI (1) 30 %	0.019	0.911
S/AgI (2) 30 %	0.006	0.957
S/AgI (1) 50 %	0.046	0.983
S/AgI (2) 50 %	0.044	0.981
AgI	1.638	0.961
S (1)	0.001	0.898
S (2)	0.001	0.867

Biological activity. The resistance of the microstructures to microorganisms was measured relying on the MBC (MFC). The MBC (MFC) values were calculated from the dilutions. As concentration of the water suspensions of the samples was 10 mg/mL (10000 $\mu\text{g/mL}$), the calculations were done by the next scheme: 1:1 dilution corresponds to 5000 $\mu\text{g/mL}$, 1:2 dilution corresponds to 2500 $\mu\text{g/mL}$ and etc. These calculations were performed for all formulations and all dilutions (from 1:1 to 1:128). According to the study, pure substances and microstructures of all compositions did not show the ability to suppress microorganisms, only S/AgI (2) 50 % was active. It was able to suppress *S. aureus* ATCC

BAA-39, *P.aeruginosa* ATCC 9027 and *Erwinia amylovora* at MBC/MFC 5000 $\mu\text{g/mL}$. As for *E. coli* ATCC 8739, the S/AgI (2) 50 % was effective at 2500 $\mu\text{g/mL}$. Such results may indicate that there is a bond between sulfur and AgI, which leads to the manifestation of biological activity. This percentage ratio and the method of obtaining were the optimal conditions for this system. The results indicate the need for further investigation of the synthesis conditions and their effect on the manifestation of biological activity. Hence, precipitation of sulfur by water during the synthesis and the equal amount of the components were optimal conditions for obtaining of the S/AgI microstructures with antimicrobial action.

Conclusion

S/AgI microstructures were prepared by solvothermal DMSO-mediated synthesis using two methods of sulfur precipitation: at room temperature (method 1) and by water (method 2). The samples were represented by the next percentages of AgI: 10, 30 and 50 %.

XRD and Raman spectroscopy revealed that all samples contain sulfur and AgI. According to EDS elemental mapping, sulfur is present in the form of both large and small grains. The large grains are covered by a thin layer of AgI. SEM results have shown that sulfur have irregular shape for both methods of synthesis. As for a size particles, first synthesis method produced sulfur with greater size (20-50 μm). AgI particles have triangular and hexagonal shape. 10 % samples represented by AgI size range from 0.5 to 3 μm , 30 % – from 0.2 to 0.3 μm , 50 % – from 1 to 3 μm . The second method yielded sulfur particles with size from 5 to 20 μm . The size of the AgI particles was the next: 10 % – 0.3 – 0.9 μm ; 30 % – 0.4 – 1 μm ; 50 % – 0.5 – 2 μm . The morphology of AgI particles is represented by non-defined shape. In general, method 1 gives larger particles of sulfur in comparison with method 2.

The potential application of the S/AgI (1, 2) 10, 30 and 50 % in the photocatalysis was not confirmed, as neither of the samples was able to degrade molecules of Orange II under visible light irradiation. The kinetics of the photocatalytic process was accepted as a pseudo-first-order reaction.

Biological activity was studied on the six types of the test strains. Only S/AgI (2) 50 % was able to inhibit test strains of *S. aureus* ATCC BAA-39, *P. aeruginosa* ATCC 9027 and *Erwinia amylovora* at MBC/MFC 5000 $\mu\text{g/mL}$, and *E. coli* ATCC 8739 at 2500 $\mu\text{g/mL}$. The manifestation of biological activity by only one sample can be explained by the formation of a bond between sulfur and AgI. Thus, the precipitation of sulfur with water and a 50 % content of sulfur and AgI are optimal for obtaining microstructures with the ability to suppress certain microorganisms.

Acknowledgements

This work was financially supported by scientific project of Ministry of Education and Science of Republic of Kazakhstan AP08855868 and done on state assignment of IGM SB RAS.

References

1. Singh R.P., Singh P., Singh K.R. (2021) Introduction to Composite Materials: Nanocomposites and their Potential Applications. Composite Materials CRC Press, 28 p. ISBN 9781003080633
2. Jaspal D., Malviya A. (2020) Composites for wastewater purification: A review. *Chemosphere*, vol. 246, pp. 125788. <https://doi.org/10.1016/j.chemosphere.2019.125788>
3. Egbo, M. K. (2021). A fundamental review on composite materials and some of their applications in biomedical engineering. *J King Saud Univ Eng Sci*, vol. 33, no. 8, pp. 557-568. <https://doi.org/10.1016/j.jksues.2020.07.007>
4. Xu X., Ye S., Liu S., Yan T. (2021). Silver Iodide as a Host Material of Sulfur for Li-S Battery. *J Electrochem Soc*, vol. 168, no. 6, pp. 060536 <https://doi.org/10.1149/1945-7111/ac0bf2>
5. Velmurugan S., Balu S., Palanisamy S., Yang T. C. K., Velusamy V., Chen S. W., El-Shafey E. S. I. (2020). Synthesis of novel and environmental sustainable AgI-Ag₂S nanospheres impregnated g-C₃N₄ photocatalyst for efficient degradation of aqueous pollutants. *Appl Surf Sci*, vol. 500, pp. 143991 <https://doi.org/10.1016/j.apsusc.2019.143991>
6. Shankar S., Jaiswal L., Rhim J. W. (2021) New insight into sulfur nanoparticles: Synthesis and applications. *Crit Rev Environ Sci Technol*, vol. 51, no. 20, pp. 2329-2356. <https://doi.org/10.1080/10643389.2020.1780880>
7. Chen W., Qian T., Xiong J., et. al. (2017) A new type of multifunctional polar binder: toward practical application of high energy lithium sulfur batteries. *Adv mater*, vol. 29, no. 12, pp. 1605160. <https://doi.org/10.1002/adma.201605160>
8. Zeng L., Wang N., Yang J., et. al. (2017) Application of a sulfur cathode in nucleophilic electrolytes for magnesium/sulfur batteries. *J Electrochem Soc*, vol. 164, no. 12, pp. A2504. <https://doi.org/10.1149/2.1131712jes>
9. Barce Ferro C. T., Dos Santos B. F., da Silva C. D., et. al. (2020) Review of the syntheses and activities of some sulfur-containing drugs. *Cur Org Synt.*, vol. 17, no. 3, pp192-210. <https://doi.org/10.2174/1570179417666200212113412>
10. Valle S. F., Giroto A. S., Klaic R., et.al. (2019) Sulfur fertilizer based on inverse vulcanization process with soybean oil. *Polym degrad stab*, vol. 162, pp. 102-105. <https://doi.org/10.1016/j.polymdegradstab.2019.02.011>

11. Kim Y. H., Kim G. H., Yoon K. S., et. al. (2020) Comparative antibacterial and antifungal activities of sulfur nanoparticles capped with chitosan. *Microb Pathog*, vol. 144, pp. 104178. <https://doi.org/10.1016/j.micpath.2020.104178>
12. Saedi S., Shokri M., Rhim J. W. (2020) Antimicrobial activity of sulfur nanoparticles: Effect of preparation methods. *Arab J Chem*, vol. 13, no. 8, pp. 6580-6588. <https://doi.org/10.1016/j.arabjc.2020.06.014>
13. Ahmad N., Alshehri A. M., Khan, Z. R., et. al. (2022) Tailoring of band gap, dielectric and antimicrobial properties of silver iodide nanoparticles through Cu doping. *Mater Sci Semicond Process*, vol. 137, pp. 106239. <https://doi.org/10.1016/j.mssp.2021.106239>
14. Wang K., Li Q., Liu B., et. al. (2015) Sulfur-doped g-C₃N₄ with enhanced photocatalytic CO₂-reduction performance. *Appl Catal B*, vol. 176, pp. 44-52. <https://doi.org/10.1016/j.apcatb.2015.03.045>
15. Chen L., Zhu D., Li J., et. al. (2020) Sulfur and potassium co-doped graphitic carbon nitride for highly enhanced photocatalytic hydrogen evolution. *Appl Catal B*, vol. 273, pp. 119050. <https://doi.org/10.1016/j.apcatb.2020.119050>
16. Wen X. J., Shen C. H. Fei, et. al. (2020) Recent developments on AgI based heterojunction photocatalytic systems in photocatalytic application. *Chem Eng J*, vol. 383, pp. 123083. <https://doi.org/10.1016/j.cej.2019.123083>
17. Li J., Liu B., Han X., et.al. (2021) Direct Z-scheme TiO₂-x/AgI heterojunctions for highly efficient photocatalytic degradation of organic contaminants and inactivation of pathogens. *Sep Purif Tech*, vol. 261, pp. 118306. <https://doi.org/10.1016/j.seppur.2021.118306>
18. Soltaninejad V., Ahghari M. R., Taheri-Ledari R., Maleki A. (2021) Bifunctional PVA/ZnO/AgI/Chlorophyll Nanocomposite Film: Enhanced Photocatalytic Activity for Degradation of Pollutants and Antimicrobial Property under Visible-Light Irradiation. *Langmuir*, vol. 37, no 15, pp. 4700-4713. <https://doi.org/10.1021/acs.langmuir.1c00501>
19. Rehan M., Khattab T. A., Barohum A., et al. (2018) Development of Ag/AgX (X= Cl, I) nanoparticles toward antimicrobial, UV-protected and self-cleanable viscose fibers. *Carbohydr polym*, vol. 197, pp. 227-236. <https://doi.org/10.1016/j.carbpol.2018.06.010>
20. Jiang X., Ma Y., Zhao C., et. al. (2018) Synthesis of flower-like AgI/Bi₅O₇I hybrid photocatalysts with enhanced photocatalytic activity in rhodamine B degradation. *J of Mater Res*, vol. 33, no. 16, pp. 2385-2395. <https://doi.org/10.1557/jmr.2018.201>
21. Yuan D., Huang L., Li Y., et. al. (2020) A novel AgI/BiOI/pg-C₃N₄ composite with enhanced photocatalytic activity for removing methylene orange, tetracycline and *E. coli*. *Dyes Pigm*, vol. 177, pp. 108253. <https://doi.org/10.1016/j.dyepig.2020.108253>
22. Li Q., Wang K., Lu X., et. al. (2020) In situ synthesis of AgI/SnS₂ heterojunction photocatalysts with superior photocatalytic activity. *Int J Electrochem Sci*, vol. 15, pp. 9256-9270. doi: 10.20964/2020.09.77
23. Ujjan Z. A., Bhatti M. A., Shah A. A., et. al. (2022) Simultaneous doping of sulfur and chloride ions into ZnO nanorods for improved photocatalytic properties towards degradation of methylene blue. *Ceram Int*, vol. 48, no. 4, pp. 5535-5545. <https://doi.org/10.1016/j.ceramint.2021.11.098>
24. Shao-you L., Yuan-dao C., Tao-yu Q., et. al. (2018) Sulfur doped lead monoxide superfine powder materials: solid-state synthesis, characterization, adsorption and photocatalytic property of methylene blue. *J Inorg and Organomet Polym Mater*, vol. 28, no. 6, pp. 2584-2595. <https://doi.org/10.1007/s10904-018-0942-4>
25. Madruga G. M., Crivellenti L. Z., Borin-Crivellenti S., et. al. (2017) Comparative use of dimethyl sulphoxide (DMSO) in different animal species. *Vet Med (Praha)*, vol. 62, no. 4, pp. 179-185. doi: 10.17221/176/2015-VETMED
26. Tashrifi Z., Khanaposhtani M. M., Larijani B., Mahdavi M. (2020) Dimethyl Sulfoxide: yesterday's solvent, today's reagent. *Adv Synth Catal*, vol. 36, no. 1, pp. 65-86. <https://doi.org/10.1002/adsc.201901021>
27. Khademian M., Zandi M., Amirhoseiny M., Dorrani D. (2017) Synthesis of CuS nanoparticles by laser ablation method in DMSO media. *J Clust Sci*, vol. 28, no. 5, pp. 2753-2764. <https://doi.org/10.1007/s10876-017-1257-2>
28. Borreguero A. M., Rodríguez J. F., Velencoso M. M., et. al. (2019) DMSO as solvent on the synthesis of flame-retardant polyether polyols. *J Appl Polym Sci*, vol 136, no. 6, pp. 47042. <https://doi.org/10.1002/app.47042>
29. Burkitbayev, M. M., Urakaev, F. Kh. (2020) Temperature dependence of sulfur solubility in dimethyl sulfoxide and changes in concentration of supersaturated sulfur solutions at 25° C. *J Mol Li*, vol. 316, p. 113886. <https://doi.org/10.1016/j.molliq.2020.113886>

30. Khan N. V., Burkitbayev M. M., Urakaev F. Kh. (2019) Preparation and Properties of Nanocomposites in the Systems S-AgI and S-Ag₂S-AgI in Dimethyl Sulfoxide. *Mater Sci Eng*, vol. 704, no. 1, pp. 012007). doi:10.1088/1757-899X/704/1/012007
31. Khan, N. V. (2022). Synthesis of the S/AgBr nano/micropowder in DMSO-water system. *Chem Bull Kaz Nat Univ*, vol. 104, no. 1, pp. 4-10
32. CLSI standard M07 (2018) Methods for Dilution Antimicrobial Susceptibility Tests for Bacteria That Grow Aerobically; 11th ed. Wayne, PA, USA.
33. CLSI standard M27 (2017) Reference Method for Broth Dilution Antifungal Susceptibility Testing of Yeasts. 4th ed..Wayne, PA, USA.
34. Cui L., Jiao T., Zhang Q., et. al. (2015) Facile preparation of silver halide nanoparticles as visible light photocatalysts. *Nanomater Nanotechnol*, vol. 5, pp. 20. <https://doi.org/10.5772/60910>
35. McEvoy J. G., Cui W., Zhang Z. (2014) Adsorption and visible light degradation of methyl orange by Ag/AgCl-activated carbon composites. Carbon-enhanced photocatalysts for visible light induced detoxification and disinfection, 85.

© This is an open access article under the (CC)BY-NC license (<https://creativecommons.org/licenses/by-nc/4.0/>). Funded by Al-Farabi KazNU

I.Yu. Silachyov^{1*} , V.A. Glagolev² ¹Institute of Nuclear Physics, Almaty, Kazakhstan²Institute of Geological Sciences named after K.I. Satpayev, Almaty, Kazakhstan

*e-mail: silachyov@inp.kz

(Received 16 October 2021; received in revised form 19 May 2022; accepted 25 May 2022)

Comparator neutron activation analysis of the solid volumetric rock samples for gold content

Abstract. The application of comparator instrumental neutron activation analysis (INAA) combined with the internal standard method was considered to analyze solid volumetric samples of different rocks, 15–20 g of the mass, for Au content. Fe was used as the internal comparator with its mass fraction determined by X-ray fluorescence method (XRF) with the help of a laboratory energy dispersive XRF spectrometer RLP-21T, Kazakhstan. The puck-like samples about 29 mm across diameter and about 10 mm of the thickness were sliced up from rock drill-cores with a diamond saw. No other pretreatment was applied. Sample dimensions were fitted in compliance with that of the XRF spectrometer dishes to substitute them during analysis, i.e. they were the highest possible allowed by the spectrometer. Relative corrections for neutron self-shielding and for gamma-ray self-absorption by the samples of the same dimensions corresponding by their macrocomponent composition to the different types of common rocks turned out rather small, simply accounted using the internal standard, and almost irrespective of the rock types. By the example of serpentinite, picrite and diabase-picrite samples (Western Ulytau Belt, Central Kazakhstan) the whole approach was found as rather expedite and reliable being applied to determine Au content of sufficiently homogeneous magmatic and metamorphic rocks. More efforts resulting in Fe multiple measurements due to its heterogeneous distribution are necessary to analyze industrially significant Au contents in sedimentary rocks like black shales (Bakyrchik, Eastern Kazakhstan).

Key words: Neutron activation analysis, internal standard, gold, volumetric samples.

Introduction

Various analytical methods of rock investigation for gold content are known in multitudes [1-3]. Most of them include decomposition of the powdered samples followed by a separation and concentration technique and a highly sensitive instrumental determination. Intensive chemical pretreatment is the main drawback of the methods since it is often laborious and expensive, depends on reagent blank, and doesn't prevent loss of analyte and/or solution contamination. Overall Au content can be significantly underestimated if gold is locked-in or encapsulated in silicates or in a refractory (sulphide) matrix [1, 4].

Sample preparation for chemical digestion presents a separate problem. Gold mainly occurs in the rocks as native grains extremely variable in size and as diverse compounds incorporated in the common sulphide minerals [5]. Due to the substantially different density of the ground particles gravitational separation easily occurs, hence

homogeneous analytical subsamples can be hardly picked. To minimize this and the inherent “nugget effect”, the sample mass should be increased to 10 g and even more [6]. Moreover, soft and malleable gold grains are highly resistant to grinding. The grains may adhere to the walls of milling vessels causing losses of gold from some samples [3, 5] and contaminating the others.

The most dependable way of overcoming these difficulties is to exclude sample grinding and chemical pretreatment (i.e. to apply an initially instrumental method) and to use larger assays for analysis. Few analytical techniques can meet these requirements taking account of the sensitivity of gold determination close to ppb level necessary in geochemical explorations.

Rapidly developing laser ablation inductively coupled plasma mass spectrometry (LA-ICP-MS) having become a highly demanded way of Au local determination in the gold-bearing minerals [7-9] could be such a technique. Heterogeneity of laser-ablation target is tided over by using fused samples

prepared by the same way as for X-ray fluorescence (XRF) [10-11] and this makes possible to implement bulk analysis [12]. The studied rocks are completely turned into borate glasses including refractory minerals. Sample contamination with flux or crucible material is not crucial in case of Au determination, but limit of detection (LOD) is increased due to dilution. However, the uncertainty resulting from initial geological sample grinding still persists since only the powdered rock material is fused in an oven.

High energy instrumental photon activation analysis (IPAA) based on the photoexcitation reaction $^{197}\text{Au}(\gamma, \gamma')^{197\text{m}}\text{Au}$ is the best suited to analyze large, up to 0.5 kg of the mass, samples with gold inhomogeneous distribution [13]. A rather short half-life $T_{1/2}$ of $^{197\text{m}}\text{Au}$ isomer (7.3 s) is considered as its only inconvenience¹. IPAA soundly found its broad application in gold mining but it can be scarcely employed in geochemistry due to insufficient LOD values reaching 0.1–0.2 ppm at the best (0.5–1.0 ppm most commonly) using a semiconductor detector [14].

Apart from 14 MeV instrumental neutron activation analysis (INAA) which doesn't compete in sensitivity with INAA by thermal neutrons [15] the latter seems being the most appropriate for gold geochemical survey owing to its extremely low LOD value in rocks up to 2 ppb [3]. Individual sample mass varies over a very wide range – from ≈ 100 mg [8, 16] to several hundreds of g and more to reduce severe heterogeneity [3, 17]. If it exceeds 0.5–1.0 g, a sample can no longer be considered as «a point source», and neutron self-shielding, neutron-flux gradients in the sample and self-absorption of gamma rays must be accounted [18]. Without discussing different ways to overcome these difficulties, internal standard based INAA applying in-situ relative detection efficiency should be mentioned since it takes care of the neutron flux perturbation inside the samples [19]. A suitable reference element determined by a convenient analytical technique is used as the internal standard. The method found its broad application to analyze large heterogeneous samples including industrial dross for noble elements [20].

In the present work comparator INAA was tried to determine Au content of solid samples – plane cylindrical pieces of the drill cores, 15–20 g of the mass, cut from several types of common rocks. Minimum nondestructive pretreatment excluded any losses of gold or sample contamination. Iron was chosen as the internal standard with its mass fraction

found by XRF as in some previous investigations of rock element composition [21-23].

Materials and methods

Total content of the natural gold including its nanoforms (“invisible gold”) was studied in picrites, diabase-picrites, and serpentinites picked in the Karatugay Complex of the Western Ulytau Belt (Central Kazakhstan) with a view of searching new ore occurrence of the non-ferrous and noble metals. The drill-core samples 28.5–29.0 mm across diameter were cut with a diamond saw into planar cylinders 9.5–10.0 mm of the thickness. This was the end of the whole preparation. The obtained analytical samples came in smooth enough, without visible roughness of the flat surfaces; small lateral chips of the hard rock, if any, were ignored. An exterior view of several similar analytical samples is presented in Fig. 1.

The sample sizes were determined by the dimensions of the measuring chamber of an energy dispersive XRF spectrometer RLP-21T used in the investigation. The rock samples were installed instead of the steel dishes for powdered specimens inside the sample changer. Their diameter corresponded to the external diameter of the dishes, and the height depended on the gap between the cover and the collimator. So, the sample sizes were close to the maximum one for the given equipment. Fig. 2 demonstrates the charged sample changer of the spectrometer.

RLP-21T was designed and produced by LLP “AspapGeo” (Almaty, Kazakhstan) to study element composition of rocks, minerals, ores, and concentrates. The accuracy of its software was repeatedly confirmed with the help of different corresponding certified reference materials (CRMs). The ascribed uncertainty of iron content measuring in rock samples is 2–8%. RLP-21T is enrolled in the State Register of Measuring Devices (Certificate № 670, valid to 27.07.2025), and the corresponding analytical technique is registered by the National Body for Certification of Kazakhstan (Certificate № 69-2022, valid to 15.02.2027).

To implement INAA each puck-like sample was sealed in polyethylene and then wrapped in aluminium foil. Several samples (no more than six at once) were stacked up and fixed in the same wrapping. Taking account of their dimensions, the packages were placed upright in the irradiation container to be oriented along the channel axis. Samples layout in the irradiation channel is presented in Fig. 3. In this case the flats of the cylindrical samples were

¹ The more convenient $^{197}\text{Au}(\gamma, n)^{196}\text{Au}$ reaction ($T_{1/2} = 6.2$ d) results in lower sensitivity.

lined parallel to the radial component of the neutron flux gradient (about 9% per 1 cm). This is the least favorable orientation if the gradient were considered either empirically or theoretically. However, it didn't matter in the present investigation since the neutron flux gradient was accounted automatically by using the internal standard method.



Figure 1 – Sliced up samples of serpentine drill-core prepared for the investigation



Figure 2 – RLP-21T with open lid and charged sample changer

All the packages were irradiated one by one for 1 min including the transportation time in the position №4 inside the peripheral vertical channel №10-6 of the light-water research reactor WWR-K (Almaty) by the thermal neutron flux density $8.9 \times 10^{13} \text{ cm}^{-2} \text{ s}^{-1}$; the fast neutron flux density amounted to $6.0 \times 10^{12} \text{ cm}^{-2} \text{ s}^{-1}$ [24]. The first package included a zirconium monitor of the neutron flux – 10 mg of ZrO_2 (the Institute of Reference Materials, Ekaterinburg, Russian Federation) sealed in small thin double polyethylene bag placed in the middle. Due to the short-timed irradiation, the neutron flux parameters were considered invariable.

Gamma-spectrometric measurements of the studied samples were conducted after 9–10 days of decay when radionuclide ^{24}Na mainly in charge of the background rise due to the Compton continuum practically completely decayed. Counting time was about 40 min and the distance from the detector cap to the bottom of the volumetric samples was 19 mm or 24 mm to their centers.

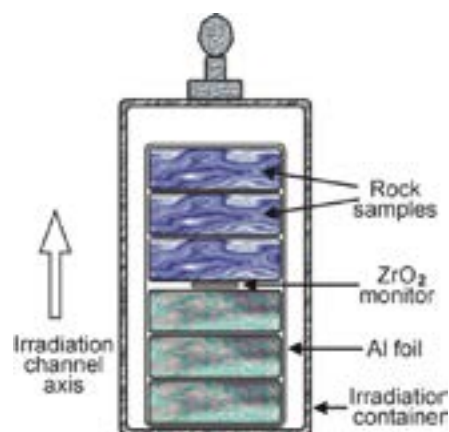


Figure 3 – Samples layout in the irradiation channel

All the measurements were performed using an extended-range HPGe detector GX5019 with a relative efficiency of 50% and an energy resolution of 1.86 keV at the 1332 keV peak of ^{60}Co , connected to a Canberra multi-channel analyzer DSA-1000. Detector calibration for relative detection efficiency was made with the help of a multi-gamma ray standard MGS-1 (^{152}Eu , ^{154}Eu , ^{155}Eu) and an isotopic source ^{133}Ba , both by Canberra. A fourth power polynomial was used for the fitting of calibration curve. Spectra collection and subsequent treatment were carried out by the “AnalGamma” software developed in the Institute of Nuclear Physics to provide gamma-ray spectrometric analysis. The software approximates a part of gamma-ray spectrum in the treatment window by Gaussian curves and a flat background and calculates peak count rates in cps. Partly overlapping peaks can be reliably resolved. Quality of the approximation is checked by the X^2 test.

Gold content of the samples was determined by the only intensive gamma-line of the radionuclide ^{198}Au with the energy E equals to 411.80 keV and quantum yield P_γ reaching 95.6%. Actually there are no unresolved spectral interferences to this gamma-line when different rocks are analyzed with the exception of the low-intensive line of ^{152}Eu ($E = 411.12 \text{ keV}$, $P_\gamma = 2.2\%$) which should be accounted if gold mass fractions get close to the LOD values for these objects.

Results and discussion

Au as well as other element contents of the samples C_a (%) can be calculated according to the next equation of simple comparator method of standardization in INAA [25] using the internal standard method [26] (lower case indices a and c mean an analyzed element and the comparator, respectively):

$$C_a = C_c \frac{k_{0,c} J_a \varepsilon(E_c)(f + Q_0^c)(SD)_c G_c F_c}{k_{0,a} J_c \varepsilon(E_a)(f + Q_0^a)(SD)_a G_a F_a} K_{a,c} \quad (1)$$

where C_c is the element comparator content of the sample (%), k_0 is k_0 -factor relatively to 411.8 keV gamma-line of radionuclide ^{198}Au for the gamma-lines of the comparator and an analyzed element [27], J is the full-energy peak count rate of the corresponding radionuclide analytical gamma-ray (cps), $\varepsilon(E)$ is the relative detection efficiency of the measured gamma-line (%), Q_0 is the resonance integral I_0 (cm^2) to the thermal neutron cross-section σ_0 (cm^2) ratio, f is the thermal to epithermal neutron flux ratio, $S = 1 - \exp(-\lambda t_{irr})$ is saturation factor, $D = \exp(-\lambda t_d)$ is decay factor (t_{irr} and t_d are irradiation and decay time), G is the correction factor for neutron self-shielding by the sample, F is the correction factor for analytical gamma-ray self-absorption by the sample.

When INAA of rock samples for the long-lived radionuclides is carried out correction for the measuring time is always $<1\%$ and can be neglected.

The empirical correction factor $K_{a,c}$ is applied to compensate for an analytical bias caused by the errors of detector calibration for detection efficiency, absence of Q_0 correction for the deviation of thermal neutron flux from $1/E$ law, and by other reasons. In particular, using the same counting geometries, there is no need to correct J for true coincidences. In case of gold analysis $K_{a,c}$ value was determined with the help of a European Commission CRM IRMM-530R (Al-0.1% Au alloy) and an assay of chemically pure (reduced) iron. Then it was verified using some multi-element CRMs certified for gold contents (see below).

The model ratio $1/f$ was evaluated by the “bare bi-isotopic method” with the help of a ZrO_2 monitor of the neutron flux spectral composition. The corresponding expression was adduced more than once in the previous investigations [21-23]. As for the present work, $1/f$ value amounted to 0.0330 ± 0.012 ($P = 0.95$).

To assess thermal and resonance neutron self-shielding by the analyzed puck-like samples, a

similar model one, i.e. 29 mm across diameter and 10 mm of the thickness, was considered corresponding by its composition to the average content of the main rock-forming oxides of the continental crust [28]. Mass fractions of Sm, Eu and Gd characterized by the maximum values of σ_0 were taken equal to their average crustal abundance (Clarke numbers) [29]. With the density equal to 2.8 g cm^{-3} close to the rocks mean value the model sample mass reached 18.5 g.

The effective neutron self-shielding factors for gold $G_{eff, Au}$ and iron $G_{eff, Fe}$ were evaluated with the help of the spreadsheet by C.Chilian, et al. [30] kindly granted by the authors. The model values are presented in Table 1. Both factors appeared close to a unit and differ by no more than 1% one from another. The latter confirms that conducting INAA for Au content, Fe as the internal standard can effectively take account of the neutron self-shielding by the model rock sample.

To verify this conclusion for broader cases which take place in geochemical investigations the same assessment was made for a range of magmatic rocks differing by their silica content – from felsic to ultramafic ones. Typical macrocomponent composition of the rocks was picked up from the CRM catalogues (Russian Federation). $G_{eff, Au}$ and $G_{eff, Fe}$ factors for different rocks appeared very close to that for the continental crust (Table 1) with their ratio practically a constant.

If Sm, Eu, and Gd contents of the model rock sample are increased by one order of magnitude, coefficients $G_{eff, Au}$ and $G_{eff, Fe}$ decrease to 0.946 and 0.919 correspondingly, and their ratio differs from a unit by no more than 3%. It's interesting to note that in this case, including even higher contents of the rare earths, another element such as Rb, Cs, As, Ba, Sm, or Th characterized by high values of Q_0 can take account of thermal and resonance neutrons self-shielding more correctly with their mass fractions being determined by an independent method [31].

Finally, $G_{eff, Au}$ and $G_{eff, Fe}$ values very slightly depend on rock density and their ratio remains a constant.

Correction for analytical gamma-ray self-absorption was estimated according to the equation providing its simplified description in cylindrical samples [32]:

$$\frac{F_c}{F_a} = \frac{\mu(E_a)(1 - \exp(-\rho\mu(E_c)h))}{\mu(E_c)(1 - \exp(-\rho\mu(E_a)h))}, \quad (2)$$

where $\mu(E)$ is photon mass attenuation coefficient ($\text{cm}^2 \text{ g}^{-1}$); ρ – sample density (g cm^{-3}) and h

– sample thickness (cm). $\mu(E)$ values of ^{198}Au and ^{59}Fe analytical gamma-lines in the chemical compounds corresponding to the main rock-forming oxides were picked up from an NIST database [33] and presented in Table 2. It takes note, that due to the high enough energy of these radionuclides gamma-lines, $\mu(E)$ values are quite close for different compounds since interaction of gamma-rays with the matter in this case is mainly brought to the

scattering processes. Hence the corresponding total mass attenuation coefficients $\mu_{\Sigma}(E)$ are practically independent of the rock composition (Table 1). The same is correct for F factors too, and their ratio is practically a constant for different types of magmatic rocks: $F_{\text{Fe}}/F_{\text{Au}} = 1.045$. According to Eq. 2, this ratio very slightly linearly depends on the rock density; it changes by no more than 1% if ρ varies within 2.3–3.2.

Table 1 – Composition of the continental crust and different magmatic rocks (wt.%,) their total photon mass attenuation coefficients of ^{198}Au and ^{59}Fe analytical gamma-lines, and the corresponding self-absorption and neutron self-shielding coefficients for the puck-like solid samples

	Continental crust [28]	Felsic rocks		Intermediate rocks		Mafic rocks		Ultramafic rocks	
		Granite (SG-3)	Granodiorite (MK-2)	Quartz diorite (SKD-1)	Synnyrite (SSN-1)	Anorthosite (MO-6)	Gabbro (SGD-2A)	Dunite (SDU-1)	Hornblendite (MU-3)
SiO ₂	59.1	74.8	64.5	60.5	55.0	51.8	46.6	39.6	37.9
Al ₂ O ₃	15.8	10.6	16.6	16.6	22.5	22.8	14.9	0.97	14.2
Na ₂ O	3.2	4.24	4.27	3.57	1.19	4.04	2.72	0.035	2.14
K ₂ O	1.88	4.64	3.12	2.98	18.0	0.76	3.09	0.010	0.382
MgO	4.4	0.10	1.58	3.05	0.18	2.10	6.81	41.9	12.7
CaO	6.4	0.32	3.83	4.84	0.49	10.1	10.68	1.52	11.0
TiO ₂	0.7	0.26	0.63	0.86	0.091	1.87	1.72	0.018	1.91
MnO	0.11	0.12	0.083	0.086	0.0093	0.076	0.167	0.13	0.144
Fe ₂ O ₃	6.6 ^a	4.50	4.64	5.55	1.35	6.26	11.3	8.91	18.3
P ₂ O ₅	0.2	0.024	0.229	0.17	0.058	0.140	1.03	0.010	0.032
SO ₃	-	-	0.020	0.033	0.0625	0.173	0.038	0.103	0.135
CO ₂	-	-	0.10	0.18	-	0.36	-	1.61	0.13
$G_{\text{eff, Au}}$	0.982	0.981	0.982	0.982	0.973	0.982	0.979	0.985	0.977
$G_{\text{eff, Fe}}$	0.973	0.972	0.973	0.973	0.960	0.974	0.968	0.978	0.966
$\mu_{\Sigma}(412 \text{ keV}), \text{cm}^2 \text{g}^{-1}$	0.0927	0.0939	0.0938	0.0926	0.0931	0.0945	0.0934	0.0893	0.0932
$\mu_{\Sigma}(1099 \text{ keV}), \text{cm}^2 \text{g}^{-1}$	0.0593	0.0601	0.0600	0.0593	0.0596	0.0604	0.0596	0.0571	0.0594
F_{Au}	0.881	0.879	0.879	0.881	0.880	0.879	0.880	0.885	0.880
F_{Fe}	0.921	0.920	0.921	0.921	0.921	0.920	0.921	0.924	0.921

^a – FeO

Table 2 – Coefficients of photon mass attenuation of ^{198}Au and ^{59}Fe analytical gamma-lines by the Earth crust rock-forming oxides

Rock-forming oxide	$\mu(412 \text{ keV}), \text{ cm}^2 \text{ g}^{-1}$	$\mu(1099 \text{ keV}), \text{ cm}^2 \text{ g}^{-1}$
SiO_2	0.0947	0.0608
Al_2O_3	0.0930	0.0597
Na_2O	0.0917	0.0588
K_2O	0.0939	0.0596
MgO	0.0941	0.0604
CaO	0.0960	0.0609
TiO_2	0.0916	0.0580
MnO	0.0910	0.0569
Fe_2O_3	0.0932	0.0579
P_2O_5	0.0936	0.0600
SO_3	0.0949	0.0608
CO_2	0.0945	0.0608

So, the effects of neutron self-shielding by the regularly-shaped samples of common rocks like represented in Fig. 1, and of gamma-ray self-

absorption, are not too significant and are simply corrected if needed. Therefore accuracy of gold determination by comparator INAA using Eq. 1 can be verified with the help of usual powered CRMs certified for Au content.

To minimize the influence of gold heterogeneous distribution in the CRMs produced from gold-bearing ores, recommended sample mass of the latter taken for an analysis must be not less than 5 g. Such a wasteful expenditure of the CRMs was avoided by selecting the ones prepared from the homogeneous products of ores chemical processing – flotation concentrates and similar (Table 3). All these CRMs are produced in Russian Federation: the first two by the Scientific-Research and Design Institute of Non-Ferrous Metallurgy (Krasnoyarsk), the others by the Vinogradov Institute of Geochemistry (Irkutsk). About 100 mg of the CRMs were sealed in plain double polyethylene bags and irradiated for 1 h. Their masses corresponded to the minimum ones recommended by the producers to guarantee gold homogeneous distribution. The samples were counted using the same gamma-ray spectrometer after 10–12 d of decay at the distance of 24 mm from the detector cap.

Table 3 – Gold content of the powered CRMs by comparator INAA using iron as the internal standard ($P = 0.95$)

CRM name	CRM type	Fe, %	Au, mg kg $^{-1}$		E_n -number
			Certified value	Measured value	
SHT-1	Matte of ore thermal melt	49.43 ± 0.67	1.62 ± 0.16	1.57 ± 0.15	-0.23
FSHT-42	Copper-nickel nis matte	2.64 ± 0.17	2.55 ± 0.11	2.60 ± 0.25	0.18
GSO 1787	Flotation concentrate	29.45 ± 0.50	36 ± 1	36.0 ± 3.0	0
GSO 1788	Flotation concentrate	26.97 ± 0.50	33 ± 1	32.4 ± 3.0	-0.19
GSO 2739	Flotation concentrate	28.44 ± 0.50	34 ± 1	34.3 ± 3.0	0.09
GSO 2740	Flotation tailings	4.24 ± 0.17	0.9 ± 0.1	0.94 ± 0.09	0.30

The first two CRMs in Table 3 are characterized by maximum total contents of medium-heavy elements (Fe, Ni, Cu, Se) amounting to 71% and 78%, correspondingly. Nevertheless, due to high values of ^{198}Au and ^{59}Fe analytical gamma-lines and small bag thickness (≈ 1 mm) relative correction for gamma-ray self-absorption evaluated by Eq. 2 is lower than 1% and can be neglected.

Expanded uncertainty of the INAA results $U(C_a)$ was estimated as follows ($P = 0.95$):

$$U(C_a) \approx 2C_a \sqrt{\frac{u(J_a)^2}{J_a^2} + \frac{u(J_c)^2}{J_c^2} + \frac{u(C_c)^2}{C_c^2} + \delta_a^2}, \quad (3)$$

where $u(J_a)$, $u(J_c)$, and $u(C_c)$ are standard uncertainties of the corresponding values as in Eq. 1, δ_a is the standard deviation of gold determination (methodical uncertainty) by comparator INAA (all the ratios and δ_a are in %). The last value assessed earlier with the help of the CRMs equals $\approx 3\%$. Standard uncertainty of iron internal comparator content of a sample by XRF corresponded to the ascribed values according to the certified analytical technique.

The results of CRM analyses for gold mass fraction by comparator INAA using Eq. 1 ($P = 0.95$) are presented in Table 3. Iron content of the samples was determined by XRF. The measured values are

well comparable with the certified ones with <5% of discrepancy. Expanded uncertainty of all the six CRM analyses by comparator INAA doesn't exceed the allowable standard deviation of the results of their determination directed by the III category of precision (of analysis) (5.4–27% for the intervals including these contents) according to OST 41-08-221-04 [34]².

On the other hand, E_n -number usually used as a recommended by IUPAC criterion to verify laboratory performance [35] also showed good agreement between all certified and measured values within acceptable value ± 1 .

The results of Au determination in volumetric samples of several types of rocks by comparator INAA are presented in Tables 4–7 together with their values of mass and density. To assess heterogeneity of Fe content of the samples used as the internal standard they were measured twice changing the sides faced to the collimator of RLP-21T. During gamma-ray counting to find Au mass fraction, the samples were accordingly turned over as well.

Fe content of the first four serpentinite samples (Table 4) differs up to 10% depending on the side faced to the collimator. However, Fe was found to be distributed more homogeneously within each flat surface of the samples. Rotating each sample around its axis, Fe mass fraction varied by less than 5%. Au mass fraction of the serpentinite samples doesn't exceed its four limits of detection evaluated according to the next expression commonly applied in spectroscopic methods: $LOD = 3.3\sigma_b/b$ [36]. Here σ_b is standard deviation of the blank signal (counting statistics of the background count rate at the peak area) and b is concentration sensitivity of the method. If a linear calibration function is used like in INAA, b is a constant: $b = \Delta J / \Delta C$. The limit of Au detection reached very low value $< 0.001 \mu\text{g g}^{-1}$ in the serpentinite samples since this ultramafic rock is characterized by negligible content of Sc ($\approx 3 \mu\text{g g}^{-1}$) which corresponding radionuclide is often mainly in charge of the Compton continuum under ^{198}Au analytical gamma-line after ^{24}Na completely decayed.

The next three Tables (5–7) present rather homogeneous distribution of iron in the rock samples, especially in picrites. Au content of all diabase-picrites is lower the LOD value for these samples which turned out four times as high comparing with that of serpentinite samples. This is caused by

high Sc mass fraction reaching its threefold Clarke number ($\approx 65 \mu\text{g g}^{-1}$) and higher Fe content comparing with serpentinites. Maximum content of Au in picrite samples doesn't exceed $\approx 0.01 \mu\text{g g}^{-1}$ that is five times as high as the corresponding LOD value ($C_{sc} \approx 18 \mu\text{g g}^{-1}$).

On the whole Au mass fraction in the several types of common magmatic and metamorphic rocks was found close to its Clarke number [29]. Fe is fairly homogeneously distributed, so only two measurements are sufficient to evaluate its content of the sample, i.e. to analyze Au reliably.

Solid volumetric samples of rocks being used in INAA can't offer an advantage of the sensitivity improvement comparing with the small powdered ones. However, they permit to avoid the sample preparation difficulties mentioned above, particularly representative sub-sampling [37], and therefore can be preferable in geochemical investigations of gold behavior. In any case, the gained limit of Au detection is quite enough for this purpose.

The volumetric sample advantages become of the distinctive excellence when the industrially significant Au contents are concerned. One of such potentially promising source of gold is associated with a sedimentary rock – black shales [38] widely spread in the upper crust. Three corresponding puck-like samples like the ones above were prepared from the large pieces of rock picked in the gold deposit Bakyrchik, Eastern Kazakhstan. 29 mm across the diameter, they differed in their thickness (7.5 or 10 mm) and hence in mass. XRF showed considerable As content of the samples about 3%, hence gold can be associated with the mineral fraction including arsenopyrite.

Unlike the samples of magmatic and metamorphic rocks investigated above, that of the black shales revealed high heterogeneity of Fe mass fraction by XRF. Each side of a sample was measured four times being rotated by 90° around its axis. The values of relative standard deviation of these measurements are presented in Table 8.

Such contradictory results of separate determination of iron content in the heterogeneous sedimentary rock samples are obviously caused by very low maximum penetration depth d (cm) of Fe characteristic X-rays. According to “the 1% approximation” (i.e. 99% of the X-rays with the certain energy are completely absorbed by the medium), this value was evaluated as follows [39] taking account of approximate macrocomponent content of the samples:

² For the samples with fine-dispersed gold < 0.1 mm of the size.

Table 4 – Iron and gold content of the serpentinite samples ($P = 0.95$), site Akzhal

Sample name	Sample mass, g	Sample density, g cm ⁻³	Fe, %		Au, μg g ⁻¹	
			First side	Reverse side	First side	Reverse side
Akzhal 7/1	14.19	2.23	4.64 ± 0.17	4.22 ± 0.17	<0.001	<0.001
Akzhal 7/2	14.20	2.27	4.83 ± 0.17	5.35 ± 0.30	<0.001	<0.001
Akzhal 7/3	13.43	2.26	4.97 ± 0.17	4.85 ± 0.17	0.0040 ± 0.0006	0.0045 ± 0.0006
Akzhal 7/4	14.22	2.30	5.05 ± 0.30	4.57 ± 0.17	<0.001	<0.001
Akzhal 7/5	14.03	2.23	4.50 ± 0.17	4.78 ± 0.17	0.0015 ± 0.0005	0.0016 ± 0.0005
Akzhal 7/6	14.52	2.31	5.28 ± 0.30	5.02 ± 0.30	0.0021 ± 0.0005	0.0015 ± 0.0005

Table 5 – Iron and gold content of the diabase-picrite samples ($P = 0.95$), site Akzhal

Sample name	Sample mass, g	Sample density, g cm ⁻³	Fe, %		Au, μg g ⁻¹	
			First side	Reverse side	First side	Reverse side
Akzhal 8/1	19.18	3.17	14.43 ± 0.45	13.98 ± 0.45	<0.004	<0.004
Akzhal 8/2	18.87	3.12	14.11 ± 0.45	13.61 ± 0.45	<0.004	<0.004
Akzhal 8/3	18.87	3.12	13.70 ± 0.45	14.06 ± 0.45	<0.004	<0.004
Akzhal 8/4	18.41	3.04	14.18 ± 0.45	14.38 ± 0.45	<0.004	<0.004
Akzhal 8/5	17.05	2.92	13.15 ± 0.45	14.23 ± 0.45	<0.004	<0.004

Table 6 – Iron and gold content of the picrite samples ($P = 0.95$), site Karatugay

Sample name	Sample mass, g	Sample density, g cm ⁻³	Fe, %		Au, μg g ⁻¹	
			First side	Reverse side	First side	Reverse side
Karat 12/1	18.76	2.99	9.24 ± 0.30	9.20 ± 0.30	<0.002	<0.002
Karat 12/2	17.64	2.91	9.30 ± 0.30	9.66 ± 0.30	0.011 ± 0.002	0.010 ± 0.002
Karat 12/3	18.26	2.90	9.30 ± 0.30	9.31 ± 0.30	<0.002	<0.002
Karat 12/4	18.44	2.93	9.24 ± 0.30	9.41 ± 0.30	<0.002	<0.002
Karat 12/5	18.35	3.03	9.16 ± 0.30	8.92 ± 0.30	0.006 ± 0.002	0.006 ± 0.002

Table 7 – Iron and gold content of the picrite samples ($P = 0.95$), site Karatugay

Sample name	Sample mass, g	Sample density, g cm ⁻³	Fe, %		Au, μg g ⁻¹	
			First side	Reverse side	First side	Reverse side
Karat 13/1	16.67	2.66	9.10 ± 0.30	9.46 ± 0.30	<0.002	<0.002
Karat 13/2	16.94	2.70	8.92 ± 0.30	8.80 ± 0.30	<0.002	<0.002
Karat 13/3	16.79	2.68	9.03 ± 0.30	8.88 ± 0.30	<0.002	<0.002
Karat 13/4	17.68	2.82	9.05 ± 0.30	8.97 ± 0.30	<0.002	<0.002
Karat 13/5	18.05	2.88	8.89 ± 0.30	8.90 ± 0.30	<0.002	<0.002

$$d = \frac{4.61}{\rho(\mu_i(E_i)/\sin\varphi_i + \mu_x(E_x)/\sin\varphi_x)}, \quad (4)$$

where indices i and x mean the primary and characteristic X-rays, respectively, φ_i and φ_x are the incidence and take-off angles. The calculated r value of the black shale samples was about 3.3 g cm^{-3} . Then taking φ_i and φ_x both close to 45° , $E_x = 6.4 \text{ keV}$ (Fe K -alpha line) and $E_i = 23.2 \text{ keV}$ (K -alpha line of Cd intermediate target) the penetration depth of Fe characteristic X-rays amounted $\approx 0.15 \text{ mm}$ only. Though that of As characterized by more high-energy X-ray lines reached $\approx 0.30 \text{ mm}$, As was rejected as the internal standard since its distribution turned out even more heterogeneous (Table 8).

Thus, to evaluate Au content of the black shale volumetric samples the mean values of eight Fe measuring by XRF were used (Table 9). The presented Fe mass fractions are averaged over four measurements of each side.

Because of As high content the irradiated samplers were counted after three weeks of decay when ^{76}As count rate became acceptable. In accordance with

the model realized in the spreadsheet, $G_{\text{eff, Fe}}$ to $G_{\text{eff, Au}}$ ratio for the black shale samples (Eq. 1) equaled 0.985 irrespective of their different thickness and As mass fraction. Correspondingly $F_{\text{Fe}}/F_{\text{Au}}$ ratio amounted to 1.056 for the thicker sample and to 1.042 for the other two (Eq. 2). Then taking these corrections Au contents were calculated (Table 9). They were found very close turning over the samples during counting. This can seemingly witness to the homogeneous distribution of gold in the samples (along the axes at least) i.e. to its preferable presence as the invisible nanoforms.

Table 8 – Relative standard deviation (%) of iron and arsenic determination in the black shale samples ($n = 4$), gold deposit Bakyrchik

Sample name	Fe		As	
	First side	Reverse side	First side	Reverse side
ZHB 4/1	20.8	12.4	18.5	12.7
ZHB 4/2	9.0	6.9	11.8	10.0
ZHB 4/3	4.1	7.0	5.9	12.2

Table 9 – Iron and gold content of the black shale samples ($P = 0.95$)

Sample name	Sample mass, g	Sample density, g cm^{-3}	Fe, %		Au, $\mu\text{g g}^{-1}$	
			First side	Reverse side	First side	Reverse side
ZHB 4/1	15.82	3.26	11.31 ± 0.45	13.18 ± 0.45	3.66 ± 0.36	3.60 ± 0.36
ZHB 4/2	21.63	3.30	13.33 ± 0.45	16.19 ± 0.45	4.43 ± 0.44	4.48 ± 0.44
ZHB 4/3	16.24	3.28	16.48 ± 0.45	15.46 ± 0.45	5.15 ± 0.53	5.18 ± 0.50

According to the peculiarities of gold behavior during sample preparation mentioned in Introduction, correctness of Au determination in volumetric samples by comparator INAA can be hardly confirmed by other analytical techniques. In this case accuracy of the results is ensured by the following:

- total absence of any sample preparation including grinding;

- verification of the accuracy of detector calibration and concentration standardization with the help of high-quality powered CRMs certified for Au content;

- application of the internal standard method allowing to minimize all main corrections making them practically independent of the sample composition and therefore almost negligible;

- reliable determination of the internal standard content of the samples by an independent method.

The last condition depends not on the method itself but on the samples too, i.e. on their intrinsic heterogeneity, and is seemingly discussable. Different instrumental methods and different internal standards can be tried. At last, a part of the samples can be crushed and powdered after INAA measurements are completed to find internal comparator content in case of its high heterogeneity. In any case, this doesn't deny the whole approach.

Conclusion

An internal standard based variant of comparator INAA was tried to determine Au content of solid volumetric samples of several

types of the widely spread rocks. Fe content of the samples as the internal comparator was determined by XRF. No pretreatment of the geological material was applied. Shape and dimensions of the samples cut as plane cylindrical pieces of the drill cores corresponded that of the dishes being used to implement elemental analysis with the help of an energy dispersive XRF spectrometer RLP-21T. Significantly enlarged sample mass to 15–20 g makes possible to take account of gold distribution heterogeneity to a great extent, if any. Application of Fe as the internal standard allowed essentially reducing corrections for neutron self-shielding and for gamma-ray self-absorption by the volumetric samples to the values no more than 1% and 5%, correspondingly. The corrections were shown to be practically irrespective of major constituents of different types of rocks.

High penetrability of neutrons and high-energy gamma-rays being taken into account, when the corresponding analytical signals of ^{198}Au and ^{59}Au are formed by the whole sample volume, reliability of gold determination depends on the correctness of iron analysis by XRF. The demonstrated simple high-sensitive approach can be considered as a rather convenient and reliable one in case of geochemical exploration of homogenous rocks, when low penetration depth of Fe characteristic X-rays (<1 mm) doesn't matter. XRF should be gingerly applied to determine Fe if sedimentary and other rocks characterized by its significant heterogeneity are analyzed for industrially significant Au contents. Other macroelements surely determined both by INAA and XRF may be tried then as the internal standards, or another method of Fe determination can be applied.

Acknowledgments

The work was supported by the grants BR09158958 from Ministry of Education and Sciences of the Republic of Kazakhstan and BR10264324 from Committee of Geology, Ministry of Ecology, Geology, and Mineral Resources of the Republic of Kazakhstan.

References

1. Balaram V. (2008) Analytical methods for gold and other precious metals in exploration studies. *J Appl Geochem*, vol. 10(2A), pp. 545-562.
2. IAEA-TECDOC-1443 (2005) Nuclear analytical methods for platinum group elements. Vienna: IAEA, 53 p. ISBN 92-0-102405-3.
3. Hoffman E.L., Clark J.R., Yeager J.R. (1998) Gold analysis – fire assaying and alternative methods. *Explor Min Geol*, vol. 7, pp. 155-160.
4. Helmeczi W., Helmeczi E., Baker L.A., et al. (2018) Development of a general acid method for the digestion of gold ore samples together with a comparison of extraction solvents for gold and determination by microwave-induced plasmaatomic emission spectrometry (MIP-AES). *J Anal At Spectrom*, vol. 33, pp. 1336-1344. <https://doi.org/10.1039/c8ja00136g>.
5. Kontas E. (1993) Analytical methods for determining gold in geological samples. Report of investigation, Geological survey of Finland. Espoo, 43 p, ISBN 951-690-476-9.
6. Liu Y.H., Wan B., Xue D.S. (2019) Sample digestion and combined preconcentration methods for the determination of ultra-low gold levels in rocks. *Molecules*, vol. 24, pp. 1778-1797. <https://doi.org/10.3390/molecules24091778>.
7. Gao F., Du Y., Pang Zh., et al. (2019) LA-ICP-MS trace-element analysis of pyrite from the Huanxiangwa gold deposit, Xiong'er shan district, China: implications for ore genesis. *Minerals*, vol. 9(3), pp. 157-171. <https://doi.org/10.3390/min9030157>.
8. Vikentyev I.V. (2015) Invisible and microscopic gold in pyrite: methods and new data for massive sulfide ores of the Urals. *Geol Ore Deposits*, vol. 57(4), pp. 237-265. <https://doi.org/10.1134/S1075701515040054>.
9. Zhang J., Deng J., Chen H., et al. (2014) LA-ICP-MS trace element analysis of pyrite from the Chang'an gold deposit, Sanjiang region, China: implication for ore-forming process. *Gondwana Res*, vol. 26, pp. 557-575. <https://doi.org/10.1016/j.gr.2013.11.003>.
10. Kil Y., Yung H. (2015) LA-ICP-MS analysis of natural rock samples using XRF glass beads. *Geosci J* (Seoul, Repub. Korea), vol. 19(1), pp. 45-52. <https://doi.org/10.1007/s12303-014-0063-1>.
11. Tamura A., Akizawa N., Otsuka R., et al. (2015) Measurement of whole-rock trace-element composition by flux-free fused glass and LA-ICP-MS: evaluation of simple and rapid routine work. *Geochem J*, vol. 49, pp. 243-258. <https://doi.org/10.2343/geochemj.2.0353>.
12. Stoll B., Jochum K.P., Herwig K., et al. (2008) An automated iridium-strip heater for LA-ICP-MS bulk analysis of geological samples. *Geostand Geoanal*, vol. 32(1), pp. 5-26. <https://doi.org/10.1111/j.1751-908X.2007.00871.x>.
13. Segebade C., Starovoitova V.N., Borgwardt T., et al. (2016) Principles, methodologies, and

applications of photon activation analysis: a review. *J Radioanal Nucl Chem*, vol. 312(1), pp. 443-459. <https://doi.org/10.1007/s10967-017-5238-6>.

14. Řanda Z., Špaček B., Mizera J. (2006) Fast determination of gold in large mass samples of gold ores by photoexcitation reactions using 10 MeV bremsstrahlung. *J Radioanal Nucl Chem*, vol. 271(3), pp. 603-606. <https://doi.org/10.1007/s10967-007-0314-y>.

15. Nat A., Ene A., Lupu R. (2004) Rapid determination of gold in Romanian auriferous alluvial sands, concentrates and rocks by 14 MeV NAA. *J Radioanal Nucl Chem*, vol. 261(1), pp. 179-188. <https://doi.org/10.1023/B:JRNC.0000030954.29323.39>.

16. Ahmad K., Dampare S.B., Adomako D., et al. (2004) The use of neutron activation analysis in gold prospecting in small-scale mining in Ghana. *J Radioanal Nucl Chem*, vol. 260(3), pp. 653-658. <https://doi.org/10.1023/B:JRNC.0000028227.81455.f7>.

17. Yudakov A.A., Ivannikov S.I., Sheleznov V.V., et al. (2015) Neutron activation determination of gold in technogenic raw materials with different mineral composition. *Nucl Technol Radiat Prot*, vol. 30(4), pp. 273-279. <https://doi.org/10.2298/NTRP1504273Y>.

18. Menezes M.Â., Jaćimović R. (2014) Implementation of a methodology to analyse cylindrical 5-g sample by neutron activation technique, k_0 method, at CDTN/CNEN, Belo Horizonte, Brazil. *J Radioanal Nucl Chem*, vol. 300(2), pp. 523-531. <https://doi.org/10.1007/s10967-014-3074-5>.

19. Nair A.G.C., Acharya R., Sudarshan K., et al. (2003) Development of an internal monostandard instrumental neutron activation analysis method based on in situ detection efficiency for analysis of large and nonstandard geometry samples. *Anal Chem*, vol. 75(18), pp. 4868-4874. <https://doi.org/10.1021/ac034457d>.

20. Swain K.K., Ajith N., Acharya R., et al. (2012) Large sample neutron activation analysis of dross for gold and silver. *J Radioanal Nucl Chem*, vol. 294(2), pp. 319-322. <https://doi.org/10.1007/s10967-011-1519-7>.

21. Silachyov I.Yu. (2018) Determination of rare earths in uranium raw material by neutron activation analysis and X-ray fluorescence. *News of the Academy of Sciences of RK, ser. chem. & technol.*, vol. 429(3), pp. 28-38.

22. Silachyov I.Yu. (2020) Instrumental neutron activation analysis of rhenium in uranium raw material. *IJBC*, vol. 13(1), pp. 161-169. <https://doi.org/10.26577/ijbch.2020.v13.i1.17>.

23. Silachyov I.Yu. (2020) Combination of neutron activation analysis with X-ray fluorescence spectrometry for the determination of rare-earth elements in geological samples. *J Analyt Chem*, vol. 75(7), pp. 878-889. <https://doi.org/10.1134/S106193482007014X>.

24. Koltchinsk S.N., Sairanbayev D.S., Chekushina L.V., et al. (2018) Comparison of neutron spectrum in the WWR-K reactor with LEU fuel against HEU one. *NNC RK Bulletin [Vestnik NYATS RK]*, vol. 76(4), pp. 14-17 (in Russian).

25. Hamidatou L., Slamene H., Akhal T., Zouranen B. (2013) Concepts, instrumentation and techniques of neutron activation analysis. In: *Imaging and radioanalytical techniques in interdisciplinary research – fundamentals and cutting edge applications*. Rijeka, Croatia, pp. 141-178. <http://dx.doi.org/10.5772/53686>.

26. Silachyov I. (2020) Elemental analysis of vegetation samples by INAA internal standard method. *J Radioanal Nucl Chem*, vol. 324(1), pp. 97-108. <https://doi.org/10.1007/s10967-020-07051-6>.

27. Nuclear data sub-committee. K0-neutron activation analysis link page (accessed Oct 15, 2021). <http://www.kayzero.com/k0naa/k0naaorg/Links.html>.

28. Rudnick R.L., Gao S. (2014) 4.1 – Composition of the Continental Crust. *Treatise Geochem*, 2d edition, vol. 4, pp. 1-51. <https://doi.org/10.1016/B978-0-08-095975-7.00301-6>.

29. Haynes W.M. (Ed.) (2016) Abundance of elements in the earth's crust and in the sea. CRC handbook of chemistry and physics, 97th edition. Boca Raton, Florida: CRC press, pp. 14-17. ISBN: 9781498754286.

30. Chilian C., St-Pierre J., Kennedy G. (2008) Complete thermal and epithermal neutron self-shielding corrections for NAA using a spreadsheet. *J Radioanal Nucl Chem*, vol. 278(3), pp. 745-749. <https://doi.org/10.1007/s10967-008-1604-8>.

31. Silachyov I.Yu. (2014) Neutron activation analysis of gold in volumetric samples of gold-bearing sulphides using atomic reactor of the INP WWR-K. Proceedings of international conference "Progressive methods of dressing and complex processing of natural and technogenic mineral resources". Plaksinsky readings – 2014. Almaty, Kazakhstan, pp. 155-157 (in Russian).

32. Jodłowski P. (2006) Self-absorption correction in gamma-ray spectrometry of environmental samples – an overview of methods and correction values obtained for the selected geometries. *Nukleonika*, vol. 51(suppl. 2), pp. S21-S25.

33. Hubbell J.H., Seltzer S.M. (accessed Oct 15, 2021) X-ray mass attenuation coefficients. NIST

standard reference database 126. <https://www.nist.gov/pml/x-ray-mass-attenuation-coefficients>.

34. OST 41-08-212-04 (2004) Standart otrasli. Upravlenie kachestvom analiticheskikh rabot. Normy pogreshnosti pri opredelenii himicheskogo sostava mineralnogo syr'ya i klassifikatsiya metodik laboratornogo analiza po tochnosti rezultatov (Industrial standard. Quality management of analytical work. Error guidelines for chemical analysis of mineral resources and precision classification of laboratory analytical techniques). Moscow, VIMS, 23 p. (in Russian).

35. ISO 13528:2015 (2015) Statistical methods for use in proficiency testing by interlaboratory comparisons. Genève, Switzerland, 89 p.

36. Desimoni E., Brunetti B. (2015) About estimating the limit of detection by the

signal to noise approach. *Pharm Anal Acta*, vol. 6, 4 pp. <http://dx.doi.org/10.4172/2153-2435.1000355>.

37. Bode P., Romanò S., Romolo F. (2018) Large sample neutron activation analysis avoids representative sub-sampling and sample preparation difficulties: An added value for forensic analysis. *Forensic Chem*, vol. 7, pp. 81-87. <https://doi.org/10.1016/j.forc.2017.10.002>.

38. Robert F., Poulsen, K.H., Dubé B. (1997) Gold deposits and their geological classification. Proceedings of Exploration 97: Fourth decennial international conference on mineral exploration. Ottawa, Canada, pp. 209-220.

39. Zawisza B., Sito R. (2012) Quantification in X-Ray fluorescence spectrometry. In: X-ray spectroscopy. Rijeka: InTech, pp. 138-162.

© This is an open access article under the (CC)BY-NC license (<https://creativecommons.org/licenses/by-nc/4.0/>). Funded by Al-Farabi KazNU

A.N. Gurin* , Ye.T. Chakrova , A.R. Borissenko , Z.V. Medvedeva ,
A.V. Kulakov , A.P. Sylnyagin 

Institute of Nuclear Physics, Almaty, Kazakhstan

*e-mail: gurin.andrey@inp.kz

(Received 18 May 2022; received in revised form 30 May 2022; accepted 05 June 2022)

Experience in production of ^{18}F isotope in the Cyclone-30 for synthesis of fluorinated radiopharmaceuticals

Abstract. This article provides a brief overview of the ^{18}F isotope production using the Cyclone-30 cyclotron and two liquid targets with the volume of 0.5 and 2.0 ml, water enriched with the ^{18}O isotope was used as the target material. The obtained isotope was used for serial production of the [^{18}F]FDG radiopharmaceutical and supply of this medicine to the operating PET centers in Almaty. The isotope was also used for experimental syntheses of [^{18}F]PSMA-1007 and Na[^{18}F]F to assess the possibility of implementation these medicines into the production and medical practice of the Republic of Kazakhstan. The need for the implementation of [^{18}F]PSMA-1007 is associated with the problem of early diagnosis and control of prostate cancer treatment, and Na[^{18}F]F – with the earliest possible detection of bone metastases in malignant tumors of various localization.

This paper provides the average radiochemical yield and the main quality parameters for [^{18}F]FDG, [^{18}F]PSMA-1007 and Na[^{18}F]F.

This scientific and practical work allows us to evaluate the three-year production experience and the possibilities of fluorine production by reaction (p,n) on the cyclotron C-30, and also reflects the prospects of using fluorine in the development of new-generation radiopharmaceuticals for the diagnosis of oncological diseases.

Key words: ^{18}F , cyclotron, radiosynthesis, radiochemical yield, radiopharmaceutical, diagnostics, PET, nuclear medicine.

Introduction

Positron emission tomography (PET) is a modern method of nuclear medicine that enables us to obtain *in vivo* information about disturbances of physiological and biochemical processes at the molecular level by determining the concentrations of compounds labeled with positron emitters in biological tissues specified by the researcher [1].

More than 90% of PET procedures in the world are implemented with ^{18}F isotope due to the longest half-life (110 min) among ultra-short-lived radioisotopes as well as the ability to synthesize a fairly wide range of labeled compounds, such as ^{18}F -fluorodeoxyglucose, ^{18}F -PSMA, ^{18}F -tyrosine, ^{18}F -fluorocholine, ^{18}F -fluorothymidine, ^{18}F -fluoromisonidazole, ^{18}F -DOPA, ^{18}F -flumazenyl, ^{18}F -fluoropurine, ^{18}F -fluoroputrescine, ^{18}F -fluoruredine, ^{18}F -fluorocytidine, ^{18}F -flunarizine, etc. [2]. During the last three years, the “Institute of Nuclear Physics” (Almaty) has been performing serial production of Deoxy-2-[^{18}F] Fluoro-D-glucose ([^{18}F]FDG) on the synthesis module Synthera and experimental work on labeling an artificially

synthesized protein tropic to prostate-specific membrane antigen (PSMA) with isotope ^{18}F ([^{18}F]PSMA-1007) and preparation of Na[^{18}F]F in the research facility SynthraRNplus.

Electrophilic and nucleophilic fluorination methods are used to introduce ^{18}F into the structure of various molecules [3,4,5]. The first method is associated with production of fluorine by irradiation of neon by the reaction $^{20}\text{Ne}(d,\alpha)^{18}\text{F}$, when the daughter radionuclide is stabilized in the chemical form [^{18}F]F₂ and characterized by the strongest electrophilic properties. The second method is based on preparation of fluorine from oxygen $^{18}\text{O}(p,n)^{18}\text{F}$, which leads to formation of fluoride anion [^{18}F]F⁻, which is subsequently used in nucleophilic substitution reactions.

Each of the methods for preparation of compounds with ^{18}F has its advantages and disadvantages. The advantages of the electrophilic method include high rate of the fluorination reaction [6]. The disadvantages of the method include low selectivity of fluorination and the resulting low specific activity of the labeled compound [3]. The advantage of the method for preparation of ^{18}F by nucleophilic

substitution is high selectivity of labeling and production of the preparation with high specific activity; the disadvantages include possible adverse reactions during synthesis, which requires more stringent maintenance of the specified technological parameters of synthesis [7].

Despite the above-mentioned disadvantages of the nucleophilic method, most modern PET centers use the nucleophilic method to prepare ^{18}F compounds, including the radiopharmaceutical production site at the “Institute of Nuclear Physics” in Almaty.

This paper describes the experience of ^{18}F isotope production and production of fluorinated radiopharmaceuticals, obtained in the INP over the past 3 years.

Materials and methods

All chemicals, reagents and solvents, required for the synthesis of $[^{18}\text{F}]\text{FDG}$, $[^{18}\text{F}]\text{PSMA-1007}$ and $\text{Na}[^{18}\text{F}]\text{F}$, were purchased from ABXGmbH (Germany). In addition, the synthesis kits, disposable synthesis cassettes and reference compounds, used for quality control, were purchased from ABXGmbH. The purchased disposable synthesis cassettes and reagent kits were used as received, with no adjustment of the factory parameters. Methods and standard operating procedures were developed and implemented at the site of radiopharmaceutical production at the “Institute of Nuclear Physics” in Almaty. Synthesis was performed on two different modules: SynthraRNplus and Synthra (Fig.1). Reagents for gas chromatography (GC), high-performance liquid chromatography (HPLC) and

(thin-layer chromatography) TLC were purchased from Sigma-Aldrich.

The HPLC analysis was performed using the Agilent Infinity 1260 system with ultraviolet (G1314B) and refractometric (G1362A) detectors, as well as a radiochemical detector from LabLogic. The HPLC system is controlled by the Laura software. Before quality control, reference standards of each compound were used to determine the retention time. Gas chromatography (Agilent 7890A, ChemStation software) was used to determine the number of residual solvents using a DB-WAX column (0.32 mm, length 30 m). Identification of radionuclides was verified by measuring the half-life using a dose calibrator (VDC-404). Radionuclide purity was determined by gamma-spectrometry with a multichannel high purity germanium detector (Canberra Industries). The level of cryptophix was determined by comparing the staining intensity on chromatography paper. The radiochemical purity was determined by TLC (ScanRAM Radio-TLC Detector LabLogic and Laura software) using silica gel plates F254 (20×100 mm) and a mixture of acetonitrile: water (95:5, v/v) as a stationary and mobile phase, respectively.

^{18}F production

The utilized in INP ^{18}F production technology is based on the nuclear reaction $^{18}\text{O}(\text{p}, \text{n})^{18}\text{F}$. The threshold of the nuclear reaction is 2.6 MeV, the cross section is growing and reaches its maximum 300 mb at 8 MeV, then it slopes down and at 20 MeV is 16 mb [8]. This means that to produce ^{18}F isotope, it is necessary to irradiate the ^{18}O oxygen nuclei with protons of energies not lower than 3 MeV and not higher than 20 MeV.



A



B

Figure 1 – synthesis modules A- Synthra, B – SynthraRNplus

In addition to the target nuclear reaction, other reactions occur with the formation of side isotopes [9]. All the resulting isotopes are characterized by very short half-lives, about tens of seconds [10]. The most “long-lived” of them is the isotope ^{13}N , the half-life of which is 10 minutes. It is produced in the reaction of $^{16}\text{O}(\text{p},\text{a})^{13}\text{N}$. The nuclei of the oxygen isotope ^{16}O are inevitably present in the target material, although in small quantities. In addition, at proton energies above 18 MeV, the reaction of ^{13}N production will already take place on ^{18}O nuclei: the nuclear reaction $^{18}\text{O}(\text{p},\alpha 2\text{n})^{13}\text{N}$. This is a limitation on the maximum energy of the proton beam used for ^{18}F production.

The Cyclone-30 cyclotron manufactured by the Ion Beam Applications SA (IBA, Belgium) is used to produce the accelerated proton beam. The target material is water, 95% enriched with ^{18}O isotope. The target is a niobium capsule filled with water, covered from the beam side with a foil, made of Havar alloy. The cyclotron, the beam transportation line and the target station are a single complex, which is controlled from the cyclotron control panel.

Taking into account that the energy of the proton beam, produced by the C-30 cyclotron, can be varied from 15 to 30 MeV, the 18 MeV operation mode is an optimal one for the production of ^{18}F . It allows obtaining the maximum yield of the target isotope ^{18}F with a minimum production of by-products. The target provides full absorption of the proton beam. The irradiated water is pumped for further synthesis through the capillaries 0.9 mm in diameter into a

receiving tank located in a hot cell. This process is performed automatically using high-purity helium gas. The transportation line is pre-purged with helium, and then the liquid is pumped, the line is re-purged.

Two targets manufactured by IBA are successfully operated in the INP for the production of ^{18}F isotope: a small-volume target of 0.5 ml and a large-volume target of 2 ml for irradiation with currents of 25 and 40 μA , respectively.

^{18}F Separation

The first stage of ^{18}F FDG, ^{18}F PSMA-1007 and Na^{18}F F synthesis is the extraction of ^{18}F isotope from irradiated H_2^{18}O . Extraction is performed by solid-phase extraction using a cartridge with anion exchange resin QMA Sep-Pak[®], conditioned with 2 ml of ethanol and 2 ml of water. Irradiated ^{18}F -containing water is passed through a pre-conditioned cartridge with anion exchange resin QMA Sep-Pak[®], while the fluoride ion is retained on the resin. Various eluents were used for elution of the ^{18}F fluoride ion, for example, during the synthesis of ^{18}F FDG, an aqueous solution of acetonitrile containing potassium carbonate and an average equimolar amount of the interfacial cryptofix catalyst (K222) was used, where potassium cation in the carbonate composition was used as a counterion for ^{18}F . In the synthesis of ^{18}F PSMA-1007, a 0.075 M solution of tetrabutylammonium bicarbonate (TBAHCO_3) was used as an eluent, and in the synthesis of Na^{18}F F -0.9% sodium chloride solution was used (Fig. 2).

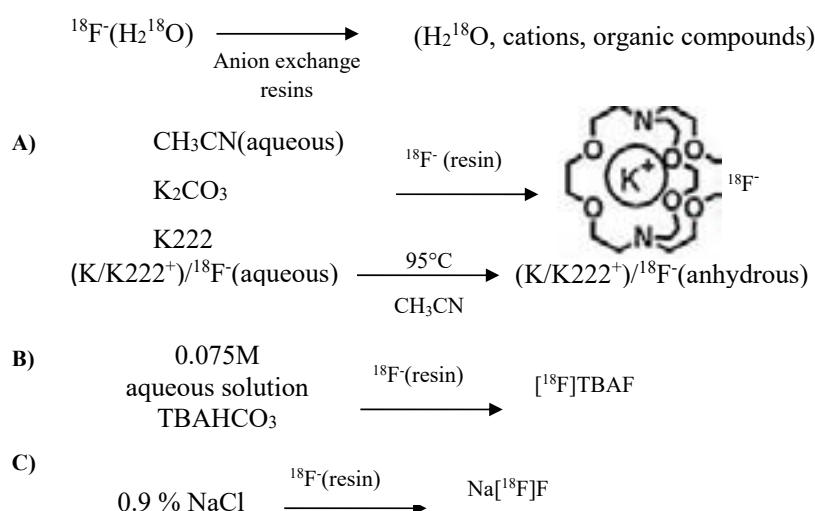


Figure 2 – A) scheme of ^{18}F extraction from irradiated target for ^{18}F FDG production, B) scheme of ^{18}F extraction from irradiated target for ^{18}F PSMA-1007 production, C) scheme of ^{18}F extraction from irradiated target for Na^{18}F F production

The yield at the stage of $^{18}\text{F}^-$ extraction from the irradiated target in case of listed elements is from 87 to 95% of the ^{18}F obtained activity. In case of [^{18}F]FDG and [^{18}F]PSMA-1007 production, for preparation for the next stages of synthesis the eluates are dried in a helium current at a high temperature. In case of $\text{Na}[^{18}\text{F}]\text{F}$ production, the eluate is not dried.

Results and discussion

During serial production of [^{18}F]FDG radiopharmaceutical using the Synthra radiosynthesis module, the following averaged data for 3 years were obtained:

According to the results of 685 cycles of irradiation in the Cyclotron C-30 a target with 2 ml of enriched water with protons of 18 MeV energy and $38 \pm 2 \mu\text{A}$ current and subsequent cycles of [^{18}F]FDG synthesis using the Synthra module, it was shown that activity of ^{18}F in the preparation [^{18}F]FDG was $75 \pm 12 \text{ GBq}$ at the end of synthesis. The irradiation time was $160 \pm 15 \text{ min}$, and the synthesis time was $27 \pm 2 \text{ min}$.

The quality parameters of the preparation corresponded to the pharmacopoeia requirements.

The activity of the resulted preparation was sufficient for daily injection up to twenty patients, depending on their weight (target activity is $370 \text{ MBq/body weight}$).

For experimental syntheses of [^{18}F]-PSMA-1007 and $\text{Na}[^{18}\text{F}]\text{F}$, 6 irradiation cycles were carried out in a target Cyclotron C-30 with 0.5 ml of enriched water with protons of 18 MeV energy and $20 \pm 2 \mu\text{A}$ current. The target was irradiated for 30-60 minutes. The synthesis was carried out at the SynthraRNplus research facility.

[^{18}F]-PSMA 1007

Three experimental syntheses of ^{18}F -PSMA-1007 were carried out. The synthesis time was 45 minutes, the average activity of ^{18}F -PSMA-1007 was $1.6 \pm 0.4 \text{ GBq}$, which corresponds to a radiochemical yield of $31 \pm 9\%$.

$\text{Na}[^{18}\text{F}]\text{F}$

Three experimental $\text{Na}[^{18}\text{F}]\text{F}$ series were produced using the SynthraRNplus synthesis module. The synthesis time was 15 minutes, the average activity of $\text{Na}[^{18}\text{F}]\text{F}$ was $5 \pm 1 \text{ GBq}$, which corresponds to a radiochemical yield of $75 \pm 2\%$.

Conclusion

The process of ^{18}F isotope production using the cyclotron C-30 is stable and provides ^{18}F activity sufficient for both serial production of [^{18}F]FDG and experimental work on the introduction of technologies for the production of new preparations for PET, such as [^{18}F]-PSMA-1007 and $\text{Na}[^{18}\text{F}]\text{F}$.

The application of the automated synthesis system for mass production is quite reliable since only 5 equipment failures were recorded for 685 production cycles, which is 0.7%.

The synthesis module SynthraRNplus for experimental works is suitable for the production of new radiotracers. The research module was used to produce [^{18}F]-PSMA-1007 and $\text{Na}[^{18}\text{F}]\text{F}$ with a radiochemical yield comparable to that of commercially available cyclotron synthesis modules.

Domestic production of a wide range of radiopharmaceuticals will improve the quality of medical care, reduce the mortality rate and increase the overall survival rate and progression-free survival in patients with various forms of cancer and improve the quality of life of patients.

This research is funded by the Science Committee of the Ministry of Energy of the Republic of Kazakhstan (Grant No. BR09158958).

References

1. Shukla, A.K., & Kumar, U. (2006). Positron emission tomography: An overview. *Journal of medical physics*, 31(1), 13–21. <https://doi.org/10.4103/0971-6203.25665>.
2. Lau, J., Rousseau, E., Kwon, D., Lin, K. S., Bénard, F., & Chen, X. (2020). Insight into the Development of PET Radiopharmaceuticals for Oncology. *Cancers*, 12(5), 1312. <https://doi.org/10.3390/cancers12051312>.
3. Jacobson, O., Kiesewetter, D. O., & Chen, X. (2015). Fluorine-18 radiochemistry, labeling strategies and synthetic routes. *Bioconjugate chemistry*, 26(1), 1–18. <https://doi.org/10.1021/bc500475e>.
4. Francis, Felix, and Frank Wuest. (2021). «Advances in [^{18}F]Trifluoromethylation Chemistry for PET Imaging» *Molecules* 26(21), 6478. <https://doi.org/10.3390/molecules26216478>.
5. Halder, R., & Ritter, T. (2021). ^{18}F -Fluorination: Challenge and Opportunity for

Organic Chemists. *The Journal of organic chemistry*, 86(20), 13873–13884. <https://doi.org/10.1021/acs.joc.1c01474>.

6. Cole, E. L., Stewart, M. N., Littich, R., Hoareau, R., & Scott, P. J. (2014). Radiosyntheses using fluorine-18: the art and science of late stage fluorination. *Current topics in medicinal chemistry*, 14(7), 875–900. <https://doi.org/10.2174/1568026614666140202205035>.

7. Yu S. (2006). Review of F-FDG Synthesis and Quality Control. *Biomedical imaging and*

intervention journal, 2(4), e57. <https://doi.org/10.2349/bij.2.4.e57>.

8. Calculator and graphical system for parameters of atomic nuclei and characteristics of nuclear reactions and radioactive decays, http://cdfesinp.msu.ru/services/calc_thr/calc_thr_ru.html.

9. TENDL-2021, TALYS-based evaluated nuclear data library, <https://tendl.web.psi.ch/home.html>.

10. Decay Radiation database, https://www.nndc.bnl.gov/nudat3/indx_dec.jsp.

© This is an open access article under the (CC)BY-NC license (<https://creativecommons.org/licenses/by-nc/4.0/>). Funded by Al-Farabi KazNU

A.T. Olzhabay^{1*}, P.I. Urkimayeva¹, Z.A. Kenessova¹,
Sh.O. Yespenbetova², El-Sayed Negim³

¹Al-Farabi Kazakh National University, Almaty, Kazakhstan

²Korkyt Ata Kyzylorda University, Kyzylorda, Kazakhstan

³Satbayev University, Almaty, Kazakhstan

*e-mail: ispeniz777@gmail.com

(Received 26 March 2022; received in revised form 24 May 2022; accepted 10 June 2022)

Development of a technology for processing waste plastic bottles and bags to obtain various types of biodegradable polymer films

Abstract. Currently, one of the most important problems in the world is waste bottles made of polyethylene terephthalate, the number of which is currently growing every hour, polluting the environment. One of the ways to protect the environment from polyethylene terephthalate waste is the invention of biodegradable polymer materials from PET waste. Currently, several methods for processing polyethylene terephthalate waste have been proposed, but the work on the production of biodegradable materials has not been fully solved. Currently, various technologies for recycling plastic bottles and bags are being developed. The most promising technology in this direction is chemical processing, which is based on obtaining the final product in the form of a monomer or oligomer, which can be used as a new raw material for the synthesis of polymers. In this work, these polyethylene terephthalate wastes were chemically degraded with ethylene glycol solvent in the presence of zinc acetate catalyst and bis-hydroxy ethylene terephthalate was obtained. This work aims to obtain bis-2-hydroxyethyl terephthalate (BHET) by glycolysis of polyethylene terephthalate (PET) waste for the synthesis of various types of biodegradable polymer films. Biodegradable films based on polyvinyl alcohol and BHET have been synthesized. Water-soluble copolymers based on BHET and PVA were obtained by grafted copolymerization. (PVA) polyvinyl alcohol (5; 15; 25 wt. %) was dissolved in distilled water at 75-80°C until complete dissolution, ammonium persulfate, used as an initiator, was added to the initial mixture and biodegradable films based on PVA and BHET were obtained for the first time. It has also been proved that the resulting biodegradable films are formed by hydrogen bonds using IR spectroscopy.

Key words: PET, depolymerization, recycling, biodegradable films, BHET.

Introduction

In recent years, intensive work has been carried out to obtain biodegradable polymer materials that do not harm the environment and the human body. The problem of environmental protection is global, so the increase in the amount of synthetic plastic waste hourly raises serious concerns. The most suitable way to solve these problems is to create environmentally friendly biodegradable polymer materials. Currently, many methods have been proposed for the development of biodegradable polymer materials, but the production of biodegradable polymers has not been completely solved [1-5]. Recycling of used plastic materials is the main problem of polymer production, mainly due to the harmful effects of plastic waste on the environment. Plastic materials are stored for a long time under normal conditions due

to their high resistance to environmental influences. We can consider the recycling of plastic materials as an important economic factor, since the material and energy are reused. This will reduce the cost of raw materials, reduce the use of the necessary energy source, and bring economic benefits. In the global world, various types of recycling are offered [5-12].

Currently, mechanical and chemical methods of recycling are used. In addition, during chemical processing, monomers are removed, and then new polymer raw materials, chemicals and fuel are obtained. Methods of incineration and disposal of waste polymer materials have lost their importance, as new directions of methods of processing polymer materials are being introduced. Currently, strategies for the processing of biodegradable polymers and the secondary use of polymer materials are being considered [13-16].

The following incentives are necessary for the implementation of secondary use: legal requirements, low price, consumer demand, environmental aspect. Recycling of polyethylene terephthalate waste in the global world has received rapid development and is just beginning in Kazakhstan.

Materials and methods

Development of a technology for processing waste plastic bottles and bags to obtain various types of biodegradable polymer films. Obtaining bis-2-hydroxy ethylene terephthalate by glycolysis of polyethylene terephthalate waste from plastic bottles. Currently, different technologies are developed for the recycling of waste plastic bottles and bags. The most promising technology in this direction is chemical processing, which is based on obtaining the final product in the form of a monomer or oligomer, which can be used as a new raw material for the synthesis of polymers.

The aim of this work is to obtain bis-2-hydroxy ethylene terephthalate (BHET) by glycolysis of polyethylene terephthalate waste (PET) for the synthesis of various types of biodegradable polymer films. After the mechanical rinsing with acetone and methanol, removing glue and other substances, the beverage bottles produced by Bonaqua™ were crushed into small pieces.

Depolymerization of PET waste was carried out in a three-necked flask equipped with a thermometer, a refrigerator, and a mechanical stirrer, in the temperature range $140 \div 190^\circ\text{C}$ at a mass ratio of ethylene glycol to PET equal to 1:1, in the presence of a catalyst – zinc acetate (0.5% by weight PET), is the most effective catalyst for PET glycolysis. The degree of PET degradation (or conversion) was determined gravimetrically. For this, samples were taken at regular intervals, weighed with an accuracy of 0.0002 g, and calculations were performed. The reaction was carried out until the complete glycolysis of PET, after which distilled water was added to the resulting destructive at a ratio of 1:100. For the complete precipitation of BHET, the contents of the flask were kept for at least 24 hours. The formed precipitate was filtered off, after which the filtrate containing water was concentrated by evaporation of water at a temperature of $80\text{--}90^\circ\text{C}$, and then cooled in a refrigerator at a temperature of $3\text{--}5^\circ\text{C}$. The filtration residue was dried in a vacuum oven to constant weight. The output of BHET is 77%.

Figure 1 presents data on the study on the effect of temperature on the conversion of PET in the presence of zinc acetate. The results showed that as the temperature rises from 140 to 190°C , there is a regular increase in PET conversion. Thus, the complete glycolysis of PET at 140°C takes 2 times longer than at 160°C and 3 times longer than at 190°C .

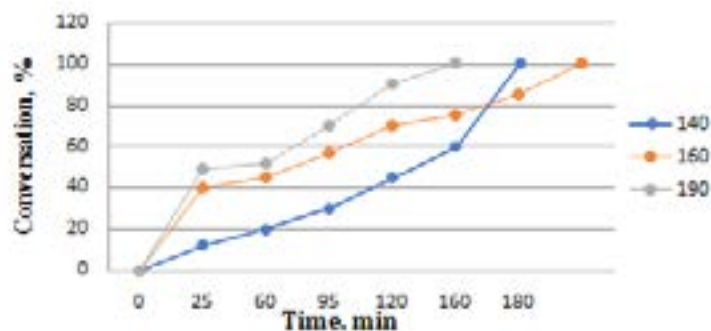


Figure 1 – Effect of temperature on PET conversion in the presence of zinc acetate as catalyst

The synthesis of biodegradable films is based on copolymers of polyvinyl alcohol and bis-2-hydroxyethyl terephthalate

Synthesized biodegradable films based on polyvinyl alcohol and BHET. Water-soluble copolymers based on BHET and PVA (FlukaChemie GmbH (Switzerland), Mw = 145000 kDa) were

prepared by the graft copolymerization method. PVA (5 wt. %) was dissolved in distilled water at $75\text{--}80^\circ\text{C}$, till complete dissolution, ammonium persulfate, used as an initiator, was added to the initial mixture. A 15% aqueous solution of BHET was added through a dropping funnel at a rate of 20 drops/min. To adjust the pH of the reaction mixture (the optimum pH of the

reaction medium is 3.8), a certain amount of glacial acetic acid was added to the reactor, the reaction mixture was heated for 2 hours at 75°C. At the end of the process, the reaction mixture was cooled to room temperature. In this case, a white homogeneous mass is obtained.

Results and discussion

The obtained PET Glycolized production is the form of a white crystalline powder with a melting point of 108°C. To confirm the structure of the obtained product, IR spectroscopy was investigated (Fig. 2).

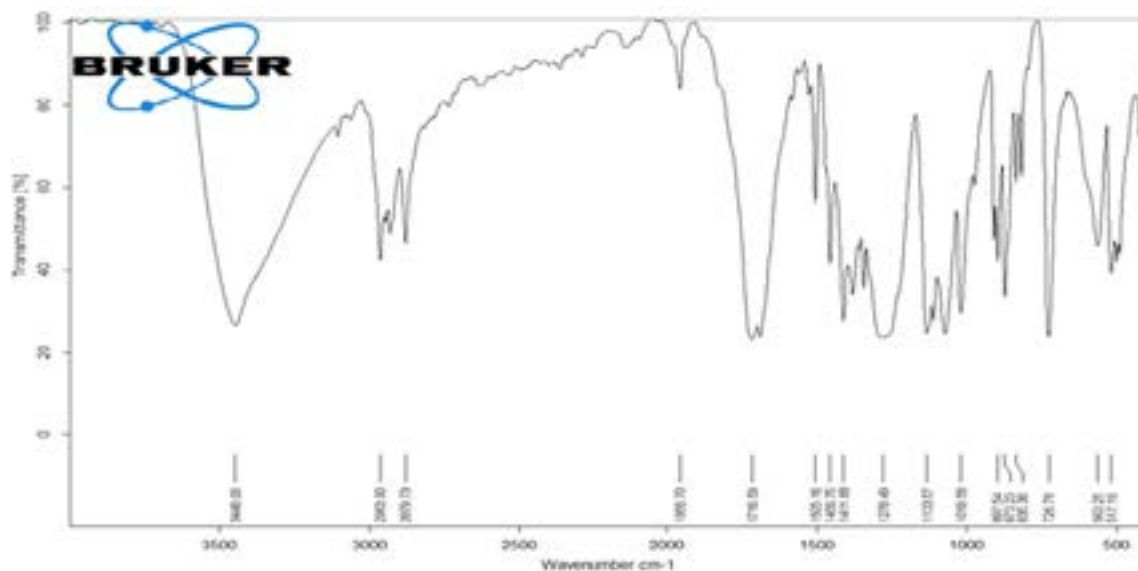


Figure 2 – IR spectrum of bis-2-hydroxyethyl terephthalate.

Thus, by the glycolized PET waste, bis-2-hydroxyethyl terephthalate was obtained for the synthesis of various types of biodegradable polymer films. Figure 2 shows the IR spectrum of the BHET of the pure product obtained. If we compare the spectra of the obtained copolymer and BHET, it turns out that the monomers are obtained in pure form and do not have chemical bonds. Benzene rings are located in the spectrum of the BHET, demonstrating the absorption of 1716-1677 cm^{-1} and 726-875 cm^{-1} , and 1133 cm^{-1} C-O-C bonds were also observed. Two vertices connected in the spectrum at 3447 cm^{-1} and 2931 cm^{-1} showed us the existence of hydroxyl groups, i.e., they manifested themselves acutely, which tells us about the elongation of the O-H groups in the composition of the $\text{CH}_2\text{-CH}_2\text{-OH}$ bonds and can serve as a basis for the fact that we have obtained a pure monomer.

To confirm the interaction reaction between PVA and BHET, IR spectra analysis was studied. As shown in Figure 3, the obtained films based on PVA and BHET showed an absorption band at about

3265.13 cm^{-1} , attributed to OH groups. The band at 1712 cm^{-1} characteristic of the carbonyl group ($\text{C}=\text{O}$) is related to the presence of residual acetate groups in the copolymer, which remained after the preparation of PVA by hydrolysis of polyvinyl acetate. The absorption bands at 1126 and 1066 cm^{-1} are due to stretching vibrations of the C-O, C-O-C groups, and the band at 724 cm^{-1} refers to the C-H₂ groups. In addition, at 1712 cm^{-1} , an absorption peak characteristic of the carbonyl group of acetic acid is observed, and at 568 and 670 cm^{-1} , a band of vibrations of C-H groups characteristic of aliphatic compounds appears.

Polymer films of the obtained copolymers were prepared by pouring a 4% aqueous solution of copolymers into polyethylene Petri dishes, followed by evaporation of the solvent at room temperature and keeping in a vacuum drying oven at 30°C until constant weight. Photographs of the obtained films based on PVA and BHET copolymers are shown in Figure 4. It can be seen that films based on PVA and BHET interpolymers are equally homogeneous and elastic.

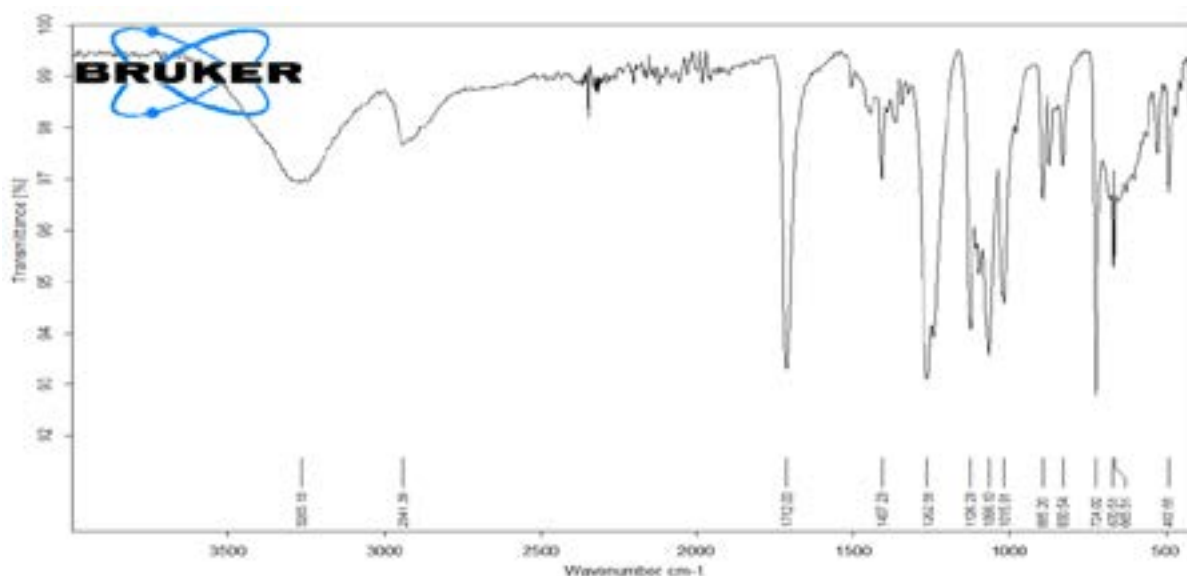


Figure 3 – IR spectra of P(PVA-co-BHET)

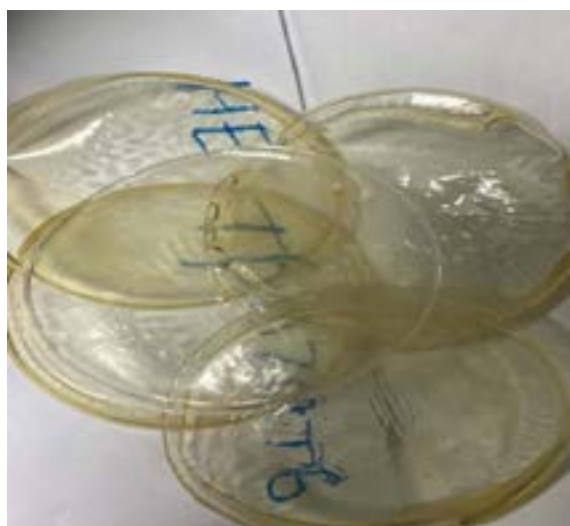


Figure 4 – Photographs of films based on P(PVA-co-BHET)

Development of a technological scheme for the processing of waste plastic bottles and bags

Completed work:

- A technological scheme for the processing of waste plastic bottles and bags has been developed.

These studies, showed the fundamental possibility of obtaining secondary BHET by glycolysis polyethylene terephthalate from waste, and indicate the advantage of the ethylene glycol solventless over water.

The optimal conditions for the PET destruction process are:

- temperature – 190°C;
- the mass ratio of ethylene glycol and PET, equal to 1: 1;
- catalyst – zinc acetate (0.5% to the weight of PET).

Based the laboratory results, a technology for producing BHET from secondary PET was proposed. This technology includes several stages (Figure 5):

- in the reactor at a temperature of 180-190°C and a pressure of 1 MPa for 1 h, PET is mixed with ethylene glycol in the presence of zinc acetate as a catalyst;
- separation of unreacted PET from the solution;
- separation of BHET from ethylene glycol and water is carried out by filtration in a drum vacuum filter;
- separation of a mixture of ethylene glycol with water is carried out in a column separation at a temperature of 200°C, where part of the ethylene glycol is returned to the first stage of processing to soften PET.

Shredded polyethylene terephthalate is fed into the reactor (R-1) from the vessel (B-1), zinc acetate is pumped from the tank (E-2) by the pump (N-3), and recycled ethylene glycol at the temperature of 206°C is also pumped into the reactor. In the reactor (R-1), the process of glycolysis polyethylene terephthalate occurs at a temperature of 190°C.

To maintain the temperature of the process, due to the exothermicity of the target reaction, the reactor (R-1) is equipped with a jacket, into which water vapor is supplied with a pressure of 2.4 MPa.

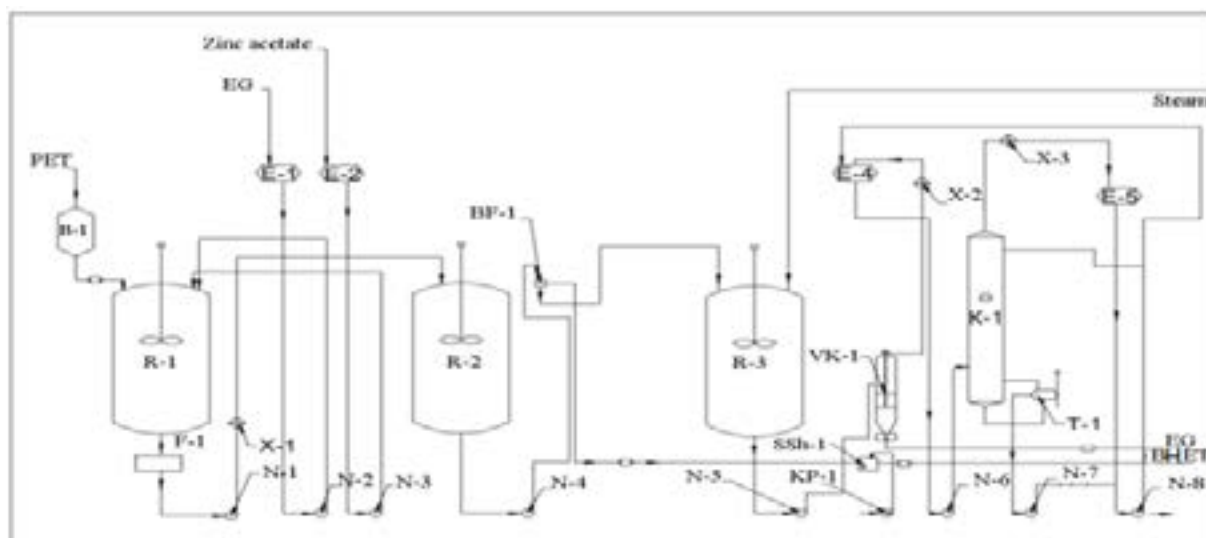


Figure 5 – Flow diagram of the process of obtaining BHET from glycolysis polyethylene terephthalate.

Note: B-1 – storage hopper; BF-1 – drum filter; VK-1 – evaporator-crystallizer; E-1, 2, 3, 4, 5 – containers; K-1 – rectification column; KP-1, 2 – compressors; N-1, 2, 3, 4, 5, 6, 7, 8 – pumps; R-1, 2, 3 – reactors; SSh-1 – drying apparatus; T-1 – heat exchanger; X-1, 2, 3 – condenser refrigerator; F – filter

From the reactor (R-1), the mixture is fed to the filter (F-1), where the unreacted PET is separated from the solution. The solution after F-1 is cooled in a refrigerator X-2 to a temperature of 2-3°C and transferred to receive BHET in the reactor (R-2), in which BHET is released at a temperature not exceeding 60°C and pressure at 101.3 kPa.

The mixture of reaction products from the reactor (R-2) is pumped out by using the pump (N-4) into the vacuum drum filter (BF-1), where the BHET is separated from the liquid part of the mixture. A mixture of water and ethylene glycol is fed to the R-3 reactor. Then BHET goes for drying to the dryer (SSh-1), where the air is supplied by the compressor (KP-1). The dried BHET is removed from the plant as a finished product.

From the R-3 reactor, the resulting mixture of water and ethylene glycol is fed to the VK-1 crystallizer through the H-5 pump and cooled in the X-3 refrigerator, and the mixture is fed to the K-1 Steam column through the H-6 pump. Water vapor is removed from the top of the column, which condenses in the (X-2) refrigerator. Water condensate enters the (E-4) tank, from which the (H-8) pump is pumped to the sewage system. From the bottom of the (K-1) column, the (N-7) pump pumps out ethylene glycol, part of which is heated in the (T-1) heat exchanger with water vapor, returns to the K-1 column cube as irrigation, and the other part enters the (R-1) reactor. The balance amount of EG is removed from the installation.

Process flow diagram of the production process of biodegradable polymer films based on PVA and BHET

To obtain polymer films based on CPL PVA-BHET, the method of casting films from solutions on a substrate (“dry” method) was used. This method is economic and technological advantages, firstly, the “dry” method is more industrially applicable due to the prostate equipment and low cost, and secondly, it allows you to obtain films with high-performance characteristics.

The basic and principle of this method is to form a viscous polymer solution. The mixture is thoroughly mixed, the excess air is removed under a vacuum. A film is formed from the resulting solution, dried and then cut to the required size.

The production of film materials consists of two technological lines for the production of water-soluble and grafted films. The main stages of the technological process of forming water-soluble films:

- Dissolution of copolymers;
- Preparation of copolymer solutions (solution filtration);
- Deaeration of the molding solution;
- Forming a film on the surface of the dryer belt;
- Film stretching and drying;
- Reception, winding and cutting of finished film;
- Stamping, packaging, and marking of finished products.

In the production of grafted films, the stages of thermal grafting and saturation of films with drugs are additionally included.

For the pilot production of new water-soluble films based on CPL of polyvinyl alcohol and BHET, a technological scheme has been developed, shown in Figures 6 and 7.

From the measuring tank – dispenser (MD-1), the pure polyvinyl alcohol dissolves in distilled water in the mixer (C-1) with a corrosion-resistant inner coating, equipped with a frame mixer. As a solvent, CPL PVA and BHET uses water, which is obtained from a metering meter (MD-2). The loading of the CPL PVA and BHET into the mixing apparatus is carried out with the mixer operating. First, using a pump N-1, water is supplied in an amount of 10-20% of the total volume of the solvent and CPL PVA-BHET is loaded in small portions through the hopper, then after a short stirring, half of the water is introduced through the dispenser. After swelling of the CPL PVA and BHET, the remaining amount of solvent water is fed into the mixer. The dissolution process lasts 12 – 24 hours with constant stirring at a temperature of 65-70°C. The prepared solution of CPL PVA and BHET is fed by a gear pump (N-2) under a pressure of several atmospheres to multistage filter presses (PF-1) to remove undissolved particles of CPL PVA and BHET.

In the filtration process of the solution, an increase in pressure is observed due to the clogging of filters. When the critical pressures are reached, the flow is switched to a backup filter press, and the clogged one is washed with water and then blown with compressed air.

To produce a water-soluble film, the filtered PVA and BHET solution was transferred to the mixer (C-1) and (C-2) to obtain a homogeneous molding solution. After prolonged mixing, a plasticizer is added to obtain homogeneous solution. The duration of the preparation of the film-forming solution at a stirrer speed of 40 – 60 rpm is 2 hours.

The mixing process of solutions can inadvertently introduce air bubbles into the liquid, therefore deaeration is a prerequisite for obtaining a homogeneous polymer solution. The film-forming solution is evacuated in a deaerator (D-1) and (D-2) for 4-6 hours and fed into the storage tank (E-1) and (E-2).

From the container (E-1), the copolymer solution is fed into the container of the smearing die (MF-1), from which it is applied to the surface of the moving continuous belt of the casting machine (FM-1). The forming speed is 1-5 m/min. The optimal drying

mode was experimentally established at 28-30°C. The drying process takes 24 hours.

In the casting machine, the film is dried to a residual solvent content of 15 – 20%, after which the film is removed from the substrate with a knife and enters the drying chamber (KD-1), where, passing through a system of rollers, it is pulled out for hardening and finally dried with heated air.

After that, the film transfers to the cutting unit (PM-1). It passes through a shaft equipped with a trimming device, after which it enters the winding machine, where it is cut along the web into 6 × 3 plates, first packed in plastic bags then into paper boxes, marked and sent to the finished product warehouse. Waste is recycled.

The formation of a polymer solution to obtain grafted films is carried out in a mixer (C-2). At the beginning, the filtered copolymer solution enters the mixer, and then the dissolved grafting agent and plasticizer are introduced. The duration of the solution formation at a stirrer speed of 40-60 rpm is 2 hours.

The molding solution is transferred to the deaerator (D-1), where it is processed for several hours, and then under pressure is fed into the container of the smearing die. The die ensures the formation of a layer of polymer solution of a given thickness and distributes it evenly over the entire width of the ground surface of the metal substrate strip stretched over the surface of the casting machine.

The solution layer is dried to a residual solvent content of up to 15-20%, the film is separated from the substrate surface and through a tear-off roller and a compensator is directed into a heat chamber (T-1) formed by several electric heating plates located in a horizontal plane. The film, passing through the rollers of the speed control system, is captured at the edges by using clamping clips and transported through the chamber using Gall roller chains. The speed of the chains is synchronized with the speed of the belt of the forming apparatus. The temperature in the chamber is 100°C; the duration of the stay of the film in the chamber is 4 hours. After the heating chamber, the film is directed into the bath (VO-1) to wash off the ungrafted part of the polymer. Then the film enters the drying chamber (VN-1).

The dried film is cut into oval-shaped plates 10 × 20 mm in size, 10 plates are packed in contour-cellular packaging made of PVA film and aluminum foil and marked.

All packed boxes are gas sterilized with ethylene oxide and then sent to the warehouse.

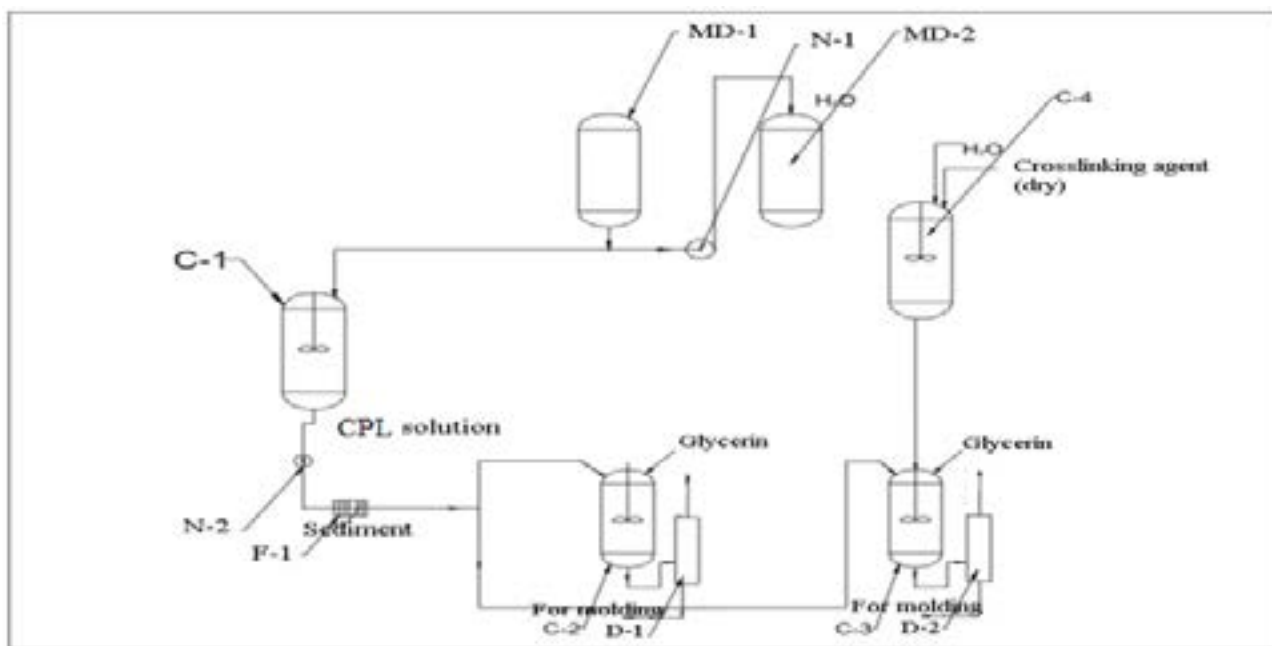


Figure 6 – Technological scheme of pilot production of linear and grafted films based on CPL PVA and BHET.

Note: MD-1, 2 – measuring tank-dispenser; C-1, 2, 3, 4 – mixer; H-1, 2 – centrifugal pump; F-1 – filter press; D-1, 2 – deaerator

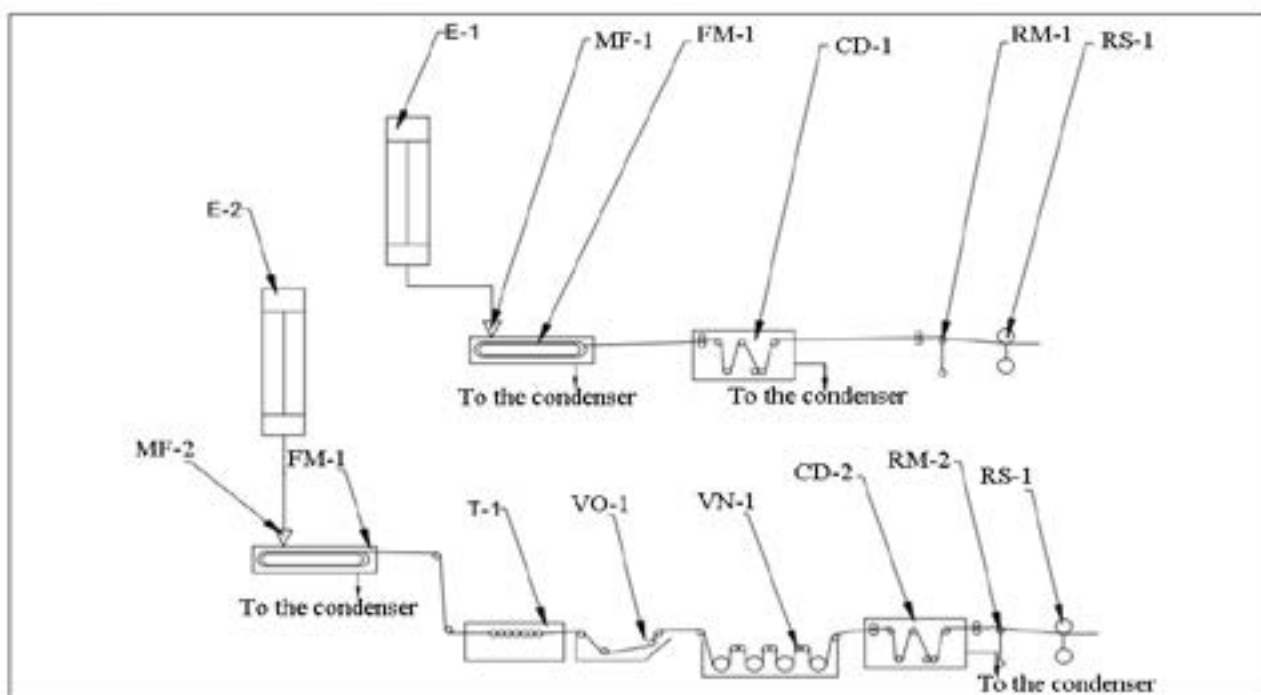


Figure 7 – Technological scheme of pilot production of linear and grafted films based on CPL PVA and BHET.

Note: E-1, 2-storage capacity; MF-1, 2-smearing die; FM-1,2-forming machine;
 CD-1, 2-drying chamber;RM-1, 2-stretching machine; RS-1, 2-cutting machine;
 T-1-heat capacity; VO-1 – bath for washing; VN-1-bath for saturation

Conclusion

In this article, the method of secondary chemical treatment of polyethylene terephthalate waste is studied. The remains of PET bottles were first sorted by color and cleaned, disassembled into flexi. Optimal conditions for the chemical method of processing polyethylene terephthalate waste have been determined, i.e. it has been established that PET waste is destroyed in the presence of ethylene glycol solvent and zinc acetate (0.5% to the weight of PET) as a catalyst. In addition, 190°C was designated as the optimal destruction temperature. Biodegradable films based on polyvinyl alcohol and bis-hydroxy ethylene terephthalate were obtained by graft copolymerization, during which ammonium persulfate was used as an initiator. This method of obtaining biodegradable films based on PVA and BHET has not yet been considered in scientific research at all. Optimal conditions for the production of films based on polyvinyl alcohol and bis-hydroxy ethylene terephthalate have been established, i.e. the optimal temperature is 75-80°C and with a ratio of PVA and BHET 1:3 and pH = 3.8-4.0, it has been established that in the presence of glacial acetic acid, very strong and flexible, water-soluble films are obtained. It has been established that biodegradable films based on PVA and BHET are interconnected by hydrogen bonds along the IR spectrum and can attract water to it as a result of the presence of C-O-C bonds in the composition, and a technological scheme of a biodegradable film based on PVA and BHET. In addition, biodegradable films based on PVA and BHET were obtained for the first time.

References

1. Nabid M.R., Bide Y., Jafari M. Boron nitride nanosheets decorated with Fe₃O₄ nanoparticles as a magnetic bifunctional catalyst for post-consumer PET wastes recycling // *Polym. Degrad. Stab.* Elsevier Ltd. – 2019. – Vol. 169. – P. 108–962. <https://doi.org/10.1016/j.polymdegradstab.2019.108962>
2. Nguyet L. et al. Enhanced catalytic glycolysis conditions for chemical recycling of glycol-modified poly(ethylene terephthalate) // *Polym. Degrad. Stab.* Elsevier Ltd. – 2018. – Vol. 155. – P. 15–21. <https://doi.org/10.1016/j.polymdegradstab.2018.07.003>
3. Passos R. et al. Bio-based electrospun mats composed of aligned and nonaligned fibers from cellulose nanocrystals, castor oil, and recycled PET // *Int. J. Biol. Macromol.* Elsevier B.V. – 2020. – Vol. 163. – P. 878–887. <https://doi.org/10.1016/j.ijbiomac.2020.07.064>
4. Zhang R. et al. PET bottles recycling in China: An LCA coupled with LCC case study of blanket production made of waste PET bottles // *J. Environ. Manage.* Elsevier Ltd. – 2020. – Vol. 260. – P. 110–162. <https://doi.org/10.1016/j.jenvman.2019.110062>
5. Guo Z. et al. Circular recycling of polyester textile waste using a sustainable catalyst // *J. Clean. Prod.* Elsevier Ltd. – 2021. – Vol. 283. – P. 124–579. <https://doi.org/10.1016/j.jclepro.2020.124579>
6. Barış Şimşek. Bis-hydroxyethyl terephthalate cementitious composites properties: A comparative study including hydrogen bonding mechanism with the dioctyl terephthalate // *Constr. Build. Mater.* – 2020. – Vol. 258. – P. 119–691. <https://doi.org/10.1016/j.conbuildmat.2020.119691>
7. Ion S. et al. Sequential biocatalytic decomposition of BHET as valuable mediator of PET recycling strategy // *Catal. Today.* Elsevier B.V. – 2020. – Vol. 1. – P. 111–129. <https://doi.org/10.1016/j.cattod.2020.08.008>
8. Iqboljon A. et al. Influence of conditions for alcoholysis of secondary polyethylene terephthalate on the output of bis(hydroxyethyl)terephthalate texnologik kataliz va reaksiyalar influence of conditions for alcoholysis of secondary va ki myo te xno logi yas i // *Chem. Chem. Eng.* – 2019. – Vol. 23, – № 4. – P. 1–5.
9. Lalmangaihzuala S. et al. Glycolysis of Poly(ethyleneterephthalate) Using Biomass-Waste Derived Recyclable Heterogeneous Catalyst // *Polymers.* – 2021. – Vol. 37., – № 13. – P. 5–13. <https://doi.org/10.3390/polym13010037>
10. Wu H. et al. The study of the thermomechanical degradation and mechanical properties of PET recycled by industrial-scale elongational processing // *Polym. Test.* Elsevier. – 2019. – Vol. 77. – P. 105–882. <https://doi.org/10.1016/j.polymertesting.2019.04.029>
11. Puspitasari N., Tsai S., Lee C. Class I hydrophobins pretreatment stimulates PETase for monomers recycling of waste PETs // *Int. J. Biol. Macromol.* Elsevier B.V. – 2021. – Vol. 176. – P. 157–164. <https://doi.org/10.1016/j.ijbiomac.2021.02.026>
12. Maio A. et al. Poly(ethylene terephthalate) (PET) degradation by *Yarrowia lipolytica*: Investigations on cell growth, enzyme production and monomers consumption // *Process Biochem.* Elsevier. – 2020. – Vol. 95. – P. 81–90. <https://doi.org/10.1016/j.procbio.2020.04.001>
13. Thi C. et al. The advancement of bis(2hydroxyethyl)terephthalate recovered from post-consumer poly(ethyleneterephthalate) bottles compared to commercial polyol for preparation of high performance polyurethane // *J. Ind. Eng. Chem.*

The Korean Society of Industrial and Engineering Chemistry. – 2020. – Vol. 93. – P. 196–209. <https://doi.org/10.1016/j.jiec.2020.09.024>

14. Marina T. *et al.* Chemical Recycling of Poly(ethylene terephthalate) (PET) by Alkaline Hydrolysis and Catalyzed Glycolysis //Electron. J. Chem. –2018. –Vol. 10., – № 3. – P. 226–233. <http://dx.doi.org/10.17807/orbital.v10i3.1104>

15. Machado A. *et al.* Enzyme-catalyzed simultaneous hydrolysis-glycolysis reactions

reveals tunability on PET depolymerization products //Biochem. Eng. J. Elsevier B.V. – 2018. – Vol. 137. – P. 239–246. <https://doi.org/10.1016/j.bej.2018.06.007>

16. Cevher D., Sürdem S. Polyurethane adhesive based on polyol monomers BHET and BHETA depolymerised from PET waste //Int. J. Adhes. Adhes. Elsevier Ltd. – 2021. – Vol. 105. – P. 102–799. <https://doi.org/10.1016/j.ijadhadh.2020.102799>

© *This is an open access article under the (CC)BY-NC license (<https://creativecommons.org/licenses/by-nc/4.0/>). Funded by Al-Farabi KazNU*

Content

A.A. Malysheva, A.M. Kokhmetova, M.K. Kumarbayeva, D.K. Zhanuzak, A.A. Bolatbekova, Zh.S. Keishilov, E.I. Gulyaeva, A.M. Kokhmetova, V. Tsygankov, Y. B. Dutbayev, S. B. Dubekova Identification of carriers of <i>Puccinia striiformis</i> resistance genes in the population of recombinant inbred wheat lines	4
A. Perfilyeva, K. Bespalova, G. Abylkassymova, B. Bekmanov, L. Djansugurova RS2710102 polymorphism of the <i>CNTNAP2</i> gene is related to autism susceptibility in a Kazakhstani population	11
M.A. Zhaksylyk, M.S. Kyrykbayeva, A.M. Kalimagambetov Results of the comprehensive study in newborn babies with congenital phenylketonuria.....	20
L. Bekbayeva, Z. Zakaria, El-Sayed Negim, K.M. Al Azzam, G. Yeligbayeva The effect of mixed fertilizers on the vegetative growth and reproductive characteristics of tomatoes (<i>L. esculentum</i> Mill)	31
E. Altınöz, E.M. Altuner Observing the presence of efflux pump activities in some clinically isolated bacterial strains	48
S.D. Zhantlessova, Zh. Khamitkyzy, A.B. Talipova, I.S. Savitskaya, A.S. Kistaubayeva Selection and optimization of cultivation conditions for bacterial cellulose producer	55
M.K. Kumarbayeva, N.M. Kovalenko, O.Yu. Kremneva, M.N. Atishova, Zh.S. Keishilov, A.A. Malysheva, D.K. Zhanuzak, A.A. Bolatbekova, A.M. Kokhmetova Identification of wheat samples for resistance to toxins of <i>Pyrenophora tritici-repentis</i> (Ptr).....	64
S. Syraiyl, A. Ydyrys, A. Ahmet, R. Aitbekov, M.T. Imanaliyeva Phytochemical composition and antioxidant activity of three medicinal plants from southeastern Kazakhstan	73
N.V. Khan, M. Baláz, M.M. Burkitbayev, B.B Tatykayev, Zh. S. Shalabayev, A.I. Niyazbayeva, F.Kh. Urakaev Solvothetical DMSO-mediated synthesis of the S/Agi microstructures and their testing as photocatalysts and biological agents	79
I.Yu. Silachyov, V.A. Glagolev Comparator neutron activation analysis of the solid volumetric rock samples for gold content.....	90
A.N. Gurin, Ye.T. Chakrova, A.R. Borissenko, Z.V. Medvedeva, A.V. Kulakov, A.P. Sylnyagin Experience in production of ¹⁸ F isotope in the Cyclone-30 for synthesis of fluorinated radiopharmaceuticals.....	102
A.T. Olzhabay, P.I. Urkimayeva, Z.A. Kenessova, Sh.O. Yespenbetova, El-Sayed Negim Development of a technology for processing waste plastic bottles and bags to obtain various types of biodegradable polymer films	107